Homeostasis of dendritic spines in hippocampal CA1 cells

Caroline Antonia Mestrallet

Thesis submitted for the degree of

Doctor of Philosophy

Department of Neuroscience, Physiology and Pharmacology

University College London

October 2011

Abstract

Synaptic connections in the brain respond throughout their lives to the activity of incoming neurones, adjusting their biological properties to increment activity-dependent changes but also avoid run-away excitation or complete loss of transmission. To ensure synapses remain functional when inputs change over time, compensatory mechanisms, coined homeostatic plasticity, take place either globally or locally. The correlation between synaptic strength and dendritic spine size has been clearly established, and thus imaging dendritic spines under various activity conditions has become accepted as a valid way of studying homeostatic changes of postsynaptic strength. Many neurological diseases demonstrate abnormalities of dendritic spines, directly linking their properties to the efficient functioning of the network. Understanding how dendritic spines are regulated under global changes of network activity is important to unveil clues about how to tackle those deficits in disease. Studying morphology of dendritic spines requires intensive and careful analysis, and a substantial part of this work has been dedicated to finding an appropriate way to analyse the data. Dendritic spines showed a remarkably stable density in CA1 pyramidal neurones during the second week in vitro, when treatments altering plasticity or even deafferentation failed to modify the autonomous development. However, deafferentation carried out a week later decreased the overall spine density and increased spine head size, specifically in the area that normally receives inputs from the transected axons. The strong activity of the Schaffer collateral axons in organotypic slices results in enlarged spines in the apical compared with basal dendrites. This difference between pathways was abolished by inhibition of CaMKII. Activity-dependent and homeostatic plasticities are working intricately to maintain the network efficacy. They operate at a local level in an age-dependent manner and are differentially modulated by the CaMKII or PKA pathways.

Declaration

I declare that the work described in the present thesis has been done by myself, except where indicated.

Caroline Mestrallet

Acknowledgements

I would like to thank my supervisor, Dr Frances Edwards, for giving me the opportunity to carry out my PhD in her lab, for teaching me independence and perseverance in the tougher times while always remaining enthusiastic and optimistic about life and science. I am grateful to the CORTEX-Marie Curie and Bogue fellowships for providing me the means to undertake this research. I would like to thank all the Edwards lab members, past and present, and especially Dr Damian Cummings, who has been my guidance through the writing process, my Italian gang Angelo and Mario, who have made this journey rich and colourful and Dr Lion Shahab for his advice on statistics. I would also like to thank my graduate advisor, Professor Chris Yeo, for his support and encouragements.

I would like to thank Professor Robert Malinow for inviting me to his lab and for the precious advice and supervision I received during my stay at UCSD. I am very grateful to the whole Malinow lab for their support and guidance, Dr Helmut Kessels, Dr Joaquin Piriz, Dr Hiroshi Makino, Dr Christophe Proulx and Irina Chuprinova for their help, and most of all to the sunshine of my stay in California, Saddegh and Brea.

This journey would not have been the same without the support of my fellow PhD students, and especially my flatmates Karolina and Anna, who have treaded through the rough PhD waters with me, offering their shoulders and opening their hearts; my dearest Zoomers with her unfailing enthusiasm; my FFF Asheeta who has been a role model during this time and my fiote Sonia for her mental support.

After several years away, I am extremely grateful to my long-distance friends, who have remained supporting and understanding, and an even greater thank to those few who bring light when you need it without having to ask for it: my fiotes from Montpellier (Violaine, Sophie, Laure, Vero et Clémence), my childhood friend Anne-Carole, my high-school friends Marie & Claire and finally my Oz buddy Hoyoung.

Last but not least, I want to dedicate my PhD to my loving family, who has supported me in every possible way throughout my entire life, in the storm and in the sun, transmitting me their fundamental values. A last special thanks to my sister, Stephanie, for always being there for me, understanding me without a word and putting me back on track when I needed. This journey would probably not be achieved without my little ferries!

"The mind is its own place, and in itself can make a heaven of hell, a hell of heaven."
John Milton

Table of Contents

Chapter 1. Introduction 19

1.1 General introduction 19

1.2 Function and structure of the hippocampus 21

1.2.1 Role of the hippocampus in learning & memory 21

1.2.2 Structure and connectivity 22

1.2.3 Hippocampal organotypic slices 24

1.3 Synapses and synaptic transmission 25

1.3.1 Synapse formation and maturation 25

1.3.2 Dendritic spines and the synaptic machinery 26

1.4 Synaptic plasticity of CA1 pyramidal neurones 29

1.4.1 Activity-dependent plasticity 29

1.4.2 Homeostatic synaptic plasticity 38

1.5 Structure-function relationship of dendritic spines – a tool to study synaptic strength regionally 43

1.5.1 Plasticity of dendritic spine morphology 44

1.5.2 Morphological factors affecting spine plasticity 48

1.6 Summary of dendritic spines plasticity 56

Chapter 2. Materials and Methods 58

2.1 Hippocampal organotypic slice cultures 58

2.1.1 Preparation and maintenance of organotypic slices 58

2.1.2 Labelling presynaptic axons 59

2.1.3 Labelling postsynaptic cells and CA1 axons 60

2.1.4 Fixation of slices for later imaging 60

2.1.5 Long-term treatments of organotypic slices 61

2.2 Imaging and analysis of morphology 63
2.2.1 Fluorescence, confocal microscopy and image acquisition 63
2.2.2 Image analysis 67
2.3 Experimental procedure in the Malinow lab (UCSD) 70
2.3.1 Rat and mouse acute and organotypic slices 70
2.3.2 Whole cell recordings – voltage clamp, current clamp, paired patch 71
Chapter 3. Dendritic spines analysis: Optimisation of the method using Imaris *Filament Tracer* 73
3.1 Introduction 73
3.2 Spine analysis: limitations of previously used methodology 73
3.2.1 'Eyeball' morphological classification 74
3.2.2 Line-scan of spine head with ImageJ 80
3.2.3 Deconvolution 84
3.3 Spine reconstruction with Imaris *Filament Tracer* 87
3.3.1 A very powerful software 87
3.3.2 User sensitivity 91
3.3.3 On the way to achievement 99
3.4 Comparison of the different methods 101
3.4.1 ImageJ *vs* Imaris and raw *vs* deconvolved images 102
3.4.2 Automatic spine classification 103
3.5 Discussion 111
3.5.1 Continuity in spine analysis 111
3.5.2 Imaris *Filament Tracer* 112
3.5.3 Limit of definitions 113
Chapter 4. Imaris analysis of the distribution of dendritic spines in CA1 pyramidal cells on 14 DIV organotypic slices 115
4.1 Introduction 115

4.2 Control and 0.1% DMSO treated cultures 116
4.3 Comparison of apical versus basal dendrites 121
4.3.1 Differences in density 121
4.3.2 Spine head diameter 124
4.3.3 Spine length 126
4.3.4 Input from the Schaffer collateral 128
4.4 Comparison of dendritic spine population in apical dendrites, according to the degree of complexity of the branches 133
4.4.1 Density and spine type distribution 133
4.4.2 Spine head diameter 136
4.4.3 Spine length 137
4.5 Discussion 138
4.5.1 Apical *vs* basal 138
4.5.2 Branching 138
4.5.3 Schaffer collateral pathway 139
Chapter 5. Synaptic scaling in organotypic slices? 141
5.1 Introduction 141
5.1.1 Synaptic scaling or absence of activity-induced changes during development? 141
5.1.2 Experimental procedures 142
5.2 Synaptic scaling in CA1 pyramidal neurones of rat organotypic slices after 14 DIV 144
5.2.1 Model 1: Rat organotypic slices, recorded at 14 DIV 144
5.2.2 No synaptic scaling observed in CA1 cells of 14 DIV rat organotypic cultures 145
5.3 Synaptic scaling in CA1 pyramidal neurones of mouse organotypic slices after 6-9 DIV 149

5.3.1 Model 2: Mouse organotypic slices, recorded at 6-9 DIV 149

5.3.2 No synaptic scaling in CA1 neurones of mice organotypic cultures aged 6-9 DIV 150

5.4 Discussion 154

Chapter 6. Effect of partial deafferentation on CA1 dendritic spines is age-dependent 157

6.1 Introduction 157

6.2 Development of dendritic spine density in organotypic slices 158

6.2.1 Increased spine density in hippocampal CA1 cells on organotypic slices between 7 and 21 DIV 158

6.2.2 Stubby spines decrease is paralleled by an increase in more plastic spines 161

6.3 Effect of long-term deletion of Schaffer collateral input onto CA1 cells from 7 to 14 DIV on dendritic spines 163

6.3.1 Effect of partial deafferentation on CA1 cells spine density at 14 DIV .. 163

6.3.2 Effect of deafferentation on headed spines dimension 166

6.3.3 Why no change in spine density at an early age? 170

6.4 Effect of long-term deletion of the Schaffer collateral input onto CA1 cells from 14 to 21 DIV 171

6.4.1 Effect of deafferentation on spine density at 21 DIV 171

6.4.2 Effect of deafferentation on spine types representation at 21 DIV 173

6.4.3 Effect of deafferentation on headed spines dimensions at 21 DIV 174

6.5 Discussion 178

Chapter 7. Effect of long-term blockade of CaMKII or PKA on dendritic spine population 182

7.1 Introduction 182

7.2 Effect on spine density 183

7.2.1 Preparation and imaging 183

7.2.2 Overall density of spines 184
7.2.3 Effect of branching on apical spines 186
7.3 Effect on spine type 187
7.3.1 Effect on density of each spine type 187
7.3.2 Effect on spine types 189
7.4 Effect on spine shape 191
7.4.1 Spine head diameter 191
7.4.2 Spine length 192
7.5 Pathway specificity 194
7.6 Discussion 198
Chapter 8. General discussion 202
8.1 Optimising dendritic spine analysis 203
8.1.1 Heterogeneity of dendritic spine types and analysis 203
8.1.2 Limits of the analysis & significance of results 204
8.2 Experimental variability & necessity of repeating basic findings in the model used 205
8.2.1 Difference in culture preparation 205
8.2.2 Variability of results and absence of published negative results 206
8.3 Age-dependence of the activity-dependent and homeostatic synaptic plasticity 207
8.3.1 Following reorganisation 207
8.3.2 Following activity deprivation 208
8.3.3 Developmental switch in PKA/CaMKII-dependent synaptic plasticity and GABA transmission 209
8.4 Balancing output globally to maintain synaptic weight 211
8.4.1 Changes proportional to the activity disruption 211
8.4.2 Balance between activity-dependent and homeostatic changes 212

8.5 Broader picture of synaptic plasticity 213
8.5.1 Presynaptic changes 213
8.5.2 Interneurones and glial cells 214
8.5.3 PKA and CaMKII are polyvalent 215
8.5.4 The dendritic branch as preferential unit for plasticity 216
8.5.5 Implications for learning and disabilities 218
8.6 Perspectives 219
List of references 221

List of Figures

Introduction

Figure 1-1: Schema of the hippocampus circuitry 23
Figure 1-2: Schematic representation of an excitatory synapse showing the major postsynaptic cascades involved in LTP. 30
Figure 1-3: Identification of spine type by Kristen Harris and co-workers and sample of each spine type variability. 44
Figure 1-4: There is a barrier to AMPA lateral movement located at the spine neck (Ashby et al, 2006). 51
Figure 1-5: PSD95 clusters can move between shafts and spines as spines emerge, briefly transiting through a stubby-shape type. 53
Figure 1-6: Prospective analysis of morphology of dendritic protrusions over 2-4h time-lapse imaging study, in developing mouse hippocampal slice. 55

Material and Methods

Figure 2-1: Scheme of an organotypic hippocampal culture following deafferentation 63
Figure 2-2: Jablonski diagram 64
Figure 2-3: Schematic diagram of the optical pathway and principal components in a laser scanning confocal microscope (Claxton et al., 2004). 66
Figure 2-4: Schematic diagrams of the fluorescent wavelength and the different filters available with short or long pass. 67
Figure 2-5: AutoQuantX interface, which enables the deconvolution of image stacks after entering the imaging parameters. 69

Result Chapters

Figure 3-1: Disparity in spine type distributions in similar preparation attributed to individual classification. 78
Figure 3-2: Comparison of spine types determined by eye by two different users. 79
Figure 3-3: Estimation of spine head diameter from light intensity analysis over line-scan of the spine terminal point. 81

Figure 3-4: Frequency distribution of spine head size analysed with ImageJ line-scan. 82
Figure 3-5: Line-scan limitations on certain spines. 84
Figure 3-6: Effect of deconvolution on image resolution. 86
Figure 3-7: 3D reconstruction of a cell using Imaris *Filament Tracer*. 87
Figure 3-8: Building of a filament with Imaris *Filament Tracer* 7.2.0. 88
Figure 3-9: Scheme of the measurements used for the estimation of the spine head diameter with the algorithms available in *Filament Tracer*. 90
Figure 3-10 : Effect of Local Threshold on the spine terminal point diameter. 92
Figure 3-11: Effect of user implementation of dendritic spine seed point on spine head diameter 95
Figure 3-12: Effect of individual user setting of seed points. 98
Figure 3-13: Improvements of neck fitting in Imaris 7.2.0 with the *Shortest Distance* to map option. 99
Figure 3-14: Improvements necessary with *Approximate Circle* algorithm. 101
Figure 3-15: Cross-comparison of the effect of the analytical method on the size, density and distribution of spine head size. 102
Figure 3-16: Comparison of the two spine fitting algorithm from *Filament Tracer*..... 104
Figure 3-17: Correlation between spine length and spine head diameter between different categories of spines identified visually..... 106
Figure 3-18: Correlation of spine length to spine head size for the sub-group for which spine minimum diameter is equal to spine head size. 107
Figure 3-19: Distribution of spine neck length to spine head diameter ratio for thin and mushroom spines. 109
Figure 3-20: Flowchart of spine sorting using *Filament Tracer* and Matlab data analysis. 110
Figure 4-1: Density of spines in vehicle or DMSO treated CA1 pyramidal neurones. .. 117
Figure 4-2: Cumulative distribution of spine head diameter and spine length in vehicle or DMSO treated slices, on non-stubby spines. 120
Figure 4-3: CA1 pyramidal cells of the hippocampus receiving 3 types of excitatory inputs..... 122
Figure 4-4: Density and representation of spine types in CA1 hippocampal neurones of organotypic slices at 14 DIV. 123

Figure 4-5: Spine head diameter of dendritic spines in apical versus basal dendrites. 125
Figure 4-6: Spine length of dendritic spines in apical versus basal dendrites. 127
Figure 4-7: 3D isosurface reconstruction of a section of CA1 dendrite (red) showing a contact between a spine and a DiO labelled axons from a CA3 cell (green). 128
Figure 4-8: Percentage of each spine type taken from the overall sample of spines available for either the overall population, or only receiving input from the Schaffer collaterals (SC). 129
Figure 4-9: Spine head diameter of headed dendritic spines receiving any presynaptic input (apical & basal) or Schaffer collateral only (SC). 130
Figure 4-10: Spine length of dendritic spines receiving any presynaptic input (overall) or Schaffer collateral only (SC). 132
Figure 4-11: Structural organisation and branching of a CA1 pyramidal neurone. 134
Figure 4-12: Density of dendritic spines and percentage of spine type in the different branches of apical dendrites. 135
Figure 4-13: Spine head diameter of spines according to their branching order in apical dendrites. 136
Figure 4-14: Spine length of spines according to their branching order in apical dendrites. 137
Figure 5-1: Scheme of treatment on rat hippocampal organotypic slices. 144
Figure 5-2: Sample trace from mEPSCs recording on CA1 cells in rat organotypic slices of 13-15 DIV. 145
Figure 5-3: Mean rise and decay time of mEPSCs recorded in 14DIV rat CA1 cells. 147
Figure 5-4: Amplitude and frequency of mEPSCs recorded from CA1 of rat 14 DIV organotypic cultures. 148
Figure 5-5: Scheme of experiments carried out in mice organotypic cultures, for recording mEPSCs at 6-9 DIV. 150
Figure 5-6: Sample trace from mEPSCs recording on CA1 cells in mouse organotypic slices of 6-9 DIV..... 151
Figure 5-7: Rise and decay time of miniature excitatory synaptic currents in CA1 pyramidal cells of mice organotypic slices, 6-9 DIV..... 152
Figure 5-8: Amplitude and frequency of mEPSCs recorded from CA1 pyramidal cells of mice organotypic cultures at 6-9 DIV 153

Figure 6-1: Image and Filament fit of CA1 dendritic spine at 7, 14 and 21 DIV. 158
Figure 6-2: Spine density of pyramidal CA1 cells in hippocampal organotypic slices, analysed with Imaris 3D reconstruction. 159
Figure 6-3: Density of spines from apical *vs* basal dendrites. 160
Figure 6-4: Representation of the different spine types automatically identified with Imaris at 7, 14 and 21 DIV. 162
Figure 6-5: Deafferentation of CA1 cells in organotypic slices. 164
Figure 6-6: Effect of partial deafferentation to CA1 pyramidal cells spine density at 14 DIV. 165
Figure 6-7: Effect of deafferentation on spine head size at 14 DIV. 167
Figure 6-8: Effect of deafferentation on spine length at 14 DIV. 169
Figure 6-9: Effect of deafferentation for 7 days on CA1 pyramidal cells at 21 DIV. 171
Figure 6-10: Density of spines at 21 DIV following a week of deafferentation. 172
Figure 6-11: Effect of deafferentation at 21 DIV on stubby spine percentage, on the whole cell or selectively in the apical or basal dendrites. 174
Figure 6-12: Effect of deafferentation on spine head size after deafferentation, on 21 DIV pyramidal cells..... 176
Figure 6-13: Effect of deafferentation on spine length at 21 DIV. 177
Figure 6-14: Summary of the effect of deafferentation on spine density. 179
Figure 6-15: Summary of the effect of deafferentation on spine head size. 180
Figure 7-1: Deconvolved images of segments of CA1 dendrites in 14 DIV organotypic slices, filled with Alexa 594 and imaged with confocal microscopy. 183
Figure 7-2: Density of dendritic spines following the 7 days treatment, in either apical, basal or overall. 185
Figure 7-3: Density of spine in apical dendrites according to the degree of branching of the parent dendrite, in either control or KN62 treated CA1 cells. 186
Figure 7-4: Effect of prolonged alteration of plasticity on the density of the different spine types..... 188
Figure 7-5: Effect of prolonged plasticity alteration on the representation of stubby and headed spines in the dendritic spine population. 190
Figure 7-6: Distribution of spine head diameters in apical and basal dendrites of CA1 neurones in the three conditions tested. 191

Figure 7-7: Distribution of spine length on apical and basal dendrites of CA1 neurones after 7 days treatments with plasticity blocker. 193
Figure 7-8: Confocal images and Imaris *Filament Tracer* reconstruction of CA1 apical dendrites innervated by DiO labelled CA3 axons 195
Figure 7-9: Percentage of spine types in the pooled population of spines, receiving input from either any presynaptic cell or specifically from CA3. 196
Figure 7-10: Percentage of the different spine type. 197
Figure 7-11: CaMKII inhibition prevents the difference of spine head size between apical and basal dendrites. 201

Discussion

Figure 8-1: Schematic representation of the putative role of local and global plasticity, regulating synapses in both activity-dependent and homeostatic manners. 218

List of Tables

Table 2-1: Excitation and emission wavelengths of the fluorescent probes used in this work. 65
Table 3-1: Sample of definitions of spine types from the literature. 76
Table 3-2: Identification of stubby spines visually and following Imaris parameters… 108

Abbreviations

AC	*Approximate Circle* algorithm (Imaris *Filament Tracer*)
ACSF	Artificial cerebrospinal fluid
APV	(-)-2-Amino-5-phosphonopentanoic acid
AMPA	α-amino-3-hydroxy-5-methylisoxazolepropionate acid
BDNF	Brain-derived neurotrophic factor
CA	*Corpus Ammonis*
CaMKII	Ca^{2+}/calmodulin-dependent kinase II
cAMP	Cyclic adenosine mono-phosphate
CNQX	6-Cyano-7-nitroquinoxaline-2,3-dion
CREB	cAMP response element-binding
DIV	Days *in vitro*
DMSO	Dimethyl sulfoxide
F-actin	Actin filament
FBS	Fetal bovine serum
GABA	γ-aminobutyric acid
GFP	Green fluorescent protein
LTP	Long-term potentiation
LTD	Long-term depression
HEPES	4-(2-Hydroxyethyl)piperazine-1-ethanesulfonic acid
mEPSC	Miniature excitatory postsynaptic current
mGluR	Metabotropic glutamate receptor
mIPSC	Miniature inhibitory postsynaptic current
NMDA	*N*-methyl-D-aspartate

PBS	Phosphate buffer saline
PKA	cAMP-dependent protein kinase A
PSD	Postsynaptic density
Rp-cAMP	Rp-8-Br-cAMP
SC	Schaffer collateral
SD	*Shortest Distance* algorithm (Imaris *Filament Tracer*)
SEM	Standard error of the means
TTX	Tetrodotoxin

Chapter 1. Introduction

1.1 General introduction

The hippocampus has long been linked with learning and memory (Scoville and Milner, 1957, for review see Andersen et al, 2007), and thus has attracted a lot of attention from scientists, with more than 100,000 publications on PubMed. Activity-dependent synaptic plasticity shapes the connectivity of the network by selectively modulating synaptic strength (reviewed in Cooke and Bliss, 2006) or by formation or deletion of synapses (Engert and Bonhoeffer, 1999; Nägerl et al., 2004). In parallel, compensatory mechanisms, called homeostatic plasticity, aim to maintain cellular excitability and network efficiency: they drive synaptic changes in the direction needed to avoid wind-up or silencing of the network (reviewed in Turrigiano, 2008 and Pozo and Goda, 2010). Previous experiments in the Edwards lab revealed that organotypic and acute slices have similar distribution of dendritic spine types (De Simoni et al., 2003). However, though the overall spine population is the same, some pathway specificity was observed: the most active pathway in the preparation, i.e. the Schaffer collateral in organotypic slices or the entorhinal cortex *in vivo*, impinge on larger spines in CA1 pyramidal neurones (Megias et al., 2001; De Simoni and Edwards, 2006; Nicholson et al., 2006). In organotypic slices, the other afferent pathways to those neurones impinge on smaller spines (De Simoni and Edwards, 2006), revealing the existence of homeostatic plasticity responding to activity-dependent activity in a pathway-dependent manner.

Studying how neurones respond to long-term modification of their inputs, either locally or globally, is important for the understanding of the maintenance of neuronal excitability and network stability. The very tight correlation between dendritic spine head size and synaptic strength in pyramidal cells of the hippocampus enables study of global and local changes of synaptic strength via the evolution of the dendritic spine population (Matsuzaki, 2007; Kasai et al., 2010). Organotypic slices were used here as a model to study the balance between activity-dependent dendritic spine organisation

and pathway specific homeostatic plasticity in CA1 pyramidal neurones of the developing hippocampus.

Using principally imaging to study excitatory synaptic transmission requires reliable methods to optically characterise dendritic spines. A large part of my work consisted in evaluating the tools available for such a task, questioning previous analytical methods and optimising a new method based on the recently available image analysis software, *Filament Tracer* from Bitplane, in order to ensure the least biased and most accurate measurements, while keeping in mind the limitation of this technique.

The new method for dendritic spine analysis gave access to several more parameters than were available with the method originally used in the lab, such as spine length and spine head diameter or volume, which reflect dendritic spine plastic properties.

Starting with the characterisation of dendritic spines both globally and locally on CA1 pyramidal neurones of organotypic cultures, the work moved on to the study of adaptive changes following chronic perturbation of the network activity.

During a stay in the Malinow lab at UCSD, I was aiming at silencing individual neurones by expressing the inward rectifier Kir2.1 channel, and comparing synaptic transmission in individually silenced cells to control cells in organotypic slices, *in vivo* and in GluA1 knock-out mouse, where the abolition of GluA1 was expected to occlude the effect of silencing. The project could not be successfully carried out during my stay there, but in parallel I studied the driving factor of synaptic connectivity in the developing hippocampal slices, testing whether blocking activity during development induced a lack of activity-driven synaptic strengthening or on the contrary synaptic scaling. Age and preparation dependence of the activity-driven *vs* homeostatic plasticity dominance led to further investigation of those mechanisms at two ages during development, by inducing a strong remodelling of CA1 pyramidal cells with a transection of the Schaffer collateral input. A more subtle approach was used to test the activity-dependence of pathway specificity, by blocking fundamental intermediates of synaptic plasticity. Preventing activity-dependent plasticity with the CaMKII antagonist abolished the pathway specificity observed.

The results here suggest that activity drives the synaptic strength at the most active pathways, and homeostatic compensation ensures the balance of total synaptic weight, in an age-dependent manner. Moreover, pathway specificity also corroborates the theory that there is an intermediate unit for plasticity and homeostatic plasticity, the dendritic branch fitting that role. Understanding the level and conditions for homeostatic plasticity to occur would enable different approaches for the treatment of many diseases such as epilepsy or AD.

1.2 Function and structure of the hippocampus

1.2.1 Role of the hippocampus in learning & memory

Historically, the hippocampus was considered, like the limbic system, as the centre of emotion. Around 1900, it was linked with memory by the Russian scientist Vladimir Bekhterev (see *The Hippocampus Book*, Andersen et al., 2007). More recently, the hippocampus has been linked with the laying down of new memories, as well as with the retrieval of older ones (Scoville and Milner, 1957). Following bilateral resection of the medial temporal lobe in order to treat severe epilepsy, the most famous patient H.M. was left with no short term memory (anterograde amnesia) and a loss of memory of recent events (retrograde amnesia), after the surgery which damaged part of his hippocampus. The retrograde amnesia of patients with lesions in the hippocampus is more severe for more recent events (Rempel-Clower et al., 1996). This suggests that older memories become less dependent upon the hippocampus with time, forming a more permanent memory in another part of the brain, probably the neocortex, which is many fold bigger than the hippocampus (Squire et al., 2004). Learning and memory require a permanent synaptic change at the final storage location, while in the hippocampus, which could be assimilated as a processing unit, bidirectional plasticity is essential to maintain on going function and avoid “saturation” of the network (Neves et al., 2008). In its role of temporary memory storage, the hippocampus is continually laying down, transferring or deleting memories throughout life. Considering this constant changing of synaptic strength, the network requires synaptic readjustment to

maintain a functional window of activity, which translates into homeostatic modulation of dendritic spine morphology and distribution.

1.2.2 Structure and connectivity

The hippocampus is deeply embedded in the brain and is connected to several other brain regions in both hemispheres. Figure 1-1 (Neves et al., 2008) is a scheme of the hippocampus, its position in the brain and its connectivity with other brain structures. The hippocampus receives inhibitory fibres from the contra-lateral side via the associational/commissural fibres, as well as modulatory input from the hypothalamus, and the septal nucleus median and nucleus of the diagonal band of Broca by the fimbria/fornix. During the transversal slicing of the hippocampus, the commissural fibres connections are lost, but the trisynaptic loop, which connects the hippocampus to and from the entorhinal cortex, is well preserved. The dentate gyrus receives inputs from the layer II of the entorhinal cortex (red line) and impinges on the *Cornu Ammonis* 3 (CA3) cells via the perforant path (orange line). Output from CA3 is conveyed via axons towards the proximal apical CA1 dendrites via the Schaffer collateral (blue line). Axons from CA1 neurones innervate mainly layer V of the entorhinal cortex. CA1 pyramidal cells are very interesting regarding homeostasis because they receive inputs from three main excitatory routes: from the CA3 region via the Schaffer collateral; from layer III of the entorhinal cortex (brown line) via the temporoammonic pathway; and from neighbouring CA1 cells (green line). They represent an important centre of integration of the activity occurring in the neighbouring areas and, as such, offer many possibilities to study homeostasis. To ensure efficiency and survival of neuronal cells and to prevent excessive firing or silencing, an important homeostatic mechanism maintains electrical excitation within physiological range, the result of a fine tuning of excitation and inhibition.

The hippocampal cell structures are highly organised, and the network is very dense and highly connected. Previous studies identified patterns of connectivity in the whole hippocampus. The temporoammonic pathway from the entorhinal cortex selectively

innervates the distal apical dendrites of CA1, in the *stratum lacunosum moleculare* (Blackstad, 1958). CA1 to CA1 connections have a very low occurrence in acute slices, less than 1% (Deuchars and Thomson, 1996), except in slices prepared from developing brain (Anikszteijn et al., 2001). The proportion of CA1-CA1 connections might be more important *in vivo*. They occur exclusively in the basal dendrites, the CA1 axons never entering the *stratum radiatum* (Ishizuka et al., 1995).

The Schaffer collateral pathway forms synapses on both apical dendrites in the *stratum radiatum* and basal dendrites in the *stratum oriens* (Blackstad, 1958). About 20% of CA3 cells make multiple synapses on a single CA1 cell (Sorra and Harris, 1993). In organotypic slices, the temporoammonic pathway makes more connections per axons with the CA1 cells than the Schaffer collateral (De Simoni and Edwards, 2006).

The synaptic attenuation induced by the structure of the dendritic tree in CA1 pyramidal cells (Jaffe and Carnevale, 1999) is compensated by an increased synaptic conductance the further away from the soma the synapse is situated (Magee and Cook, 2000), partly due to an increasing number of enlarged synapses (Nicholson et al., 2006).

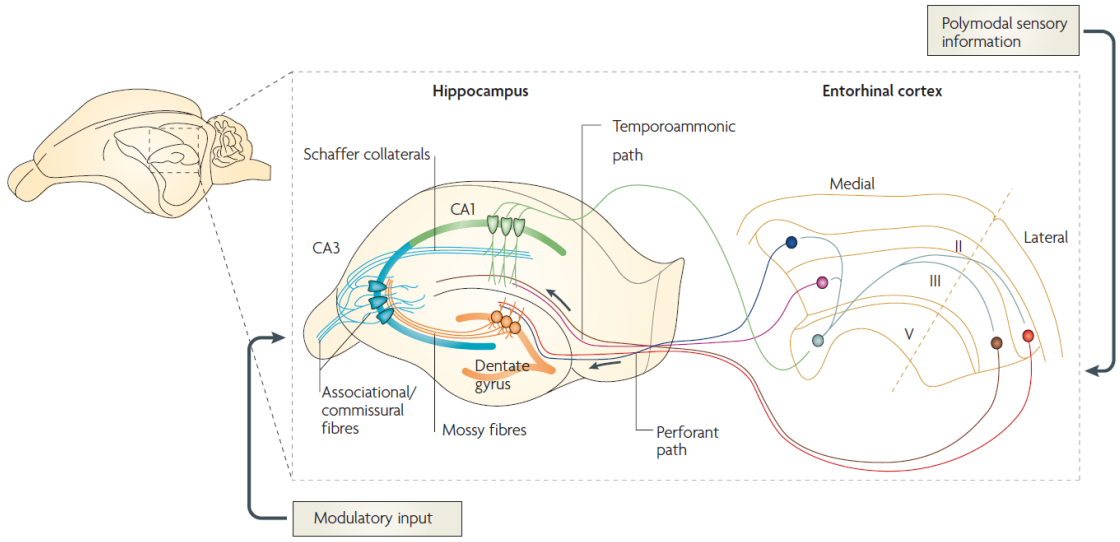

Figure 1-1: Schema of the hippocampus circuitry

Showing the trisynaptic loop from and to the entorhinal cortex (EC) as well as the three different inputs impinging on CA1 cells: the Schaffer collateral from CA3 cells (blue), the temporoammonic from the third layer of the entorhinal cortex (brown), and neighbouring CA1 axons (green), (Neves et al., 2008).

In epileptic patients, frequent seizures submit cells to excessive activity. The consequences are direct perturbation of synaptic plasticity (Wong, 2005), leading to the recognised symptoms of cognitive deficits, memory impairments and learning disabilities (Williams, 2003; Elger et al., 2004), as well as a variety of dendritic abnormalities, mainly loss of dendritic spines (Swann et al., 2000).

1.2.3 Hippocampal organotypic slices

Studying network connectivity over the course of several days requires a model both preserving the original brain structure as much as possible and that can be kept long enough to study long-term changes. Hippocampal organotypic cultures regroup both these criteria, and therefore present many advantages to the study of homeostatic mechanisms.

Acute and organotypic hippocampal slices may present some differences regarding connectivity, density of cells, and survival rate of different cell types. Transverse slices of hippocampus preserve the trisynaptic pathway, i.e. the main excitatory loop described in figure 1-1. The output of the hippocampal circuit is fine-tuned along the loop by inhibitory interneurones releasing γ-aminobutyric acid (GABA) (reviewed in Freund and Buzsáki, 1996). In hippocampal organotypic slices, the laminar structure, morphological features of dendrites as well as receptor expression are well-preserved and very similar to acute slices of similar age (Frotscher and Heimrich, 1995; Gahwiler et al., 1997; Holopainen and Lauren, 2003; De Simoni et al., 2003).

Organotypic hippocampal slices are more inter-connected than acute slices of equivalent age, possibly because of the limited number of cells present in a slice compared to the whole hippocampus. The balance between the different inputs on CA1 pyramidal cells may differ in organotypic cultures from *in vivo* because the slicing may not affect similarly all pathways. For instance, original CA1-CA1 connections are probably lost during the slicing, since most CA1 axons cannot be followed in acute slices (personal observation), while CA3-CA1 connections are very well preserved.

The research described here is supported by previous data gained in the Edwards lab about the development of organotypic slices compared to acute slices. A paper published in 2003 (De Simoni et al., 2003) compares several criteria such as complexity of branching, percentage of spine types, miniature excitatory postsynaptic (mEPSCs) and inhibitory currents (mIPSCs) amplitudes and frequencies. The study showed surprisingly that organotypic slices, although expressing a more complex dendritic tree and thereby expressing an increased mEPSCs frequency, develop very similarly to acute slices regarding synaptic transmission and dendritic morphology (De Simoni et al., 2003). The synaptic development of CA1 neurones in organotypic slices is thus comparable with the one occurring in living animals, housed in a standard (non-enriched) environment.

1.3 Synapses and synaptic transmission

Synaptic transmission in the central nervous system can be either excitatory or inhibitory. In this section, both pre- and postsynaptic sites of the synapse will be described. In the later part of the work, the description will focus more specifically on the dendritic spines, which represent the postsynaptic sites of most excitatory connections in CA1 cells of the hippocampus, and constitute the principal object of investigation in this work.

1.3.1 Synapse formation and maturation

Ramón y Cajal observed at the end of the 19th century that density of dendritic spines in pyramidal neurones was higher at some early stages during development than during adulthood (Ramón y Cajal, 1899). Those early observations were confirmed many years later by several groups, showing an initial proliferation of spines, followed by a selective decrease in spines (Miller and Peters, 1981; Rakic et al., 1986). Interestingly, dendritic spines can develop with very little environmental influences, like in the brain of guinea pigs during prenatal days (Yuste and Bonhoeffer, 2004), or in the cerebellum, where parallel fibre spines on Purkinje cells seem to be able to develop independently of incoming axons (Sotelo, 1978).

In mouse and rat, which are born with relatively immature brain (Yuste and Bonhoeffer, 2004), spinogenesis and synaptogenesis in the forebrain seems to rely on more complex interactions between autonomous and external factors (Miller and Peters, 1981; Katz and Shatz, 1996).

The elongated and highly motile dendritic filopodia, which are only present in younger tissues, are one of the proposed models for spinogenesis and subsequent synaptogenesis on CA1 pyramidal neurones (Ziv and Smith, 1996; Fiala et al., 1998), but other models propose very early development of synapses from dendritic shafts or stubby protrusions (Miller and Peters, 1981; Pokorny and Yamamoto, 1981).

The majority of dendritic spines (~96%) were shown to make synaptic contacts in the mouse adult neocortex (Arellano et al., 2007b). Excitatory synapses were identified with electron microscopy by the presynaptic presence of an active zone with glutamate-containing vesicles and a postsynaptic electron-dense, protein-rich thickening on the cytoplasmic surface, the postsynaptic density (PSD) (Harris et al., 1992). The pre- and postsynaptic membranes are separated by the 20 nm wide synaptic cleft, which represents a very small gap extending over a large area. This allows the concentration of neurotransmitter to increase very rapidly upon vesicular release and decrease quickly by diffusion (Isaacson and Nicoll, 1993; Savtchenko and Rusakov, 2007), thus optimising synaptic transmission while reducing neurotoxicity.

1.3.2 Dendritic spines and the synaptic machinery

Dendritic spines, the major postsynaptic sites of excitatory connections in the brain, play a major role in synaptic plasticity. Abnormalities in spine density, length or stability are observed in neurological diseases such as Alzheimer's disease (Knobloch and Mansuy, 2008; Knafo et al., 2009; Smith et al., 2009) or fragile X syndrome (Comery et al., 1997; Irwin et al., 2000; Cruz-Martin et al., 2010). Dendritic spines are fundamental units in the synaptic transmission machinery of most excitatory synapses within the forebrain.

In the hippocampus, dendritic protrusions are typically less than 3 µm in length and 1 µm in diameter and cover the largest part of dendrites in pyramidal neurones. Their size, shape and number vary greatly depending on age, cell type, location and previous activity undergone. The two main characteristics of dendritic spine morphologies, their head and neck, led to their classification in three major categories: stubby spines, which are typified by a protrusion with no constriction to the parent dendrite; thin spines, which have a long and narrow neck followed by a small head; mushroom spines, which have a short neck and a large head. In rat hippocampal neurones, more than 65% of spines are thins, while mushrooms account for less than 25% (Harris et al., 1992). The headless filopodia disappear with age, while the stubby spines, predominant at early ages, decrease significantly but are still present in adult cortices (Benavides-Piccione et al., 2002). However, the classification of dendritic spines in such types, which usually follows the descriptions set in one of Kristen Harris' early papers, leaves almost a third of the spines studied with electron microscopy not classified because of ambiguity (Harris et al., 1992). Some authors have tried to apply exclusive criteria, which lead to neat classification on paper (e.g. Oray et al., 2006) but those are generally less relevant physiologically. It is not fully established whether dendritic spines are really represented by three different and clearly identifiable types, each of them reflecting a specific functional state or if rather there is a continuum between them, guided by development and plasticity. This question will be studied both from the literature in section 1.5.2, and from an experimental point of view in Chapter 3.

On all types of spines, the pre- and postsynaptic densities contain hundreds of proteins involved in a multitude of biochemical pathways. Presynaptically, the docking and release of the neurotransmitter follows calcium entry via activation of voltage gated channels (Katz and Miledi, 1967) and Ca^{2+}-induced Ca^{2+} release from internal stores (Emptage et al., 2001). To detect glutamate release, the postsynaptic density is enriched with glutamate-binding receptors: N-Methyl-D-Aspartate (NMDA), α-amino-3-hydroxy-5-methyl-4-isoxazolepropionic acid (AMPA), kainate and metabotropic glutamate (mGlu) receptors.

The main type of receptors involved in ionotropic fast synaptic transmission at membrane resting potential is AMPA receptors. AMPA receptors are heterotetramers of GluA1-4 subunits (Hollmann and Heinemann, 1994), which are mainly permeable to monovalent cations Na^+ and K^+ . Also, their subunit composition can modify Ca^{2+} permeability, GluA2-containing receptors being Ca^{2+} impermeable (Hollmann et al., 1991). However, not all dendritic spines contain AMPA receptors, giving rise to so-called silent synapses, which contain NMDA but no AMPA receptors. Silent synapses are found in the young brain but progressively disappear and could underlie the maturation of the synaptic network (reviewed in Kerchner and Nicoll, 2008).

NMDA receptors, heterotetramers composed of NR1 and NR2A-D or NR3 subunits, are always present at the PSD of synapses, whether active or silent (Takumi et al., 1999). They are highly permeable to Ca^{2+} ions, but are blocked by Mg^{2+} at resting membrane potentials. Depolarisation of the postsynaptic membrane is thus needed for the removal of the Mg^{2+} block on NMDA receptors, while glutamate binding is necessary for the opening of the channel and Ca^{2+} influx. NMDA receptors are ideal sensors of coincident pre- and postsynaptic activity at dendritic spines synapses (Yuste and Denk, 1995; Yuste et al., 1999).

NMDA and AMPA receptors subunit compositions and number at the synapses can be modulated by synaptic activity, as will be discussed in the next section (for reviews see Malinow and Malenka, 2002; Perez-Otano and Ehlers, 2005).

The major cytoskeletal component of dendritic spines is composed of a network of short and long branches of actin filaments, localised under the PSD in the spine head (Landis and Reese, 1983). Actin plays a fundamental role in the stabilisation of postsynaptic proteins (Renner et al., 2009) and in the modulation of spine head morphology following NMDA and AMPA receptor-mediated activity (Fischer et al., 2000; Okamoto et al., 2004). Actin filaments (F-actin) reorganise rapidly following plasticity inducing signals, relying on different pools of F-actin which help to support dendritic spine enlargement (Honkura et al., 2008). In the same paper, the enlargement was maintained in time only when the pool of F-actin was physically

isolated from the dendrite by the presence of a neck, emphasising the role of spine morphology on plasticity. Moreover, F-actin is tightly regulated by a key protein involved in plasticity, Ca^{2+}/calmodulin-dependent protein kinase II (CaMKII), which is involved in the regulation of many proteins important for the maintenance of activity-dependent synaptic changes (called plasticity related protein). Thus F-actin could be used as a synaptic tag, its upregulation tightly following the activation of CaMKII specifically at activated synapses (Okamoto et al., 2007).

Synapses are highly dynamics structures which can be modified in an activity-dependent manner, suggesting that synaptic plasticity could be a molecular correlate of learning and memory (Martin et al., 2000). The next section describes some of the different forms of synaptic plasticity that occurs in CA1 pyramidal neurones of the hippocampus, whether they are rapid input-specific activity-dependent modifications of synaptic strength or the result of homeostatic changes aimed at maintaining the cellular excitability within physiological limits.

1.4 Synaptic plasticity of CA1 pyramidal neurones

The mechanisms behind activity-dependent synaptic plasticity have long been investigated because of their potential role in learning and memory. I briefly review here the different steps of those long-term synaptic changes with a particular focus on CA3-CA1 synapses: induction, expression, persistence and functions, before reviewing some characteristics of their physiological counterpart, homeostatic synaptic plasticity, which corresponds to synaptic strength adaptation to long-term changes of activity detection.

1.4.1 Activity-dependent plasticity

1.4.1.1 Long-term potentiation and long-term depression

Since its discovery by Bliss & Lømo in 1973, long-term potentiation (LTP) has received a lot of interest because of its putative role in the formation of memory (Morris et al., 1990; Kandel, 2001; Tonegawa et al., 2003). Its counterpart, long-term depression

(LTD), which shares some mechanisms with LTP, has been implicated more recently for learning and memory in the hippocampus (Kemp and Manahan-Vaughan, 2004; Etkin et al., 2006). The property of synapses to undergo both types of plasticity is essential to enable the brain to store vast amounts of information. Bidirectional plasticity enables the network to increase many fold its computing power/processing ability (Bliss and Collingridge, 1993; Malenka and Bear, 2004).

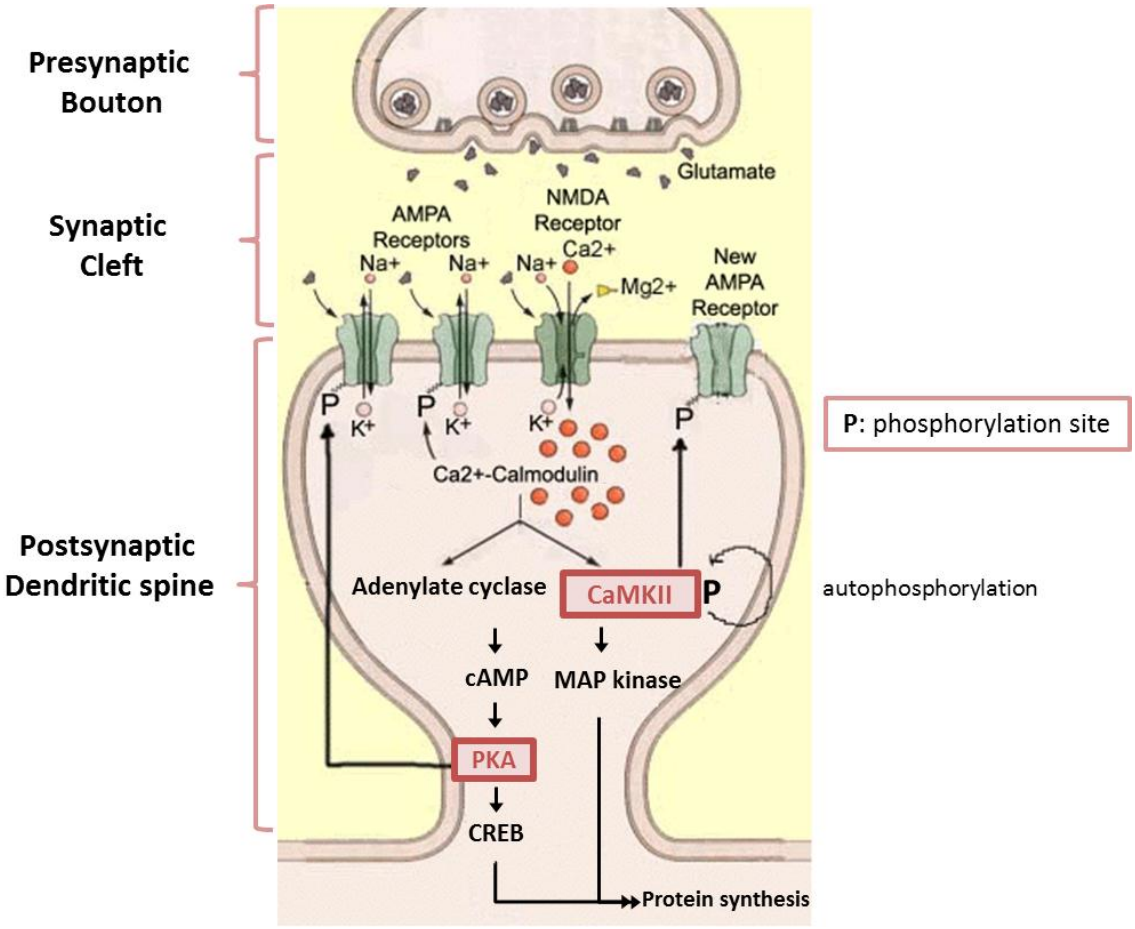

Figure 1-2: Schematic representation of an excitatory synapse showing the major postsynaptic cascades involved in LTP.

The presynaptic terminal releases vesicular glutamate into the synaptic cleft following depolarisation of the afferent axon by an action potential. If coincident with postsynaptic depolarisation, the block of NMDA receptors is lifted, allowing Ca2+ to enter the postsynaptic dendritic spine head, and activate the two main cascades necessary for LTP: via Ca2+/calmodulin kinase II and cAMP/PKA (adapted from http://thebrain.mcgill.ca/flash/a/a_07/a_07_m/a_07_m_tra/a_07_m_tra.html, retrieved 2011).

1.4.1.1.1 Induction mechanisms

LTP can be induced by many conditioning paradigms, usually consisting of high-frequency stimulation (HFS) (Bliss and Collingridge, 1993; Liao et al., 1995). LTD is induced by repetitive low-frequency stimulation (LFS) (Dudek and Bear, 1992). At intermediate frequencies, the effect of stimulation of the axon bundles depends on the previous activity encountered by the synapses, which might have modified the threshold for synaptic plasticity: a phenomenon called metaplasticity. The Bienstock – Cooper – Munro (BCM) theory states that there is a sliding threshold for LTP/LTD induction (Bienenstock et al., 1982; Mayford et al., 1995). Following that rule, LTP is more difficult to induce in pathways which previously received LTP-inducing stimulation. Similarly, impaired spatial learning was observed in rats after saturation of LTP (Moser et al., 1998), suggesting that LTP mimics and can occlude spatial learning.

These features are important for the hippocampus, which is believe to be a place for temporary storage of information and needs to avoid saturation to remain functional. The newly expressed LTP needs time to be consolidated, and is vulnerable to depotentiation by LFS in the 5 minutes following induction (Lynch et al., 2007).

Bidirectional synaptic plasticity is thought to be an essential part for information storage (Bear, 2003). LTP and LTD are not mirrors of each other, and the phosphorylation of distinct AMPA receptor sites on GluA1 at Ser 845 and Ser 831 could explain the dissymmetric bidirectionality of plasticity (Lee et al., 2000). However, contrary to previous speculation about the “forgetting” role of LTD in a model where LTP would be the “learning” mechanism, LTD is now recognised as an encoding mechanism as well (Kemp and Manahan-Vaughan, 2004), which would have to be balanced by reversed changes such as LTP to avoid learning and memory impairments (Parsley et al., 2007). LTP itself can be reversed by several other mechanisms mechanistically distinct from LTD, such as depotentiation, de-depression, run down or active decay (Villarreal et al., 2002; reviewed in Kemp and Manahan-Vaughan, 2007).

The special properties that make LTP and LTD good candidates for learning and memory are their associativity, cooperativity, input specificity and longevity (Cooke and Bliss, 2006).

At CA3-CA1 synapses, both LTP and LTD induction is typically dependent on NMDA receptor activation, which requires postsynaptic depolarisation to relieve the Mg^{2+} block (Cull-Candy et al, 2001). Thus LTP at CA3-CA1 synapses corresponds to Hebbian plasticity, where coincident pre-and postsynaptic activity leads to the strengthening of the synapses (Hebb, 1949). NMDA receptors activation induces an elevation of Ca^{2+} concentration which triggers several Ca^{2+}-dependent cascades (Lynch et al., 1983; Malenka et al., 1992). The concentration of Ca^{2+} is essential for the initial phase of synaptic plasticity, as low concentration leads to LTD while high concentration activates several pathways leading to synaptic potentiation (Dudek and Bear, 1993). Postsynaptically (figure 1-2), two main cascades are activated by the Ca^{2+} rise, involving Ca^{2+}/calmodulin protein kinase II (CaMKII) (Lisman et al., 2002) and the 3'-5'-cyclic adenosine monophosphate/ protein kinase A (cAMP/PKA) pathway (Abel and Nguyen, 2008).

LTP-inducing stimuli can activate several cascades the importance of which varies during development. PKA, which is activated by cAMP, seems to be necessary to induce LTP in younger tissues (before postnatal day 9 [P9]) (Yasuda et al., 2003; Esteban et al., 2003), while CaMKII becomes a fundamental mediator of LTP as neurones mature (reviewed in Lisman et al., 2002). CaMKII, via its Ca^{2+}/calmodulin activation, is one of the major Ca^{2+} sensor postsynaptically, and thus a good candidate as a signalling integrator of synaptic plasticity (Xia and Storm, 2005). In mature CA1 neurones, the activation of the cAMP pathway is important for the late phase of LTP, as it triggers protein synthesis necessary for the structural maintenance of LTP via the phosphorylation of cAMP response element-binding (CREB) by PKA (Matsushita et al., 2001; Ahmed and Frey, 2005).

1.4.1.1.2 Expression mechanisms

The transmission efficacy of an excitatory synapse can be measured by its ability to transmit the presynaptic signal at resting membrane potential. The main fast ionotropic receptor at excitatory synapses which can open at resting potential is the AMPA receptor, and thus their presence and density at the PSD plays a fundamental

role for synaptic transmission and plasticity. Changes in synaptic efficacy following LTP/LTD can be expressed both pre- and postsynaptically.

Following LTP, the observed potentiation and decrease in failures of synaptic transmission (Malinow and Tsien, 1990) can result from two main phenomena:

1) *postsynaptic*: insertion of AMPA receptors at the PSD, usually containing GluA1 subunits (Hayashi et al., 2000; Shi et al., 2001; Makino and Malinow, 2009), thus increasing transmission or unsilencing synapses (Kullmann, 1994; Isaac et al., 1995).

2) *presynaptic*: increase in release probability (Emptage et al., 1999; Emptage et al., 2003; Enoki et al., 2009), possibly involving diffusible molecules such as BDNF, nitric oxide or endocannabinoids (Wilson and Nicoll, 2001; Tao and Poo, 2001) or *trans*-synaptic signalling through cell adhesion proteins such as neuroligin and N-cadherin/β-catenin (Chavis and Westbrook, 2001; Gottmann, 2008).

Reciprocally, the decrease in synaptic transmission in LTD is expressed postsynaptically by the removal of AMPA receptors from the PSD (Carroll et al., 1999; Beattie et al., 2000; Man et al., 2007), and by presynaptic changes such as a decrease in the size of the readily releasable pool (Goda and Stevens, 1998) or decrease in synaptic contacts (Becker et al., 2008).

1.4.1.1.3 Persistence mechanisms

LTP can be divided into two mechanistically different phases: the “early-phase”, which is the increased synaptic transmission that immediately follows LTP-induction stimulus, lasts for about an hour and is protein-synthesis independent; and the “late-phase”, which can last from hours *in vitro* and weeks or months *in vivo* and relies on protein synthesis (Abraham and Williams, 2003; Raymond, 2007). New protein synthesis can rely on local messenger RNA (mRNA) pre-existing in the dendrite, and is thus independent from gene transcription (Kelleher, III et al., 2004). Protein synthesis-dependent LTP has been shown to occur in dendrites physically isolated from the soma (Cracco et al., 2005), and local protein synthesis inhibition in apical or basal dendrites impaired LTP only in the inhibited region without affecting other regions (Bradshaw et al., 2003), emphasising the role of local protein synthesis for late LTP and its independence from nuclear gene transcription.

The gene-transcription-dependent phase of LTP relies on the phosphorylation of CREB (Montminy, 1997). Following stimulation-induced increase in cAMP, PKA translocates to the nucleus where it can phosphorylate CREB at Ser 133 (Bacskai et al., 1993), thus initiating the transcription of CRE-associated genes (Yamamoto et al., 1988). Other signalling cascades are thought to be involved in late LTP, such as CaMKIV and MAPK, which can also activate CREB and other immediate early genes (Abraham and Williams, 2003). Ca^{2+} and calmodulin also plays an important role in the activation of the brain derived neurotrophic factor (BDNF)-induced protein synthesis and neuroplasticity (Zhou et al., 2010).

1.4.1.1.4 LTP and LTD links to learning and memory

Recent evidence from behavioural experiments brings together long-term synaptic changes with learning and memory. A recent review by Kessel and Malinow highlights the latest evidences linking synaptic AMPA receptor plasticity with experience-induced changes in behaviour (Kessels and Malinow, 2009). Learning and memory share several mechanisms with LTP and LTD, like the delivery/removal of AMPA receptors to synapses. For instance, in the rodent barrel cortex, activity-dependent learning induced an LTP-like potentiation *in vivo* (Finnerty et al., 1999; Hardingham et al., 2003) which also requires synaptic delivery of GluA1-containing AMPA receptors (Clem and Barth, 2006; Takahashi et al., 2003). The impairment/rescue of the mechanisms necessary for LTP also impair/rescue learning: Spatial working memory can be partially rescued in GluA1-deficient mice by expressing GluA1 in the deficient mouse hippocampus (Schmitt et al, 2005). Inhibition of protein kinase Mξ *in vivo*, a molecule necessary for maintaining late LTP in hippocampal slices (Serrano et al., 2005), abolished LTP and prevented the retention of 1 day old spatial information. (Pastalkova et al., 2006). These results emphasise the parallel between LTP expression and maintenance and the formation and retention of new memory.

Long-term depression has been viewed as a homeostatic depotentiation mechanism (Bear and Abraham, 1996; Lee et al., 2000), but LTD has also been found to encode different aspects of novelty acquisition (Manahan-Vaughan and Braunewell, 1999; Kemp and Manahan-Vaughan, 2004; Parsley et al., 2007). LTD was also found to be

necessary for long-term spatial learning in rats tested in the Morris water maze, after intrahippocampal injection of a peptide that inhibits AMPA receptor endocytosis prevented learning (Ge et al., 2010).

1.4.1.2 Role of Ca^{2+}/calmodulin kinase II

The putative importance of CaMKII as a molecular switch for bidirectional synaptic plasticity has led to extensive studies, up to the generation of a mouse model with the point mutation T286A in CaMKII which prevents autophosphorylation (Giese et al., 1998). CaMKII is an oligomeric protein kinase present at the postsynaptic density (Braun and Schulman, 1995; Cheng et al., 2006). CaMKII is present in four isoforms (α, β, γ and δ), α and β being both specific to and predominant in the brain (Tobimatsu and Fujisawa, 1989). In the hippocampus, the levels of βCaMKII are already adult-like at P4, while αCaMKII levels, detectable at very low levels before P4 in the CA1 region (Parsley et al., 2007), increase 5-fold between P5 and P16 (Burgin et al., 1990).

CaMKII is one of the main Ca^{2+} sensors at the PSD, and its activation is required for LTP induction in the hippocampus (Otmakhov et al., 1997; Lisman et al., 2002). Inhibition of CaMKII activity in adult neurones almost completely blocks the induction of LTP (Malenka et al., 1989; Malinow et al., 1989). Conversely, injection of constitutively active CaMKII into postsynaptic neurones induced potentiation of the synapses, and occludes further LTP (Lledo et al., 1995), suggesting that CaMKII is both necessary and sufficient to induce LTP (Lisman et al., 2002). Activated upon binding of the Ca^{2+}/calmodulin complex, autophosphorylation of CaMKII at the threonine 286 allows the kinase to remain autonomously active after the decay of the Ca^{2+} transient (Hanson et al., 1989), but this autonomous activity is not required for the expression of LTP (Lengyel et al., 2004). Interestingly, CaMKII seems to be necessary for the induction (early phase) but not for the persistence (late phase) of LTP, since blocking CaMKII after induction has no effect on LTP (Yang et al., 2004). Late-phase LTP may be mediated by protein synthesis pathways involving the phosphorylation of cAMP and PKA (Abel et al., 1997; Bach et al., 1999; Wong et al., 1999).

NMDA receptors are one of the main binding targets of active CaMKII at the PSD (Colbran, 2004), but its affinity for the C-tail of NR2B is much greater than that for

NR2A (Mayadevi et al., 2002). The change in subunit compositions from NR2B to NR2A observed following activity (Barria and Malinow, 2002; Bellone and Nicoll, 2007) or learning (Quinlan et al., 2004) could control synaptic plasticity by regulating binding of activated CaMKII at the PSD (Barria and Malinow, 2005). Active CaMKII is also a determining factor of LTP expression through its direct phosphorylation of GluA1 subunit of AMPA receptors at Ser-831 (Lee et al., 2000), which drives the anchoring of GluA1-containing AMPA receptors at the synapses following their vesicular delivery into the extrasynaptic membrane (Hayashi et al., 2000; Makino and Malinow, 2009).

Like LTP, activation of CaMKII is input-specific. Stimulation of single dendritic spines by glutamate-uncaging induces NMDA receptor and L-type voltage-sensitive Ca^{2+} channel -dependent activation of CaMKII which is restricted to the stimulated spines (Lee et al., 2009). However, the translocation of CaMKII to activated sites was not limited to activated synapses but propagated to the distal dendrite arbour, resulting in an accumulation of CaMKII at neighbouring synapses and providing a molecular mechanism for heterosynaptic plasticity (Rose et al., 2009). Blocking CaMKII with the inhibitor KN62 at Schaffer collateral-CA1 synapses in 7-11 DIV hippocampal organotypic slices completely abolished LTP, as well as the persistent increase in volume generally observed following synaptic potentiation at the stimulated spines (Matsuzaki et al., 2004).

CaMKII is also fundamental for structural plasticity through its binding to F-actin in the dendritic spines (Shen et al., 1998; reviewed in Okamoto et al., 2009). Binding of βCaMKII to F-actin is crucial for dendritic spine morphogenesis and structural stability (Okamoto et al., 2007; Lin and Redmond, 2008). Inhibition of CaMKII blocks the sustained but not the initial enlargement of spines following LTP (Matsuzaki et al., 2004), suggesting that CaMKII is involved in the stabilisation of plastic changes, probably by acting as a molecular tag bound to anchoring proteins at the synapses, thus identifying potentiated ones and consolidating LTP.

1.4.1.3 Role of cAMP-dependent protein kinase

The Ca^{2+} influx in the spine head also activates the cAMP/PKA pathway, which is involved at two different levels of LTP mechanism: 1) during the induction, where PKA

is involved in the phosphorylation of the GluA1 subunit of AMPA receptor at Ser-845 (Esteban et al., 2003), and which might play a role as a switch in synaptic activity depending on the previous history of the synapse (Lee et al., 2000); 2) during the late phase of LTP, where phosphorylation of CREB by PKA induces the transcription of genes necessary for the structural maintenance of LTP (Nguyen and Kandel, 1996; Deisseroth et al., 1996). The critical role of PKA for the gene-dependent expression of LTP has been shown repeatedly (Abel et al., 1997; reviewed in Abel and Nguyen, 2008). The inhibition of PKA activity by delivery of a PKA antagonist to the nucleus abolishes the late-phase of LTP in CA1 pyramidal neurones (Matsushita et al., 2001; Nguyen and Woo, 2003), and inhibition by H89 blocks estradiol-induced formation of new spines (Murphy and Segal, 1997). Phosphorylation of GluA1 at Ser-845 by PKA induces AMPA receptors insertion and reduces their endocytosis (Man et al., 2007), thus strengthening synaptic transmission.

Repeated activation of PKA induced long-lasting enhancement of synaptic transmission (Shinoda et al., 2003; Yamamoto et al., 2005), which was inhibited by PKA antagonists. The reliance on PKA for LTP-induction shows an age-dependent component. In immature synapses, GluA4-containing AMPA receptors, the level of which becomes nearly undetectable by postnatal day 10 [P10], play a critical role in plasticity and are delivered to synapses in an activity and NMDA-dependent manner which does not require CaMKII (Zhu et al., 2000). During those early postnatal days, PKA inhibitors completely block the induction of LTP (Esteban et al., 2003; Yasuda et al., 2003) but, in older animals, they only attenuate the potentiation at Schaffer collateral-CA1 synapses (Skeberdis et al., 2006; Yang et al., 2008). Interestingly, through its interaction with A kinase-anchoring proteins, PKA has been involved in synaptic tagging for L-LTP (Young et al., 2006).

PKA-dependent phosphorylation of proteins, necessary for late LTP, can be reversed by the activation of phosphatases such as calcineurin or its downstream target protein phosphatase 1, which dephosphorylates CREB at Ser-133 (Hagiwara et al., 1992) and is involved in bidirectional synaptic plasticity (Jouvenceau et al., 2006).

1.4.2 Homeostatic synaptic plasticity

Activity-dependent synaptic plasticity, such as LTP and LTD, induces long lasting modifications of synaptic strength and has been linked with learning and memory. Those chronic perturbations of the neuronal activity are, however, compensated by reversed changes in synaptic efficacy, known as homeostatic synaptic plasticity. Those changes are thought to counteract the destabilising effect of activity-dependent plasticity in neuronal networks, and aim at preserving global excitability within physiological limits to maintain information coding capacity.

1.4.2.1 Synaptic scaling

The abilities of neurones to detect activity in neighbouring neurones and to encode new information by synaptic plasticity are essential for the functionality of the network. The global network activity in which neurones are embedded impact on the threshold for synaptic plasticity. In the adult dentate gyrus, neurones born in an epileptic brain show a reduced excitability, receiving less excitatory and more inhibitory inputs (Jakubs et al., 2006). This result points out the adaptive compensatory changes happening at a cellular level in the brain to maintain intrinsic excitability and to promote stability. Failure in this ability to compensate for experience-dependent modulations by homeostatic mechanisms is responsible for common neuropsychiatric disorders (Ramocki and Zoghbi, 2008).

1.4.2.1.1 Scaling of synaptic quantal size

Global scaling of synaptic activity has been first observed following chronic activity perturbation of the network in dissociated neocortical neurones. The silencing of the network by inhibition of sodium channels with tetrodotoxin (TTX) induces a general scaling up of miniature excitatory postsynaptic current (mEPSC) amplitudes, while increasing excitation by blocking $GABA_A$ receptor-mediated inhibition induces a down scaling of mEPSC amplitudes (Turrigiano et al., 1998). Chronic inhibition of activity with TTX induces postsynaptic insertion of AMPA receptors at the synapses, which proportionally increases both GluA1 and GluA2 (Wierenga et al., 2005). Synaptic scaling seems to rely on the GluA2 C-tail (Gainey et al., 2009), conversely to activity-dependent insertion of AMPA receptors which relies predominantly on GluA1 C-tail

(Kopec et al., 2007). However, insertion of GluA1 homomers was found to contribute to synaptic scaling of existing synapses in dissociated cultures following prolonged blockade of AMPA receptors (Thiagarajan et al., 2005). Frequency of mEPSCs is unchanged following chronic activity inhibition with TTX, suggesting a predominantly postsynaptic mechanism (Turrigiano et al., 1998).

1.4.2.1.2 Different expressions of synaptic scaling

The induction protocols as well as the preparation used for long-term modification of activity reveal the existence of several mechanisms for global homeostatic plasticity which rely on different molecular pathways. Dissociated cultures are a very malleable model for studying synaptic inputs, but they lack a closer resemblance to network structures compared to organotypic cultures, which preserve part of the original connectivity. The structural differences between these commonly used models could explain the discrepancy observed in synaptic scaling and reveal the existence of various mechanisms of homeostatic plasticity. For instance, the cell adhesion molecule β3 integrin is necessary for TTX-induced synaptic scaling in both dissociated and organotypic hippocampal cultures, but affects the variability of mEPSCs amplitudes only in organotypic slices (Cingolani and Goda, 2008). Moreover, in the same study, chronic activity deprivation treatment induced an increase in frequency in organotypic slices which was absent in dissociated cultures, emphasising another aspect of the differences between those two preparations. In dissociated hippocampal cultures, chronic NMDA receptor blockade induces a downstream PKA activation and clustering of NMDA receptors at the synapses (Crump et al., 2001). The effect of chronic blockade of AMPA receptors is prevented by inhibition of several CaM kinases (CaMKI, CaMKII, and CaMKIV) with KN93 (Thiagarajan et al., 2002). In the same study, the method used for inducing chronic inactivity modifies the α/β CaMKII ratio, which consequently alters mEPSCs amplitude, frequency and decay time. However, blocking CaMKII in control cells with a dominant-negative form of CaMKII had no effect on mEPSC amplitude (Ibata et al., 2008).

Using imaging to study the effect of chronic activity blockade on dendritic spines, TTX was found to increase spine density on rat acute slices after 5 hours incubation (Kirov et al., 2004), but no change in density was observed when organotypic slices were

treated for 7 days (McKinney et al., 1999). In mature rat organotypic cultures, deafferentation, blockage of AMPA receptors or inhibition of presynaptic release with botulinum toxin induced a significant loss of dendritic spines in CA1 pyramidal neurones, which affected more specifically synapses with small PSDs (Mateos et al., 2007). In contrast, blocking NMDA receptors increased the sprouting of thin spines (McKinney et al., 1999; Mateos et al., 2007). Local application of AMPA on the synapses was sufficient to rescue spine density, suggesting that spontaneous glutamate release was sufficient to maintain dendritic spines.

Synaptic scaling can take several forms, affecting dendritic spine density and transmission of miniature currents depending on several factors such as type and age of culture and mode of induction. Because this work is based on developing cultures, age-dependence of homeostatic plasticity is a major factor of interest here.

1.4.2.1.3 Age dependence

Several studies show that the maturation stage of the neurones and the network impacts on the homeostatic responses. *In vivo* studies in the visual system shows three distinctive periods for plasticity: an initial formation of the network independent of activity; a critical period for plasticity; finally followed by a less plastic adult stage (Hooks and Chen, 2007). Dark rearing increases excitatory transmission and AMPA receptor abundance in visual cortical layer II/III and IV, but layer II/III homeostatic plasticity extends beyond the end of the critical period (Goel and Lee, 2007) while this is not the case for layer IV (Desai et al., 2002). *In vivo* blockade of hippocampal function with TTX for two days induced an increase in mEPSCs amplitude in juvenile (P15) but not in young adult (P30) rats, suggesting an age-dependence of homeostatic plasticity (Echegoyen et al., 2007). TTX and Ca^{2+} deprivation for 5 hours in acute hippocampal slices did not affect dendritic spine density of CA1 pyramidal neurones from younger animals (P6 or P15), but significantly decreases density in slices from P20-22 animals or in adults (Kirov et al., 2004). In the same study, the absence of Ca^{2+} shortened dendritic spines at P11-12, but not at any other age, revealing once more the age-dependence of homeostatic plasticity. By using individually silenced neurones over-expressing the inward rectifying channel Kir2.1, Burrone and colleagues showed

that reducing neurones excitability during development induces a loss of functional synaptic inputs (Burrone et al., 2002), which corresponds to the absence of increased transmission observed from P4 to P7 in the absence of spontaneous activity in high Mg^{2+} conditions (Barria and Malinow, 2005). Once the network activity is established, suppressing excitability in individual neurones induced a homeostatic increase of synaptic input and a restoration of the neurone excitability after four days. Experiments in neocortical cultures found that synaptic scaling is predominantly postsynaptic in young cultures (Wierenga et al., 2005), while other evidence points out presynaptic mechanisms for homeostatic plasticity, such as increased mEPSCs frequency and increased number of readily available vesicle (Branco et al., 2008; Han and Stevens, 2009).

1.4.2.2 Local non-Hebbian synaptic changes

The various forms expressed by homeostatic plasticity are not restricted to global changes in synaptic weight, but could result in more localised compensatory mechanisms. Improvement of imaging techniques and the possibility of selectively suppressing the activity of a presynaptic neurone allowed the study of synapse-specific compensatory mechanisms (Abraham, 2008). Using green fluorescent protein (GFP) tagged-Kir2.1 to identify silenced presynaptic input on active cortical neurones, Hou and colleagues found that TTX induced a synapse-specific increase in mEPSC amplitude (Hou et al., 2008). The increased amplitude of mEPSCs was accompanied by an increase in receptor conductance due to the replacement of Ca^{2+} impermeable GluA2-containing AMPA receptors by Ca^{2+} permeable GluA2-lacking receptors (Hou et al., 2008). This increased synaptic transmission was not accompanied by a change in spine volume (Beique et al., 2006), in contrast to what has been observed previously (Matsuzaki et al., 2001; Beique et al., 2006). Another mechanism involved in single synapse homeostatic plasticity is a switch in NMDA receptor subunits mediated by spontaneous glutamate release, thus controlling Ca^{2+} transients and thereby adjusting individual spine threshold for the induction of plasticity (Lee et al., 2010). Moreover, knock-out of the activity-regulated cytoskeleton-associated protein (Arc, also known as Arg3.1), a member of the immediate-early gene family, abolishes AMPA receptor scaling, thus establishing a role for local protein synthesis in homeostatic plasticity (Shepherd et al., 2006; reviewed in Shepherd and Bear, 2011).

Global synaptic scaling presents the advantage of preserving the relative importance of each input, while input-specific changes would erase previous activity-dependent modification of synaptic transmission. Rabinowitch and Segev (2008) review the advantage of a local model of homeostatic plasticity based on weakening of the neighbouring synapses of a potentiated spine. This computer simulation integrates individual spine changes with a broader perspective restricted to the dendritic branch (Rabinowitch and Segev, 2008). This theory would work accordingly to the "clustered plasticity model" of long-term memories proposed previously (Mehta, 2004; Govindarajan et al., 2006) implying that dendritic branches and not individual spines are the functional units for memory storage (Govindarajan et al., 2011).

1.4.2.3 Pathway specific homeostatic changes

The negative feedback mechanisms that represent homeostatic synaptic plasticity could occur at the various branch levels, depending on the activity received in those compartments. Hence, on the dendritic tree receiving inputs from different cell types with various activity patterns, synaptic plasticity could have a local component competing with a more global component for gene transcription and somatic protein synthesis.

Homeostatic synaptic plasticity seems indeed to depend on the activity and nature of the input received, as it has been observed in organotypic slices (De Simoni and Edwards, 2006; Kim and Tsien, 2008). The adaptation to inactivity is synapse specific: at CA3-CA1 synapses, TTX induces an increase in mEPSC amplitude but no change in frequency, while at CA3-CA3 synapses, it induces a decrease in mEPSC frequency, which shortens reverberatory bursts observed in organotypic slices due to the hyperconnectivity of CA3 cells, finally preventing wind-up excitation (Kim and Tsien, 2008).

Studying the impact of different pathways on the dendritic tree, the Edwards lab labelled axons with the lipophilic dye DiO from a localised group of neurones in hippocampal organotypic slices to identify specifically the presynaptic inputs received by dendritic spines. The Schaffer collateral largely impinged on mushroom spines

(50%) in CA1, an elevated number compared with the less than 15% of synapses from entorhinal cortex or CA1 axons impinging on mushroom spines. Studies from acute slices showed that 30% of synapses between entorhinal cortex and CA1 cells impinge on mushroom spines (Nicholson et al., 2006), compared to about 10% *in vitro* (De Simoni and Edwards, 2006). The pathway specificity seemed to be very dependent on the environment in which the cells develop, offering more mushroom spines to the most activated pathway, i.e. the temporoammonic pathway *in vivo*, and the Schaffer collateral *in vitro* and consequently dampening the other pathways to maintain global excitability.

Setting the dendritic branch as the principal unit for plasticity also found supporting evidence in the result from presynaptic observation on dissociated hippocampal neurones, where release probability within the same branch were very similar, and inversely correlated with the number of spines on that particular branch (Branco et al., 2008). Moreover, homeostatic adaptation of presynaptic release was correlated with the activity of the postsynaptic dendrite, showing again a local mechanism for synaptic plasticity.

Homeostatic plasticity acts as a negative feedback, integrating local and global information in order to maintain the total synaptic weight through balancing excitatory and inhibitory inputs, as well as by bidirectional changes in distant locations to maintain global stability (Royer and Pare, 2003; Bourne and Harris, 2010).

1.5 Structure-function relationship of dendritic spines – a tool to study synaptic strength regionally

Growing evidence links dendritic spine morphology not only to synaptic strength but also to the synapse's propensity for plasticity. The shape of spines has a significant impact on their ability to induce plasticity and retain plasticity-related proteins (reviewed in Kasai et al., 2010). Dendritic spines are plastic entities, whose head size tightly correlates synaptic strength, both statically and dynamically. These properties enable the use of imaging of dendritic spines as a functional read-out of synaptic strength in steady state or following plasticity. A review of biophysical properties

playing a role in plasticity is used to distinguish fundamental morphological features. The recent knowledge gained about the most determinant morphological characteristics for plasticity makes it possible to assess whether the separation of spines into distinct morphological categories –mushroom, thin and stubby- is still relevant or whether spines could be separated on more appropriate criteria.

1.5.1 Plasticity of dendritic spine morphology

1.5.1.1 Dendritic spine populations and development

Following electron microscopy studies, dendritic spines have been categorised into three main types present throughout life: mushroom, thin and stubby spines, to which is added filopodia, present essentially during development (Harris et al., 1992). Figure 1.3A summarises the three main categories of dendritic spines as defined by Kristen Harris and co-workers. In that regard, thin "learning-spines" and mushroom "memory spines" (Kasai et al., 2003; Bourne et al., 2007) have received most of the attention of plasticity labs.

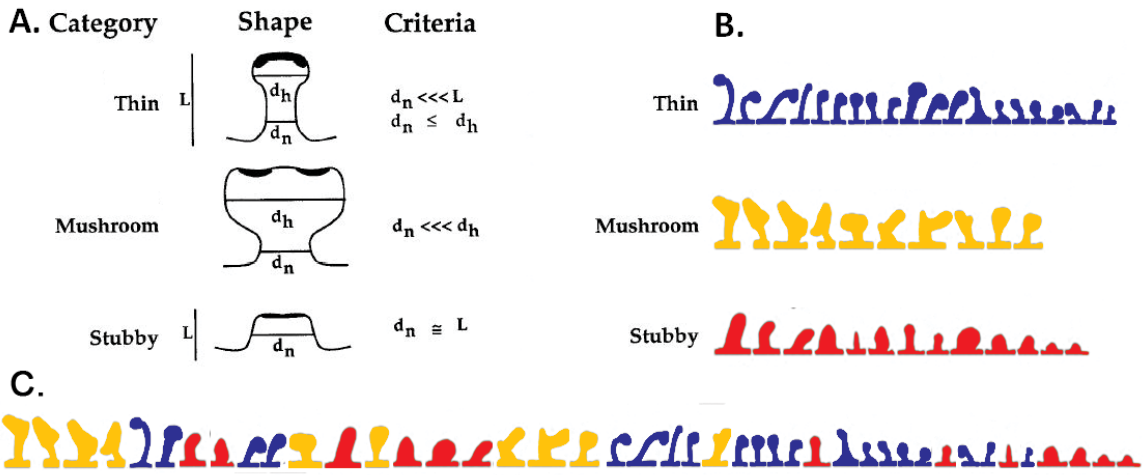

Figure 1-3: Identification of spine type by Kristen Harris and co-workers and sample of each spine type variability.

(A) The three main type of dendritic spines as classified originally by the Harris lab (adapted from Harris et al., 1992) present non-strict criteria for identification. Definitions: dn neck diameter, dh head diameter, L spine length. (B) A sample of the diversity of spine morphologies highlights the diversity of spine shapes and illustrates the difficulty of sorting some spines which could fit more than one type (adapted from Oray et al., 2006). (C) The alignment of the dendritic spines classified in (B) shows a continuum of shapes.

The morphology of dendritic spines is highly plastic and evolves dramatically during development. In the hippocampus, stubby shape is the most abundant form of spine in young preparations (P14: 50%; 7 DIV: 40%), but decreases significantly with age, representing 30% in P21 slices, and 20% at 21 DIV (De Simoni et al, 2003). Serial electron microscopy sections of hippocampus reveal that stubby spine density decreases from 0.6 in young animals to less than 0.2 spines/µm in adults, then representing less than 10% of the total population. Percentage of mushroom spines remains stable at around 20-25% from P15 to adults. The overall spine density measured in CA1 pyramidal neurones of rats more than doubles between P15 and adult, growing from 1.4 spines/µm to plateau around 3.0 spines/µm (Harris et al, 1992). Dendritic spine types and densities develop very similarly in organotypic and acute hippocampal slices of equivalent ages, thus demonstrating the stability of their distribution across different preparations preserving the network structure (De Simoni et al., 2003).

As detailed above, the proportion of the different spine types and the total spine density are constantly changing during development. Dendritic spines are motile entities which keep on evolving and transforming throughout life, as part of a developmental process early on, but mainly in response to network activity. The first observation of dendritic spine growth following stimulation was made by administering a local superfusion of normal artificial cerebrospinal fluid (ACSF) to dissociated hippocampal cultures under a blocking solution (Engert & Bonhoeffer, 1999). Later, morphological changes in spines were observed by several independent studies, corroborating a strong correlation between synaptic modifications and spine head size alterations (Matsuzaki et al., 2004; Ostroff et al., 2002; Zhou et al., 2004; Kopec et al., 2006), see 1.5.1.3. The variability of shapes within one type, as illustrated on figure 1.3B&C, shows the difficulty inherent in separating spines on pure morphological grounds without bias. Limitations incurring from resolution limits and measurement approximations lead to the diversity of dendritic spine classifications, as discussed in more detail in Chapter 3.

1.5.1.2 Correlation between spine head size and synaptic strength

Dendritic spines have been studied extensively using electron microscopy, which enables precise measurement of parameters such as the size of the presynaptic active zone, PSD, neck length and diameter. The dimensions of the neck do not correlate very well with that of the head. There is, however, a clear linear relationship between the size of the PSD, the head volume (Harris et al., 1992) and the number of AMPA receptors (Baude et al., 1995).

In parallel, the development of live-imaging has allowed a non-static approach of dendritic spine study. Time-lapse imaging and glutamate uncaging enable the study of individual dendritic spines over time, while achieving localised excitation restricted to the tiny focal volume in the range of the 1 μm^3 (Matsukazi et al., 2001). The relationship between the size of the spine head and the sensitivity to glutamate was confirmed with glutamate uncaging and 2-photon imaging in the Kasai lab (Matsuzaki et al., 2001; Kasai et al., 2003), larger spines showing much larger uncaging EPSCs than thin spines.

1.5.1.3 Correlated changes of spine head after LTP or LTD

Long-lasting synaptic plasticity has progressively been linked with alterations in spine number, size and shape. Engert and Bonhoeffer, 1999 (reviewed in Kasai et al., 2010) made the first confocal study showing the formation of new spines following LTP induction in organotypic slices. The new spines were later found to be innervated by presynaptic terminals (Goldin et al., 2001). Long-term synaptic plasticity in pre-existing spines is accompanied by morphological changes. A few important studies revealed that the volume of individual spines increases with LTP, and decreases with LTD (Maravall et al., 2004; Matsuzaki et al., 2004; Okamoto et al., 2004; Zhou et al., 2004), giving support to the hypothesis that the number of mushroom spine synapses increases following high frequency stimulation or theta burst stimulation (Edwards, 1995; Buchs and Muller, 1996; reviewed in Dhanrajan et al., 2004). This is also in accordance with the high plasticity of thin spines, which can either shrink or disappear following low-frequency stimulation, or increase in size following high-frequency stimulation.

Activity-dependent changes in spine morphology have been reported in several live imaging studies using glutamate uncaging or chemical LTP, revealing an increase in spine head size of the stimulated synapses (Matsuzaki et al., 2001; Kopec et al., 2006). The postsynaptic density also increases accordingly to the enlargement of spine head size, in parallel with a translocation of polyribosomes (Ostroff et al., 2002), which are transferred from the dendritic shafts, where most of them reside before stimulation, to the head of the spine.

Delivery of AMPA receptors to hippocampal synapses, and specifically of the GluA1 subunit (Hayashi et al., 2000), is a good indicator of local potentiation, and difference between spine types could emphasise the tight relationship between morphological and functional properties (Kasai et al., 2003; reviewed in Matsuzaki, 2007). LTD was shown to induce endocytosis of AMPA receptors from the synaptic sites which correlates with a decrease in spine head size observed (Zhou et al., 2004). Spine morphology also impacts on its ability to retain and stabilise plasticity-related proteins. Mushroom spines were found to incorporate GluA1 subunits more easily than other spine types following stimulation (Matsuo et al, 2008). Short spines were found to be more prone to expressing GluA1 at synapses following LTP than longer spines, because of a better coupling between their head and the parent dendrite (Korkotian and Segal, 2007). However, other studies found that thin spines, with longer necks and more isolated heads, would sustain enlargements more readily than larger spines because of the better retention of the "enlargement pool" of F-actin (Honkura et al., 2008).

1.5.1.4 Learning-induced changes in dendritic spines

Activity-induced trafficking, phosphorylation and activation of certain proteins in the postsynaptic density lead to synaptic plasticity and are believed to underlie learning, memory and modification of animal behaviours (Malenka and Nicoll, 1999; Kessels and Malinow, 2009). As mentioned previously, changes in both morphology and stability of dendritic spines can be linked to experience-dependent learning. Using the motor cortex as the platform to study synaptic transmission of neurones and dendritic spine plasticity, several recent papers have visualised postsynaptic changes following motor learning tasks. The upper location of the motor cortex in the brain allows easy access

for *in vivo* field recording or imaging of neurones. Spines transiently increased in layer I of the primary motor cortex after learning a new motor skill (Harms et al., 2008). Within an hour of learning a forelimb reaching task, the contralateral motor cortex neurones of mouse showed selective elimination and formation of new spines, which subsequently are preferentially stabilised (Xu et al., 2009). *In vivo* imaging studies in rats (Yang et al., 2009) or zebra finches (Roberts et al., 2010) demonstrated an important spine remodelling after behavioural learning, inducing spine density increase, stabilisation and enlargement of spines, which correlated with the behavioural improvement.

Modulation of dendritic spines can clearly be related to experience-dependent learning. The tight correlation between spine head size and synaptic strength at any moment enables an estimation of local synaptic strength using image analysis of postsynaptic heads. Moreover, the dynamic changes of spine heads following plasticity confer the ability to visualise synaptic changes through the morphological modification of dendritic spines, thus providing a functional read-out of plasticity. However, initial morphologies of dendritic spines may affect their ability for plasticity, and it is important to establish if all spines respond similarly to those changes.

1.5.2 Morphological factors affecting spine plasticity

The previous section reviewed morphological changes observed in spines either during development, following activity-dependent stimuli or potentially during learning. The changes could be due to active constriction or expansion of the neck and/or the head. Cytoskeletal remodelling, such as actin-filament polymerisation or depolymerisation, as well as organelle distribution from dendritic shafts to spine head or redistribution of membrane proteins from the non-synaptic zones to the synaptic area could also be responsible for the measured perturbations of spines during synaptic plasticity (Hotulainen and Hoogenraad, 2010). Dendritic spine morphology will affect a synapse's ability to undergo such plastic changes, revealing that some types of spines may be more plastic than others. This point will be discussed below.

1.5.2.1 Biophysical properties of dendritic spines

The variation of thin spine numbers compared to the relative stability of mushroom spines has led some to hypothesise that thin spines were small and plastic "learning spines", while mushrooms were large and stable "memory spines" (Matsuzaki, 2007; Bourne and Harris, 2007). The differences in morphology induce several functional differences regarding plasticity and signal integration.

1.5.2.1.1 Diffusion between head and dendrite

Dendritic spine length and neck width are essential parameters when studying dendritic spine plasticity. Thin spines have a long and narrow neck, which can trap transiently expressed molecules such as inositol 1,4,5-triphosphate, the scaffolding protein PSD95, or even Ca^{2+} influx (Gray et al., 2006). Theoretical analysis suggested that longer and narrower necks have much slower diffusion rates, and thus the heads of such spines are more isolated from the parent dendrite (Kato et al, 2004; Biess et al, 2007). The small conductance of longer necks could play an important role in thin spine plasticity, preventing Ca^{2+} from diffusing to the parent dendrites, and consequently by raising the Ca^{2+} concentration in the spine head following activation of NMDA receptors (Noguchi et al., 2005). Thin spines also have more NR2-B-containing NMDA receptors (Sobczyk and Svoboda, 2007), which deactivate more slowly than other subtypes. Following synaptic activity, NR2-B-containing NMDA receptors favour larger Ca^{2+} transients and thus increase the probability for potentiation in thin spines.

However, a faster coupling between head and neck can also be an advantage for insertion of GluA1-containing AMPA receptors following activity-induced plasticity (Korkotian and Segal, 2007). In that study, long spines (>1.5 µm) loaded GluA1 only when the Ca^{2+} concentration was raised at the base of the neck, while shorter spines (<1.5 µm) accumulated GluA1 following local rises of intracellular Ca^{2+} in their heads. These differences are attributed to the ability of the Ca^{2+} transient to diffuse from the spine head to the parent dendrite, i.e. to the degree of coupling between them.

Large mushroom spines have bigger PSDs, more AMPA receptors, and often larger necks allowing a more rapid diffusion of Ca^{2+} transients to the parent dendrite, observations consistent with the difficulty to induce further LTP in large mushroom spines (Noguchi et al., 2005).

The total spine length is not the only crucial element for diffusional coupling: the cross-sectional area of the neck also regulates spine/dendrite diffusional coupling (Bloodgood and Sabatini, 2005).

Those results suggest that both length and neck width are fundamental for plasticity. However, no linear correlation was found between spine head size and neck width or length (Harris et al., 1992), possibly because of the continuity of headed spine morphologies evolving from the extreme structures represented by the stereotypical types identified as mushroom, thin and stubby spines. It is therefore difficult to separate thin from mushroom spines based on these characteristics.

1.5.2.1.2 Lateral diffusion in the membrane

Lateral diffusion of membrane proteins from reserve pools located on the dendritic shafts to the spine head can be restricted by the influence of membrane architecture. A study on membrane protein trafficking in headed spines found that increased spine length and/or head volume, both of which proportionally increase the membrane area, slowed the exchange between dendritic shaft and spine head compartments (Hugel et al., 2009). Focusing on the rate of diffusion of membrane-bound proteins along the neck, a study from the Henley lab found that a GFP-tagged membrane protein diffused more rapidly in stubby spines than in mushroom spines of equivalent membrane area (see figure 1-4, Ashby et al, 2006).

Hippocampal neurones infected with SEP-GluA2, a pH sensitive variant of enhanced-GFP, were photobleached to study the diffusion rate and half recovery time of different regions of the spines (base, neck and head). The spatial resolution achieved with two-photon imaging can be applied to fluorescence recovery after photo-bleaching techniques (FRAP), thus enabling the study of tiny fractions of dendritic spine membrane of a few tens of micrometres, considering the impact of spine morphology on lateral diffusion of membrane proteins. The study revealed that

mushroom and stubby spines have different fluorescent recovery time after bleaching their spine terminal point (Ashby et al, 2006). Diffusion was clearly slower in the head of mushroom spines, the recovery time being more than double that of stubby spines (figure 1-4B). No difference in volume between stubby and mushroom spines was observed, but the spine neck morphology, more than the head volume, was the chief parameter determining membrane protein trafficking.

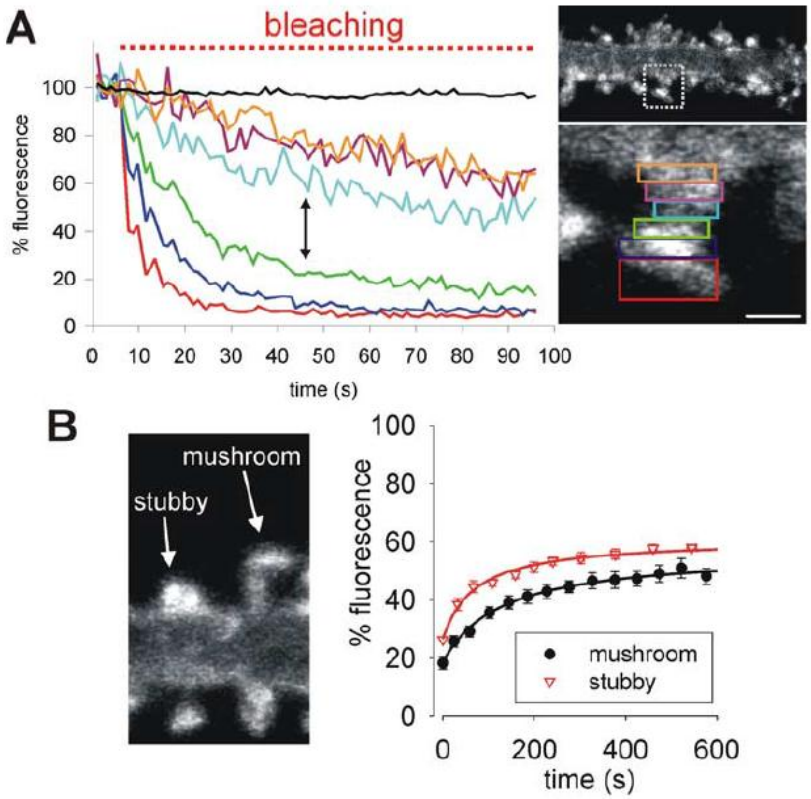

Figure 1-4: There is a barrier to AMPA lateral movement located at the spine neck (Ashby et al, 2006).

(A) Continuous photobleaching at the top of the spine head (red region) leads to loss of fluorescence in nearby regions (regions shown in accompanying image; the black line is fluorescence in neighbouring spine) as SEP–GluA2 moves around the membrane of the spine. The loss of fluorescence is relatively slow in regions at or near the neck, suggesting that movement in this region is reduced. Scale bar, 1 µm. (B) Image shows typical examples of SEP–GluA2 fluorescence from stubby and mushroom spines. Chart shows pooled and averaged FRAP curves from stubby and mushroom spine heads.

Altered lateral mobility of membrane-bound protein emphasises the role of dendritic spine shape in expressing synaptic plasticity. Furthermore the rapid alteration of dendritic spine shape following LTP/LTD induction would alter its susceptibility for further plasticity. The neck appears as a key player for plasticity, regulating both trafficking of membrane-bound proteins and diffusional coupling between head and dendrite. Headed spine morphology may vary between "thin-learning" and "mushroom-memory", but in a progressive manner, and many headed spines would probably fall halfway between the two stereotypical shapes. From the literature, it seems more appropriate to regroup both thin and mushroom spines in a category called "headed", which comprises all spines with a neck constriction separating the head from the shaft, and distinct from stubby spines.

1.5.2.2 Are stubby spines as plastic as headed spines?

Stubby spines are quite an abundant type of dendritic spine, but far less studied than their headed counterparts. The previous sections have shown that the neck of dendritic spines gate many functions related to plasticity, and the absence of neck could be a serious restraint for plasticity. What is the part played by stubby spines in plasticity then? Do stubby spines undergo similar plastic changes as headed spines? Stubby spines are often described as small neckless protrusions (figure 1-4B), which could be identified by their low total length-to-neck-diameter ratio (Harris et al., 1992). In general agreement, stubby spines are often called headless while thin and mushroom spines are considered headed spines. Given that stubby spines possess a PSD and glutamate receptors, it seems more correct to say that stubby spines are neckless, and so thin and mushroom spines would become "necked" spines. To avoid confusion, the new terms have not been used in this thesis. Their identification differs slightly from paper to paper, ranging from the visual absence of a neck (De Simoni et al., 2003) to the equivalent size of its length and width (Harris et al., 1992) via more strict measurements such as spine length/neck diameter ≤ 2 (Oray et al., 2006).

In the following sections, I will discuss the plasticity of stubby spines, showing that the absence of neck constriction seems to limit their plasticity to early developmental stages or within their own subtypes, and thus suggesting that stubby spines are a separate category from their headed counter-parts.

1.5.2.2.1 Early plasticity of stubby spines

The changes occurring in the representation of stubby spine synapses with age lead to the conclusion that stubby spines are an important intermediary in the development of the neuronal network, though they progressively become less and less important in the adult hippocampus, representing then only 10% of synapses. Shaft synapses, abundant at P1 in rat, are recruited early on to become dendritic spines, possibly transiting through the state of stubby spines, which is the dominant type of postsynaptic protrusion around P14 (Marrs et al, 2001). In figure 1-5, the formation of a dendritic spine imaged over several minutes shows in red PSD95, an essential component of the PSD, at the tip of the newly formed spine, transiting through a stubby-like state before transforming into a headed spine. Stubby spines could also correspond to retracting filopodia, which are highly prevalent and motile during early development, and which may be pruned if they don't find a postsynaptic partner.

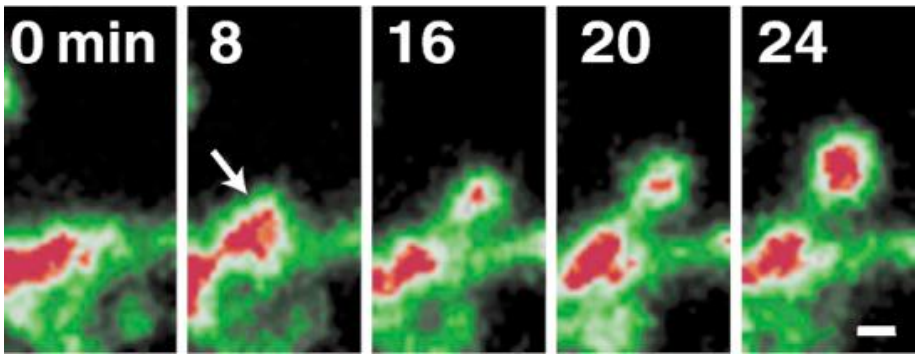

Figure 1-5: PSD95 clusters can move between shafts and spines as spines emerge, briefly transiting through a stubby-shape type.

A preformed shaft cluster moves outward with an emerging stubby spine (arrow), progressively transforming into a headed spine. Scale bar, 1 µm (Marrs et al., 2001).

Surprisingly, the motility measured in the mouse visual cortex shows very similar values for stubby spines compared with mushroom spines, at either P28 or P42. At P21, the motility is slightly higher for both, but actually reveals a disparity: stubby spine motility fits a Gaussian curve centred on the average motility value, while mushroom spines comprise two population of spines, one very stable and the other highly motile (Majewska and Sur, 2003).

Nevertheless, stubby and headed spines were found to mainly remain within their own group (figure 1-6). In a time-lapse imaging study carried out in developing mouse hippocampal slices, dendritic spines from CA1 or CA3 pyramidal neurones were found to predominantly preserve their original morphological properties. Filopodia rapidly transformed into stubby or headed spines, but few stubby spines actually evolved into headed spines, or vice versa (Parnass et al., 2000).

It is possible that during early development, the abundance of stubby spines reflect the transient states of nascent spines, while at a later age, they form a pool of synapses with different propensity for plasticity than headed spines, but necessary for basal synaptic transmission.

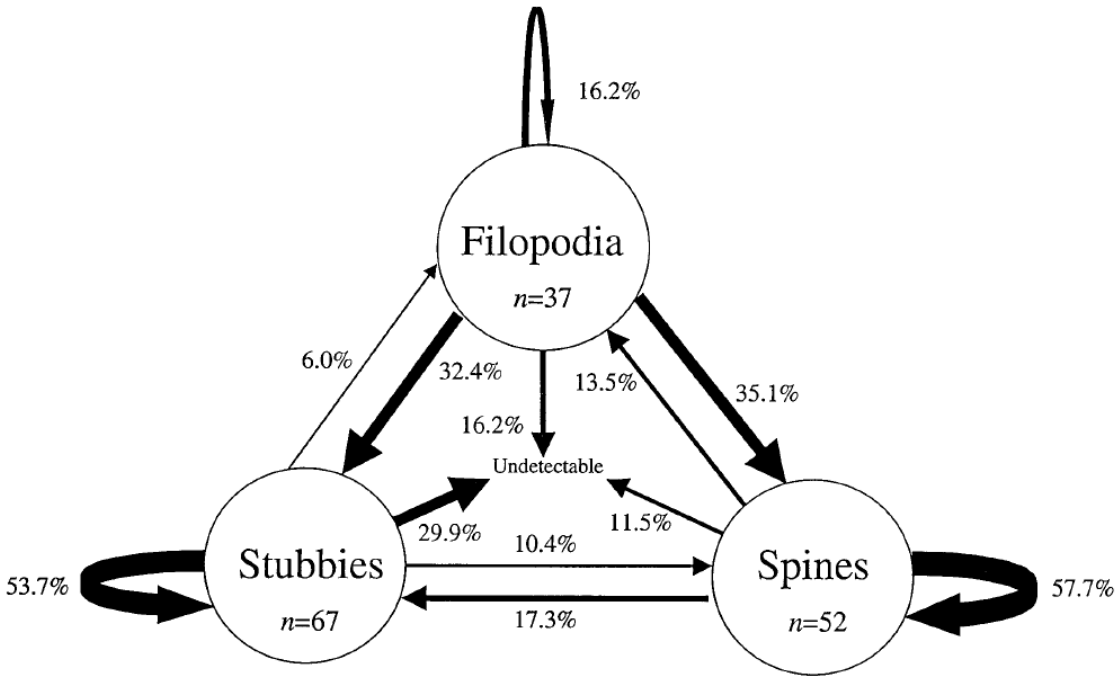

Figure 1-6: Prospective analysis of morphology of dendritic protrusions over 2-4h time-lapse imaging study, in developing mouse hippocampal slice.

Each circle represents the population of protrusions categorised as filopodia, stubby, or headed spines at the beginning of the time-lapse sequences. Arrows indicate the class in which those protrusions were categorized at the end. Thickness of a line is proportional to the percentage of the initial protrusions. Note how, in contrast to filopodia, most stubbies and spines are still classified in the same group at the end of the sequences (Parnass et al., 2000).

1.5.2.2.2 Morphological changes following activity of stubby spines

When examining spine morphological changes following activity-dependent synaptic plasticity, several papers found that stubby spine properties differ from that of headed spines (Ashby et al., 2006; Honkura et al., 2008). Stubby spines were found to be less responsive to plastic changes than other types and were thus excluded from the analysis, under the argument that they brought in noise which prevented detecting changes in headed spines (Korkotian and Segal, 2007). Spine length and head area are the main parameters that are significantly altered in thin and mushroom spines while stable in stubby spines. However, observations of individual spines or pieces of dendrites in plasticity experiments show that stubby spines can result from the shrinkage of a headed spine (Parnass et al., 2000; Majewska and Sur, 2003), or as the transient state between a shaft and a headed spine (figure 1-5, Marss et al, 2001).

Those two spines, similar in shape, could represent, in reality, two functionally different entities, one stable and one transient.

Stubby spines, with a PSD usually about the same size as thin spines (Harris et al., 1992), and no constriction between the PSD and the dendrite, have very fast diffusion coupling, limiting Ca^{2+} rise from homosynaptic activation (Sabatini et al., 2002). Photo-activated GFP has been introduced to visualise the diffusion barrier created by the neck. Once activated near the PSD of a spine to mimick Ca^{2+} entry, these free intracellular molecules diffuse from the head to the parent dendrite, and can also passively propagate from the main dendrite to the heads of neighbouring spines with large necks (Bloodgood and Sabatini, 2005). Also, stubby spines were found to be capable of incorporating AMPA receptors at their synapses following activity, in a study where they are regrouped with "short spines" of any type (Korkotian and Segal, 2007). Therefore, stubby spines could act as heterosynaptic captors of activity, sensing and benefitting from the activity of nearby activated spines. This possibility is corroborated by the work of Rose and colleagues, who found that locally induced accumulation of CaMKII at synapses could translocate to the neighbouring synapses along the dendrite in a Ca^{2+}-dependent manner (Rose et al., 2009).

1.6 Summary of dendritic spines plasticity

Dendritic spines, the recipients of most excitatory synapses in the hippocampus, are found in a large variety of shapes on the dendritic branches of pyramidal neurones. The particularity of their morphology, such as the presence or absence of a neck, alter several properties important for plasticity, such as diffusional coupling to and from the dendritic shaft (Bloodgood and Sabatini, 2005; Noguchi et al., 2005) or lateral diffusion of membrane-bound protein (Ashby et al., 2006; Hugel et al., 2009). The various shapes of dendritic spines seem to present a continuum which makes it difficult to separate unequivocally dendritic spines into exclusive types (figure 1-3B). However, all spines morphologies are not equal regarding plasticity. There is usually a good correlation between dendritic spine head size and synaptic strength (Kasai et al., 2010), but the presence of a neck constriction seems to have the biggest impact for

spine plasticity. Hence, stubby spines, though presenting functional synapses, cannot raise Ca^{2+} concentration in the postsynaptic site, a prerequisite for plasticity (Bloodgood and Sabatini, 2007). Consequently, stubby spines seem less able to undergo plastic changes, mainly remaining in their own category (Parnass et al., 2000), and potentially masking the detection of changes in headed spines (Korkotian and Segal, 2007).

Stubby spines share with their headed counterparts most features of active synapses, such as a PSD facing a presynaptic active zone and an average PSD is about the same as thin spines (Harris et al., 1992), although their volume can vary greatly (figure 1.3B). Thus, the correlation between head size and synaptic strength is not as clear as with headed spines. The absence of a constriction between head and dendrite produces a high diffusion constant, which makes it difficult to increase the Ca^{2+} concentration as necessary for potentiation, but makes them better sensors of neighbouring activity.

For the purpose of my analysis, which focuses on dendritic spine plasticity based on imaging, stubby spines are thus distinguished from mushroom and thin spines which will not be distinguished but regrouped under the term headed spines. Stubby and headed spines will be analysed separately in order to increase the detection of possible morphological plasticity in headed spines.

The hypotheses are that the characteristics of spines in a particular pathway will depend on activity, and that changes of strength, reflected in spine type, in one pathway will be balanced by reversal in another pathway. The results obtained previously in the lab are the starting point to study further the repartition of spine types under other types of activation/inhibition, trying to block *in vitro* the inputs from CA3 cells, and enhanced those from the EC.

Electrophysiological recording and confocal imaging of dendritic spines are used here to reveal local age-dependent plasticity that maintains overall synaptic weighting by balancing activity-dependent and homeostatic synaptic changes.

Chapter 2. Materials and Methods

The materials and methods presented here results from the work carried out during my PhD in two different places:

- the vast majority was done at UCL in Dr Frances Edwards' lab (2.1-2.2), and involved mainly *in vitro* work on organotypic cultures and imaging
- a shorter part was carried out at UCSD in Prof. Robert Malinow's lab (2.3), and involved electrophysiology on organotypic and acute slices and several techniques for *in vivo* injection of viruses.

2.1 Hippocampal organotypic slice cultures

2.1.1 Preparation and maintenance of organotypic slices

Organotypic slices were prepared using the method of Stoppini et al. (Stoppini et al., 1991). Six well plates were prepared with 1ml of serum culture medium (pH 7.3): 25% horse serum, 50% Modified Eagle Medium (MEM), 23% Hank's balanced salt solution (HBSS) (all from GIBCO BRL, Paisley, Scotland), 5000 Units/100 ml Penicillin (0.08 mM), 1200 Units/100 ml Nystatin (both from Sigma-Aldrich Co., Poole, Dorset, England). Millicell culture plate inserts (Millipore UK, Watford, England) were added in each well, and 3 halves of autoclaved culture membranes (Millipore LCR membrane filter, 0.5 µm, 13 mm) were put with sterilized twisters onto each insert. The plate was then incubated at 37°C, 5% CO_2 until plating.

Hippocampal slices were obtained from 5-day old male rat pup, decapitated under the flow cabinet. The brain was removed gently and quickly (less than 1 min) and put in ice-cold slicing medium (EBSS with HEPES). The brain was cut in two, glued on a slicing platform, immersed in slicing medium. Using a ceramic blade, 300 µm thick parasagittal slices were cut with a manual vibroslicer (Campden Instruments, UK). Each slice was then placed on a culture membrane, and incubated at 37°C. The culture medium is changed on the day following the dissection, and then every two days. Individual slices were removed from the incubator for experiments on the appropriate

day *in vitro*. All work was carried out following UK Home Office regulations and with agreement with national ethics committee guidelines.

2.1.2 Labelling presynaptic axons

Long-chain dialkylcarbocyanine DiO crystals (Invitrogen Molecular Probes, Leiden, The Netherlands) are lipophilic dyes that dissolve into the membranes of the cells with which they come in close contact. The dyes do not dissolve in the culture medium during incubation, or in the ACSF during imaging because of their hydrophobic properties and hence the dyes only diffuse through the lipid membrane. The dyes diffuse at a rate of 6mm per day in living tissue, and at a much slower pace of 0.2–0.6 mm per day in fixed tissue (Godement et al., 1987).

The crystals can be used to determine the origin of labelled axons, and thus determine the morphology and connectivity of the dendritic tree of fluorescent cells. Labelled axons, even located far from the area on which the crystals were put, belong to the cells marked by the crystal. The crystals are applied on the desired cell type using a fine glass pipette, working under the flow cabinet with a low magnification objective (5X). The amount of crystals placed on the slice directly affects the background noise for imaging, therefore it is important not to add too many crystals. Also, it is essential that no crystal jump on the slice over any other area than the one selected, as they would label the axons as well, and consequently the labelled axons could not be certified as originating only from the desired type of cell.

When added on the slice, the crystals were put on the cell body layer of either CA3 or EC, to label respectively the Schaffer collateral or the perforant path. The dye must be applied the day before imaging, to allow overnight diffusion of the molecules in the membrane.

2.1.3 Labelling postsynaptic cells and CA1 axons

Whole-cell patch-clamp of CA1 pyramidal neurones were made at a holding potential of –70 mV with an Axopatch 200B (Axon Instruments, Union City, CA), at room temperature (22–25°C). Electrodes pulled from borosilicate glass (World Precision Instruments, Sarasota, USA) at a resistance of 4–5 MΩ were filled with a CsCl based intracellular solution (see below). ACSF: NaCl 125 mM, KCl 2.5 mM, $NaHCO_3$ 26 mM, NaH_2PO_4 1.25 mM, glucose 25 mM, $CaCl_2$ 2 mM, $MgCl_2$ 1 mM; bubbled with 95% O2 / 5% CO2. Intracellular solution: CsCl 140 mM, 4-(2-Hydroxyethyl)-1-piperazineethanesulfonic acid (HEPES) 5 mM, EGTA 10 mM, MgATP 2 mM, pH 7.4 with CsOH.

The fluorescent dye was introduced into the cell through the electrode via the intra-cellular solution. Alexa Fluor 594 (Molecular Probes Europe BV, Leiden, The Netherlands, absorption 590 nm, emission 617 nm) was diluted at 0.2 mg/ml in the CsCl internal solution, aliquoted and kept at -20^{o}C. Once the whole-cell patch was achieved, the dye was left to diffuse into the cell for at least 20 minutes to allow distant dendrites to be filled properly (Edwards et al, 1989).

In a previous study, De Simoni compared detailed morphology (spine density and shape as well as dendrite complexity) and synaptic transmission of CA1 neurones containing either one of the two different Alexa dyes or Texas Red (De Simoni et al., 2003). Neither the particular dye used nor imaging the cells with or without fixation altered the measured morphology of the cells nor did the dye used affect the synaptic properties (De Simoni et al., 2003).

2.1.4 Fixation of slices for later imaging

If slices could not be imaged immediately, slices containing cells filled with the fluorescent probe Alexa 594 were taken out of the bath and fixed for later imaging, following the paraformaldehyde (PFA) fixation protocol carried out at room

temperature. The slices were fixed with a 15 min bath in a solution containing 4% PFA/4% Sucrose (pH adjusted at 7), then rinsed twice for 10 min in a fresh Phosphate Buffered Saline (PBS) bath. A glass microscope slide was mounted with transparent nail polish in a 1 cm x 1 cm square to delineate the area where the slice was to be placed. The excess solution was removed with absorbent paper. A drop of Antifade (Vectashield) was finally added over the slice before adding a coverslip and sealing it with nail polish. The slide was maintained at -20°C.

If the slice contains lipophilic dyes, such as DiO, it cannot be fixed with antifade agents, because the glycerol contained in it dissolves such dyes. DiO containing slices can be fixed by mounting them on a slide and adding PBS onto them. The slice should be protected by placing a coverslip on top, and can be stored in the fridge for a maximum of a week.

2.1.5 Long-term treatments of organotypic slices

2.1.5.1 Long-term drug treatments

Prior to long-term treatments of organotypic slices with drugs, such as 48 hours incubations with Tetrodotoxin (TTX) or CNQX/APV or 7 days for the CaMKII and PKA antagonists, respectively KN62 and Rp-8-Br-cAMPs (Rp-cAMP), the solubility of the drug in the culture medium was tested prior to the beginning of the experiment, to ensure that the drug would not precipitate out of solution.

To avoid potential modification of the drug if stored in the culture medium, the drugs were stored in concentrated aliquots of 100X (or 1000X) final concentration in buffer solution, and 10 µl (or 1 µl) were added to the freshly changed 1 ml of culture medium in each individual well at the time of treatment. The operation was repeated every time the culture medium needed to be changed for the whole duration of the treatment.

For activity blockade, tetrodotoxin with citrate (TTX) from Tocris was aliquoted at 100 µM in distilled water, and used at a final concentration of 1 µM in culture medium.

For blockade of α-amino-3-hydroxy-5-methyl-4-isoxazolepropionic acid receptors (AMPA-R) and *N*-methyl *D*-aspartate receptors (NMDA-R), aliquots of 5 mM of 6-Cyano-7-nitroquinoxaline-2,3-dione disodium salt hydrate (CNQX) and 10 mM of D-(-)-2-amino-5-phosphonopentanoic acid (D-APV or simply APV here) were prepared in distilled water, and used at the final concentration of 50 µM for CNQX and 100 µM APV.

For plasticity blockade, the PKA type-1 antagonist Rp-cAMP (BioLog) was dissolved in water at 20 mM, for a final concentration of 200 µM once diluted in culture medium.

The CaMKII antagonist KN62 from Tocris was first dissolved in dimethyl sulfoxide (DMSO) as it is not very soluble in water. The 1000X solution at 4 mM was then aliquoted and stored at -20°C. Aliquots were diluted on the day of use in culture medium for a final concentration of 4 µM. The concentration of DMSO was 1/1000 (or 0.1%) volume.

2.1.5.2 Deafferentation of CA1 cells from the Schaffer collateral

For long-term study of dendritic spine changes following cutting of an afferent input, here of the Schaffer collateral (figure 2-1), hippocampal organotypic slices of either 7 or 14 DIV were dissected in a flow cabinet under a microscope, using fine needles mounted on syringes as a blade. The Schaffer collateral pathway was disrupted following the removal of a small wedge of the slice orthogonally to the CA3-CA1 axis. The disruption was checked after 4 days, and the pathway was cut again if some cells or axons had spread through the gap.

One day before recording, DiO crystals were dropped on CA3 cell bodies, and the absence of DiO labelled axons was confirmed under fluorescent imaging.

The slices remain without input from the Schaffer collateral pathway for a total of seven days.

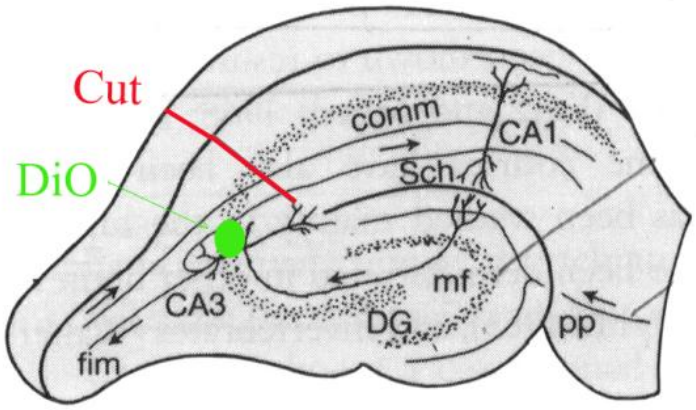

Figure 2-1: Scheme of an organotypic hippocampal culture following deafferentation, showing the deposition of DiO crystals over CA3 body layer (green), and the cut (red) made perpendicular to the Schaffer collateral pathway, seven days before imaging (adapted from http://graulab.tamu.edu/J-Grau/Psyc606/Figures/LTP-LTD-Hippocampus.jpg).

2.2 Imaging and analysis of morphology

2.2.1 Fluorescence, confocal microscopy and image acquisition

The technical advancements of microscopy, fluorescent molecules and image analysis has provided the tools necessary to take the study of biological molecules and mechanisms one step further, constantly improving the detection power of microscopic events and thus reducing photodamage by less intense exposure of the tissue.

2.2.1.1 Principle of fluorescence imaging & fluorochromes

The electrons of a fluorescent molecule can be excited at a certain wavelength (figure 2-2), also called excitation wavelength (blue arrow), which give them enough energy to jump from their ground state (S_0) to a higher energy state (S_1, S_2 or S_3). Once the electrons have absorbed this high energy from short wavelength light, they return to their basal energy level by rapidly emitting fluorescent light (green arrow) of longer wavelength and lower energy, or by transiting to the triplet states, delaying their return and emitting photon of lower energy, called phosphorescence (red arrow).

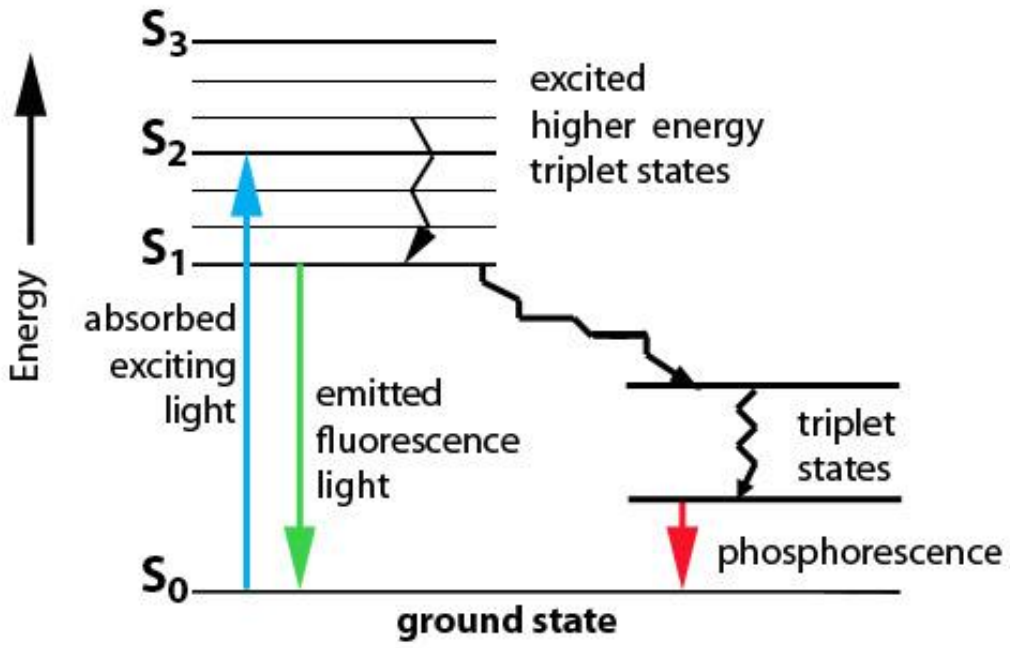

Figure 2-2: Jablonski diagram

It shows the different energy levels of electrons from an excited molecule, and the different routes electrons can take to return to their basal energy state (University of Victoria, 2005, http://web.uvic.ca/ail/techniques/epi-fluorescence.html).

The energy of light (E) is determined by its wavelength (λ) following the equation:

$$E = \frac{hc}{\lambda}$$

where *c* is the speed of light, and *h* Planck's constant. Absorption (excitation) and emission wavelengths are important parameters in confocal microscopy because the fluorescent probes used have to be adapted to the characteristics of the optical system. Moreover, when dealing with multiple fluorescent probes at once, their excitation-emission properties have to be studied to avoid overlapping of one probe's fluorescence into the detection spectrum of the others. Optical filters can be used to correct such overlap (see 2.4 below).

The properties of the fluorescent probes used in this piece of work are regrouped in table 2-1.

Table 2-1: Excitation and emission wavelengths of the fluorescent probes used in this work.

	Excitation wavelength (nm)	Emission wavelength (nm)
DiO	488	506
EGFP	488	509
Alexa 594	594	615

2.2.1.2 Laser-scanning confocal microscopy & image acquisition

The imaging of dendritic spines on hippocampal CA1 pyramidal neurones was performed with an Olympus Fluoview confocal microscope (figure 2-3) on an upright Olympus BX50WI. In a confocal microscope, the laser beam is focused on a focal plane, and the emission light resulting from excited fluorescent molecules in the sample is filtered from the excitation light through a dichromatic mirror, then collected through a pinhole and detected by the photomultiplier (PMT), a photo-detection device which then converts the light signal into an electrical one. The detector pinhole obstructs the light which is not coming from the focal plane, resulting in sharper images than conventional microscopy.

The system magnification was 3.43, to which was added the following Olympus objectives: 60X water immersion, Numerical Aperture (NA) 0.9 or 40X water immersion, NA 0.8. The confocal microscope is equipped with Argon/Krypton laser: Argon laser (488 nm, 10 mW), Krypton laser (568 nm, 10 mW), used respectively with the confocal aperture of 3 for 60X objective and 2 for 40X objective. The theoretical resolution limit (R) of an optical instrument can be determined by the formula:

$$R = 1.22 \frac{\lambda}{NA(objectif) + NA(condenser)}$$

In the case of a confocal microscope, the resolution may actually exceed the limits placed by this equation (Abramowitz and Davidson, 2010). The resolution limit for microscopy is considered with a similar formula to be around 0.2 µm.

The laser intensity is set at 6% of maximal intensity to avoid damage to the neurone and bleaching of the fluorescent probes. When the dendrites are deep in the slice, the power can be turned up to 20% to compensate for the loss of intensity by dispersion through the tissue. However, it is preferable to avoid taking images over a large depth, since the fluorescent intensity across it might not be homogeneous, and exposure to higher intensity light necessary to image deeper into the slice could damage the tissue. Consequently, most images are taken close from the surface of the slice, on portion of dendrites running almost perpendicular to the z-axis.

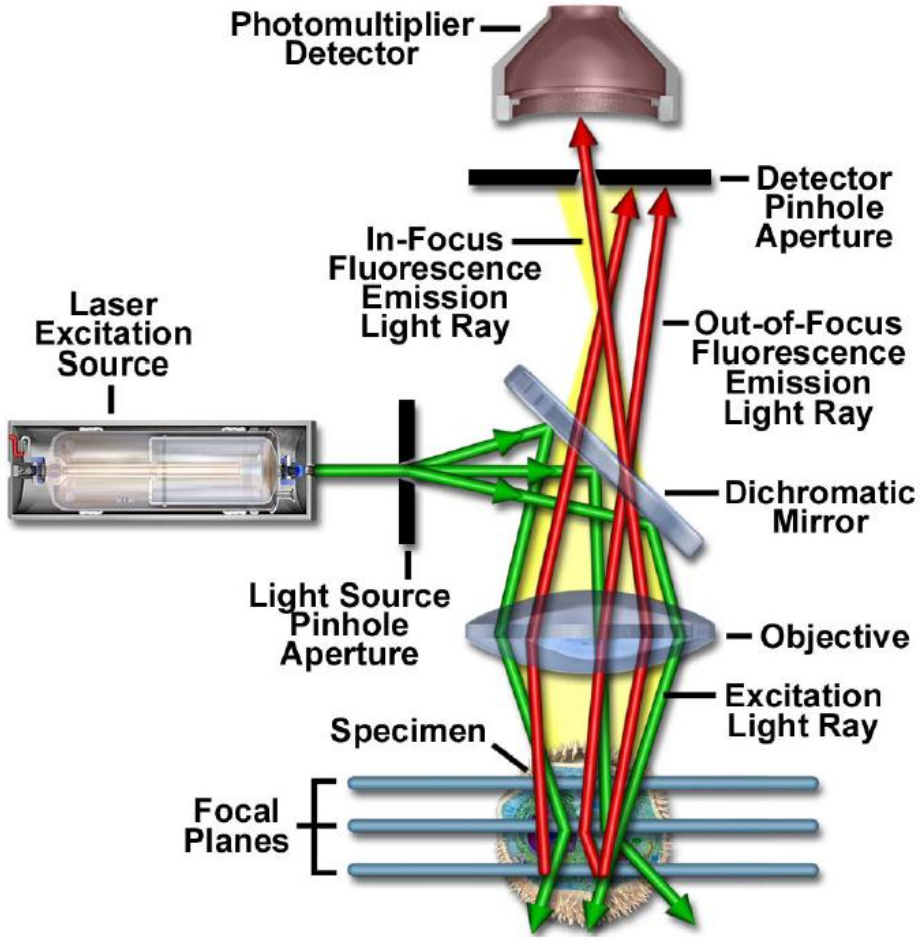

Figure 2-3: Schematic diagram of the optical pathway and principal components in a laser scanning confocal microscope (Claxton et al., 2004).

The Fluoview software was used to record stack of images taken with the Olympus confocal microscope. Three parameters could be adjusted to improve the contrast and quality of the images: the photomultiplier, the gain and the offset. The software had

an Auto set mode, but the settings could be adjusted manually to reach the "optimum balance" between contrast and intensity. Thus, the PMT was usually pushed up (around 80%), the gain was kept at 1 and the offset did not have to be used when the background noise was low. Saturation had to be avoided in order to analyse the spines with the whole range of intensity, which could be visualised by the use of pseudocolors intensity coding.

In order to avoid leaking of one fluorescent probe emission light into the channel of the second one, cut-off filters can be added individually to each channel. When working with both DiO and Alexa 594, two filters were used to separate the fluorescence: on channel 1 (Argon laser, 488 nm excitation) a short pass filter BA 550RIF was used to cut-off light of a wavelength higher than 550 nm, while on channel 2 (Krypton laser, 568 nm excitation) a long pass filter BA 610IF was used to cut-off light of a wavelength shorter than 610 nm (figure 2-4).

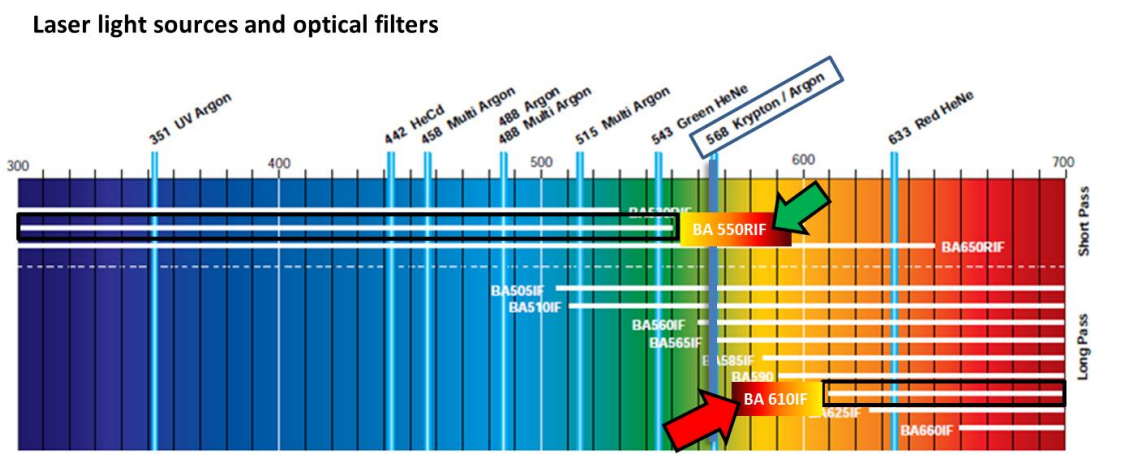

Figure 2-4: Schematic diagrams of the fluorescent wavelength and the different filters available with short or long pass.

(Adapted from http://www.olympusmicro.com/brochures/pdfs/fluoview.pdf, Olympus Fluoview brochure).

2.2.2 Image analysis

In order to set-up an appropriate and consistent method for analysing dendritic spines, it was necessary to test and further develop Imaris and in particular *Filament Tracer*. In

this section, the image analysis methods will only be briefly described, as they are the object of the first results chapter, Chapter 3.

2.2.2.1 Spine classification with ImageJ

The early analysis of spine type was carried out using ImageJ software (National Institute of Health, USA, http://rsb.info.nih.gov/nih-image/), which was used to measure spine head size and differentiate between spine types before the acquisition of Imaris.

Although spines express a large variety of shapes and sizes, they have often been classified into three major categories based on their shapes (see Introduction).

For comparison to previous work in the Edwards lab, the three categories were defined as previously published (De Simoni et al., 2003):

1. Stubby spine: the diameter of the neck is similar to the total length of the spine and no clear head is identified.

2. Thin spine: the length of neck is greater than its diameter and the head is clearly distinguishable but has a diameter less than the length of the neck.

3. Mushroom spine: the neck is shorter than it was wide and the diameter of the head is greater than the width of the neck.

2.2.2.2 Deconvolution & 3D visualisation

Before the determination of spine types, the stack images can be deconvolved and reconstructed in 3D using AutoQuantX (figure 2-5) and AutoVisualize software from Media Cybernetics. The deconvolution is a mathematical algorithm that subtracts noise due to out-of-focus light taking into account the parameters of the confocal optics and the immersion media. Deconvolution, combined with 3D reconstruction, gives higher resolution images of dendritic spines which are much easier to analyze than the original tif files, and improving spatial resolution.

The settings used for deconvolution with AutoQuantX were as follow:

- Adaptive Point Spread Function (Blind)
- Theoretical PSF
- Default settings: 10 iterations, medium noise.

The spines can be analyzed with more accuracy using the different z-sections and the 3D reconstruction. The z-direction remains however with the lowest resolution compared to that of the (x,y) plan.

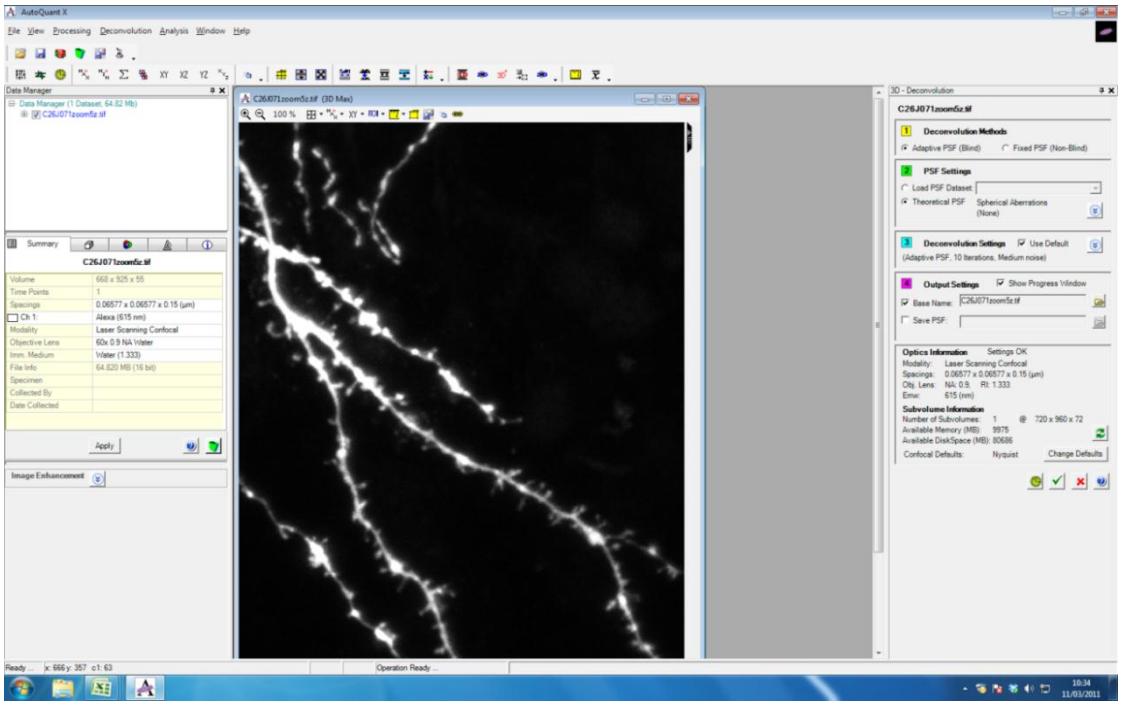

Figure 2-5: AutoQuantX interface, which enables the deconvolution of image stacks after entering the imaging parameters.

2.2.2.3 Filament Tracer from Imaris 3D Image analysis software

Filament Tracer is a recent advance from Imaris, which rebuilds neurone's dendrites and dendritic spines from stacks of images. Using a new software required many trials to ensure that the result obtained were satisfactory and unbiased. The testing method and the parameters finally selected with the last version of Imaris (7.2.0 from December 2010) are described in detail in Chapter 3 and thus not repeated here. All analyses were performed blind to experimental conditions.

NB: In this chapter, spines have been divided by types as well, but filopodia are not included in the analysis. Most of the work done which required intensive image analysis was done on 14 DIV cultures, an age when filopodia are very rare (less than 5%), in fact hardly any were found on my cultures. Hence, the very few filopodia present were either integrated among the thin spine category, or excluded if their length was more than 3.5 µm.

2.2.2.4 Statistical analyses

Spine density was calculated by adding up all the spines (both stubby and headed spines), and dividing the total number of spines by the total length of dendrite analysed for a particular cell. The density per condition was thus determined as mean ± SEM of individual cell densities, and compared between conditions using Student t-test or one-way ANOVA with Bonferroni's post-test.

Unlike spine density, which can only be measured per cell, measurements of spine parameters such as length or head size can be measured individually, thus dramatically increasing the sample size and thereby the probability of detecting changes. Only headed spines were included in the analyses of spine head size and spine length. In order to even out the weight of each individual cell on the final result, the same number of spines, randomly selected from each cell, was included in the analyses. The number of spines in each cumulative distribution is then proportional to both the number of cells in a group and the smaller number of headed spines analysed per cell in the same group (Kopec et al., 2006; Yasumatsu et al., 2008; Nakamura et al., 2011). Following D'Agostino & Pearson omnibus normality test on the sample of spine length and spine head size in all groups, most distributions differ very significantly from a normal distribution, and thus non-parametric tests were used to compare them. The distributions were compared using a Mann-Whitney test or a Kruskal-Wallis with Dunn's post-hoc test as appropriate.

2.3 Experimental procedure in the Malinow lab (UCSD)

In this section are presented the methods used during a six months rotation in Professor Malinow's laboratory at UCSD, the results for which are shown in Chapter 5.

2.3.1 Rat and mouse acute and organotypic slices

Organotypic slices were made from brains isolated from either P7 Sprague-Dawley rat or P5 C57/Black6 mouse pups, using an automatic tissue chopper on the hippocampus previously removed from the whole brain. The method differs from the one used in

the Edwards lab, where the half brain is sliced as a whole and the hippocampus is dissected from the slice and not isolated from the whole brain. The method here enables the preparation of slices from the whole hippocampus and not only from the dorsal part, as happens when slicing the half brain.

The culture medium was based on MEM Eagle medium reconstituted, and contained 20% heat inactivated horse serum, 200 nM L-Glutamine, 1 mM $CaCl_2$, 2 mM $MgCl_2$, 13 mM D-Glucose, 5 mM $NaHCO_3$, 30 mM Hepes, Ascorbic acid (from 25% solution), and 1 mg/ml of insulin. The pH was adjusted to 7.27-7.28 with NaOH, and the osmolarity was finally adjusted to 320 ± 3 with Milli-Q H_2O. The solution was sterilized by passing through 0.22 µm filter, aliquoted in 50 ml falcon tubes and stored at +4°C for up to 2 weeks. The slices were maintained very similarly to the Edwards lab protocol, in accordance with the Stoppini method (Stoppini et al., 1991).

2.3.2 Whole cell recordings – voltage clamp, current clamp, paired patch

2.3.2.1 Internal solutions

For current clamp recordings and firing experiments, a K^+ gluconate based internal solution was used, which does not block potassium channels. The internal solution contained:

Kgluconate 130 mM, KCl 5 mM, HEPES 10 mM, $MgCl_2$ 2.5 mM, Na_2ATP 4 mM, Na_3GTP 0.4 mM, NaPhosphocreatinine 10 mM, EGTA 0.6 mM, bubbled with 95% O2 / 5% CO2. pH is adjusted to 7.2 and osmolarity to 317. The medium was filtered and stored at -20°C.

For voltage clamp recordings, a Cs^+ methanesulfonate ($CsCH_3SO_3$) based internal solution was used, Cesium ions blocking potassium channels and thus reducing the flux of currents in and out of the cell, thereby making recordings more stable. The osmolarity of the solution was adjusted to 317, and pH to 7.2.

The internal solution contained: $CsCH_3SO_3$ 115 mM, CsCl 20 mM, HEPES 10 mM, $MgCl_2$ 2.5 mM, Na_2ATP 4 mM, Na_3GTP 0.4 mM, NaPhosphocreatinine 10 mM, EGTA 0.6 mM, bubbled with 95% O2 / 5% CO2.

2.3.2.2 External solutions

The ACSF was made freshly from a stock solution containing 119 mM NaCl, 2.5 mM KCl, 26 mM $NaHCO_3$, 1 mM NaH_2PO_4. The remaining components were added up to their final concentration: 11 mM glucose, 1 mM of $MgCl_2$, 2 mM $CaCl_2$. The solution was gassed with a mixture 5% CO_2 / 95% O_2, and maintained at the temperature of 32 ± 2°C. The pH was readjusted to 7.3 if necessary.

For mEPSC recordings, the solution contained the NMDA receptor blocker APV at 100 µM, TTX at 1 µM, and picrotoxin at 100 µM.

For the recordings, the glass electrode tip resistance was 3-5 MΩ, the series resistance was kept below 15 MΩ, and input resistance was at least ten times the series resistance. If the values changed more than 10% during experiments, the recording was discarded. Noise levels were controlled and were on average 3 ± 1 pA, while the current injected had to remain below 0.1 pA for the recording to be included in the analysis.

2.3.2.3 mEPSCs recordings and analyses

Recordings of mEPSCs were performed with Igor Pro software, the signals being filtered at 2 kHz and sampled at 5 kHz. Whole cell patch-clamped CA1 pyramidal neurones were held at -60 mV for the duration of the recording. Analyses of mEPSCs recordings were performed blind to the experimental conditions, using *Synaptosoft* mini analysis program. Decay time was measured from the 90 %-10 % peak value compared to the baseline determined over 2 ms of recordings, 8 ms before the peak.

Chapter 3. Dendritic spines analysis: Optimisation of the method using Imaris *Filament Tracer*

3.1 Introduction

To achieve such a high processing power and to enable the fantastic ability to learn and to remember, the brain relies on a highly elaborated machinery, capable of both adaptability to evolving inputs, and of maintenance from minutes to months of sensitive information. Synaptic plasticity is thus an essential property of neurones in the central nervous system. Dendritic spines, as the post synaptic site of most excitatory inputs in the brain, are particularly subject to plasticity, as they are believed to account in part for the material support of memories. Looking at dendritic spines population and plasticity is an effective tool to study synaptic aspects of cell adaptation under altered conditions. In this chapter, I review the various methods previously used in our lab for spine analysis and their limitations, before evaluating in depth the advantages and drawbacks of using an automated method of analysis with the Bitplane software *Filament Tracer*. After investigating the most reliable way of using the software and working extensively with Bitplane on its improvement, the results were compared to those obtained with previous methods and a new automated way of sorting spines was implemented.

3.2 Spine analysis: limitations of previously used methodology

Dendritic spines constitute a fundamental support for synaptic activity, and if their shapes and sizes can be objectively defined, they become a valuable tool in synaptic analysis in both health and disease. Many diseases such as Down's syndrome (Ferrer and Gullotta, 1990), Alzheimer's disease (Knobloch and Mansuy, 2008; Knafo et al., 2009; Smith et al., 2009) or fragile X syndrome (Comery et al., 1997; Irwin et al., 2000; Cruz-Martin et al., 2010), exhibit abnormalities in dendritic spine distribution, emphasising the role of those protrusions in the efficient transmission of information, and the necessity to understand how to restore it to its functional state.

3.2.1 'Eyeball' morphological classification

The existence of dendritic spines was first observed by Ramón y Cajal at the end the 19th century, using Golgi staining. He already suspected that these protrusions played a significant role in the transmission of information between neurones. Back in 1969, Ruiz-Marcos and Valverde studied the distribution of dendritic spines in the visual cortex of normal and dark-raised mice (Ruiz-Marcos and Valverde, 1969). The wide range of dendritic spines appeared to fall into three main categories that were described according to their shape: thin, mushroom and stubby spines. Those categories, along with filopodia and branched spines, have since then been used as a fundamental architecture to classify spine. More defined parameters have succeeded with Kristen Harris' electron microscopy imaging analyses, where the visual parameters were coupled with dimensional ones (Harris and Stevens, 1989; Harris et al., 1992). These parameters have since been used with little variations in countless studies involving spines (De Simoni et al., 2003; Matsuzaki et al., 2004; McNair et al., 2010).

However, the categorisation of spines according to measured parameters has several drawbacks:

- The different categories are not exclusive of each other, and thus about a third of the spines are unclassifiable.
- Electron microscopy offers an excellent resolution of spines, and thus easier classification, but is extremely time-consuming and thus prevents analysis of very large samples.
- Confocal or two-photon imaging techniques allow sampling of large numbers of spines, but the output images require processing such as deconvolution.

The reliance on visual determination of categories introduces a degree of subjectivity, and results differ from user to user. Analysis performed in the Edwards lab on similar organotypic hippocampal cultures revealed that the proportions of the different spine types differ greatly from one user to the next, essentially because of the difficulty of finding exclusive definitions. For instance, a mushroom spine was often defined as having a large head to neck diameter ratio by the Harris group (Harris et al., 1992), to be later redefined by the width of their head, if above 0.6 µm as measured with the precision of electron microscopy (Bourne and Harris, 2008).

Table 3-1 regroups a sample of published article dealing with dendritic spine analysis, and the various definitions used to classify them, illustrating the disparity of the criteria selected by each lab to identify certain entities. Some labs settled on strictly non-overlapping parameters (Oray et al., 2006), while others select only spines which fall into one of their set of visual criteria, and do not classify the remaining spines (Matsuo et al., 2008).

The most commonly used definition, from Kristen Harris (Harris et al., 1992), leaves many spines in an intermediate state between the mushroom and thin categories, both sharing the same feature of having the neck diameter smaller than the head. Thin spines also include a restriction on the neck diameter to spine length or neck length ratio. However, when trying to sort spines out myself, I found that many spines do have a head much larger than the neck, but the spine length was quite short and thus was not fitting the thin spines criteria. Nor did they fit the mushroom spine criteria, since their head was not huge. Moreover, resolution limits affect the visual evaluation of the neck, or its measurement with a simple line over the projection.

Table 3-1: Sample of definitions of spine types from the literature.

Key: SMinD = Spine Minimum Diameter = Spine Neck Diameter

SHD = Spine Head Diameter; SL= Spine Total Length; SNL = Spine Neck Length.

Author	Mushroom	Thin	Stubby
(Harris et al., 1992)	SMinD <<< SHD	SMinD <<< SL SMinD ≤ SHD	SMinD ~ SL
(De Simoni et al., 2003)	SHD/SMinD ≥ 2	Head visible SL > SminD SHD~ SMinD	SL~ SMinD
(De Simoni and Edwards, 2006)	SNL < SMinD SHD > SminD	SNL > SMinD SHD < SNL	SL ~ SMinD No head
(Oray et al., 2006)	SL/SMinD > 2 SHD/SMinD ≥ 1.3	SL/SMinD > 2 SHD/SMinD ≤ 1.3	SL/SMinD ≤ 2
(Matsuo et al., 2008)	large head with a neck	long neck but small head	Large head but no neck
(McNair et al., 2010)	SHD/SMinD > 1.4	SL/SNL < 1.4	SHD/SMinD ≤ 1 SL/SMinD ≤ 1
(Calabrese and Calpain, SfN, 2010)	SHD/SMinD ≥ 1.5	SHD/SMinD < 1.5 1 µm ≤ SL ≤ 3 µm	SHD/SMinD < 1.5 SL < 1 µm

Concerning stubby spines, similar aberrations can be found in their definition. The absence of a clear neck/head structure was the main criterion. However, only protrusions with a similar total length to width would be considered as stubby, as longer spines with no clear enlargement of the head would still have diffusion properties similar to that of thin spines (Korkotian and Segal, 2007), and as such would

differ from the very short and open protrusions. There is therefore a series of intermediate spines which visually reside in between stubby and thin spines, or in between stubby and mushroom, when the head is very large and the short neck may be invisible because of noise or resolution limits.

The graphs of figure 3-1 show the disparities in the measurements of spine type distributions in similar samples of CA1 pyramidal cells, labelled with the fluorophore Alexa 594 through patch clamp, in rat organotypic slices at 7 and 14 DIV. Though the preparations were similar, the difference observed in relative proportions was attributed, after thorough examination, to the individual appreciation of parameters used to define spine types, such as “much greater than”.

The major difference in the estimated proportion resided in the evaluation of mushroom spines. In both analyses their number was found to be very stable, but their percentage reached 25% in one case (Caroline), and only 12% in the second case (Anna de Simoni), (figure 3-2). Those trends were confirmed with statistical analysis, a two-way ANOVA differences showed significant differences (interaction: 7 DIV, $p=0.0002$, figure 3-2A; 14 DIV, $p=0.003$), and a Bonferroni’s post-test analysis specifically emphasised the difference in the percentage of mushroom spines.

The disparity in spine type distribution suggested that cross-experimenter comparison was not possible with eyeball determination of spines. Moreover, even a single user judgement of spines can vary significantly when analysing the same set of data on different days, emphasising that visual analysis is prone to user bias.

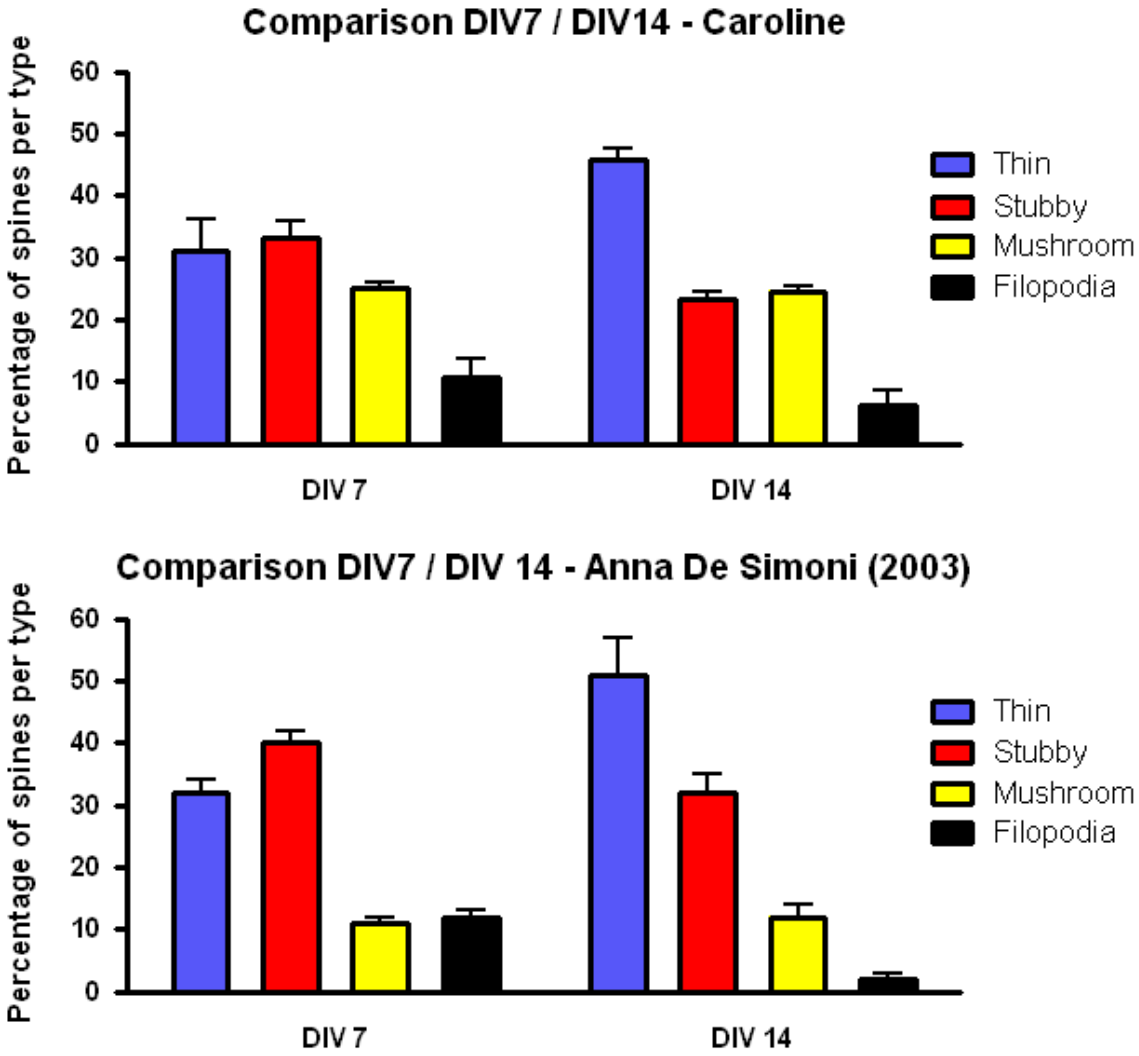

Figure 3-1: Disparity in spine type distributions in similar preparation attributed to individual classification.

Dendritic spines were analysed on similarly prepared rat organotypic slices, labelled with Alexa 594 intracellularly, then imaged with confocal microscopy after 7 or 14 DIV. In both user analyses, the different groups (thin, stubby, mushroom and filopodia spines) show a similar evolution between 7 and 14 DIV, stubby spines being equally or even more abundant at 7 DIV, and overtaken by thin spines at 14 DIV (Data: mean percentage of spine, error bar: SEM, 7 DIV: n=4 cells, 14 DIV: n=5 cells).

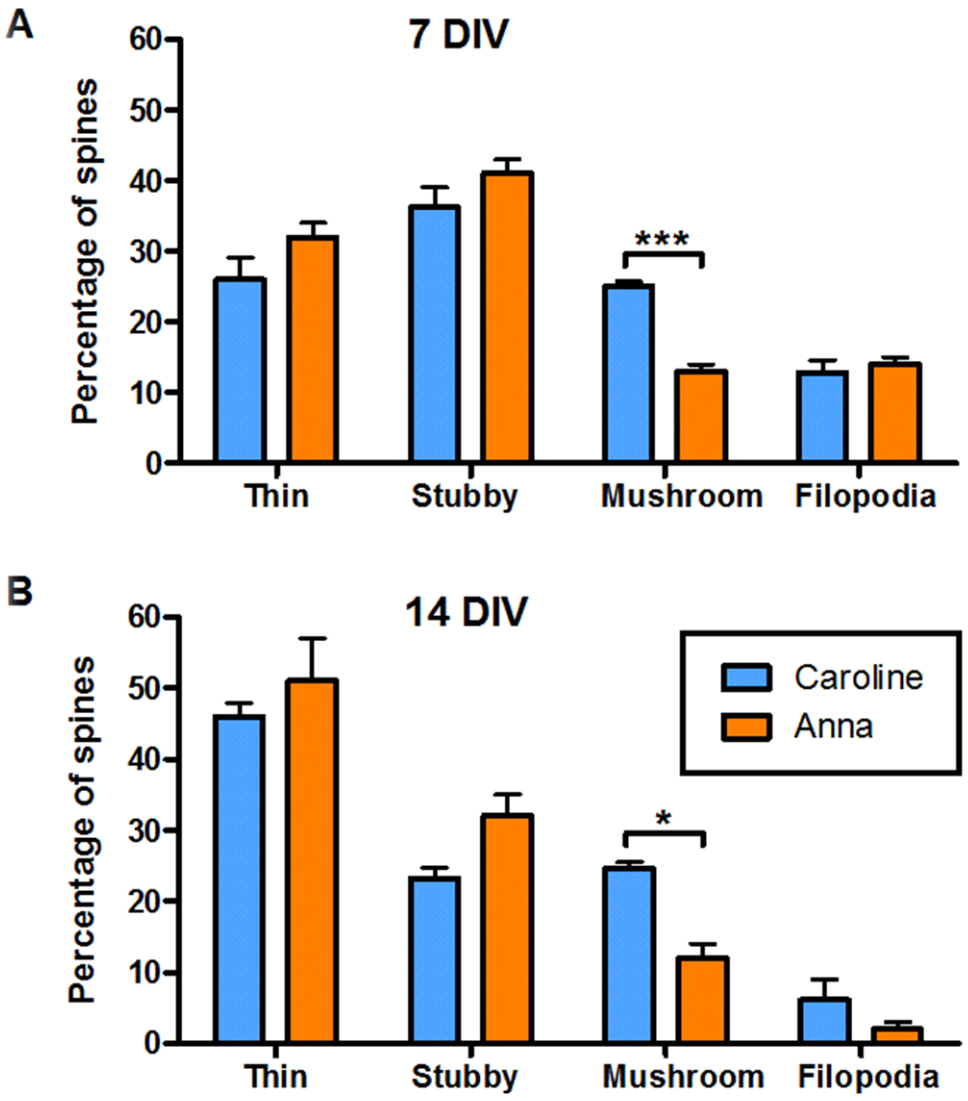

Figure 3-2: Comparison of spine types determined by eye by two different users.

Side to side presentation makes it possible to see more precisely which type of spines creates the main source of disparity. Same data as on figure 3-1. A two-way ANOVA on both groups found a significant interaction between spine type and user (figure A: 7 DIV, p=0.0002; figure B: 14 DIV, p=0.003). In both cases, a Bonferroni's post-test analysis showed differences in the percentage of mushroom spines between the two users.

The abundance of spines falling in-between multiple types, as shown by Harris' electron microscopy data (Harris et al., 1992) where 25% of spines could not be classified, and the lack of precision of 2D image analyses led us to explore a new analytical method which would take only spine terminal points into account using the NIH software ImageJ.

3.2.2 Line-scan of spine head with ImageJ

3.2.2.1 Principle

The arbitrary classification of up to 25% of dendritic spines – that percentage related to unclassified spines according to Kristen Harris' parameters in one of her earliest electron microscopy studies (Harris et al, 1992) – made us look for alternatives to eyeball classifications.

ImageJ is a free Java-based software developed at the National Institute of Health in Bethesda (Rasband, 1997), that allows powerful analysis of stack files such as tif format. Image analysis is still carried out on 2D images or z-projection, but it is easy to scroll through the z-axis to get an in-depth vision of the structure. Light intensity of a line-scan parallel to the dendrite and across the largest section of the head gave a series of points, pairing the distance x from the start of the line with the luminescence intensity i at that point (figure 3-3A). The group of (x,i) points generated can be plotted and fitted into a Gaussian curve by Prism, a software from GraphPad (figure 3-3B). The Gaussian curve can be defined by the position of its peak intensity and its standard deviation σ, a measure of the width of the distribution (figure 3-3C). The percentage below the curve corresponds to the portion covered one, two or three standard deviations from the mean value in both directions, respectively 68.2%, 91.4% and 95.6%. Since stubby spines do not have a clear head distinct from the dendrite, they cannot be analysed with a line-scan and are thus only counted for spine density but not measured here.

The estimation of the dendritic spine head is then left to the user, guided by the value of the curve fitting. When possible, a calibration can be performed by using standard-sized beads filled with fluorescent dye. A good estimation of the diameter of a bead relative to the parameters of the Gaussian curve fitting the line intensity across it is 2.35 times the standard deviation (Peter Haslehurst, unpublished data), which corresponds to the section of the curve at the point of half-maximal intensity (figure 3-3D).

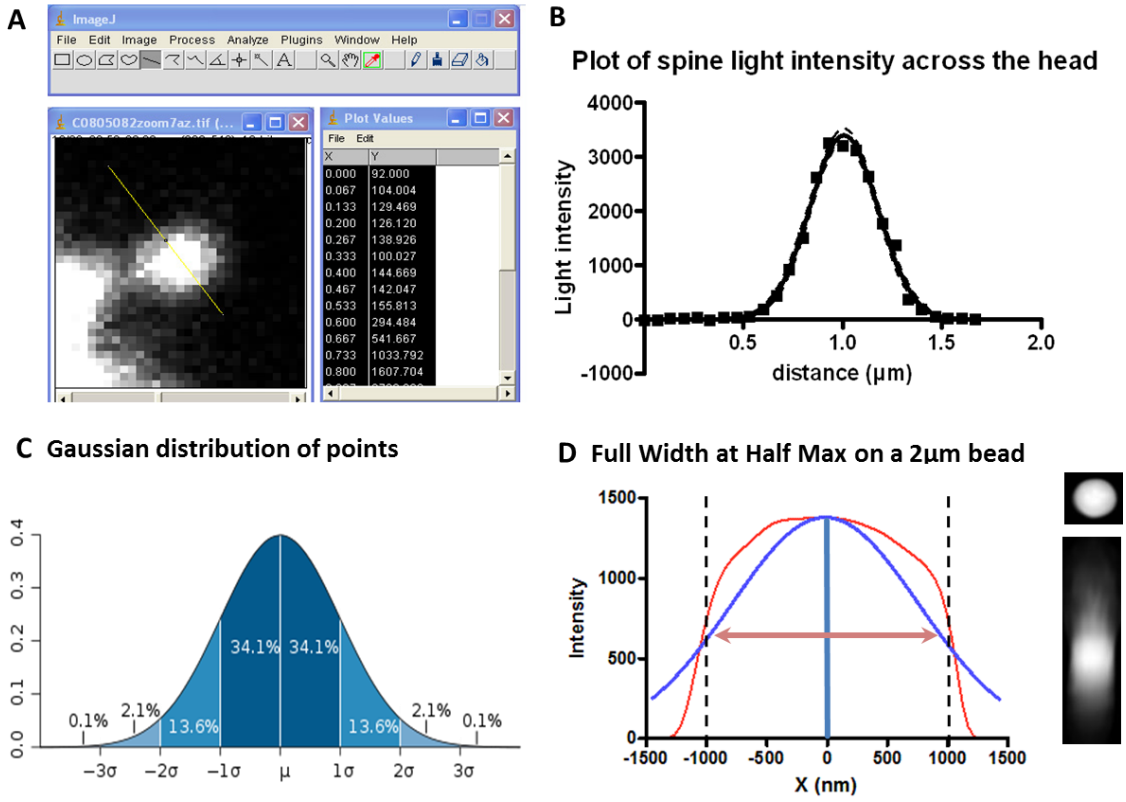

Figure 3-3: Estimation of spine head diameter from light intensity analysis over line-scan of the spine terminal point.

The largest section of the head is determined by looking through the z-stack, and the line is placed across the largest section of the head (A). The plot of light intensity across the line can be fitted with a Gaussian curve with Prism (B), and the spine head diameter can be estimated from the standard deviation σ of the curve (C) or by using standardised beads to determine the multiple of σ which estimates the head size more accurately (D, Peter Haselhurst unpublished data).

This line-scan technique is useful because it can be performed on raw data, using 2D images and thus is little affected by the scatter of light along the z-axis. Using this new method for analysing spine head size, I then plotted the distribution and examined goodness of fits with a single or a multiple Gaussian. The latter would suggest the existence of two different populations of spines, which could be identified by their average head size, each constituting a sub-category of spine.

By grouping the data of hundreds of headed spines in similar culture conditions, I found that spine head sizes are normally distributed, the distribution fitting a Gaussian curve with a high fidelity (figure 3-4, n=1149, r^2= 0.976).

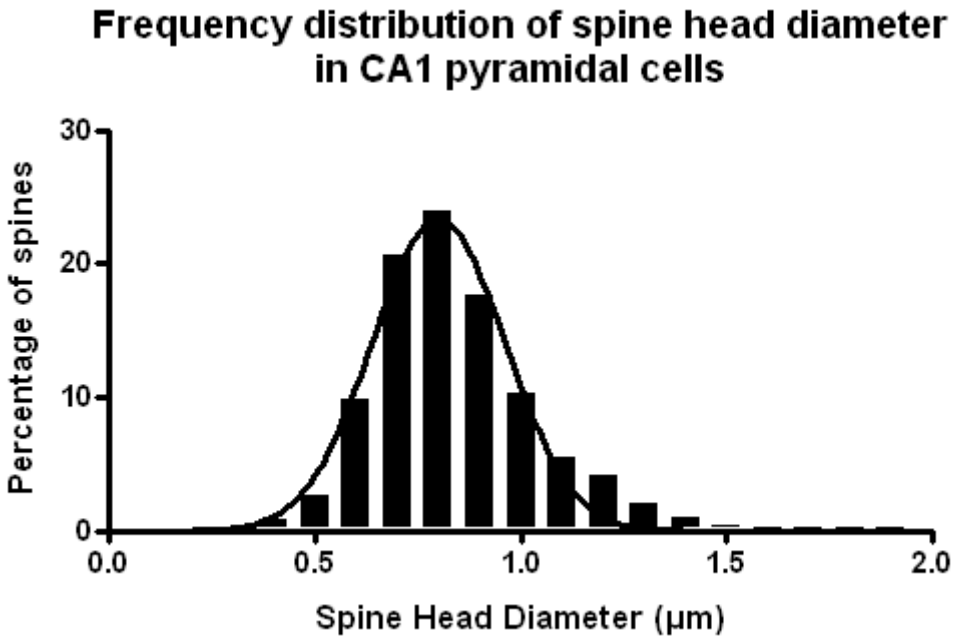

Figure 3-4: Frequency distribution of spine head size analysed with ImageJ line-scan.
Spines showing a clear neck, with the head clearly distinguishable from the dendrite, were analysed in this study, while stubby spines were discarded. A non-linear fit of the data gave a very good correlation with the Gaussian theoretical curve (n=1149, r2=0.976), strongly suggesting that spine head sizes are normally distributed.

3.2.2.2 Advantages and drawbacks

Using ImageJ line-scan intensity plot to analyse spine head size has several undeniable advantages over the 'eyeball' classification.

One of the major advantages of ImageJ is that it is freely accessible on the internet, can be downloaded on any computer and offers a large range of analytical possibilities.

The user intervention during the processing is limited to the choice of the largest and most in-focus section of the spine head by running through the images along the z-axis, and then setting the line across it, the user being of course blind to the conditions of the experiment. This assessment can be by-passed by measuring several cross sections, or using a projection of maximal intensity. However, although the latter is

often used (Korkotian and Segal, 2007; Matsuo et al., 2008; Honkura et al., 2008) , non-deconvolved projections are noisy and very sensitive to drift, and thus line-scan on a single plane was preferred. Compared with the former spine type analysis, there is no pressure to make the spine fit into one or another category, and thus removing ambiguity and subjectivity.

However, ImageJ is mainly a 2D software which can deal with image stacks. Therefore it also presents limitations for the analysis of 3D structures such as dendritic spines.

The images acquired with Fluoview are tif files, i.e. stack of (x,y) planes taken at repetitive interval along the z-axis. As mentioned above, the software cannot cope with the (x,y,z) parameters of the spines, and thus only treat the images as two-dimensional. The angle of the spine neck is not taken into account, and therefore the calculations of spine length and to a lesser extent spine head diameter are affected by it. The measures remain dependent on the parameters chosen for the determination of the edge (e.g. a multiple of the standard deviation of the Gaussian fit, see figure 3-3C), reminding us that, at this resolution, the measures are objective estimations relying on previous beads fitting (Peter Haselhurst, unpublished data) and not absolute values.

Another concern about the line-scan analysis is that it requires sufficient background space in line with the largest section of the spine to measure noise level around that spine. Thus, there are a variety of cases where spines cannot be measured: very short spines, spines presenting a large angle from the (x,y) plane and cannot be distinguished from the parent dendrite, and spines in very populated areas (figure 3-5).

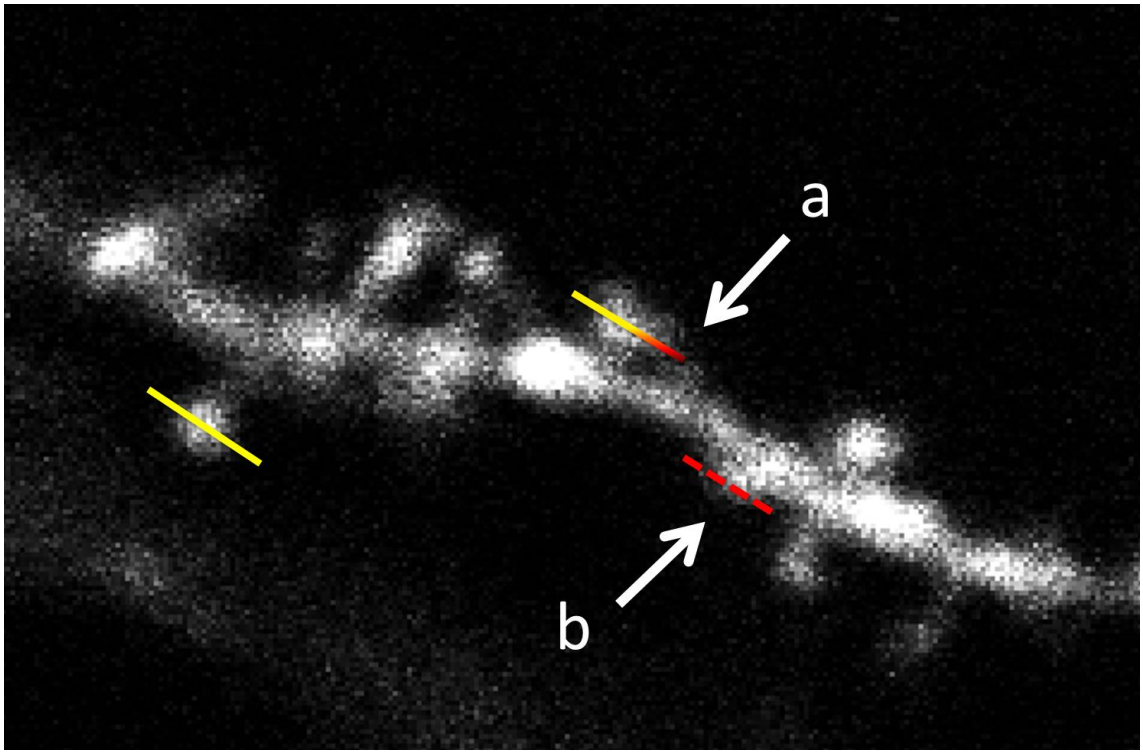

Figure 3-5: Line-scan limitations on certain spines.

This example shows the limitations of line-scan analysis, which can be easily conducted on isolated spines in a 2D plane (yellow line), but can be dampened by the proximity of two spines (a, gradient line) or when the spine cannot be distinguished from the parent dendrite (b, red dotted line), preventing a proper line-scanning of the spine head.

3.2.3 Deconvolution

The light travelling through the tissue is distorted, introducing blur on the edge of the shapes, on top of the shot noise due to the digitalisation of the data. Deconvolution is a widely used image processing technique, which reduces the optical noise generated by the contribution of out-of-focus fluorescent points and by the distortion due to the optical instrument. The image of a fluorescent dot, called Point Spread Function (PSF), can be determined theoretically from the characteristics of the optical instrument and the imaging conditions. Deconvolution software uses this PSF as the template for running the algorithm-based process that restores images, reversing the optical distortion and consequently improving the Signal-to-Noise Ratio. It is essential when examining small morphological features such as dendritic spines, co-localisation of different fluorophores, or extracting measurements from images.

The necessity of deconvolution for spine type classification depends on the type of analysis required.

- For visual classification, fine structures such as necks need deconvolution to help with their visual identification.
- When studying spine head diameter using line-scan intensity analysis, deconvolution is not strictly necessary. Indeed, spine head analysis is done on 2D images, in the (x,y) plane, while confocal microscopy images are mainly distorted along the z-axis. Thus, the absence of deconvolution is not an obstacle to the measurement of spine heads on 2D images, though the dimensions differ greatly from those obtained on deconvolved images (see 3.4.1).
- When it comes to neck measurements, the presence of out-of-focus light impacts more heavily on the estimation of the neck size, because the blur is in the same range of size as the object itself. Thus deconvolution is necessary in order to study spine necks.

The contrast in resolution, as shown on figure 3-6 before (A) and after (B) deconvolution, is striking. The deconvolution gives a smoother image of the dendrite and spines, while sharpening the edges and increasing the signal-to-noise ratio.
The resolution of spines along the z-axis can only be done after deconvolution of the data, and using 3D viewer. Indeed, the intensity on a 2D image before deconvolution is affected by the intensity of the plans above and below. Deconvolution increases greatly the number of spines identifiable on an image. However, it is important to note that deconvolution has its own limitations and new imaging techniques such as STED can prevent the necessity of using deconvolution algorithms by diminishing the out-of-focus light collected.

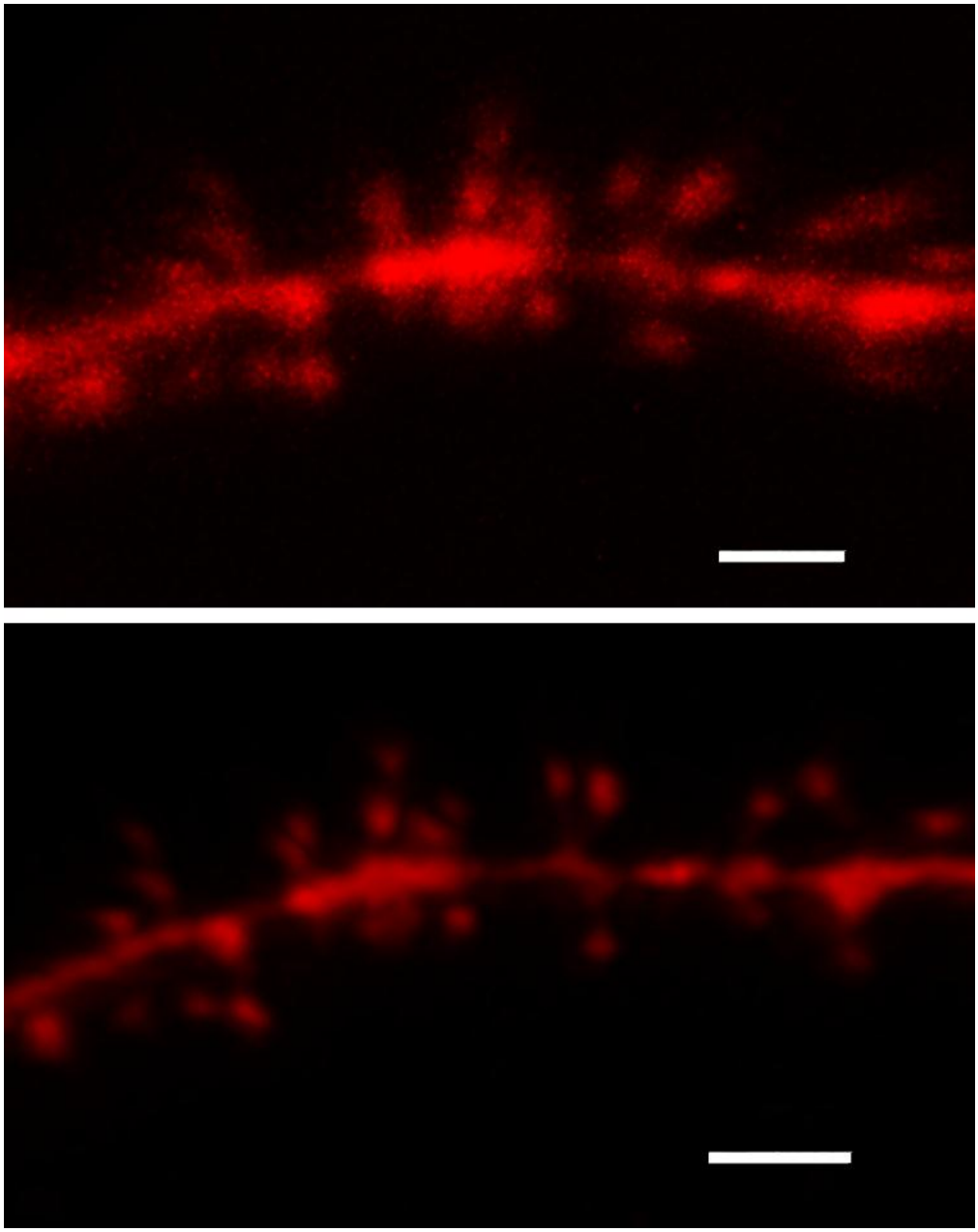

Figure 3-6: Effect of deconvolution on image resolution.

(A) 3D image of a spiny dendrite acquired with a confocal microscope, before deconvolution. (B) Same image after processing with AutoQuantX software from MediaCybernetics. Deconvolution usually enables one to identify more spines on the dendrite, which would otherwise be undistinguishable from the noise. Scale: 2 µm.

3.3 Spine reconstruction with Imaris *Filament Tracer*

As outlined above, spine analysis is both prone to bias and time-consuming. Therefore, any automated way of extracting various spine parameters in an unbiased way would greatly improve and facilitate dendritic spine analysis. Few types of software have gone to the extent of the new Bitplane software, Imaris *Filament Tracer*, which provides automatic detection of filaments in 3D microscopic images.

3.3.1 A very powerful software

Imaris *Filament Tracer* is a recent software package from Bitplane developed specifically for the analysis of 3D images of filaments and dendritic spines (figure 3-7). Some computer programs already offered 3D reconstruction of neurones, for a better visualisation of the structure in space. Imaris *Filament Tracer* is one of the very few commercially available pieces of software that allows semi-automatic rebuilding of the dendrites and the spines of neurones, thus computing many parameters from a single stack of images.

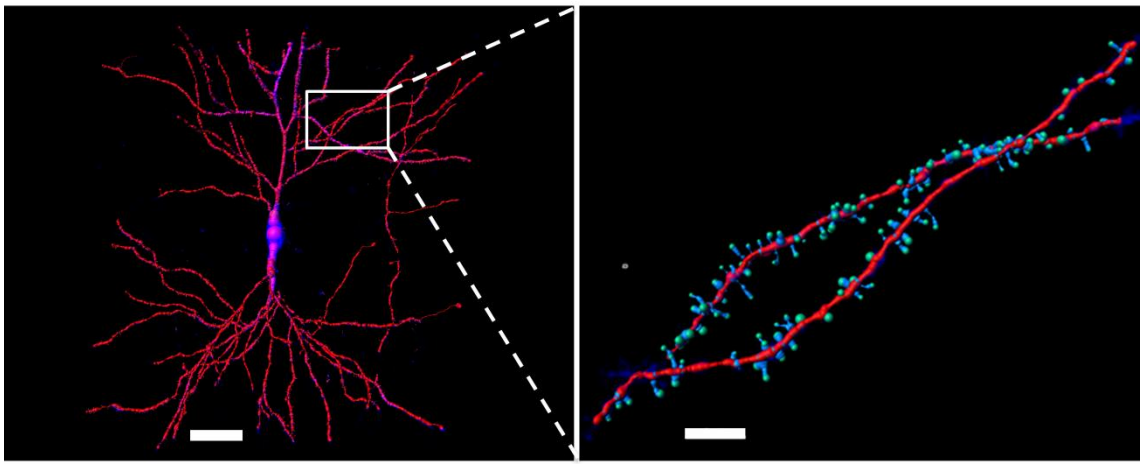

Figure 3-7: 3D reconstruction of a cell using Imaris *Filament Tracer*.

The stack of images from a neurone can be reconstructed with Imaris in a full 3D, and dendritic spines can be identified automatically. Scale: left 30 µm, right 5 µm.

The software rebuilds the dendrites by tracing a filament through the line of maximal intensity, starting from a seed point that can be adjusted manually, to encompass only the segment of interest for the analysis (figure 3-9 A&B). Once the dendrite has been rebuilt, the software automatically detects the points of strong intensity on the image, and places a seed point in them, as the centre of a dendritic spine. The seed points can be set entirely automatically, but can also be added or deleted by the user independently.

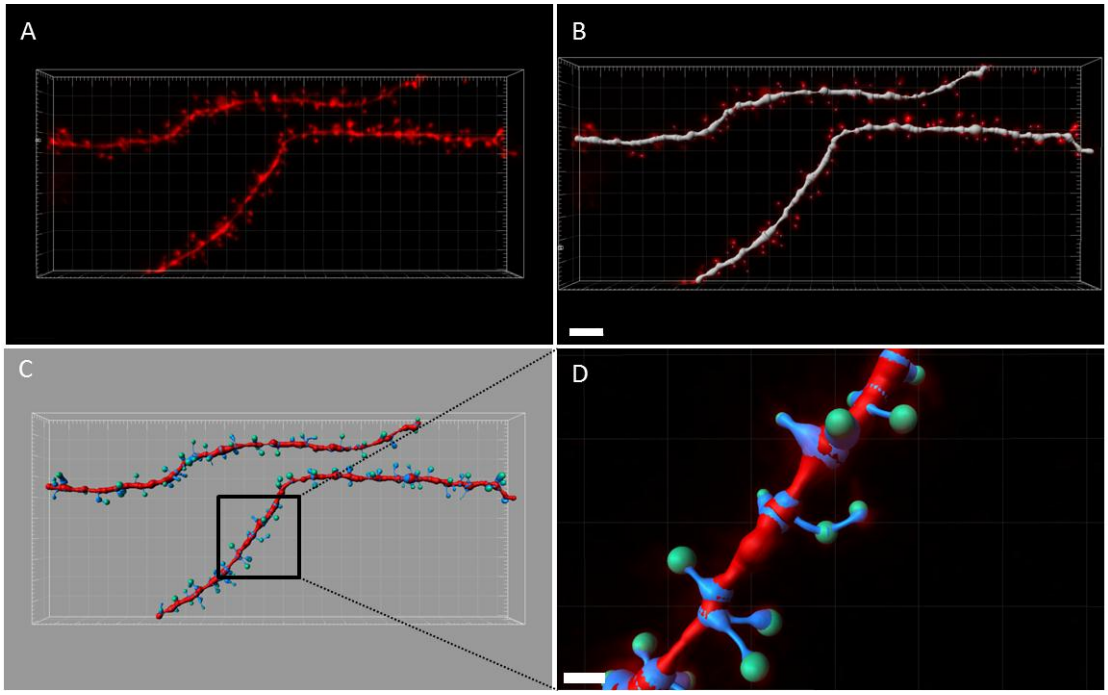

Figure 3-8: Building of a filament with Imaris *Filament Tracer* 7.2.0.

The raw image is viewed in 3D with Imaris (A), before being used as the template for building a filament, the edges of which match as closely as possible that of the dendritic spine on the image. The dendrite is rebuilt in a first step, and then the seed points are set along it, at the centre of the spine heads (B). The spines are later rebuilt, thus completing the filament (C), which match very well the original image (A). Image (D) shows an enlargement of the rebuilt filament, the dendrite labelled in red, the spines in blue, and their terminal point in green. Scale: B 3 µm, D 0.8 µm.

The size of the seed point, as well as the maximal length of a spine are set previously to eliminate all the objects which do not fit the required criteria. Once the spine seed points are correctly distributed, the software determines the "local threshold", i.e. the

intensity value which sets the most probable edges of the spines according to published data (see paragraph *1.3.2.1 Spine Local Threshold*). Two algorithms are proposed to determine the size of the spine terminal point (or spine head diameter), using 3D measurements:

- ***Shortest Distance* to map**: Considers the spine radius as the shortest distance from the seed point to the edge of the spine head, in any (x,y,z) direction (figure 3-9A).
- ***Approximate Circle* of cross-section area**: Averages the cross-section areas perpendicular to the neck axis for the whole spine head in order to determine the head volume, and returns the diameter of a sphere of equal volume (figure 3-9B).

These two algorithms will be referred to as *Shortest Distance* (or SD) and *Approximate Circle* (or AC) throughout this chapter.

By using the surface area of each section to estimate the volume of the sphere, the *Approximate Circle* algorithm evaluates much more accurately spine head size, including spines with non-spherical heads. This is very important as a significant proportion of the largest spines have heads more elongated than spherical. Since the *Approximate Circle* algorithm uses the neck axis to determine the volume of the head, stubby spines will be overestimated, as there is no constriction between the head and the dendrite. Therefore, to measure parameters relative to headed spines, the *Approximate Circle* is the most reliable algorithm. However, the sorting of stubby spines will have to be processed with the *Shortest Distance* algorithm, which is not affected by the absence of neck constriction.

NB: It is worth mentioning that, although the diameters given with the *Approximate Circle* algorithm can seem beyond the optical resolution limit of 0.2 µm at times, the value does not derive from a direct 2D measurement of the spine head diameter but from the evaluation of its volume. In order to relate to the literature, the equivalent spine head diameter is preferred to spine head volume for the plots.

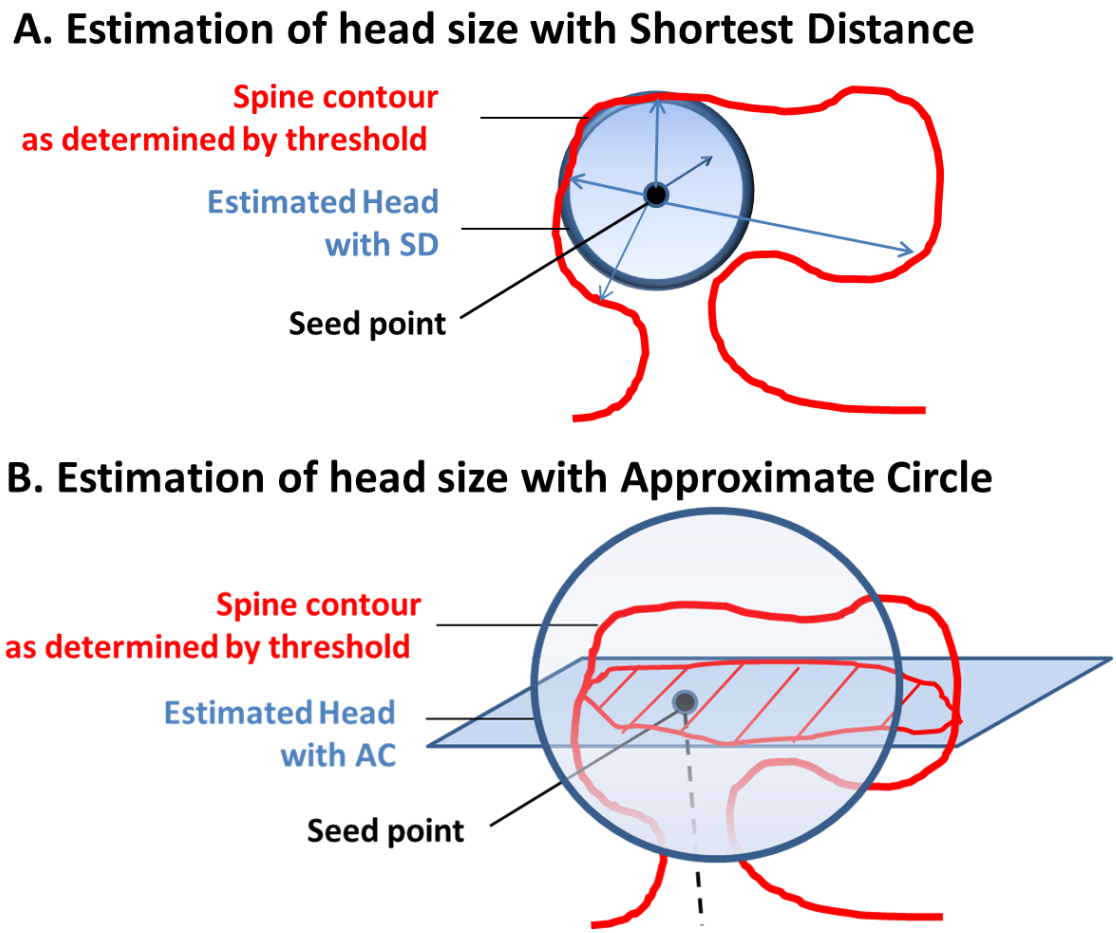

Figure 3-9: Scheme of the measurements used for the estimation of the spine head diameter with the algorithms available in *Filament Tracer*.

(A) Estimation of spine head diameter with SD leads to an underestimation of the measure. (B) The AC algorithm evaluates the whole shape of the spine head, and can estimate precisely non-spherical heads. It returns the diameter of a sphere whose volume is identical to the one measured by compiling all the cross-section areas.

Once the algorithm is selected, the edges are rebuilt and the dendritic filament and its excitatory spines are now visible on the screen (figure 3-8 C&D). The parameters relative to both the dendrite and the spines can be extracted in the very user-friendly interface of Imaris, which allows selection of the parameters to be exported into Microsoft Excel format.

3.3.2 User sensitivity

Although Imaris *Filament Tracer* is an automated alternative to manual analysis, it still requires user input at certain stages. In the following section of this chapter, the effect of users' input on the final outcome was studied following several simulations. Here are reviewed the points of concerns, where the user can introduce bias in the analysis by his implemented choices, and how it affects the measurements.

3.3.2.1 Spine Local Threshold

To ensure that the filament correctly fits the edge of the spine, the algorithm needs to be adjusted to the particular conditions of the image, which include the brightness, noise level and local contrast with the background. Those parameters, and especially the brightness, can differ greatly between the dendrite and the spines, or even between different areas on the same image. In order to adapt the modelling to the potential differences in fluorescence between dendrite and spine, the software makes it possible to set different "local thresholds".

The threshold for the dendrite was left to the automatic suggestion of the program, as it made little difference to the spines. However, when it comes to spines, the modulation of their local threshold has a significant impact on the values collected, such as the spine terminal point diameter (i.e. spine head size) or spine neck diameter. Moreover, in some cases, like when the intensity levels vary a lot across the image (e.g. when the image contains both a segment of the bright apical dendrite and segment of dimmer second order branches), the program cannot compute a local threshold, leaving the users with the responsibility of selecting the threshold manually.

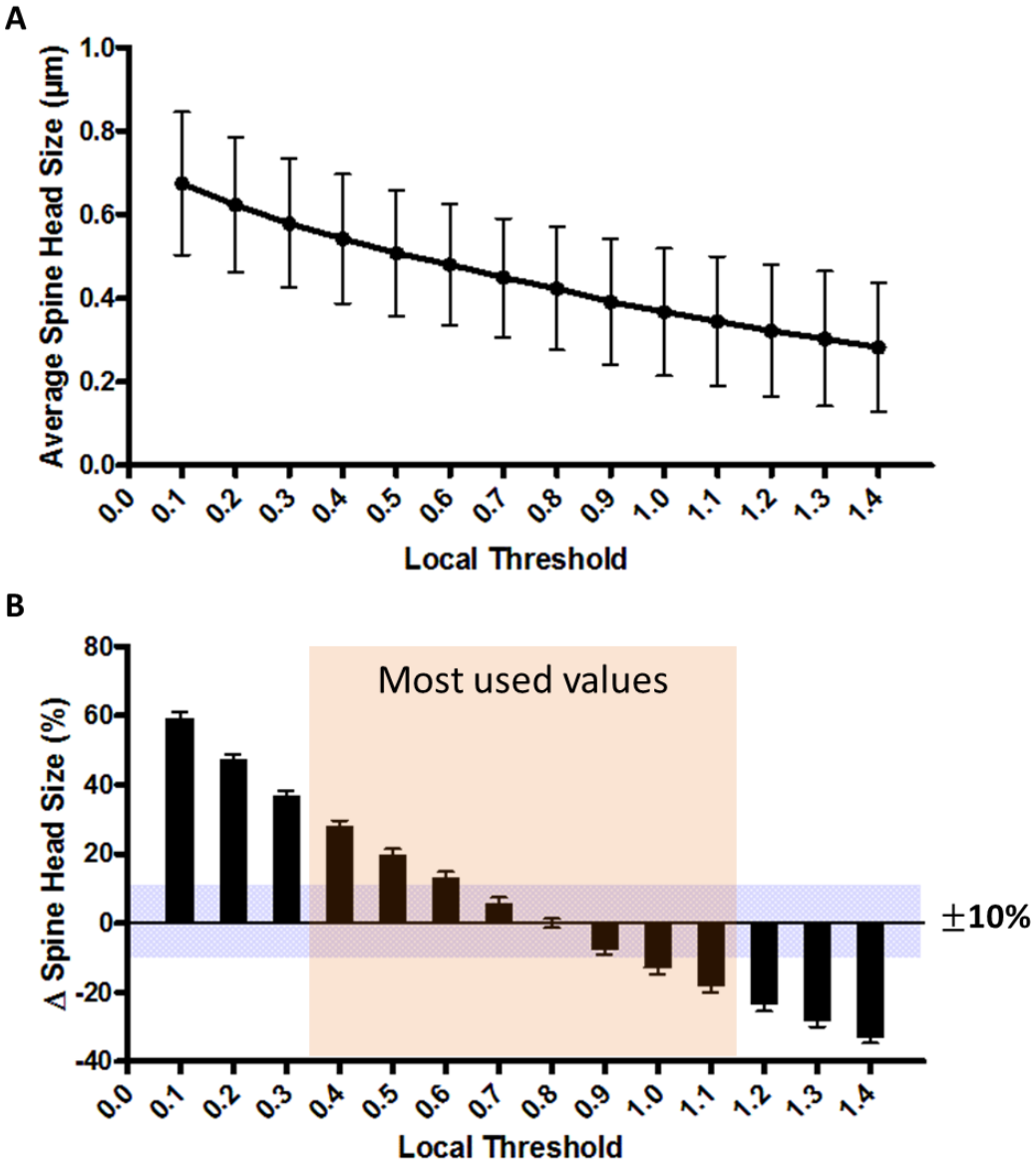

Figure 3-10 : Effect of Local Threshold on the spine terminal point diameter.

The same image was analysed several times, keeping the same settings for dendrite and spine seed points, only changing the local threshold for spines (n=115 spines per image).(A) The mean and standard error of the spine terminal point diameters (STPD) are plotted against the local threshold value. (B) The STPDs' averages were normalized to the mean STPD value obtained at the threshold of 0.8, the median value for local threshold used. The plot shows the percentage of difference in STPD when the local threshold value is changed, compared with the centred value. The grey area represents the ±10% limit of variability for the STPD, and the pink zone covers 85% of the most frequently used values for local threshold. A variation of less than 0.15 in the setting of the local threshold doesn't significantly affect the result.

The effect of local threshold on the dimensions of the spine head terminal point was examined by modifying the spine local threshold on an image already analysed. The function "Rebuild Spine Diameter" in *Filament Tracer* allows modification to the filament, even once it has been previously finished. All the previous steps, such as reconstruction of the dendrite and dendritic spines' seed points are preserved, and only the very last one, the setting of the threshold for spines, is modified. On figure 3-10A, the mean of the spine head diameters is displayed against the value of the local threshold selected. The curve clearly shows a strong inverted correlation between the local threshold and the spine head diameter.

Analysis of hundreds of images showed that the mean of automatically-set local threshold was 0.78. The closest value of 0.8 was used as a reference for comparison of the effect of different local threshold values on measured parameters. The head diameters of spines at various local thresholds were normalised to the mean spine head diameter at the local threshold of 0.8, and the percentage of difference was plotted against the local threshold (figure 3-10B). Changing the local threshold of +/- 0.1 induces a difference of less than 10% on the spine terminal point diameter values. When the local threshold is changed by 0.3 or more from the suggested value, the difference exceeds 20% difference.

The automatic threshold from *Filament Tracer* uses the powerful k-means algorithm (Ridler and Calvard, 1978), that operates on local regions along the filament axis in order to reduce the effect of brightness variations across the image. In most cases, the automatic threshold can reliably be used for spines, thus avoiding the potential bias introduced by user-defined thresholds, and has consequently been used here.

3.3.2.2 User manual setting of seed points

The optimisation of image analysis was meant to improve the reliability and thus the validity of the results, removing bias and improving consistency as much as possible.

Imaris *Filament Tracer* was one of the solutions that automated to a large extent image analysis, but a few steps of the process could still introduce user interpretation, and thus had to be evaluated to determine their impact on final measurements.

Complete automatic setting of seed points is usually impossible, mainly because of noise or brightness contrast across the image. Therefore, to ensure consistency in the analysis, all the seed points were placed entirely manually. To ensure that this step was not affecting the measurement of spine head diameter, an image was analysed by the same user in two different ways. On one hand, the "semi-automatic" method consists of letting the software Imaris place the seed points automatically, and then to add or delete a few of them to match the user choice. On the other hand, the "manual" method, which consists of setting all the seed points manually, as it has later been done for all the images. This verification was preceded by a study of a small group of spines, where individual changes were evaluated after voluntarily misplacing the seed point away from the spine head centre (figure 3-11 A&C).

The graphs in figure 3-11 B&D show that there is no difference in the spine terminal point diameters of a dendrite reconstructed either semi-automatically or fully manually. This result was confirmed with either of the two algorithms for spine fitting. The number of spines detected was very similar (n=119 *vs* n=121, $\Delta n \leq 2\%$), and the distributions, non-Gaussian for automatic *Approximate Circle* (D'Agostino and Pearson normality test) but Gaussian for the others, were not different from each other (Kruskal-Wallis non-parametric test, $p>0.7$).

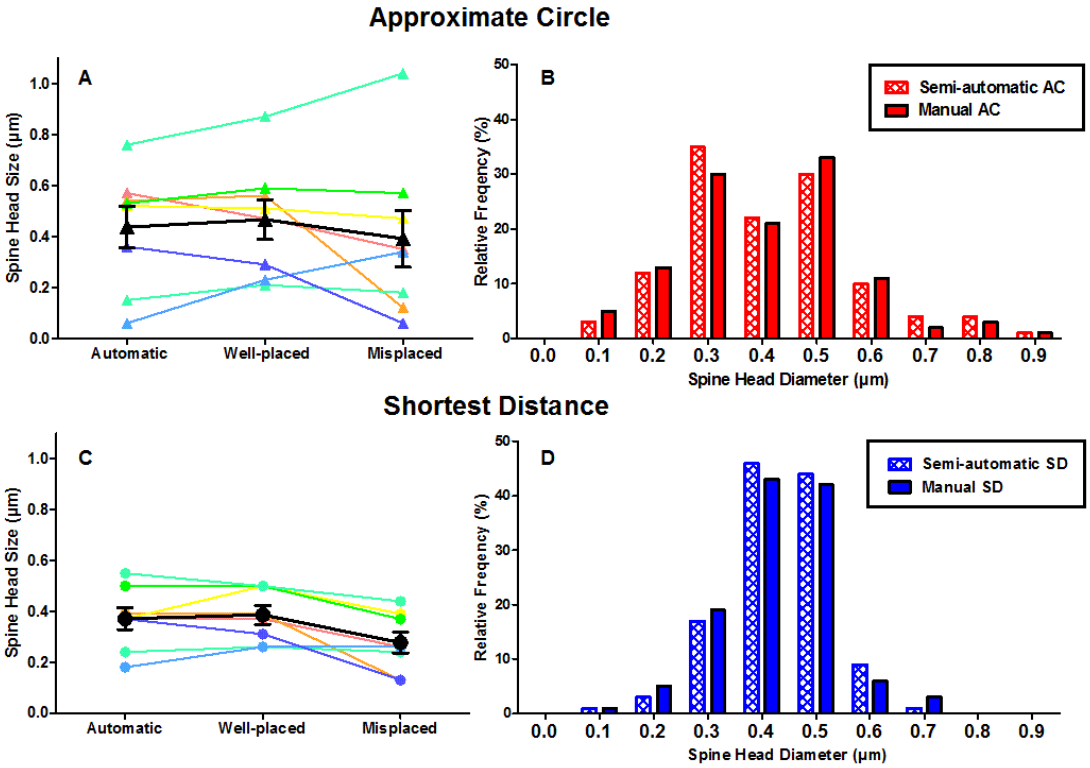

Figure 3-11: Effect of user implementation of dendritic spine seed point on spine head diameter

(A&C) The spine head diameters of the same 8 spines are compared between different spine seeding procedures: fully automatic or manual and careful, or finally manual but deliberately not at the centre of the spine head. Each colour represents a single spine, and the black line is the average with SEM. (A) Effect of changing seed point placing using the *Approximate Circle* algorithm. (C) Effect of changing seed point placing using the *Shortest Distance* algorithm. (B&D) Frequency histograms showing the distribution of dendritic spine head diameters using a semi-automatic or a fully manual spine seeding technique, with both algorithms. The distribution of spine head size is not affected by the manual or semi-automatic technique (Kruskal-Wallis non-parametric test, AC: $p>0.7$, SD: $p>0.9$).

To verify individually the effect of each algorithm, I looked at both a small number of individual spines (figure 3-11 A&C) and at the average of a larger number of spines (figure 3-11 B&D). The *Approximate Circle* algorithm fits dendritic spines to a larger range of sizes (0.1- 1.1 µm *vs* 0.1-0.8 µm for AC *vs* SD), and the misplacing of spines affects the final spine size in either direction, as individual spines on figure 3-11A show either an increase or a decrease of head sizes between careful and careless placement of the seed point. The result is different for the *Shortest Distance* algorithm, where 7

out of 8 spines ended up with a shorter estimated spine head size following a careless placement of the seed point.

This result shows, as expected, that SD is a rough underestimation of the spine head diameter, which is hardly affected by misplacement of the seed point. This turns out to be useful for the identification of stubby spines (see Automatic Spine Classification in 3.4.2). Misplacement can be overcome by an attentive placing of seed points, which is more time consuming but leads to results more similar to fully automatic seed point placing. It is worth noting that the "misplaced seed points" in this test were set purposefully quite far from the estimated centre of the head, in a way that can be very easily and quickly avoided on a large majority of spines during any analysis.

Fully manual or semi-automatic settings of seed points did not affect the distribution of spine head diameters within a particular algorithm, supporting the fact that both manual and semi-automatic methods can be used interchangeably.

To test further if the user input affects the result, and to establish if Imaris can enable one to compare data obtained by different users, I looked at inter-users analysis of the same files, using two images with large number of spines but of different quality. The first image selected for the test was considered to be noisy (figure 3-12A). The second image was selected for its absence of background noise (figure 3-12B), which unfortunately cannot always be obtained, especially when working with slices from GFP expressing cells, or with lipophilic fluorescent labelling. Both images were analysed using in parallel the two fitting algorithms available, and using the automatic threshold.

The interpretation of noisy images can vary considerably from one user to the next. The number of spines detected fluctuated greatly, more importantly on noisy images, reaching more than 25% difference between users from the average number of spines detected (figure 3-12 C&E). On the cleaner image, that difference did not exceed 10% (figure 3-12 D&F). Smaller spines can sometimes be missed, since they are closer to the

dendrite, and thus in the potentially noisy area. Stubby spines can be taken up by the dendrite as they do not have a clear neck separating them, and thus some users, like C, can fail to label them in the absence of pre-established conventions.

The effect of background noise was very detrimental with the SD (figure 3-12C), possibly because of the misplacement of seed points. Using the AC prevented those significant differences, but the absence of the largest spines by user C (figure 3-12E) showed the impact of wrongly fitted stubby spines on the distribution.

These results confirm that the subjectivity introduced by user input is not totally erased with Imaris, and conventions need to be found in order to standardise the analysis, if experiments have to be compared across different operators. The setting of the local threshold, originally done manually, was entirely switched to automatic settings after the analysis revealed the significant impact of small changes in its value and identified the threshold as a major source of bias in the analysis. Finally, those results underline the necessity to use both algorithms to study with precision stubby and headed spines.

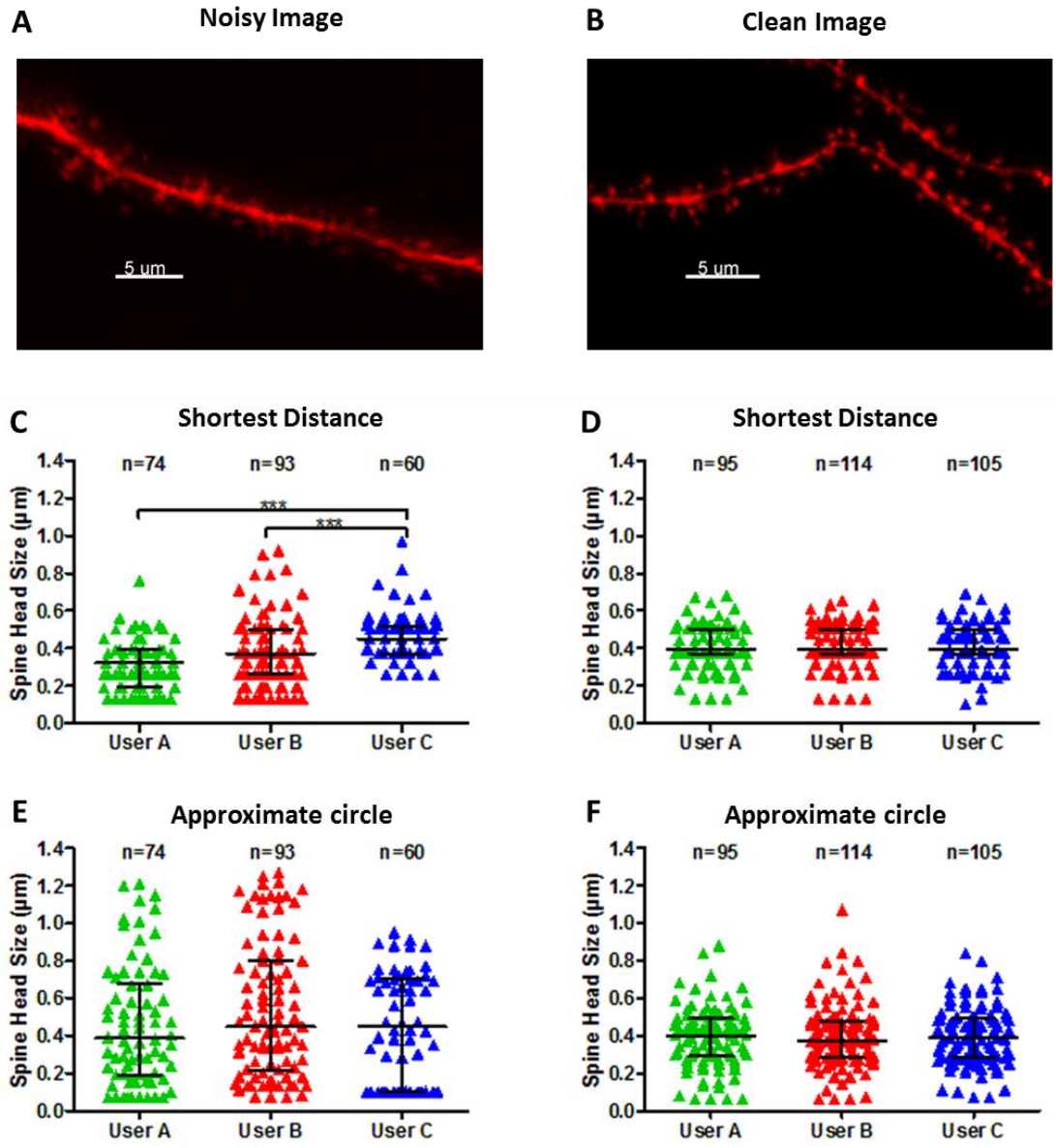

Figure 3-12: Effect of individual user setting of seed points.

Two images of different qualities were analysed separately by three users, and the effect on measured spine head diameter was compared. (A,C&E) The first image had a high level of noise around the dendrites, adding difficulty to the identification of dendritic spines. (B, D & F) The second image is of very good quality, with almost no noise. The number of spines detected varied more on the noisy image than on the clean one (mean number of spine detected ± Δ spines, Noisy image: 76±17 spines, Δ=±22%; Clean image: 104±10 spines, Δ=±9%). No difference across users was detected, except using the *Shortest Distance* algorithm on the noisy image (Kruskal-Wallis with Dunn's post-test, *** $p<0.001$).

3.3.3 On the way to achievement

The result of the analysis so far showed that previous version of Imaris *Filament Tracer* were not satisfactory, spine necks being poorly fitted, and the measurements available did not allow reliable sorting of spine types. Following back and forth communication with the development team, our feedback allowed them to focus on specific features, and solve many of our issues in their 7.2.0 version, released in December 2010.

The new release Imaris 7.2 has improved drastically the fitting of spine necks (figure 3-13), which has allowed us to use additional measurements to identify spines, remove stubby and in fact even separate mushroom from thin automatically if appropriate (cf 3.4.2.2 Thin and mushroom spines).

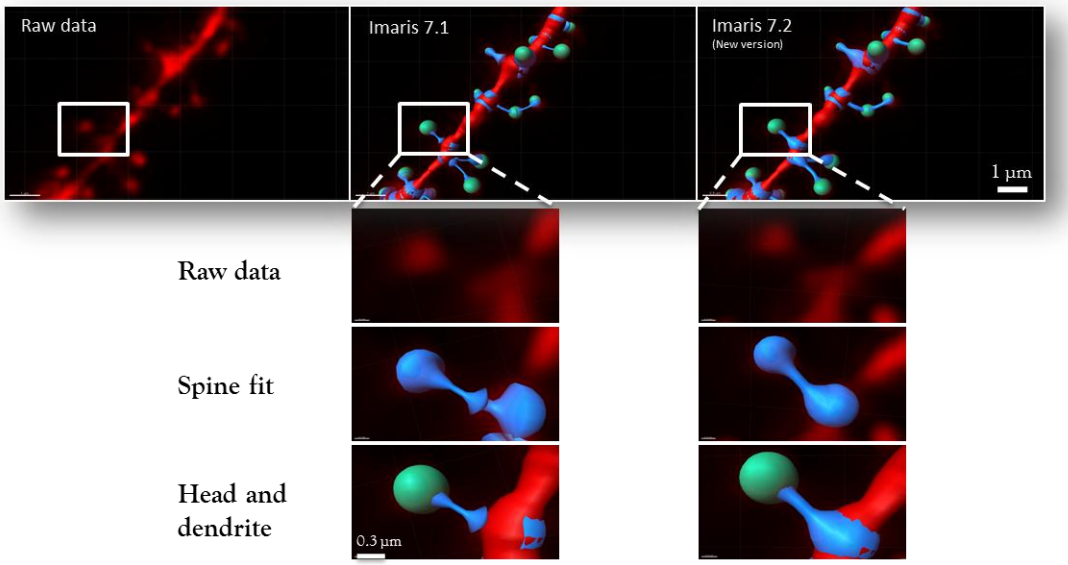

Figure 3-13: Improvements of neck fitting in Imaris 7.2.0 with the *Shortest Distance* to map option.

The images represent: the zoom taken of a CA1 dendrite labelled with intracellular Alexa 594, and imaged with confocal microscopy (Raw data), the *Filament Tracer* modelling with Imaris 7.1, and the filament modelling with the last version Imaris 7.2. The effect on the neck is clearly visible, the “saucer shape” and the constriction at the base of the neck having both disappeared.

The *Approximate Circle* of Cross Section Area algorithm is theoretically more accurate than the *Shortest Distance* to Distance Map, because it is encompassing the luminescence intensity in all 3 directions, and averaging them. The *Shortest Distance*, by taking for the radius the *Shortest Distance* between the seed point and the edge of the spine in a 3D volume as well, is underestimating the spine head diameter.

3.3.3.1 Points to improve

The distribution of spine head sizes, as shown earlier in figure 3-11 B&D, seems to be very dependent on the algorithm used for spine fitting. The *Approximate Circle* distribution is much larger and usually less discreet (or pixelated) than the *Shortest Distance* one. The average value for spine head diameter are very similar though, but smaller than those found in electron microscopy (Harris and Stevens, 1989) (mean ± SEM, *Shortest Distance*: 0.39±0.01 µm, *Approximate Circle*: 0.41±0.01 µm, electron microscopy, 0.53±0.03 µm). The *Shortest Distance* algorithm gives a discreet distribution of values, with relatively large and irregular intervals, constrained by the acquisition resolution of the image. On the other hand, the *Approximate Circle* algorithm gives a smooth distribution of values, adequate for the variety of spine head shapes.

The *Approximate Circle* is thus more representative of the continuity of spine head dimensions.

Imaris initially developed the SD algorithm which unfortunately is not adequate for measurements of spine heads. The AC improved greatly the estimation of headed spines measurements, but the necks of dendritic spines were poorly fitted, conversely to the smooth fit achieved with the SD. Therefore a compromise between the two algorithms had to be found for the present analysis, as those issues were not solved in the version 7.2.0 used for this work (December 2010).

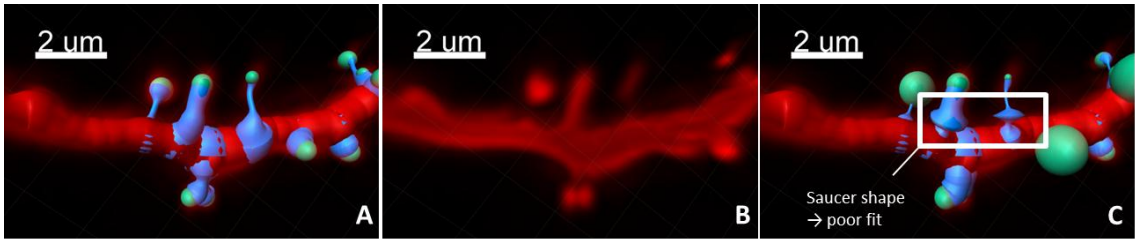

Figure 3-14: Improvements necessary with *Approximate Circle* algorithm.

The same image is shown raw (B), or fitted with Imaris *Filament Tracer* algorithms, either *Shortest Distance* (A) or *Approximate Circle* (C). In the latter case, the model shows an enlargement of the neck that is not visible on the raw image or on the other model.

The fitting of the neck, which used to have "saucer shape" forms with both algorithms, has been fixed in the *Shortest Distance* but not in the *Approximate Circle* (figure 3-14). A Matlab custom-written program allows us to easily use the parameters from both algorithms. Thus stubby spines are first separated using the neck fitting of the *Shortest Distance* and then headed spines are measured using the *Approximate Circle*.

After evaluating Filament Trace fitting of dendritic spines under various conditions and across users, and optimizing an analytical method to obtain the most consistent results, this new method was compared in the following section with previously established methods, and an automated spine sorting tool was implemented.

3.4 Comparison of the different methods

When most of the work is based on spine analysis, it is crucial to ensure that the analysis is consistent, unbiased, and reflects reality as much as possible. Image analysis softwares are not to be taken for granted, as approximations in their own modelling can induce errors in the analysis.

Imaris *Filament Tracer* was only made available from autumn 2009. Before that, spine classification and line-scan on raw data were the only means available in the lab for analysing dendritic spines. Before deciding to use this new software to reanalyse all the three year's data, it had to be shown that the software was indeed fitting our images correctly, and whether the measurements given could be used to classify spines or at least separate the stubby spines from the rest of the population.

3.4.1 ImageJ *vs* Imaris and raw *vs* deconvolved images

It was important to compare results gained previously with line-scan analysis, to those obtained from Imaris modelling of the dendritic filament. The deconvolution step was carried out as described in Material and Methods. Deconvolution had opposite effects on the estimation of spine head diameter with the two pieces of software. Line-scan analysis struggles to cope with small heads and consequently estimations of smaller spines are largely overestimated. In that context, deconvolution greatly improved the evaluation of spine head diameter on smaller spines, and also reduced the median head size considerably as shown in figure 3-15A (Mann-Whitney test, $p<0.0001$).

The spine head diameters measured by *Filament Tracer* gave opposite results to those from ImageJ, raw images presenting shorter heads than deconvolved ones (figure 3-15B). This result could be due to the lack of homogeneity of non-deconvolved images, tending to under-estimate the values for automatic local threshold.

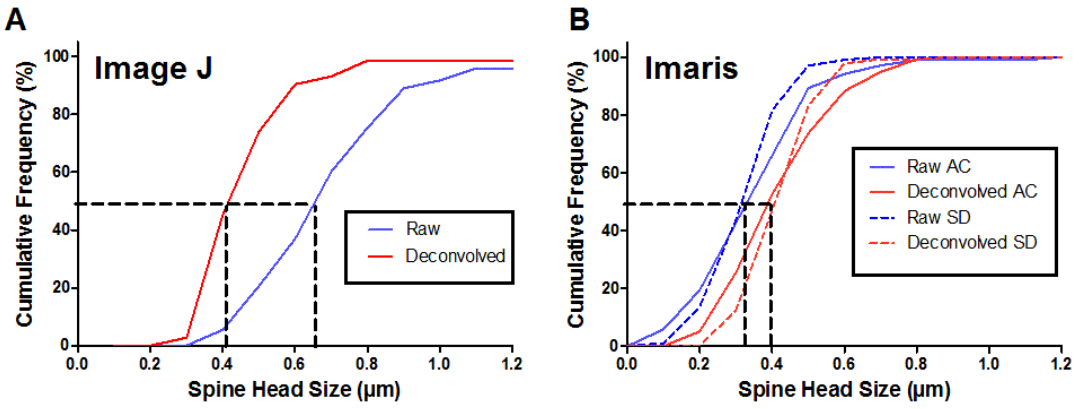

Figure 3-15: Cross-comparison of the effect of the analytical method on the size, density and distribution of spine head size.

The cumulative frequency distribution shows very different patterns between ImageJ line-scan analysis (A) and Imaris modelling (B), comparing the spine head diameter on raw or deconvolved images. Data from spines analysed with ImageJ differs significantly whether it has been deconvolved or not (A) (median, Raw: 0.71 µm *vs* Deconvolved: 0.47 µm, Mann-Whitney test, $p<0.001$). Imaris *Filament Tracer* output shows opposite results, head diameters from deconvolved data being smaller than raw data ones (Mann-Whitney test, AC $p<0.001$; SD $p<0.0001$).

3.4.2 Automatic spine classification

3.4.2.1 Identification of stubby spines

Necessity to identify stubby spines. As mentioned in the introduction, stubby spines represent a distinct category of dendritic spines. Although they possess all the characteristics of dendritic spines in terms of functionality – a postsynaptic density, glutamate receptors and active synapses – the absence of a neck constriction confers on them very different plastic properties compared with their "headed" counterparts, thin and mushroom spines. The very rapid diffusion rate of molecules between the postsynaptic density and the parent dendrite means that they are less able to retain ions and molecules within their head, and thus do not act as a biological compartment. When studying synaptic plasticity, the isolation properties of dendritic spine heads are a fundamental characteristic to their ability to react to activity patterns, the length of the neck and the size of the head impacting on spine propensity to retain necessary molecules to express and maintain long-term potentiation (Matsuo et al., 2008; Honkura et al., 2008). Moreover, only a small percentage of stubby spines (10%) develop into headed spines in the developing hippocampus (P9-12), stubby and headed spines predominantly changing within their own category (Parnass et al., 2000). Therefore, being able to separate stubby from headed spines is important to study plasticity changes of spine heads.

Useful parameters for stubby spines identification with Imaris. Using Imaris *Filament Tracer* with the aim of automating dendritic spine analysis, it was important to apply similarly impartial methods to the identification of stubby spines.

Dendritic spines from 9 different cells, imaged across four years, were individually analysed both by visual identification of spine type and by Imaris *Filament Tracer* reconstruction. To standardise the analysis, all the cells were reanalysed at the same time, using the same version of the deconvolution software and of Imaris. For spine type identification, a total of 643 spines from 9 cells were examined. All spines were included but spines falling between two categories were labelled as such and were counted as correctly identified if the automated analysis came up with either of the two types proposed. For example, a spine classified as either mushroom or thin by

visual verification would be counted as correctly identified if the automated program classifies it as a thin or a mushroom but would be counted as wrongly identified if it came up as a stubby.

In order to distinguish stubby spines from their counterpart possessing a neck, it was important to be confident that the fitting of the neck by Imaris was satisfactory. The values for spine head size or spine length given by both algorithms were plotted against each other. As mentioned earlier, the *Approximate Circle* algorithm, although more representative of spine head size variability (figure 3-16A), was not proficient with neck fitting, meaning that values such as spine minimum diameter could not be relied upon. Moreover, the *Approximate Circle* overestimates the head size of stubby spines because of the absence of neck restriction. Spine lengths, however, were unaffected by the choice of either algorithm (figure 3-16B). Therefore, values given by the *Shortest Distance* algorithm were used to distinguish stubby spines, before moving on with *Approximate Circle* values for spine head size comparisons.

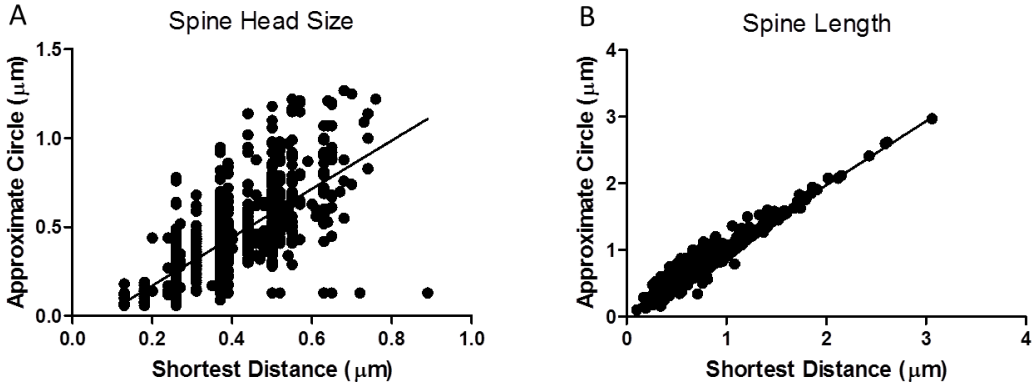

Figure 3-16: Comparison of the two spine fitting algorithm from *Filament Tracer*.

(A) The two algorithms have very different ways of fitting dendritic spines. The non-linearity of spine head diameters with the *Shortest Distance* algorithm is made visible by the vertical lines of similar diameters along the x axis. There is a substantial scatter along the linear regression linking the spine head diameters from both algorithms (slope p=1.3, R^2=0.52). (B) Conversely, the spine lengths correlate very well (slope p=1.01, R^2=0.95).

Criteria used for identifying stubby with Shortest Distance algorithm. After visual identification of stubby and headed spines, their principal parameters defined with the *Shortest Distance* were plotted to identify a reliable way to distinguish them: spine length against spine head size (figure 3-17A), and spine minimum diameter against spine head size (figure 3-17B). Stubby spines stand out from headed spines by the ratio spine minimum diameter/spine head diameter, which was equal to 1 for a majority of stubby spines (94%), and less than 1 for spines with an identifiable neck (figure 3-17A).

$$\frac{\boldsymbol{Spine\ Minimum\ Diameter}}{\boldsymbol{Spine\ Head\ Diameter}} = \mathbf{1}$$

Stubby spines also show a different pattern than most headed spines for their spine length to spine head diameter ratio, on the overall spines (figure 3-17B) or on the sub-group including only spines with no neck restrictions (figure 3-18A). In that group, stubby could be separated from headed spines by their length-to-head ratio (figure 3-18A), their distributions being significantly different (Mann-Whitney test, $p<0.0001$).

Using the cumulative probability distribution of length-to-head ratio (figure3-18B), the threshold necessary to both isolate the maximum number of stubby spines and including the minimum number of incorrectly identified stubby spines could be computed, . The best results were obtained with the following parameters:

$$\frac{\boldsymbol{Spine\ Length}}{\boldsymbol{Spine\ Head\ Diameter}} < \mathbf{1.5}$$

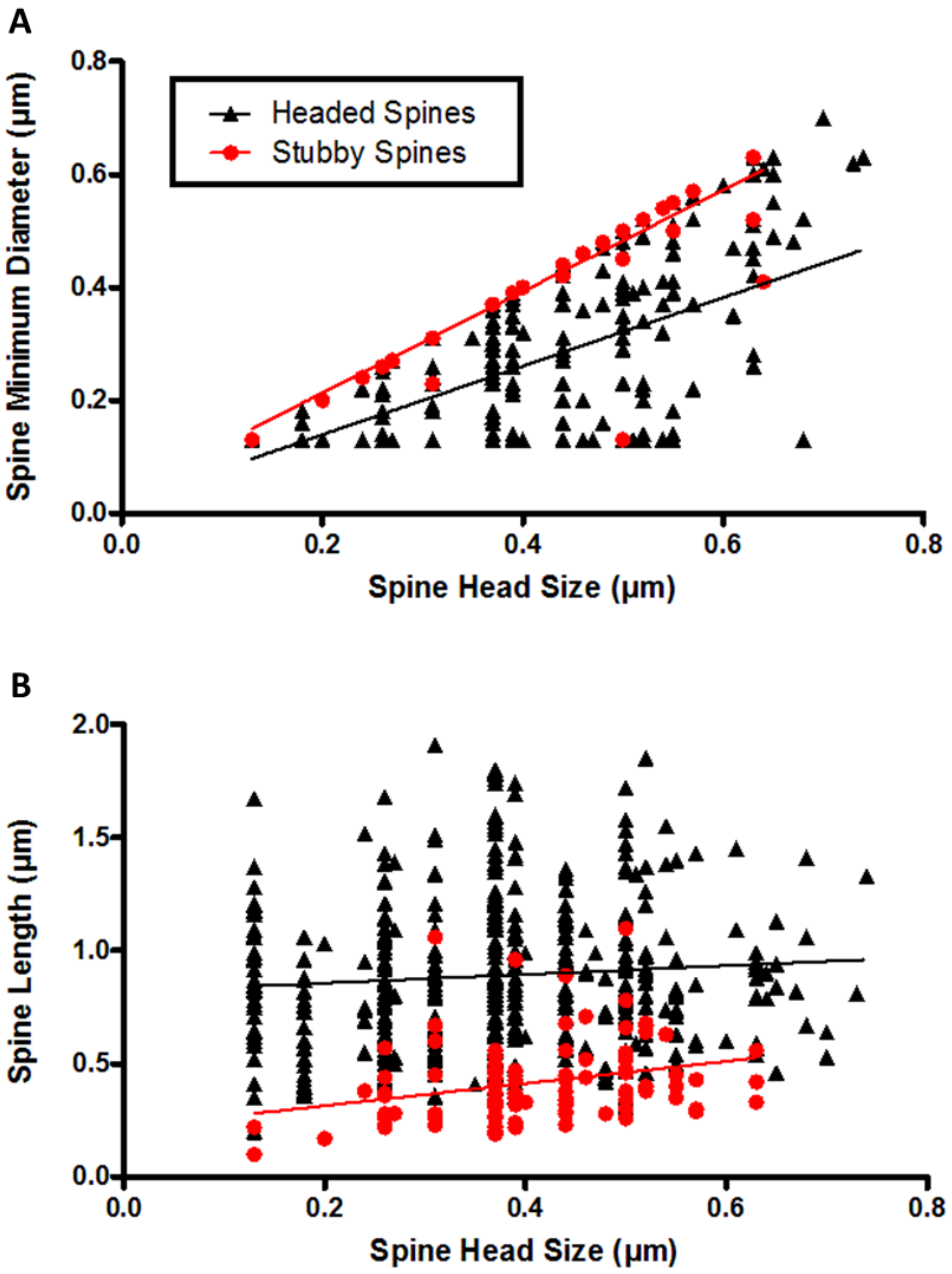

Figure 3-17: Correlation between spine length and spine head diameter between different categories of spines identified visually.

Using the *Shortest Distance* algorithm, headed spines (mushroom and thin spines) and stubby spines have overlapping spine head size pools but differ from their overall length, stubby spines being generally shorter. (A) Spines presenting a well-defined neck on their filament could easily be separated from stubby spines on their "spine minimum diameter/spine head diameter" ratio, and less than 1 in such cases. (B) Stubby spines also present shorter overall lengths than headed spines.

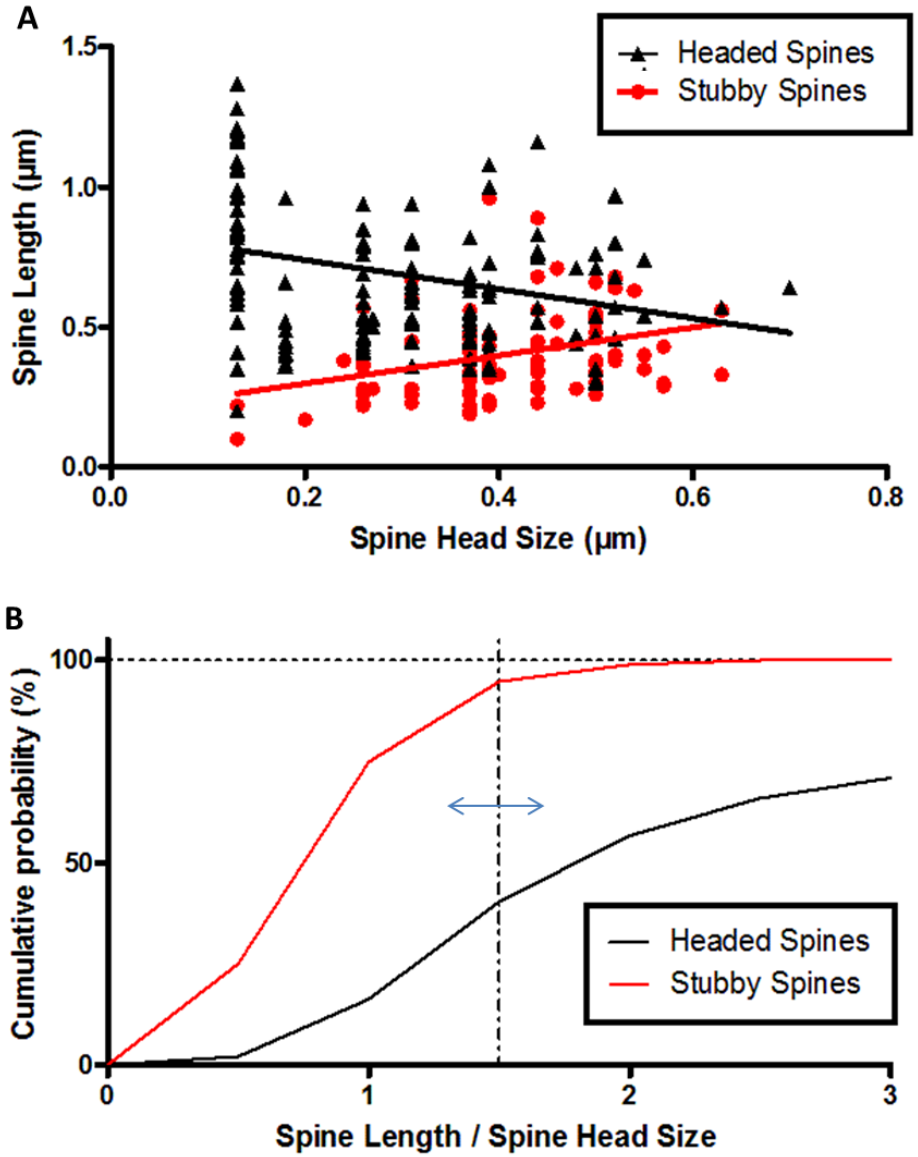

Figure 3-18: Correlation of spine length to spine head size for the sub-group for which spine minimum diameter is equal to spine head size.

Selecting spines for which Imaris has not detected a neck separates out the vast majority of stubby spines (94% of stubby spines). (A) Stubby spines (red) represent 41% of the remaining spines, and are in majority grouped on the bottom part of the graph plotting spine length against spine head size. (B) The cumulative distribution of the ratio spine length/spine head size shows a very significant shift between the two population (Mann-Whitney test, $p<0.0001$), and thus will be used to separate the stubby from the remaining headed spines. The vertical dotted line represents the threshold used for removing spines considered as stubby from the rest.

Stubby can be thus be sorted by Imaris if they answer the two equations cited previously. The summary of stubby spine sorting with Imaris *Filament Tracer* is found in table 3-2 below.

Table 3-2: Identification of stubby spines visually and following Imaris parameters.

The table summarises data from 9 CA1 cells, samples from different sets of experiments.

	Number of spines	Percentage
Total spines analysed	643	
Stubby visually identified	144	22.4% of Total
Stubby correctly identified by Imaris	127	88.2 % of Stubby
Stubby wrongly classified as headed by Imaris	17	11.8% of Stubby 3% of Total
Headed wrongly classified as stubby by Imaris	37	5.7% of Total
Total spines correctly identified	589	84.0% of Total

This sample the most satisfactory results after trying many possibilities to find the best compromise between removing the maximum of stubby spines and limiting the number of headed spines identified as stubby spines. Our percentages of total (84%) or stubby only (88.2%) matches are in accordance to what has been found previously using Neuron Studio software, matching 82.8% of stubby spines (Rodriguez et al., 2008).

3.4.2.2 Thin and mushroom spines

After finding an efficient way of sorting stubby spines from the *Shortest Distance* parameters, the remaining spines can then be analysed by using their *Approximate Circle* dimensions by using a custom-written Matlab program.

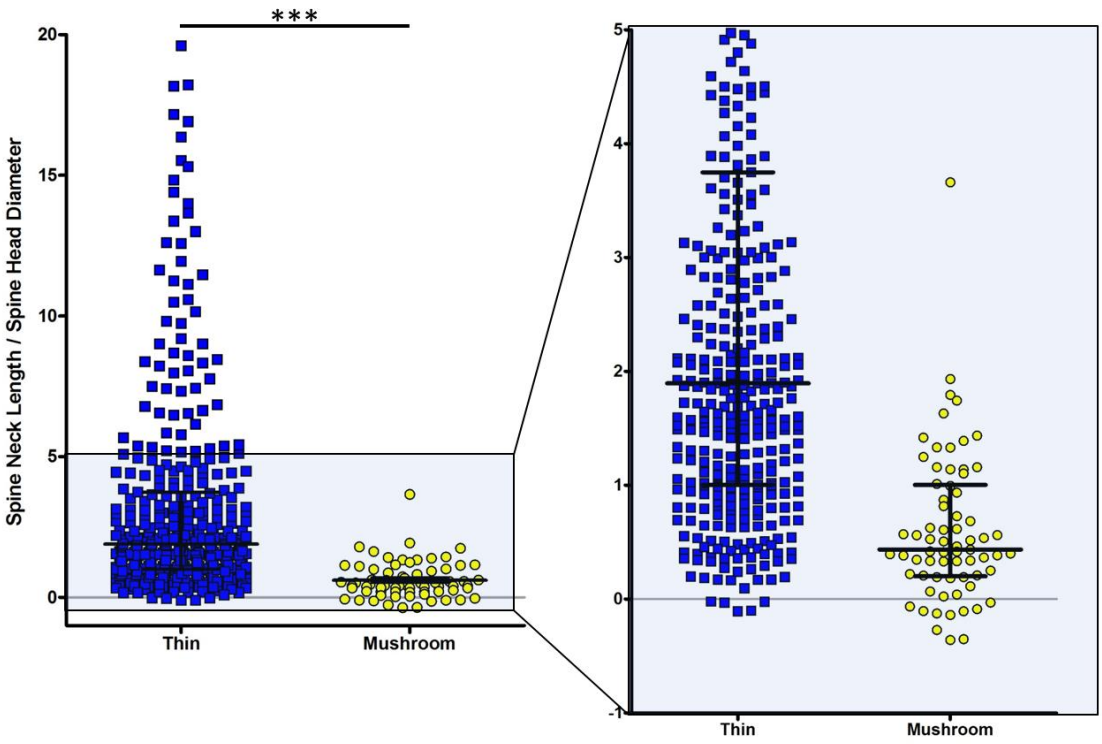

Figure 3-19: Distribution of spine neck length to spine head diameter ratio for thin and mushroom spines.

After removing stubby spines by the automatic method described previously, mushroom and thin spines (identified visually for this exercise) can be sorted by the ratio of their spine neck length to spine head diameter (median and quartile, Mann-Whitney test, $p<0.0001$). The spine neck length is calculated by subtracting the spine head diameter from the spine length.

In the introduction, I have shown that the distinction between mushroom and thin is not so simple, and for most of the following they are both regrouped in headed spines. In order to potentially compare with previous results, I tried to use Imaris and published articles (Sorra and Harris, 2000; Rodriguez et al., 2008) to define parameters to sort out thin and mushroom spines. Head size was a first obvious parameter (Thin: <0.4 µm, mushroom: >0.6 µm, but the remaining spines could be separated on their neck length to head size ratio, mushroom usually having a much larger ratio.

As shown in figure 3-19, the neck length/head size ratio shows a clear difference between the two groups of spines (Mann-Whitney test, $p<0.0001$), but some overlap remains. Trying to optimise the number of correctly identified spines while matching the percentage of mushroom spines found in the literature for 14 DIV CA1 pyramidal

cells in organotypic slices, i.e. between 10 and 25%, (McKinney et al., 1999a; De Simoni et al., 2003), the ratio that sorted mushroom spines the most accurately was:

$$\frac{Spine\ Neck\ Length}{Spine\ Head\ Diameter} = \frac{Spine\ Length - Spine\ Head\ Diameter}{Spine\ Head\ Diameter} < 0.2$$

Using that threshold, 80% of spines were fitting according to the visual identification consensus and the proportion of mushroom spines was 14.9%, very similar to both the visual estimation (15.0%), and the value found previously in the lab (12%). However, the number of correctly identified mushroom spines remained low at its best (<65%), emphasising the inappropriateness of separating mushroom from thin spines.

The flowchart of the spine categories (figure 3-20) represents the process and the parameters used for the reliable sorting of stubby versus headed, and the more ambiguous sorting of mushroom and thin spines.

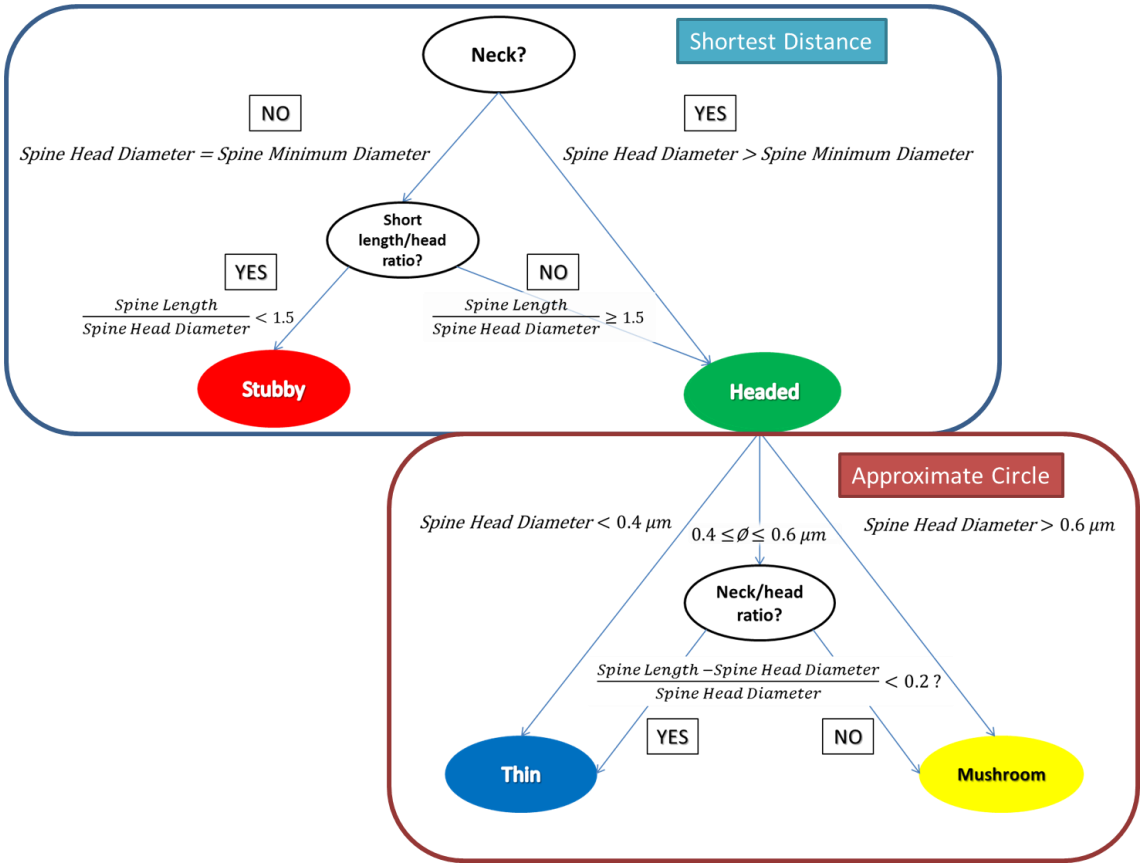

Figure 3-20: Flowchart of spine sorting using *Filament Tracer* and Matlab data analysis.

The top part of the chart corresponds to the sorting of stubby spines, using the SD algorithm fitting of spines from Imaris. The flowchart below represents the subsequent sorting of the spines defined as headed into thin or mushroom spines using the AC.

3.5 Discussion

Since their discovery by Ramón y Cajal in the 19th century, dendritic spines have attracted an increasing interest from neuroscientists, as their particular shape and density seem to impact heavily on the network connectivity, and many neurological diseases present alterations of dendritic spines. However, the small size of these protrusions, with heads between 0.2 and 1.2 µm in diameter, are close to or even beyond the resolution limit of light microscopy and thus their finest structures are harder to identify without powerful techniques, such as deconvolution and confocal/two-photons fluorescent imaging, or by using electron microscopy.

3.5.1 Continuity in spine analysis

A quick comparison with previous analysis performed in the lab revealed that spine type analysis, as adopted by several labs following the Harris parameters for classifying thin, mushroom and stubby spines (Harris et al., 1992), leads to various interpretations of spine types, not only across users but also on a repetitive analysis by the same user (Rodriguez et al., 2008). Spine type analysis of confocal images presents the additional difficulty of estimating 3D structures from a stack of 2D images, without consistent tools to evaluate parameters such as spine neck length or spine head diameter, which are necessary to categorise spines. With confocal microscopy, the spine neck dimensions are almost beyond the limits of resolution. Hence, that parameter is only used by comparison to head diameter, in order to distinguish headed from stubby spines.

Moreover, an additional degree of complexity in visual analysis of spine types is the continuity of spine morphologies, which present various forms in-between the extremes represented by the well-defined thin, mushroom and stubby spines. In Kristen Harris' in depth analysis of spines using electron microscopy, more than a quarter of the spines could not be classified, emphasising the lack of absolute categorisation (Harris et al., 1992). Those findings were determinant in the search of a better way of analysing spines, which would not rely so much on individual estimation of spine shapes and that would diminish as much as possible the user bias.

Moving on from visual identification of spine type to line-scan measurement of spine head with ImageJ software marked the first step towards unbiased spine analysis. Line-scan of dendritic spine heads has been previously established in major spine labs using confocal and 2-photons imaging (Matsuzaki et al., 2004). Stubby spines, which represent a less plastic category of spine because of the absence of a neck separating the postsynaptic density from the parent dendrite (Ashby et al., 2006), are often removed from analysis aiming at observing changes in spine head size or when using line-scan analysis, because their terminal point cannot be separated from the dendrite (Bloodgood and Sabatini, 2005; Korkotian and Segal, 2007).

Line-scan analysis is very time consuming, and only able to measure spine head size on a 2D image. The development of new image analysis software able to recognise dendritic spines was a huge improvement towards the enhancement of dendritic spine analysis.

3.5.2 Imaris *Filament Tracer*

The development of a piece of software able to distinguish spines from their parent dendrite and to compute many parameters relative to those spines on a 3D scale is a tremendous achievement towards the facilitation of truly objective dendritic spine analysis. Using a new technology, however, requires in-depth exploration of its possibilities and limitations, necessary to establish the validity of the new model. With no previous publication on Imaris *Filament Tracer*, I had to evaluate the impact of the users on the consistency of the results and determine a line of conduct for anyone using the software to maximize consistency of the analysis. The software offers two different algorithms for fitting dendritic spines' *Shortest Distance*, which offers very good fitting of spine necks but underestimates the spine head size; and *Approximate Circle*, which is more able to deal with non-round heads but for which the fitting of the neck still present incongruities.

The data from both algorithms were investigated and used in order to establish a model of spine analysis, which respond satisfactorily to our requirements: 1) Single out

stubby spines from headed spines to enable later removal of stubby spines from analysis; 2) Use the *Approximate Circle* parameters on headed spines to compare the changes in spine morphology.

In this study, I have included a sorting of spines per category but this time the categorisation is not based on visual clues and thus less prone to bias. Previous publications have sorted spines by very rough parameters, which had the advantages of being exclusive but probably not as representative of the physiological differences between spine types (Oray et al., 2006). In our study, spine categorisation is the result of a long process aiming at sorting protrusions by types of physiological differences, such as the extreme forms that represent the neckless stubby spines, and the various headed spines with a clear neck constriction. This result was achieved by using a large sample of spines, defining the parameters which differentiate those extremes easily in accordance with visual clues and setting threshold which finally sort automatically the remaining spines, usually belonging to the "unclassified" domain using other methods.

3.5.3 Limit of definitions

It is important to remember that some parameters helping the identification of spine types, such as neck diameter or the presence of mitochondria, cannot be assessed precisely or at all without electron microscopy. Among the many publications involving spine type classification, many show a variety of definitions, and thus an even variability in the results. Even electron microscopy studies result in many unclassified spines. Thin spines are the less affected by spine categorisation parameters, because they represent the larger group of spines and thus a few discrepancies between visual and automatic classification is not going to affect the proportions of thin spines. Stubby spines and more specifically mushroom spines are much more prone to misfitting, because they do not fit the theoretical model of a neck with a spherical head. Stubby spines numbers may have been overestimated, but as they are removed from further analysis of spine length and head size, the following results from headed spines would thereby be more significant with 'noise' from spinous fitting of stubby

spines omitted. Enlarged and non-spherical spine head parameters can be appropriately evaluated with the *Approximate Circle* algorithm, but the diversity of shapes makes their separation from other headed spines difficult.

With the good correlation between spine head size and the postsynaptic density of headed spines (Harris et al., 1992), combined with Imaris *Filament Tracer* 3D evaluation of the spine head volume from which is derived the spine head diameter, it is interesting and possible to follow changes in density, percentage and measurements of all types of spines to get a readout of the postsynaptic strength. A well-defined method for spine reconstruction with Imaris *Filament Tracer*, enforced by a blind analysis of the data, greatly limits any bias in spine analysis, while giving the possibility to study a large variety of parameters with a relatively less demanding technique.

Chapter 4. Imaris analysis of the distribution of dendritic spines in CA1 pyramidal cells on 14 DIV organotypic slices

4.1 Introduction

Hippocampal organotypic slices are a widely used preparation for the study of synaptic plasticity in networks and homeostasis, as they present the advantage of retaining the organisational structure of the hippocampus cellular network, while allowing long-term treatments of more than a few hours. They also respond to the criteria for the reduction of animal use in research, as they allow a maximal use of the slices generated per animal.

Dendritic spines have been described many times in the literature, as early as the end of the 19th century with Golgi staining by Ramón y Cajal. A large part of the later work was carried on with electron microscopy imaging on fixed tissue from acute slices (Gray, 1959; Harris and Stevens, 1989; Harris et al., 1992), before confocal and two-photon microscopy enabled imaging of dendritic spines in live cells (Parnass et al., 2000; Korkotian and Segal, 2001; De Simoni and Edwards, 2006). Each method present distinct advantages and drawbacks, which should be kept in mind when analysing the data and the differences observed between labs. Using a new image analysis method based on Imaris *Filament Tracer* reconstruction of the dendritic tree, it is interesting to recapitulate the morphological properties of CA1 pyramidal neurone dendritic spines, in our model of organotypic slices , which is based on the Stoppini method (Stoppini et al., 1991).

4.2 Control and 0.1% DMSO treated cultures

When studying drug effects, many treatments require the use of the dipolar aprotic solvent DMSO at a low concentration - usually below 0.1% of total volume- as it is very potent and an excellent vehicle for drug therapies.

A concentration of DMSO below 0.1% of the final volume is very commonly used in experiments, with no toxic effects on neurones (Lu and Mattson, 2001).

In our experiments, DMSO was employed to dissolve the CaMKII antagonist KN62 from Tocris, which was added to the culture medium to modify synaptic plasticity over the course of a week (see chap 7). Controls with "Vehicle", i.e. culture medium alone, were run in parallel because another drug used to study long-term changes in dendritic spines was the PKA antagonist Rp-8-Br-cAMP from BioLog, which was dissolve in distilled water. The treatment consisted of incubation of organotypic hippocampal slices made from P5 male rat with either culture medium alone or DMSO 0.1% of final volume, for 7 days starting after the preparation of slices. The slices were then taken for imaging at 14 DIV, and CA1 pyramidal neurones were filled with Alexa 594 and imaged with Olympus Fluoview confocal microscope.

As all the treatments and experiments were intertwined in time, the possibility of pooling all the controls would decrease the number of recordings needed, provided that vehicle and DMSO treated slices were similar. This section compares slices treated with media only (vehicle), or with DMSO 0.1 % Volume (DMSO).

The density of dendritic spines was not significantly affected by the 7 days treatment (figure 4-1A). The mean overall density of spines went from 1.14 ± 0.24 spines/µm (n=5 cells) in vehicle to 1.06 ± 0.22 spines/µm (n=15) in DMSO (Student t-test, p=0.51). The same results were obtained in apical (mean ± S.D. in spines/µm, vehicle: 1.15 ± 0.19, n=5 vehicle; DMSO: 1.12 ± 0.28, n=14; p=0.84) or in basal dendrites (Vehicle: 1.14 ± 0.27, n=5 cells; DMSO: 1.04 ± 0.21, n=13; p=0.39).

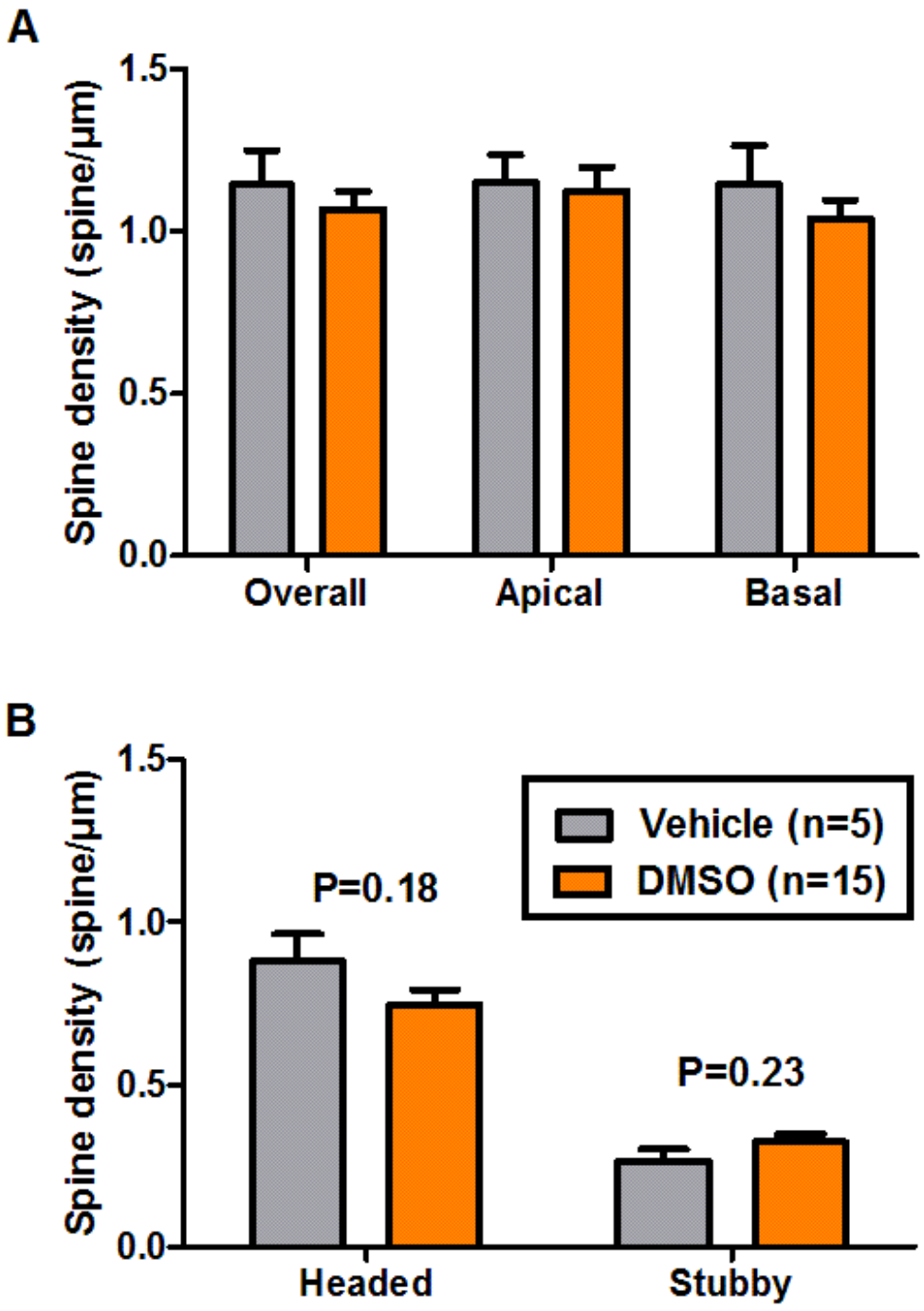

Figure 4-1: Density of spines in vehicle or DMSO treated CA1 pyramidal neurones.

(A) Spine density in organotypic slices pyramidal cells was not affected by the 7 days incubation with 0.1% DMSO (Student t-test, overall: p=0.51, apical: p=0.84, basal: p=0.39). (B) The density of spine regrouped by categories, as determined previously, shows no significant difference between vehicle and DMSO treated slices. Headed spines regroup mushroom and thin spines, and correspond to the spines which parameters are looked at in figure 4-2.

Taking a closer look at individual spine types (figure 4-1B), as classified automatically following the method described in Chapter 3 and using Imaris extracted measurements, the effect of long-term exposure to 0.1% final volume concentration of DMSO had no significant effect on them. As I have mentioned previously, stubby spines are biophysically distinct from spines with a neck -generally called headed spines. Headed spines density was 0.88 ± 0.19 spines/µm (n=5) in vehicle and 0.75 ± 0.18 spines/µm (n=15) in DMSO (Student t-test, p=0.18). The variability of density across cells often induces large standard errors and overlapping samples. The density of the stubby spines was also not significantly altered by DMSO (p=0.23).

To see if spine dimensions are affected by the DMSO, the cumulative frequency of headed spines was preferred to the comparison of the mean of medians, as it is more powerful and avoids reducing the very large number of spines analysed to the smaller number of cells. For this analysis, a similar number of spines were randomly selected from each cell sample, thus ensuring that each cell has the same weight.

To confirm the efficiency and accuracy of this analytical method, another analysis was carried out in parallel using SPSS Complex Sample on all the spines, and weighing them for potential cell clustering. The analysis with SPSS on control data brought similar results to those observed with the technique in this chapter, showing significant differences or the absence of change in exactly the same way (data not shown).

The length of spines was not affected by the treatment (figure 4-2A), and the distributions are very similar for all groups, whether observing overall spines (Mann-Whitney test, p=0.94), apical (p=0.62) or basal (p=0.26). Mann-Whitney test are used here as the sample of spine head diameters does not fit a Gaussian distribution, according to the D'Agostino & Pearson omnibus normality test run in GraphPad Prism ($p<0.0001$ for all groups).

The spine head diameter cumulative frequency distributions (figure 4-2B) were more variable than the spine length. On the overall spines, the median values were 0.39 µm (n=360) for vehicle (grey plain line) and 0.36 µm (n=1560) for DMSO (orange plain line). A Mann-Whitney test on the distribution detected no significant difference (p=0.94). That was not the case for basal spines, which presented a small increase in spine head size after 7 days exposure to DMSO (Vehicle: 0.35 µm, n=360; DMSO: 0.38 µm, n=810; p=0.036). This trend was not found in the apical dendrites, where the head diameters were similar (p=0.26, n=270 for vehicle, n=900 for DMSO).

The analysis of the most used parameters from media or DMSO treated slices present very little difference overall. Given the number of observations made (n=13 comparisons), the fact that one significant difference was observed among all the parameters tested could be a statistical probability (65% chance of getting one false positive at p=0.05). The data from vehicle and DMSO were pooled together in a new group called “Control”, which regroup the data from 14 DIV organotypic CA1 cells imaged during the same period of time. Other similar data, used for instance in the deafferentation chapter, were not included in the analysis as they were dating from a complete distinct period and the acquisition settings also might have slightly changed in the meantime.

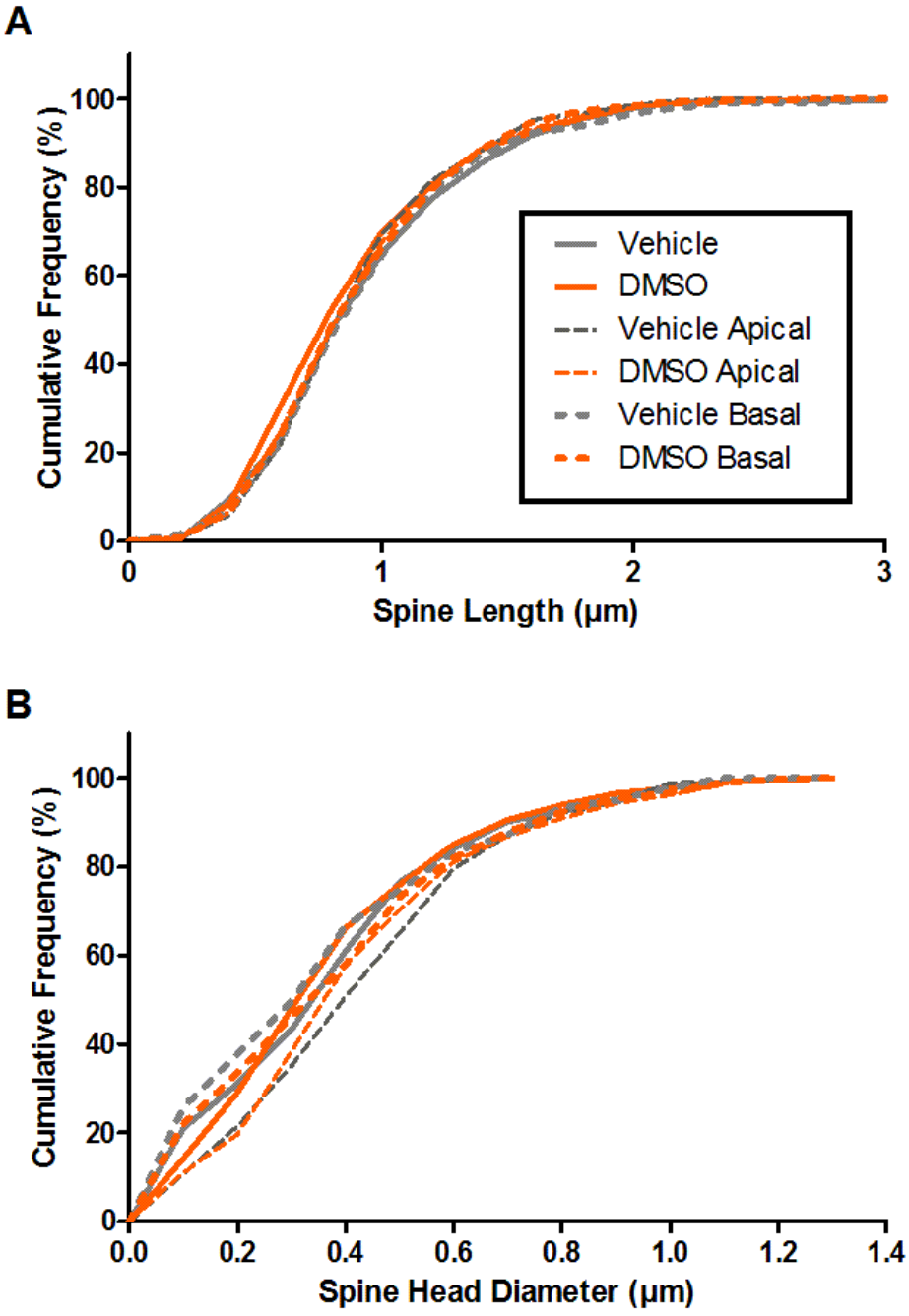

Figure 4-2: Cumulative distribution of spine head diameter and spine length in vehicle or DMSO treated slices, on non-stubby spines.

(A) The spine length was not affected by DMSO treatment (overall: p=0.94, apical: p=0.62, basal: p=0.26). (B) The frequency distribution of spine head diameters show no difference between overall vehicle and DMSO (p=0.94, n=360 spines for vehicle, n= 1560 spines for DMSO). Apical spines were not affected by the changes (p=0.26, n=270 vehicle, n=900 DMSO), while basal spine head diameters were slightly increased by DMSO (median, vehicle: 0.352 µm, n=360; DMSO: 0.381 p=0.036 µm, n=810; p=0.036).

4.3 Comparison of apical versus basal dendrites

4.3.1 Differences in density

The hippocampus is highly structured both *in vivo* and to a lesser extent in organotypic cultures, CA1 pyramidal neurones being polarised by the inputs they receive at various strata of their dendritic tree, from the entorhinal cortex in the *stratum lacunosum moleculare*, from the Schaffer collateral in the *stratum radiatum* of the apical dendrites, as well serving partly the basal dendrites, along with inputs from neighbouring CA1 (figure 4-3A & 4-7). The difference in the inputs received by apical and basal dendrites, as well as the electrical filtering operating with the degree of complexity of the branches (Sourdet and Debanne, 1999; Hausser, 2001; Silver, 2010), can induce differences in the spine populations in those different regions. Apical branches develop along the main apical dendrite (figure 4-3B), which spread some hundreds of micrometres from the soma to the distant *stratum lacunosum moleculare* towards the centre of the hippocampus. The branches in the apical dendrites spread from the main apical dendrite, with progressive complexity of the tree into first, second and third or fourth degree branches. In the basal dendrites, the dendritic tree is differently organized, forming several bundles which branch immediately into secondary dendrites (Bannister and Larkman, 1995).

Apical and basal dendrites have distinctive structures, and receive inputs from different groups of neurones (figure 4-4A). I first compared apical and basal dendrites spine density to see if the differences mentioned above were echoed in local density. The mean ± SEM density of spines was calculated by adding the number of spines counted in all the segments imaged in one region (apical or basal), and dividing it by the sum of the length of each segment, using a total of 20 CA1 pyramidal cells, coming from different slices and at least 8 different cultures. In the apical dendrites, the density was 1.13 ± 0.06 spines/µm (n=19 cells), while it was 1.07 ± 0.05 spines/µm (n=18) in the basal dendrites (unpaired Student t-test, p=0.45).

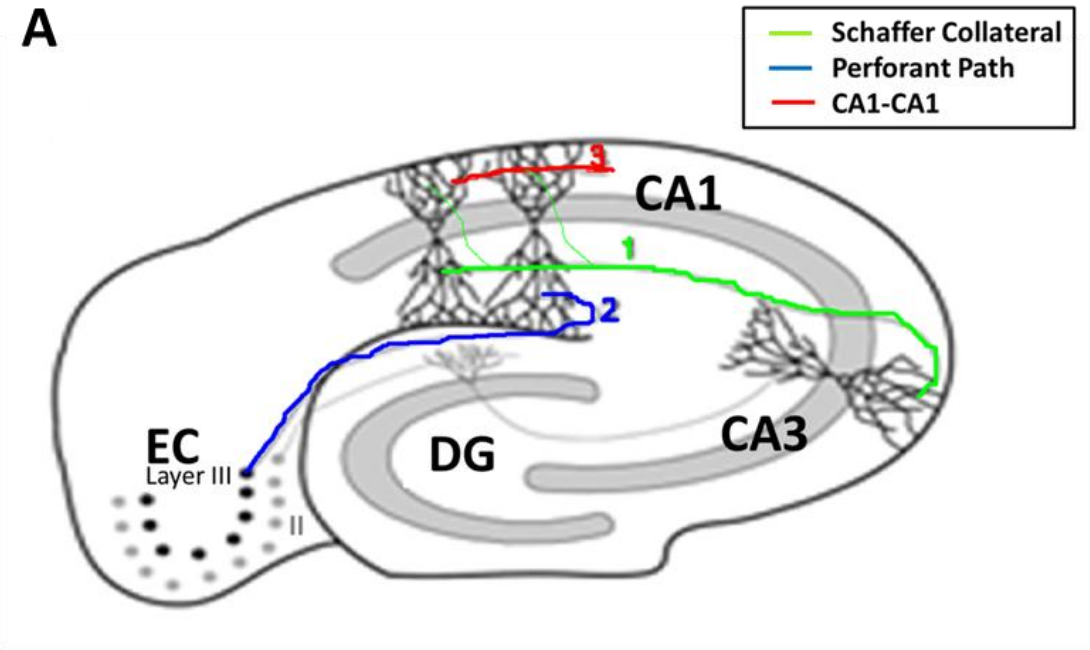

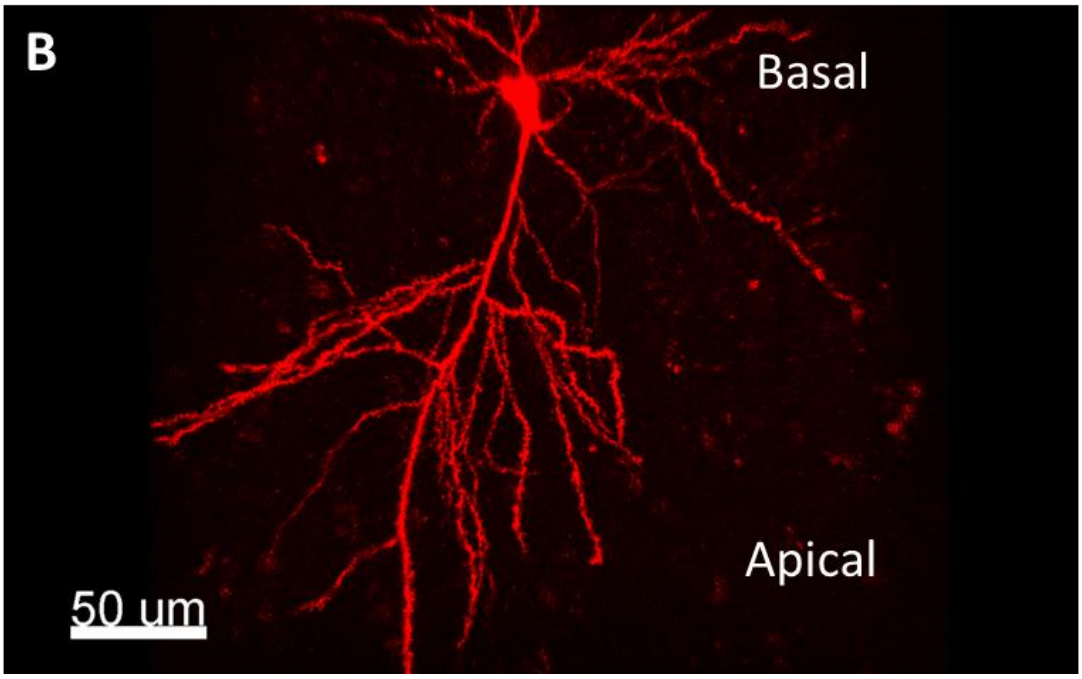

Figure 4-3: CA1 pyramidal cells of the hippocampus receiving 3 types of excitatory inputs.

(A) Scheme of the trisynaptic circuit of the hippocampus section, showing in particular the three excitatory inputs impinging on CA1 neurones: (1) the Schaffer collateral sending axons from CA3 cells, (2) the perforant path sending axons from layer III of the entorhinal cortex, and finally (3) CA1 axons connecting to neighbouring CA1 cells. (B) A projection of a large portion of a CA1 neurone from an organotypic culture at 14 DIV shows the dissymmetrical structure of the dendritic tree, and the differences in branching between apical and basal dendrites.

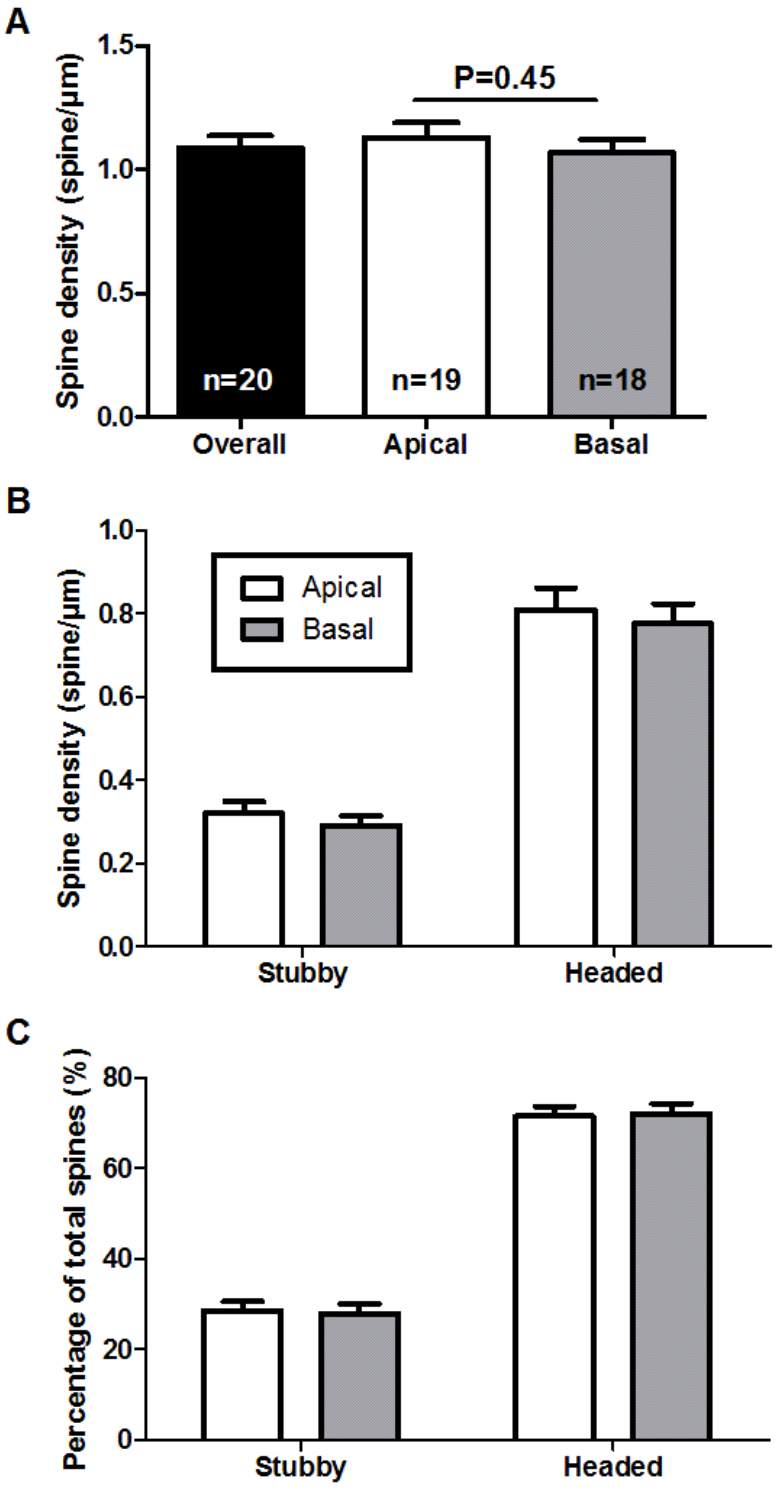

Figure 4-4: Density and representation of spine types in CA1 hippocampal neurones of organotypic slices at 14 DIV.

(A) The overall density at 14 DIV was very similar between apical and basal dendrites (Student t-test, p=0.45). Spine type density (B) and spine type percentage of total spines (C) were also very similar between apical and basal, in control conditions at 14 DIV.

Spine types, which are the product of presynaptic activity and postsynaptic ability for plasticity, were also examined in the perspective of inputs and location disparity (figure 4-4B). The mean density of stubby spines was 0.32 ± 0.03 spines/µm (n=19) in apical and 0.29 ± 0.02 spines/µm (n=18) in basal dendrites, that of mushroom spines was 0.19 ± 0.02 spines/µm (n=19) in apical and 0.17 ± 0.02 spines/µm (n=18) in basal, and finally thin spines were 0.62 ± 0.05 spines/µm (n=19) in apical and 0.62 ± 0.04 spines/µm (n=18) in basal dendrites. A two-way ANOVA comparing conditions and location found no difference whether the spines were on apical or basal dendrites (p=0.46).

The contribution of each spine type, measured as the percentage of each group on the total pool of spines (all spines are counted in our observations of density) is a parameter often looked at because it is independent of the density. The proportion of each spine type can change distinctly from the density of that subgroup if the other groups are also affected. Here, as no difference was observed between apical and basal dendrites density, the percentage of each spine type was similarly comparable between the two regions (figure 4-4C, two-way ANOVA: p=1.00).

4.3.2 Spine head diameter

Although the density of spines and the representation of the different spine types is very similar between apical and basal dendrites, the spine head diameter of headed spines was compared in the two regions (figure 4-5). The measurements of 90 randomly selected spines from each cell in one region were pooled together, thus giving the same weight to all the cells analysed. The graph on figure 4-5A shows the median of the distribution, as well as the first and third quartile on the box, and the min and max of the distribution at the whiskers. The dissymetry of the box shows that the sample of spine head diameter was not normally distributed, and it was confirmed using D'Agostini and Pearson omnibus normality test (p<0.0001 for both apical and basal dendritic spines). The comparison of the ranking of the sample showed that spines on apical dendrites had significantly larger head diameter (median, apical: 0.41 µm, n=1350 spines; basal: 0.36 µm, n=1260; Mann-Whitney test: p<0.0001).

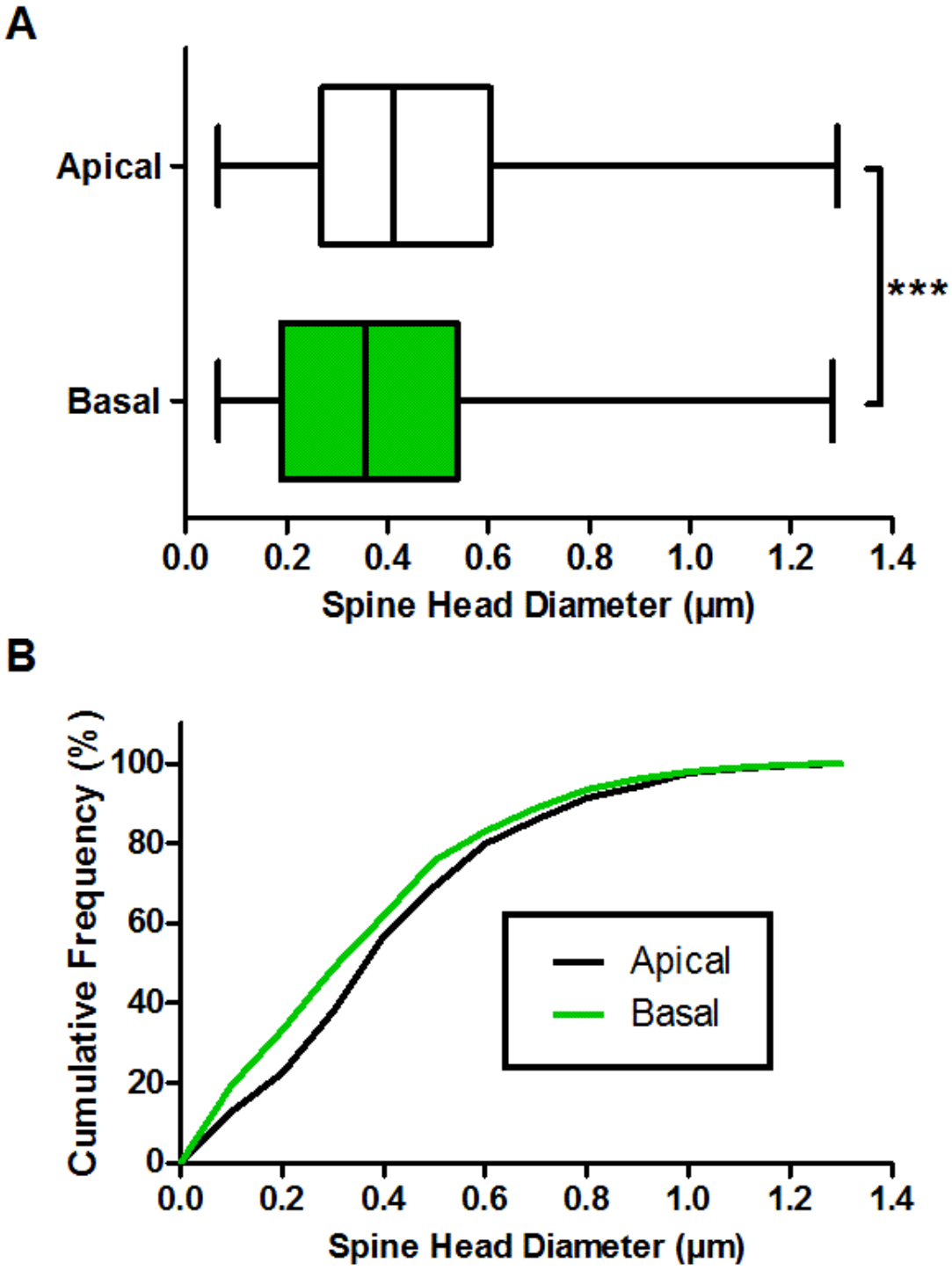

Figure 4-5: Spine head diameter of dendritic spines in apical versus basal dendrites.

(A) Box and whisker plot of dendritic spine head diameter in control conditions of CA1 pyramidal neurones at 14 DIV, showing the min and max point (whiskers), and the 25, 50 and 75% (box). (B) Cumulative distribution of spine head diameter on a sample of randomly selected 90 spines per cell in either apical (n=1350 spines from 15 cells) or basal dendrites (n=1260 spines from 14 cells).

4.3.3 Spine length

The analysis of spine length allows the evaluation of a certain degree of plasticity, longer spines being usually more motile and prone to changes (reviewed in Kasai et al., 2003). Using the same method described earlier for cumulative distribution, a random subset of spines was selected from either apical or basal dendrites, and pooled together, making sure that the same number of spine was selected from each cell. The graph on figure 4-6A shows the median of the sample for apical and basal spines. In contrast to what was observed with the spine head diameter, the two boxes are very similar, showing that the distribution of spine length was independent of the location of the parent dendrite (figure 4-6B). The median of the spine length was 0.95 µm (n=1350) in the apical, and 0.92 µm (n=1260) in the basal dendrites. The Mann-Whitney test for non-normally distributed samples found no significant difference between apical and basal spine length (p=0.14).

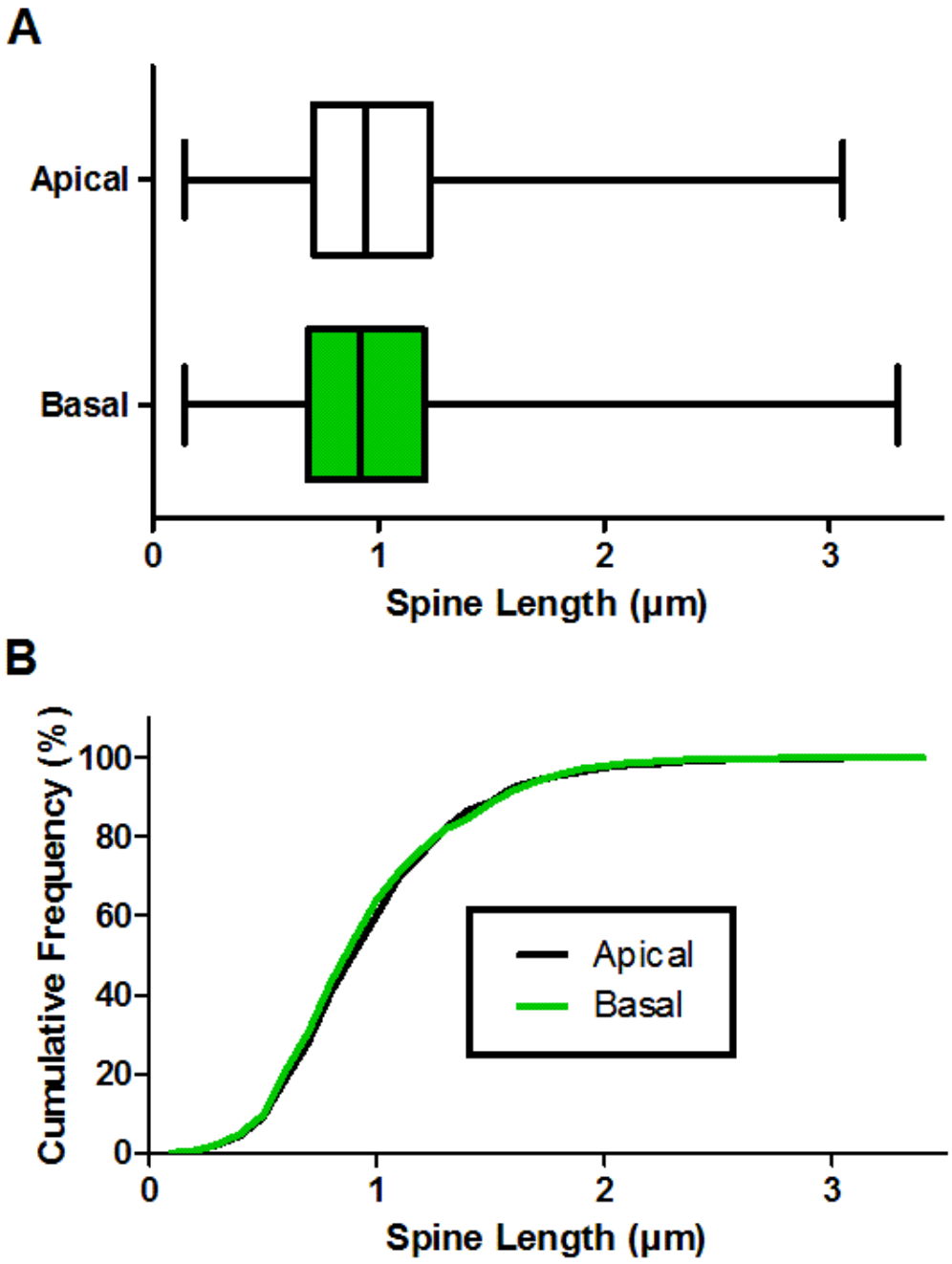

Figure 4-6: Spine length of dendritic spines in apical versus basal dendrites.

(A) Mean of medians per cell of dendritic spine length in control conditions of CA1 pyramidal neurones at 14 DIV. (B) Cumulative distribution of spine length on a sample of randomly selected 90 spines per cell in each condition (apical, n=1350 spines from 15 cells; basal, n=1260 spines from 14 cells).

4.3.4 Input from the Schaffer collateral

In this section, the focus is to compare dendritic spines receiving input exclusively from CA3 spines to the overall spine population. In organotypic cultures, all neurones tend to be hyper-connected, and especially the CA3 cells. Indeed, cutting the Schaffer collateral pathway in hippocampal organotypic cultures removes most spontaneous activity in CA1 neurones, suggesting that this pathway is the most active input to CA1 cells (De Simoni and Edwards, 2006). The Schaffer collateral pathway, which innervates mostly the proximal apical dendrite of CA1 neurones, was found to impinge largely on mushroom spines (De Simoni and Edwards, 2006). This result is in agreement with the finding presented above in 4.3.2, showing that spines on proximal apical dendrites were larger than those on basal dendrites.

The technique used here to label presynaptic axons with DiO and detect synaptic contacts has been repeatedly tested in the lab (De Simoni and Edwards, 2006), showing a nearly perfect correlation between contacts that appeared as synapses and actual synapses tested via presynaptic current injection and postsynaptic recordings. The 3D reconstruction of synapses was made with Imaris viewer, and shows in green the DiO labelled CA3 axons, contacting the Alexa 594 filled CA1 cell, in red on figure 4-7.

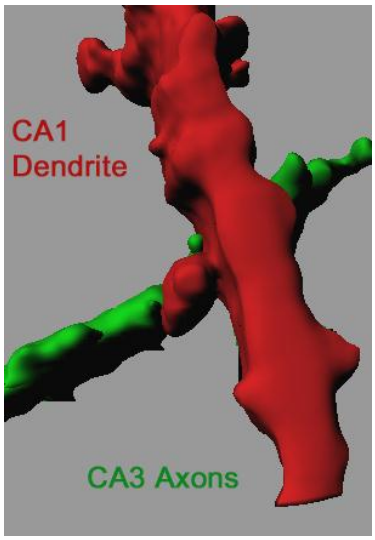

Figure 4-7: 3D isosurface reconstruction of a section of CA1 dendrite (red) showing a contact between a spine and a DiO labelled axons from a CA3 cell (green).

4.3.4.1 Spine type representation

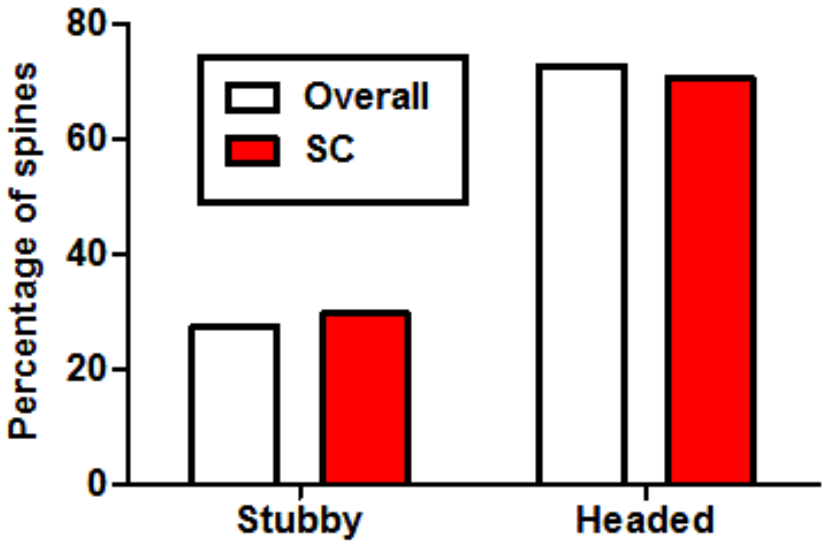

Figure 4-8: Percentage of each spine type taken from the overall sample of spines available for either the overall population, or only receiving input from the Schaffer collaterals (SC).

27 spines from 9 CA1 pyramidal neurones were identified using DiO as receiving input from the Schaffer collateral axons. These spines were compared to 10,590 spines sampled across the dendritic trees of 25 dye-filled neurones (figure 4-8). The number of spines with labelled presynaptic partner is much smaller than the overall number of spines because the identification of synapses is much more time-consuming than screening of spines with undetermined presynaptic input. Here, stubby spines account for a very similar percentage of total spines whether they receive input exclusively from the Schaffer collateral (SC, 29.6%) or from any cell (overall, 27.4%), similarly to what was observed previously (De Simoni and Edwards, 2006).

4.3.4.2 Spine head diameter and length

In this section, the cumulative frequency of head diameters from headed spines is visible on figure 4-9A, followed by the box representing the median, 1st and 3rd quartiles of the head diameter distribution (figure 4-9B).

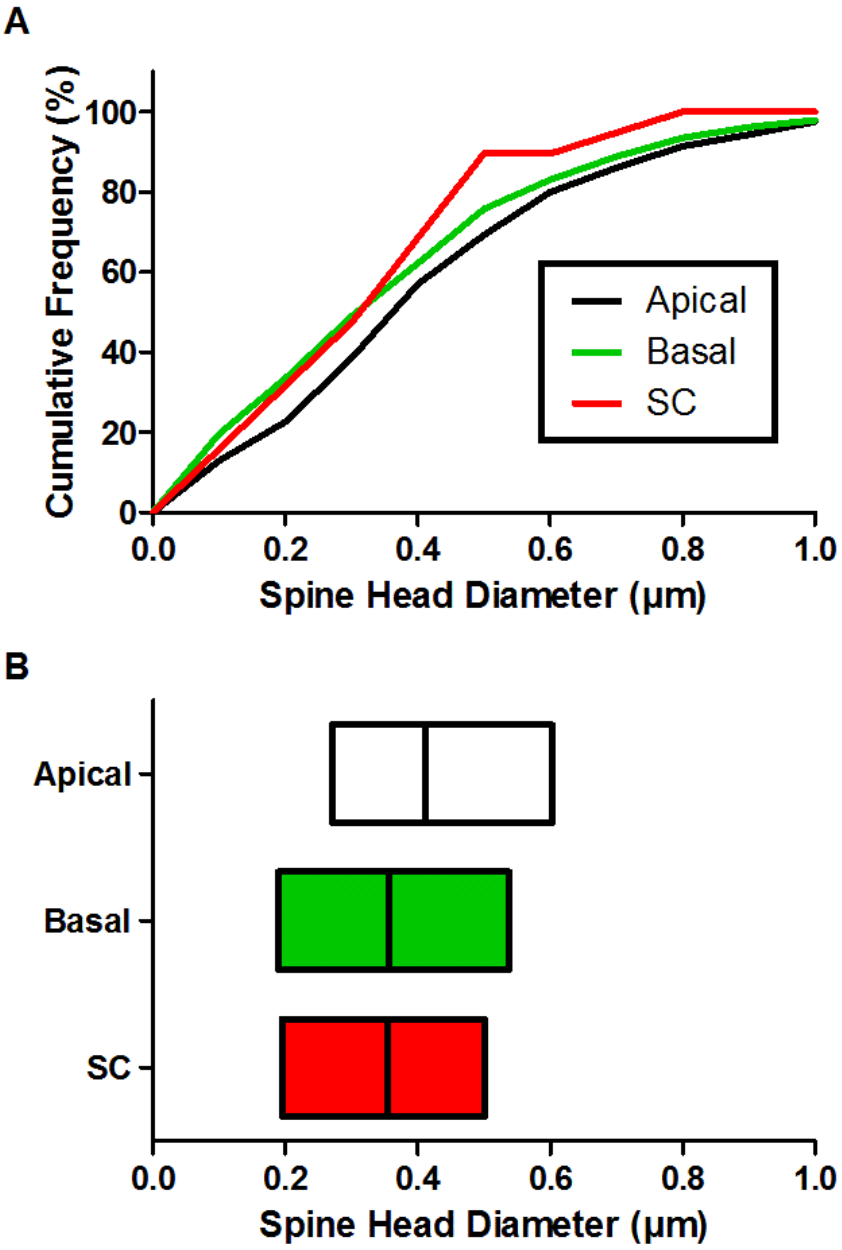

Figure 4-9: Spine head diameter of headed dendritic spines receiving any presynaptic input (apical & basal) or Schaffer collateral only (SC).

(A) Cumulative frequency of spine head size from a random sample of 90 headed spines per cell for the overall population, or from all the headed spines identified which received input from the Schaffer collateral. The Kruskal-Wallis test showed a trend towards smaller head sizes in spines receiving input exclusively from the Schaffer collateral (p=0.088). (B) Median, 1st and 3rd quartiles of the spine head diameter distribution in apical (n=1350 synapses), basal dendrites (n=1260 synapses) or spines receiving only SC input (n=19 synapses).

A Kruskal-Wallis with Dunn's post-hoc test on spine head diameters revealed no significant difference between spines receiving input from the Schaffer collateral and spines receiving any input and located either in the apical or basal dendrites (median, apical: 0.41 µm, n=1350 spines; basal: 0.36 µm, n=1260 spines; Schaffer collateral input: 0.35 µm, n=19 spines). Surprinsingly, the spines receiving input from the Schaffer collateral identified here are not bigger than the overall population, in contrast to the observations made earlier in this work and in De Simoni et al (2006). Spines in the proximal apical dendrites, mainly innervated by the Schaffer collateral, were found to have larger heads than those in the basal dendrites. The result presented above suggests that the spines identified here may represent a different population from the one previously studied in the lab with this method (De Simoni and Edwards, 2006). This hypothesis is strenghtened by the observation that spine forming CA3-CA1 connections are on average shorter than the overall population (median, overall: 0.95 µm, n=1350 spines; Schaffer collateral: 0.66 µm, n=19 spines, Mann-Whitney non parametric test, p=0.0021, figure 4-10).

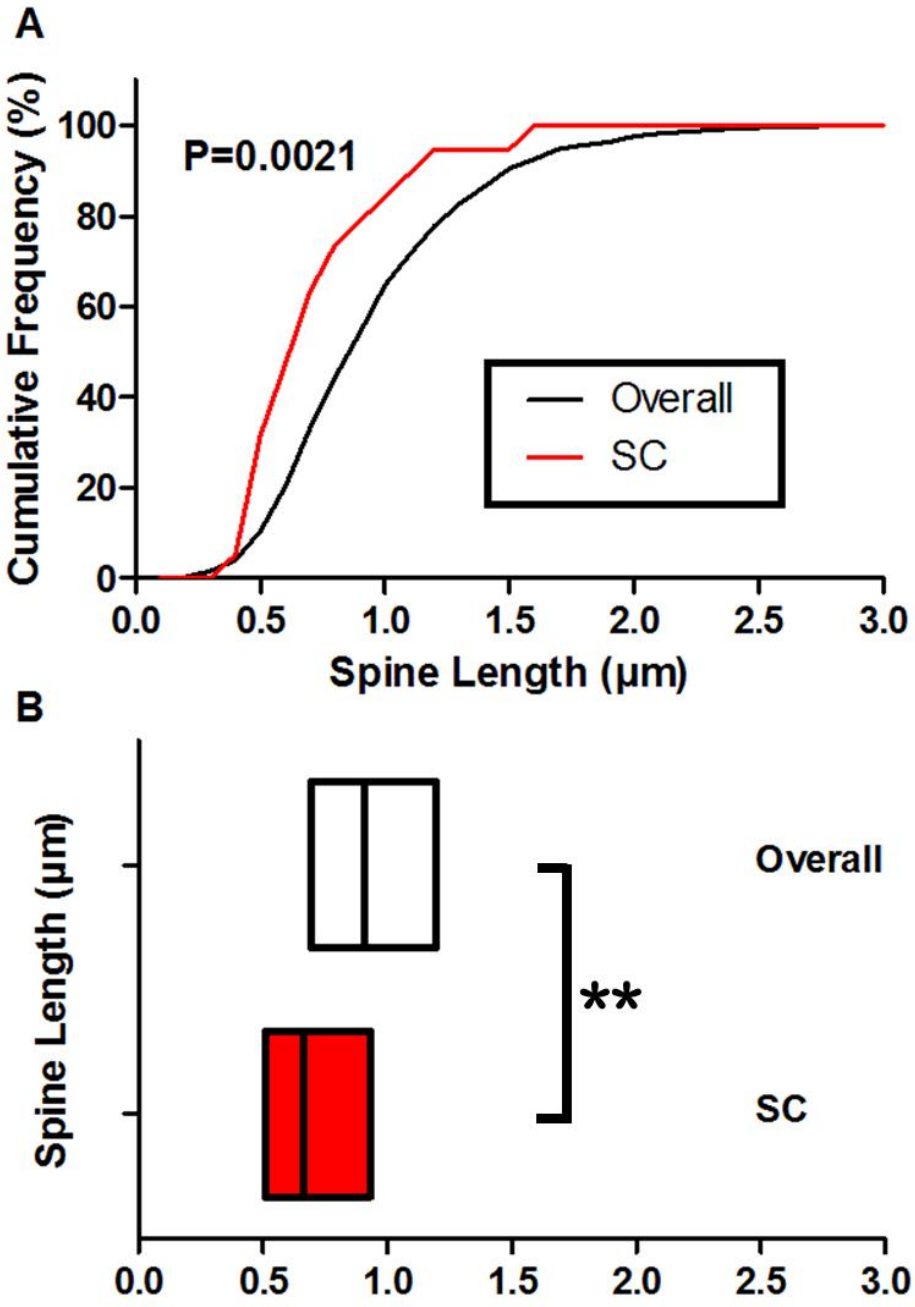

Figure 4-10: Spine length of dendritic spines receiving any presynaptic input (overall) or Schaffer collateral only (SC).

(A) Cumulative frequency of spine head size showing a decrease in spine length among spines receiving SC input only compared with the overall population (overall n=1350 spines, SC n=19 spines, Mann-Whitney test p=0.002). (B) Median, 1st and 3rd quartile of the spine length distribution.

4.4 Comparison of dendritic spine population in apical dendrites, according to the degree of complexity of the branches

4.4.1 Density and spine type distribution

Basal dendrites have a very high number of terminations and branchings, which are usually difficult to track because they develop from a few bundles (Bannister and Larkman, 1995). In contrast, apical branches have much simpler organisation, usually forming a maximum of three branches (figure 4-11). Apical branches are easily identified, and thus spines can be sorted according to the degree of branching of their parent dendrites. In the following section, the density and representation of the different type of spines was analysed on the apical dendrites of CA1 pyramidal neurones, in control hippocampal slices of 14 DIV cultures (figure 4-12).

The total density of spines was 1.16 ± 0.11 spines/µm (mean ± SEM, n=5) in the first branches, 1.07 ± 0.07 spines/µm (n=14) in the second branches and 0.91 ± 0.05 spines/µm (n=4) in the third branches (figure 4-12A). The results were analysed using one-way ANOVA, which did not detect a significant difference (p=0.30). The sample number varies a lot, the first and third branches being little represented, while second branches were more abundant. This is due to the necessity, in order to optimize imaging, to select long segments ideally within limited depth, and parallel to the main line of scanning, thus limiting scanning time, potential damage to the slice and bleaching of the fluorophore. In that context, second branches usually fit more criteria and are more often selected.

Characterisation of how density of different spine types and representation is affected by the level of branching of the parent dendrite (figure 4-12 B&C) reveals that headed spine density decreased with increasing branching (two-way ANOVA with Bonferroni's post-test, p=0.037), but not stubby spines density (p>0.05).

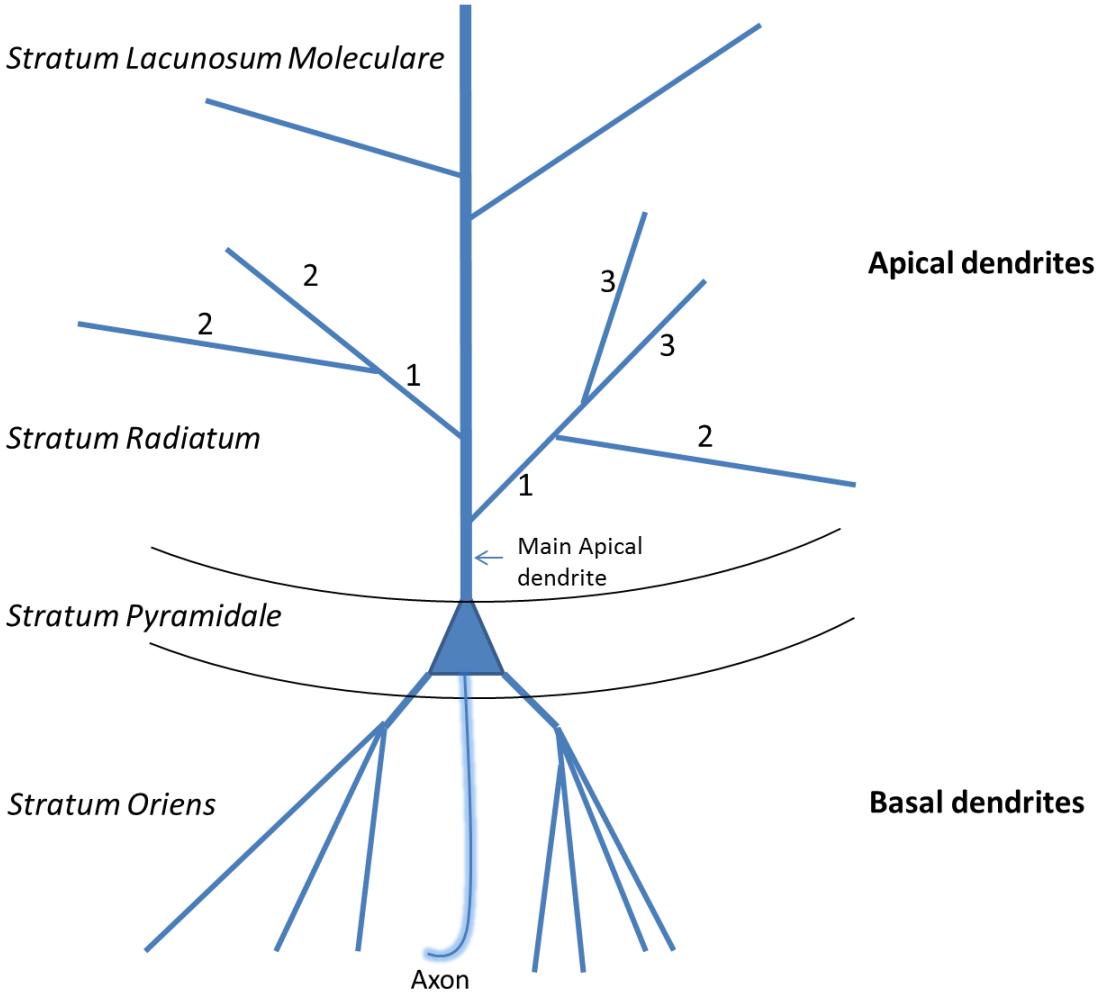

Figure 4-11: Structural organisation and branching of a CA1 pyramidal neurone.

The s*tratum pyramidale*, or cell body layer, divides the dendritic tree into highly ramified basal dendrites in the s*tratum oriens,* and apical dendrites towards the centre of the hippocampus. The apical dendrites can be separated *in vivo* between the s*tratum radiatum*, which receives input from the Schaffer collateral axons, and the s*tratum lacunosum moleculare*, which *in vivo* receives exclusively input from the Layer III of the entorhinal cortex. The numbers on the apical branches correspond to the degree of separation from the main apical dendrite.

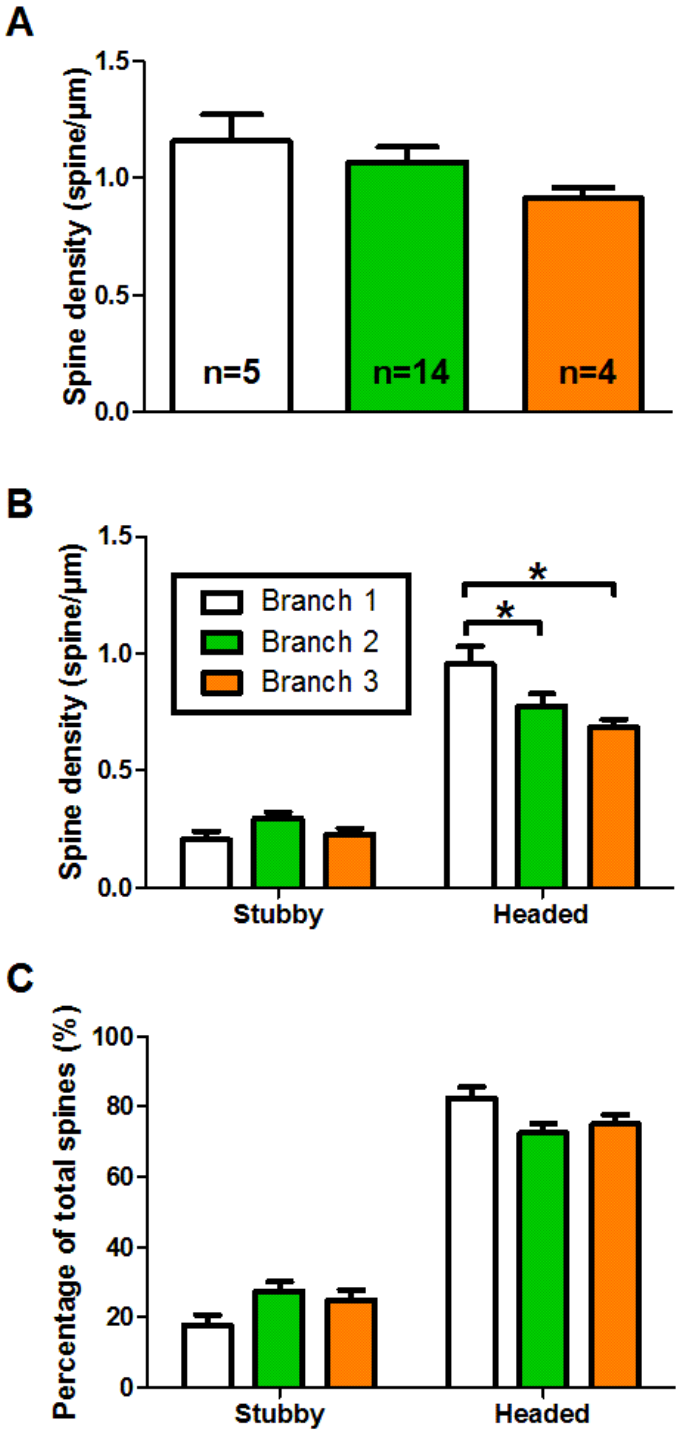

Figure 4-12: Density of dendritic spines and percentage of spine type in the different branches of apical dendrites.

(A) Density of spines was not significantly different in the branches (mean ± SEM, one-way ANOVA. p=0.30). (B) Stubby spine density was unchanged in the different branches, but headed spine density decreased with increasing ramification (two-way ANOVA with Bonferroni's post-test). (C) The percentage of spines per type was unaffected by the branching level (one-way ANOVA, p=0.15).

4.4.2 Spine head diameter

Spine head diameters in branches were compared using the min to max whiskers plot (figure 4-13A) and the cumulative frequency distribution of pooled data (figure 4-13B). The median values for spine head diameter obtained on the sample pooling an even number of spines from each cell were for Branch 1: 0.47 µm (n=475 spines), for Branch 2: 0.43 µm (n=2181 spines), and for Branch 3: 0.46 µm (n=283 spines). The differences were not significant (Kruskal-Wallis, p=0.11).

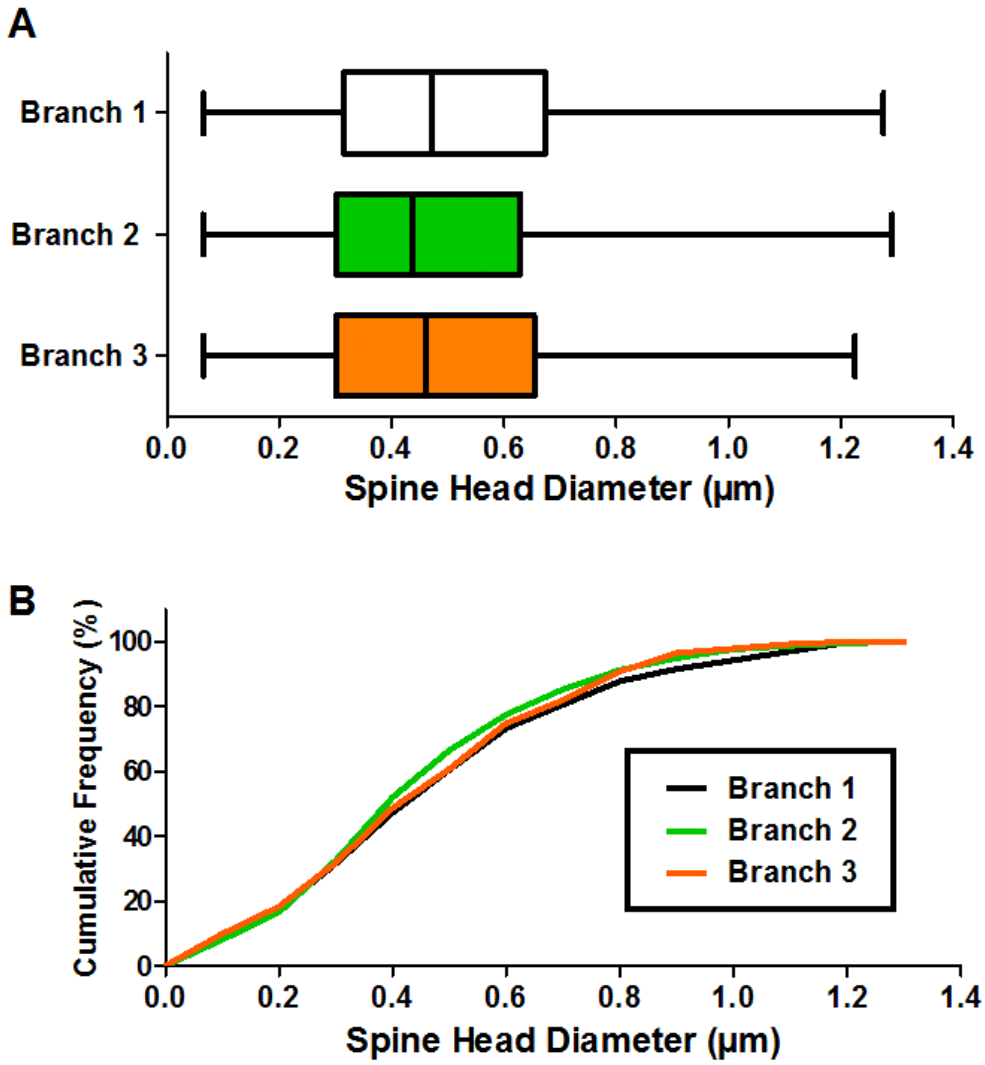

Figure 4-13: Spine head diameter of spines according to their branching order in apical dendrites.

(A) Min to max whiskers plot of dendritic spine head diameters in the three types of branches. (B) Cumulative frequency in percentage of spine length in the three types of branches in apical dendrites.

4.4.3 Spine length

The length of dendritic spines was compared across the different branches with its median, first and third quartiles, as well as the minimum and maximum values of the distribution (figure 4-14A). the cumulative frequency distribution of pooled data (figure 4-14B), The median values for spine length obtained on the sample pooling of an even number of spines from each cell were for Branch 1: 0.98 µm (n=475 spines), for Branch 2: 0.94 µm (n=2181 spines), and for Branch 3: 0.92 µm (n=283 spines). Kruskal-Wallis with Dunn's post-hoc test revealed a significant difference between first and third branches (p=0.034).

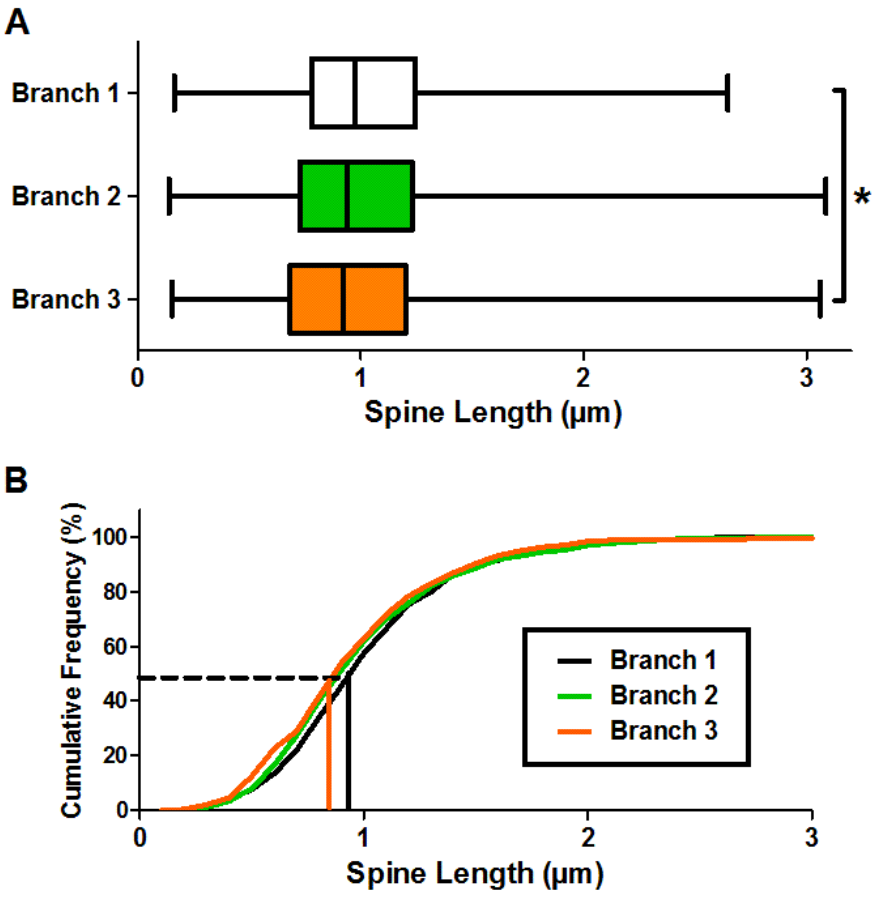

Figure 4-14: Spine length of spines according to their branching order in apical dendrites.
(A) Min to max whiskers plot of dendritic spine length in the three types of branches. (B) Cumulative frequency in percentage of spine length in the three types of branches in apical dendrites, presenting a significant decrease of length from third branches compared to first ones Kruskal-Wallis with Dunn's post-test, p=0.034).

4.5 Discussion

4.5.1 Apical *vs* basal

From the in-depth study of the dendritic tree of CA1 pyramidal neurones in control conditions of hippocampal organotypic slices of 14 DIV, apical and basal dendrites had on average very similar dendritic spine population. The overall density and the representation of spines as well as spine length were very similar in all categories. The main noticeable difference was found in spine head diameter, basal dendrites exhibiting smaller spines than their apical counterparts ($p<0.0001$). Though the difference between the medians of spine head diameter is small (apical 0.41 µm *vs* basal 0.36 µm) and may seem below resolution, it actually derives from a much larger difference in head volume. For instance, the median spine head volume of apical spines (0.036 μm^3) is 50% larger than the median head volume of basal spines (0.024 μm^3), a difference which could induce significant changes in ions transients and concentrations.

Interestingly, the difference in median head size between apical and basal dendrites partly strengthens what has been observed previously in the lab (De Simoni and Edwards, 2006). Indeed, apical dendritic spines were found to exhibit a higher percentage of mushroom –i.e. enlarged head- spines than basal spines. Moreover, the Schaffer collateral inputs predominantly innervate the *stratum radium* in the apical dendrites, and were found to impinge mainly on mushroom spines. Those results, observed by looking at spine types, have now been confirmed by studying the population of dendritic spines with more objective analysis based on Imaris *Filament Tracer* and the newly established analytical method.

4.5.2 Branching

Analysis of branching levels on apical dendritic spines shows a significant decrease in headed spines with increasing complexity. The overall density was not significantly affected, but the values found for each branch parallel previous results found in the lab in CA1 pyramidal neurones from 14 DIV organotypic cultures (De Simoni et al., 2003),

which saw a trend towards a reduced density with increasing branching. Some papers report an increase in larger spines with distance from soma (Andrásfalvy and Magee, 2001; Nicholson et al., 2006), suggesting that spines in more distant dendrites compensate for the attenuation of the signal through the propagation by increasing synaptic strength. The decrease in spine length could parallel an increase in spine stability with further branching, which can also be related to the distance from the apical dendrites, since third branches are usually further away from it than first or second branches.

4.5.3 Schaffer collateral pathway

In this chapter, the population of spines from unknown presynaptic input was compared to the sub-group of known input, here specifically from the Schaffer collateral identified by lipophilic labelling of CA3 cells with DiO crystals. If no significant changes could be detected in the proportion of the different spine types, the results seem to show that the identified spines receiving input from the Schaffer collateral are shorter than the average. In a paper previously published from the Edwards lab, the percentage of mushroom spines receiving input from CA3 cells (~50%) was much larger than the average proportion of mushroom spines (<10%) in their preparation (De Simoni and Edwards, 2006). Here the experiments were carried out on similar preparation, i.e. hippocampal organotypic cultures at 14 DIV. However, the method for analysis has largely changed and spines are not evaluated on visual criteria but following a more objective analysis. Moreover, even if the procedure to make slices and label presynaptic axons have remained similar, there was no overlapping between the previous experimenter, Anna De Simoni, and myself, and thus small changes in the practice could induce differences in the population of CA3 cells labelled or in the synapses selected for the study. Indeed, when labelling CA3 axons, Anna De Simoni was focusing only on en-passant axons which she could follow all the way through.

In my hands, it was almost impossible to follow axons across the field of view, suggesting that some differences in the preparation could have led to the labelling or identification of different synapses. The synapses thus identified were not necessarily from en-passant axons, and could result from synapses formed on sprouting axons. In

the sample of synapses identified receiving input from the Schaffer collateral, the spine length were smaller and spine head diameter not larger than the overall average, emphasising that in this subset of synapses, CA3 did not seem to be impinging preferentially on enlarged spines.

This result does not reflect what was observed in the overall population, where the apical dendritic spines, receiving mainly input from CA3 cells, were found to have larger heads than basal spines. This finding support the hypothesis that the sub-population of spines identified was not the same as those identified by Anna De Simoni previously, and the difficulty to follow them further induced us to suggest they were from recently sprouting axons.

Chapter 5. Synaptic scaling in organotypic slices?

Work carried out at UCSD, in Prof Malinow's lab

5.1 Introduction

The ability of neurones to maintain their excitability is fundamental for their capacity to respond to environmental changes and to generate action potentials while the network activity is disturbed. During long-term changes of activity, cells need to adapt their firing threshold in order to remain functional, and avoid either run-down of activity in case of hyper-activity or silencing in case of decreased network activity. How neurones adapt their plasticity rules to remain functional when their network is undergoing persistent changes of activity is a question that may find some answer in homeostatic mechanisms. Identified in Turrigiano's group as a local answer to global changes, synaptic scaling allows all synapses to scale up or down similarly to compensate for changes in general activity, thus maintaining cell excitability while preserving the relative weight of each input (Turrigiano et al., 1998). Synaptic scaling was originally observed and studied *in vitro,* in dissociated cells cultures, and has been progressively observed in other cellular models or *in vivo* (see review Pozo and Goda, 2010).

5.1.1 Synaptic scaling or absence of activity-induced changes during development?

In hippocampal organotypic slices, Kim and Tsien (2008) found an increase in mEPSCs amplitude but not frequency in CA1 cells treated for 48 hours with 1 µM TTX, and recorded at 21-25 DIV. This result concords with Turrigiano's data in dissociated cultures of visual cortex neurones and may reflect molecular mechanisms happening in mature circuits since, by that age, neurones in hippocampal cultures have reached stability (De Simoni et al, 2003). The rules of synaptic scaling, like most synaptic plasticity mechanisms happening in neurones, seem to be evolving in parallel with development (Kirov et al., 2004). As a matter of fact, chronic suppression of activity

during development was found to yield opposite results depending on the method used. For instance, reducing spontaneous activity for 3 days with high Mg^{2+} concentration on 4 DIV organotypic cultures induces a decrease in activity-driven incorporation of AMPA receptors and thus a reduction of mEPSCs amplitude (Barria and Malinow, 2005). However, in another series of similar experiments on 6-9DIV organotypic cultures, a 48 hours blockage of AMPA and NMDA receptors induced an increase in mEPSCs amplitude, in line with the commonly observed synaptic scaling (Stellwagen and Malenka, 2006).

It is therefore possible that changes in the way of inducing activity blockade and the age and type of preparation yields different adaptive responses. In order to determine the potential for synaptic scaling and homeostatic plasticity in my organotypic cultures, I first tried to reproduce chronic activity deprivation for 48 hours with TTX and separately with a cocktail of glutamate receptor antagonists CNQX/APV in 14 DIV rat organotypic slices, which were similar to the culture I was using at UCL. I tried in a second time to induce homeostatic plasticity in 6-9 DIV mice organotypic slices, reproducing the procedure used in Stellwagen paper, trying to determine whether chronic activity blockade induces a homeostatic compensation or a lack of spontaneously-driven up-scaling in developing neurones.

5.1.2 Experimental procedures

Most of the experiments carried out in the Edwards lab at UCL were done on rat organotypic hippocampal slices, made from P7 males. Since this model is the base of most of my experiments on homeostatic plasticity, it was useful to establish whether synaptic scaling was also happening in this model.

In the Malinow lab at UCSD, in contrast to the cultures done at UCL, the hippocampus was removed from the whole brain under the flow cabinet, and was chopped in 400 µm sections, the hippocampus being almost horizontal and not as curved as in its natural position in the brain. This technique allows more slices to be kept from the hippocampus, since most of them are cut similarly, preserving the tri-synaptic circuit.

This chapter comprises two series of experiments, the first one on rat organotypic slices of 13-15 DIV (section 5.2), the second on mouse organotypic slices of 6-9 DIV (section 5.3). For each type of culture, two different methods of chronic activity blockade are used. In the first method, the treatment consisted of 1 μM of TTX, which was the drug originally used to provoke synaptic scaling in dissociated cortical cultures (Turrigiano et al., 1998). In a second method, the cocktail of the glutamate receptor antagonists CNQX (50 μM) and D-APV (100 μM) were used similarly to previous publication (Stellwagen and Malenka, 2006). In that paper, they look at the effect of Tumor Necrosis Factor alpha (TNFα) levels on miniature synaptic transmission in the hippocampus, both in dissociated cell cultures and in hippocampal organotypic slices. Surprisingly, there is a discrepancy in the method they use to achieve synaptic scaling between their two different culture models. With their dissociated hippocampal cultures, they keep the commonly used protocol for dissociated cultures consisting of 1 μM of TTX which completely blocks sodium channels and thus action potentials in all cells. Similarly to the study by Turrigiano and colleagues (1998), Stellwagen and co-workers (2006) found a large increase in the mEPSCs amplitude of treated pyramidal cells under those conditions compared with control transmission. However, when they tried to repeat the experiment with organotypic cultures, which have a much more preserved architecture than dissociated culture, they used a mix of CNQX and APV to block only AMPA and NMDA receptors, thus offering a different protocol to implement the lack of excitation and induce synaptic scaling.

I thus tried to investigate the two approaches, blocking either action potential-mediated excitation with TTX or reducing the cell ability to sense excitation by blocking both NMDA and AMPA receptor channels, in CA1 pyramidal cells from organotypic hippocampal cultures.

5.2 Synaptic scaling in CA1 pyramidal neurones of rat organotypic slices after 14 DIV

5.2.1 Model 1: Rat organotypic slices, recorded at 14 DIV

The organotypic slice cultures are left for 11 to 13 days after slicing to develop in the incubator at 37°C, the culture medium being replaced every other day. For the last 48 hours before recording, the culture medium is refreshed, and the drugs necessary to block some path of the synaptic transmission are added individually into each well from a freshly thawed aliquot of the drug (figure 5-1).

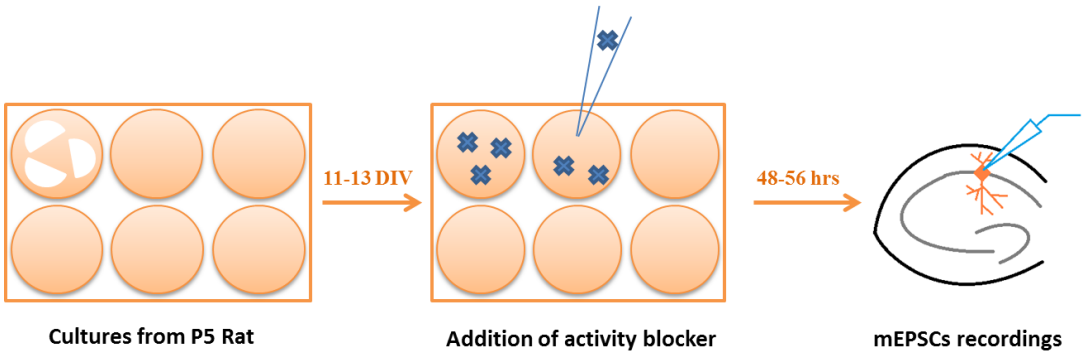

Figure 5-1: Scheme of treatment on rat hippocampal organotypic slices.
Hippocampal organotypic slices are made from male P5 rat pups, and transferred onto confettis, and placed over inserts in a 6 wells plate with 1 ml of culture medium. After 11-13 DIV, the activity blocker drug is added to the culture medium, and the slices are taken out for recordings of mEPSCs after a minimum of 48 hrs.

Hippocampal organotypic slices were taken out of their culture conditions, and incubated under a normal ACSF for the duration of the recording. Both control and treated slices were left at least 30 minutes in the recording chamber perfused with normal ACSF in order to wash out the remaining of the drugs used in treated slices, especially CNQX which blocks AMPA receptor-mediated synaptic transmission, and to have comparable conditions in the control slices. The volume of flowing solution was at least 50 ml, so as to decrease significantly the concentration of drugs potentially left. The slices were cultured in dishes of 1 ml, and were extracted by cutting the porous supporting membrane, thus transferring the minimal amount of medium between the two solutions. If a fifth of the solution was transferred, approximately 200µl, the dilution would be 1:250, leading CNQX concentration to 0.2 µM, i.e. 10-fold lower than the IC_{50} of CNQX on AMPA receptors in CA1 cells (Andreasen et al., 1989).

This concentration is sufficiently low to neglect the antagonist effect of the molecule on AMPA receptors after wash. The mEPSCs were recorded at 32°C, with a glass pipette of 3.0-4.5 MΩ resistance, in an ACSF containing 11 mM glucose, 1 mM $MgCl_2$, 2 mM $CaCl_2$, and a cocktail of 1 µM TTX, 100 µM D-APV, 100 µM picrotoxin to block sodium channels and the fast ionotropic NMDA and $GABA_A$ receptors. Recordings were used only when the input resistance was at least ten times higher than the series resistance, itself below 15 MΩ (usually between 9 and 12 MΩ) to avoid filtering of the signal.

5.2.2 No synaptic scaling observed in CA1 cells of 14 DIV rat organotypic cultures

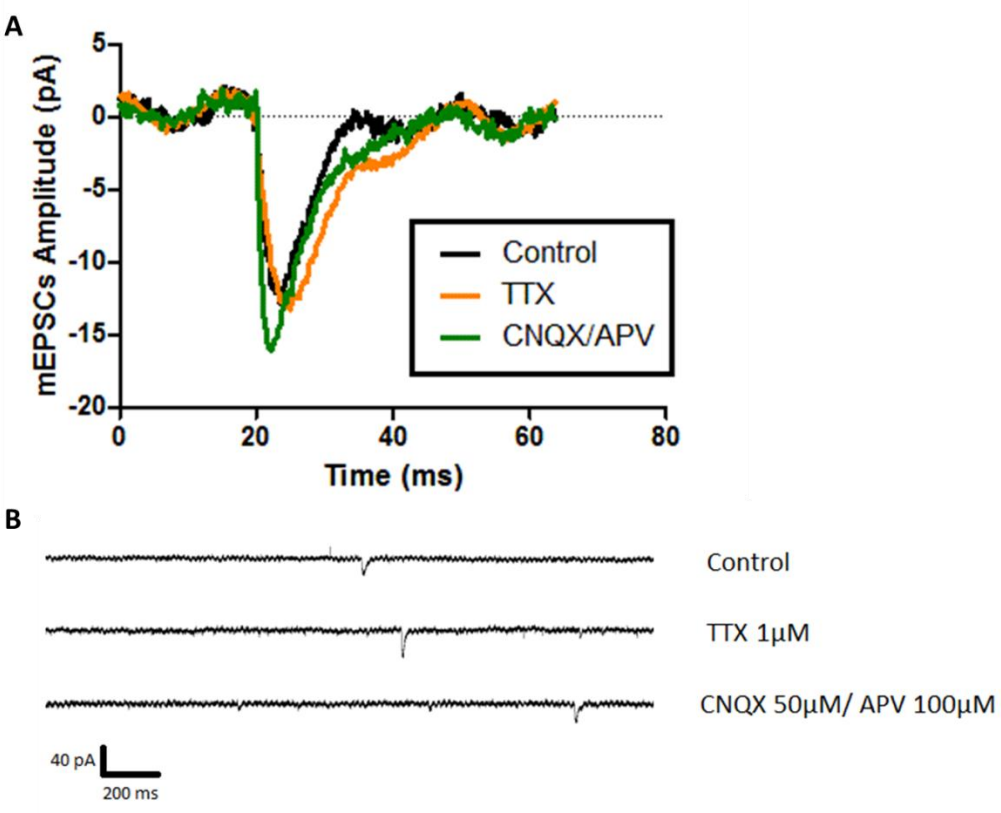

Figure 5-2: Sample trace from mEPSCs recording on CA1 cells in rat organotypic slices of 13-15 DIV.

(A) Average of 50 mEPSCs from individual cell, recorded after 48 hours treatment in either control, TTX or CNQX/APV culture medium. (B) Sample of mEPSCs recordings from a single cell, in the three conditions examined. NB: The 60 Hz cycle visible introduce a noise below 3 pA, and did not prevent either the detection or a clear reading of the events.

On figure 5-2A, the traces show the average of 50 excitatory events in a single cell from a control culture (black line), or a culture incubated for 48 hours with TTX (orange) or a cocktail of CNQX and APV (green).The traces below (figure 5-2B) are 2 seconds recordings of a single cell in the three conditions, showing the low frequency of miniature EPSCs.

To ensure that the events detected are not artefacts, rise times of events were compared in each experiment with the mean value of all experiments and to those reported in the literature. In the control group (figure 5-3A, control), the mean rise time was 3.1 ± 0.4 ms (n=14), which is within the range generally observed on organotypic slices (1.5-5 ms) (Zhang et al., 2005; Cingolani and Goda, 2008). The rise time was not affected by the 48 hours incubation with the drugs, as the average rise time values for TTX or CNQX/APV treated slices were not significantly different from control ones (mean ± SEM, TTX: 3.2 ± 0.5 ms (n=9), CNQX/APV: 3.4 ± 0.6 ms (n=12), one-way ANOVA, p=0.42).

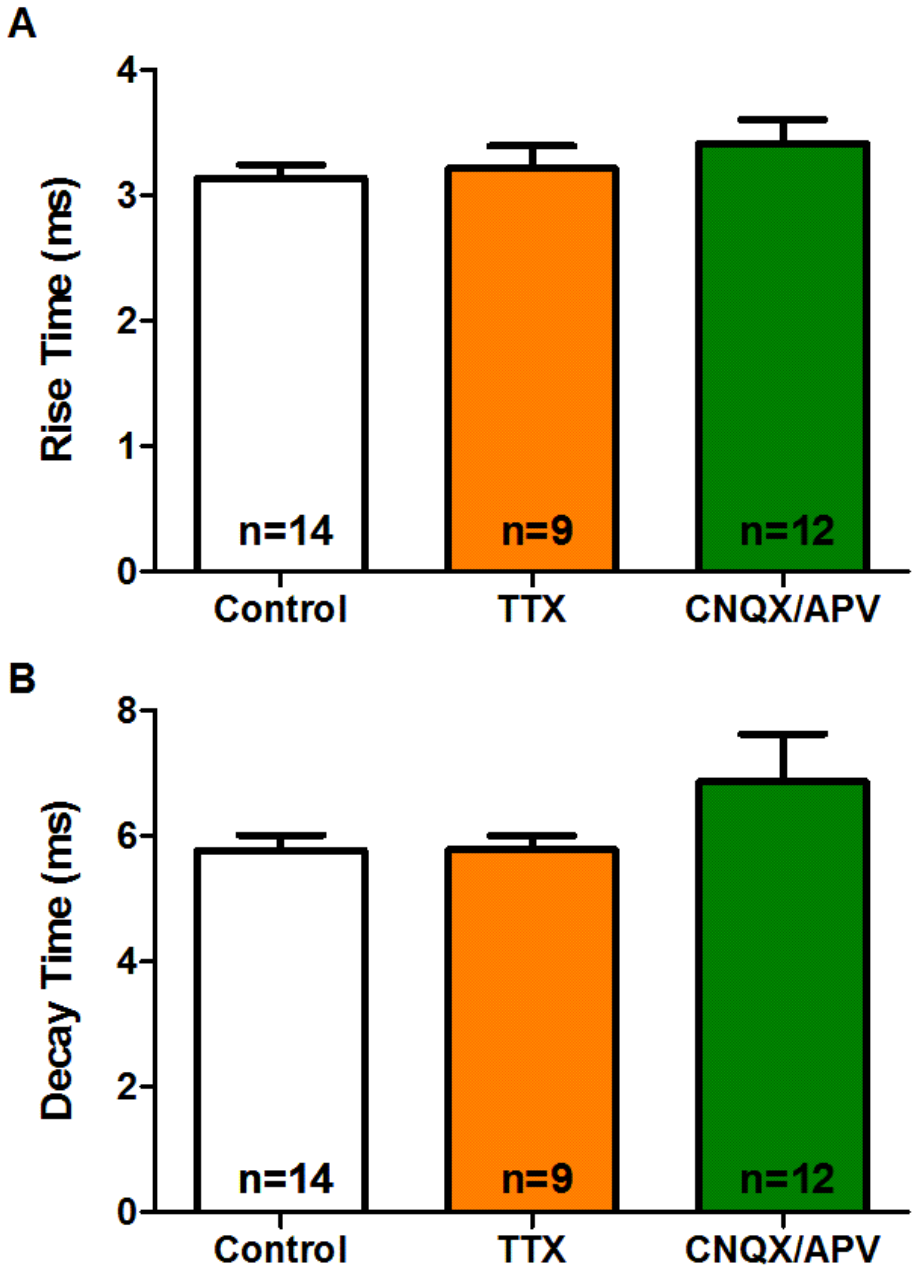

Figure 5-3: Mean rise and decay time of mEPSCs recorded in 14DIV rat CA1 cells.

(A) The mean rise time (10-90%) was not affected by the different treatment (one-way ANOVA, p=0.42). (B) The decay time was not significantly affected either, but the standard deviation was much greater on the CNQX/APV treated group (one-way ANOVA, p=0.21).

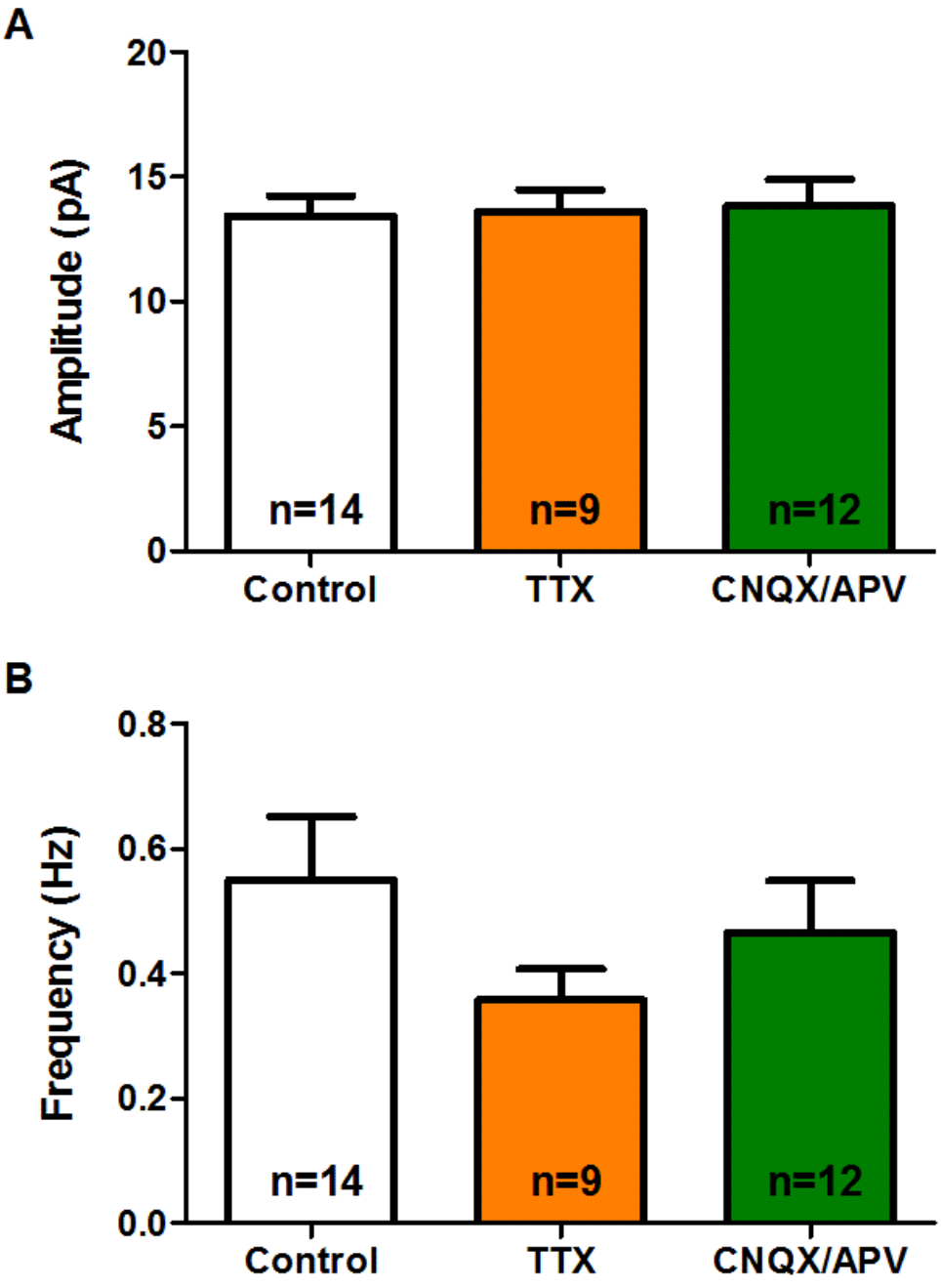

Figure 5-4: Amplitude and frequency of mEPSCs recorded from CA1 of rat 14 DIV organotypic cultures.

(A) The mean amplitudes of miniature excitatory events show no change after 48 hours of activity blockade, whether treated with TTX or CNQX/APV (one-way ANOVA, p=0.96). (B) The frequency of mEPSCs tends to decrease on average, but no significant changes were detected in our sample (one-way ANOVA, p=0.34).

The decay time of miniature excitatory events can reveal differences in opening durations of the ionotropic receptors, which could be due to changes in subunit composition (Furukawa et al., 2005), or changes in deactivation or desensitisation. However, in our series of experiments (figure 5-3B), decay was left unchanged by the two days of drug treatments (control: 5.8 ± 0.2 ms, TTX: 5.8 ± 0.2 ms, CNQX/APV: 6.9 ± 0.8 ms; one-way ANOVA, p=0.21). This first set of experiment carried out on rat hippocampal slices of 13-15 DIV did not induce the expected synaptic scaling (figure 5-4 A&B): the amplitude of mEPSCs was left unchanged by 48 hours of activity blockade (one-way ANOVA, p=0.95). The frequency of mEPSCs was not altered either (one-way ANOVA, p=0.34). Developmental changes intrinsic to the preparation could induce differences in the potential for plasticity of slices.

I decided to repeat the series of experiment on mouse hippocampal slices of a younger age (6-9 DIV), where synaptic scaling was observed (Stellwagen and Malenka, 2006), to see if the preparation could induce different results.

5.3 Synaptic scaling in CA1 pyramidal neurones of mouse organotypic slices after 6-9 DIV

5.3.1 Model 2: Mouse organotypic slices, recorded at 6-9 DIV

As the first series of experiments, aiming at observing synaptic scaling on CA1 pyramidal cells in rat organotypic slices of 14 DIV, failed to demonstrate any significant change in either amplitude or frequency of miniature excitatory events, I hypothesised that this could be due to the difference in age and model of our cultures. In the second series of experiments, I reproduced very strictly the conditions used by Stellwagen *et al* to induce synaptic scaling in organotypic slices (Stellwagen and Malenka, 2006).

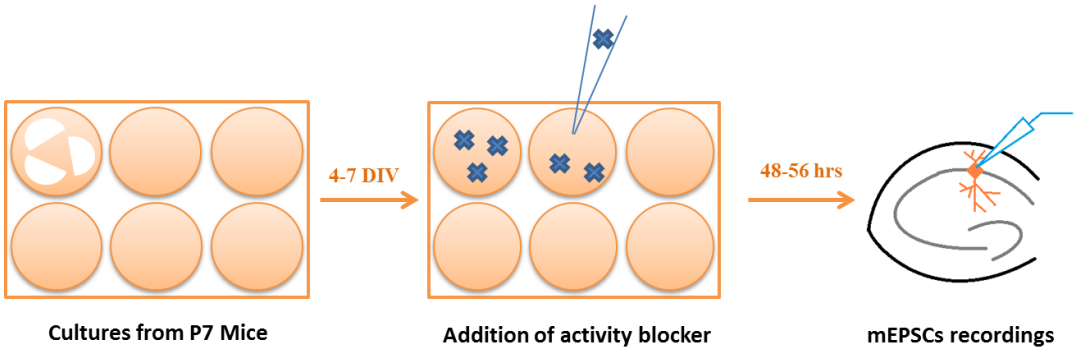

Figure 5-5: Scheme of experiments carried out in mice organotypic cultures, for recording mEPSCs at 6-9 DIV.

Hippocampal slice cultures are made from P7 male C57/Bl6 mouse pups according to the Stoppini method (Stoppini et al., 1991), and incubated for 4 to 7 days before adding either tetrodotoxin or CNQX/APV to the culture medium for a minimum of 48 hours before recording mEPSCs.

Hippocampal organotypic slices from P7 C57/Bl6 male mouse pups (figure 5-5) were kept in the incubator for 4 to 7 days before adding similar activity blocking drugs to what was used previously: TTX at 1 µM or CNQX 50 µM and D-APV 100 µM were added to the culture medium for a minimum of 48 hours.

5.3.2 No synaptic scaling in CA1 neurones of mice organotypic cultures aged 6-9 DIV

Miniature excitatory events were recorded from CA1 cells after a 30 minute wash out in the ACSF to remove all traces of CNQX, or just to establish comparable conditions. The average of 50 events from a single cell in control, TTX or CNQX/APV conditions is shown on figure 5-6A. Sample trace from an individual cell in each of the three conditions is shown on figure 5-6B.

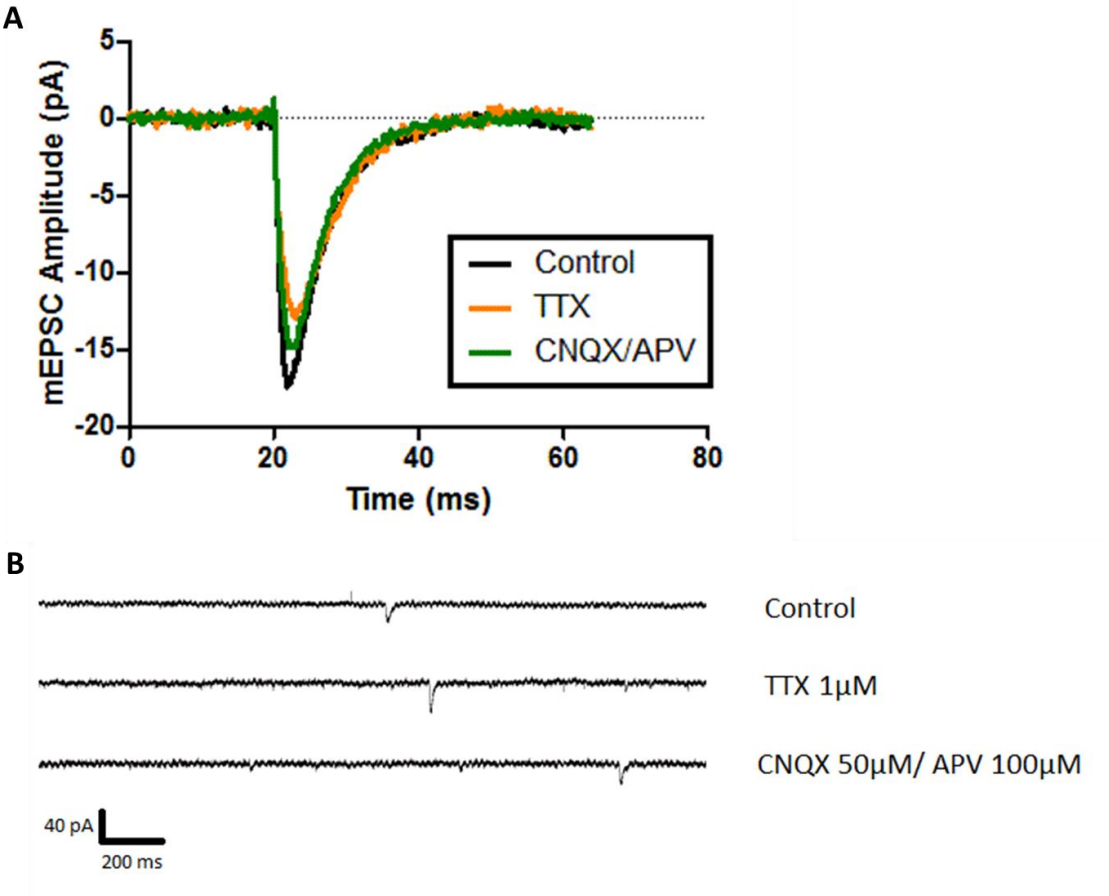

Figure 5-6: Sample trace from mEPSCs recording on CA1 cells in mouse organotypic slices of 6-9 DIV.

(A) Average of 50 mEPSCs from an individual cell, recorded after 48 hours treatment in either control, TTX or CNQX/APV culture medium. (B) Sample of mEPSCs recordings from a single cell, in the three conditions examined.

Looking at miniature excitatory synaptic currents rise time (figure 5-7A), no difference was observed (control: 3.4 ± 0.2 ms, n=14; TTX: 3.1 ± 0.3 ms, n=8; CNQX/APV: 3.7 ± 0.2 ms, n=14; one-way ANOVA, p=0.20). The decay time (figure 5-7B) was also very similar for the three conditions (control: 5.4 ± 0.2 ms, n=14; TTX: 5.2 ± 0.1 ms, n=8; CNQX/APV: 5.4 ± 0.2 ms, n=14; one-way ANOVA, p=0.61).

The results from amplitude and frequency of miniatures excitatory events were expected to show signs of synaptic scaling following prolonged blockade of activity (figure 5-8). However, amplitude of mEPSCs (figure 5-8A) was left unchanged (control: 15.4 ± 0.5 pA, n=14; TTX: 14.0 ± 0.7 pA, n=8; CNQX/APV: 14.7 ± 0.8 pA, n=14; one-way ANOVA, p=0.39), contrary to the significant increased observed in similar conditions by

Stellwagen (control, 11.2 ± 0.6 pA, n=15; CNQX/APV, 16.5 ± 0.5 pA, n=15; P<0.0001). The frequency of mEPSCs (figure 5-8B) was not affected either by long-term activity blockade (control: 0.49 ± 0.04 Hz, n=14; TTX: 0.50 ± 0.09 Hz, n=8; CNQX/APV: 0.40 ± 0.04 Hz, n=14; one-way ANOVA, p=0.34). The frequency seemed to be decreased between control and CNQX/APV treated slices, but Bonferroni's multiple comparison test revealed there was no significant difference (p>0.05). The drugs used for these two series of experiments were used regularly for other electrophysiological experiments, which validates their ability to act as expected.

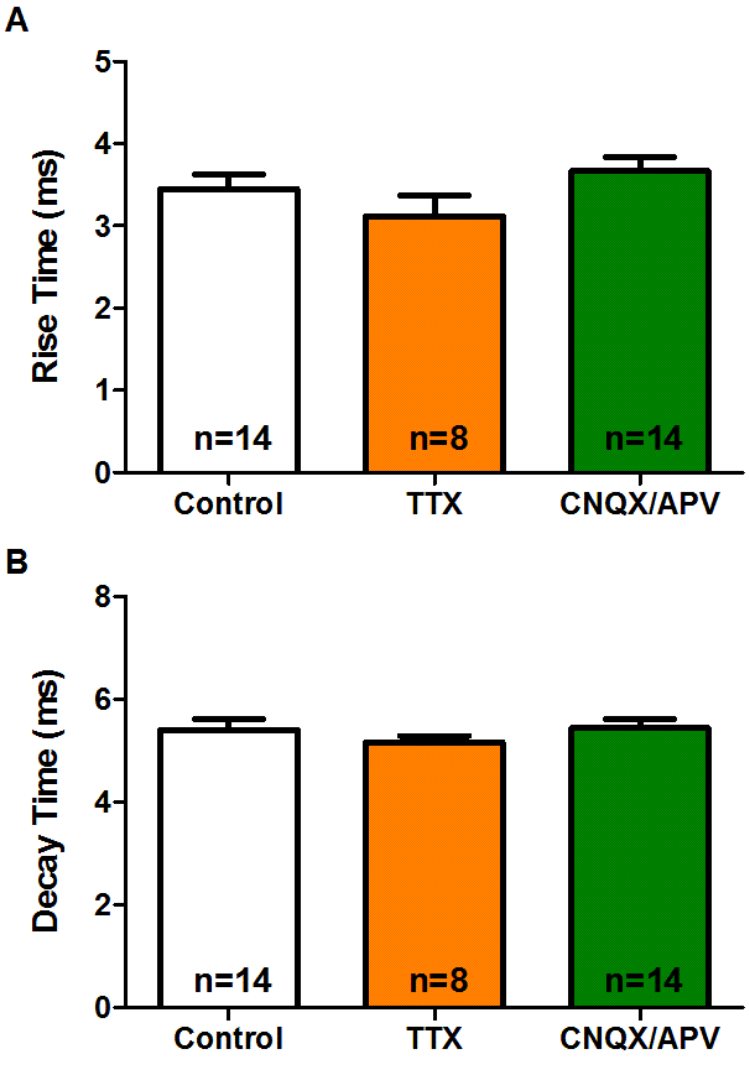

Figure 5-7: Rise and decay time of miniature excitatory synaptic currents in CA1 pyramidal cells of mice organotypic slices, 6-9 DIV.

(A) Rise time were very similar in CA1 cells after 48 hours incubation with either control (white), TTX (orange) or CNQX/APV (green) culture medium (one-way ANOVA, p=0.20). (B) Decay time was also left unaffected by the treatment (one-way ANOVA, p=0.62).

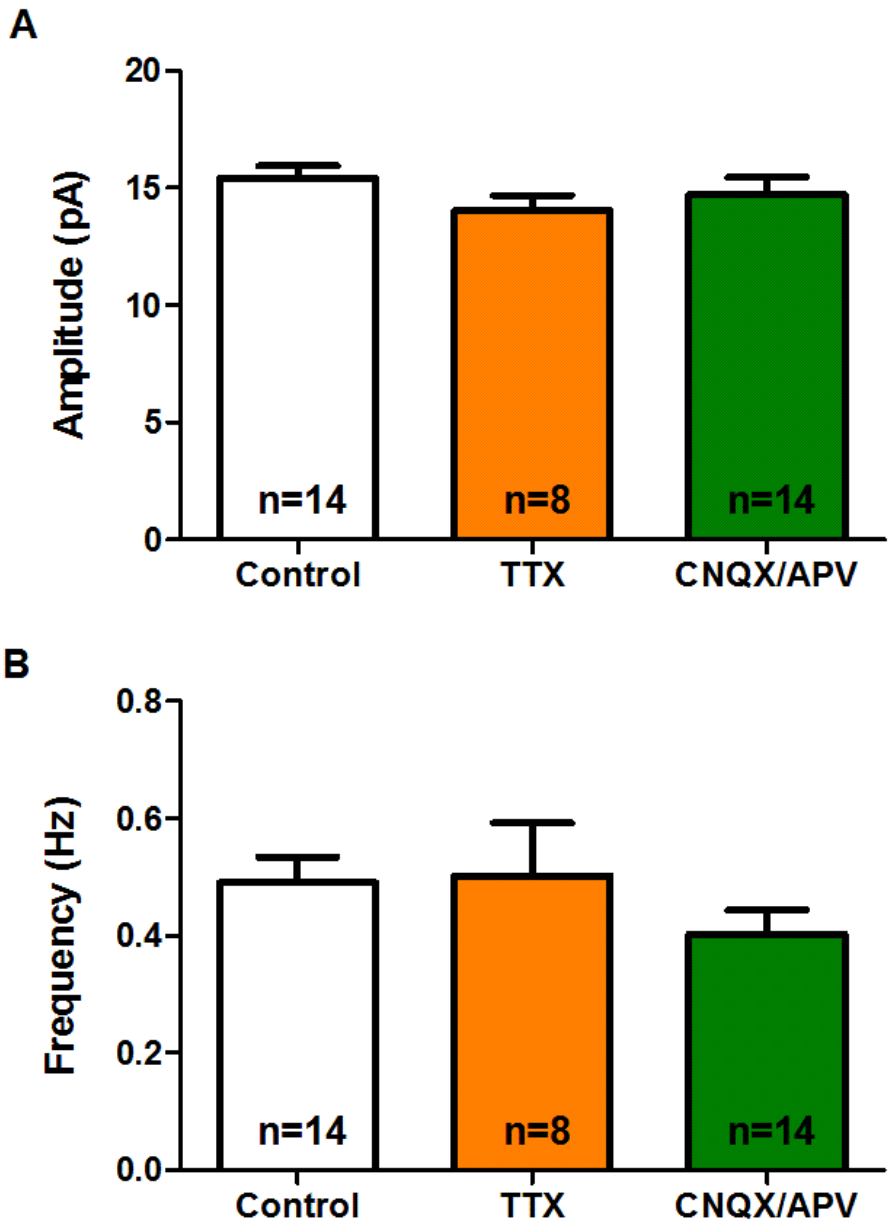

Figure 5-8: Amplitude and frequency of mEPSCs recorded from CA1 pyramidal cells of mice organotypic cultures at 6-9 DIV

(A) The mean amplitudes of miniature excitatory events show no change after 48 hours of activity blockade, whether in TTX or CNQX/APV (one-way ANOVA, p=0.39). (B) There was a slight trend towards a decrease in frequency after TTX blockade but this was not statistically significant (one-way ANOVA, p=0.34).

5.4 Discussion

In order for the network to remain functional, individual neurones need to be able to detect presynaptic activity, fire action potentials and be capable of activity-induced plastic changes. They must be able to modify their threshold for synaptic transmission and plasticity to adapt to chronic modification of network activity.

Long-term changes in global network activity have been reported to induce an increase in miniature excitatory potentials, called synaptic scaling (Turrigiano et al., 1998). In the case of an activity blockade, all synapses scale up their responses to the release of a single vesicle, thus lowering their global threshold for inducing LTP by increasing their detection power of events (Savic et al., 2003). The most commonly used agent to reduce spontaneous activity is TTX, which prevents action potentials by binding to fast voltage-gated sodium channels. Treatment with TTX for 5 hours was sufficient to induce changes in the number of synapses in organotypic cultures (Kirov et al., 2004) and a treatment of 24-48 hours induced an increase in mEPSCs amplitude in dissociated cortical cultures (Turrigiano et al., 1998). The density of neurones in dissociated cultures was found to determine fundamental properties for individual cell plasticity, such as network connectivity and basal spontaneous activity (Ivenshitz and Segal, 2010). Therefore, synaptic scaling, which is very dependent on basal network activity as a homeostatic mechanism, may have very different expressions in dissociated cultures and in models that better conserve network properties like organotypic slices.

During development, intrinsic properties and external factors drive the establishment of the network via neuronal synaptic connections. Reduction of network activity in developing neurones was shown to prevent the spontaneous activity-driven insertion of AMPA receptors at synapses (Barria and Malinow, 2005). The discrepancy between synaptic upscaling in silenced dissociated cultures (Turrigiano et al., 1998) and activity-driven increases of mEPSCs amplitude and frequency with development on organotypic slices (Barria and Malinow, 2005) led us to investigate whether synaptic

scaling also occurred in our organotypic slices. Organotypic culture, which is widely used to explore synaptic plasticity, is by itself a model of adaptation of the neuronal network to drastic changes in organisation, expressing potentially a different state of overall excitability than acute or dissociated cultures. As this model is used to study homeostatic plasticity in this work following long-term alteration of spines' ability to express LTP (see Chapter 7), two case scenarios could be predicted: 1) CA1 pyramidal neurones in developing organotypic slices respond to homeostatic rules, similarly to dissociated cultures, by up-regulating its response to single events after long-term exposure to activity blockers; 2) CA1 neurones respond according to developmental rules, showing a reduction of their activity-dependent development after chronic deprivation (Barria and Malinow, 2005).

The first set of experiments was carried out using 13 to 15 DIV rat hippocampal slices, to compare with the results previously gained in the Edwards lab. Surprisingly, the amplitude of miniature excitatory events between control and TTX treated was unchanged (figure 5-4). In parallel I had carried out 48 hours treatment with CNQX and APV, which blocked both AMPA and NMDA receptors activation. The prolonged exposure to CNQX/APV did not change the mEPSCs amplitude compared to control or TTX. No synaptic scaling was observed in those 13-15 DIV organotypic cultures, while it has been reported several times in similar types of culture (Tyler and Pozzo-Miller, 2003; Kim and Tsien, 2008; Cingolani and Goda, 2008). The question arises as to why this is different in my preparation. The lack of synaptic scaling observed in 13-15 DIV CA1 neurones from hippocampal slices could reveal some age-dependent mechanisms. Indeed, chronic activity blockade was found to depend on the age of the preparation (Kirov et al., 2004; Echegoyen et al., 2007). Surprisingly, *in vivo,* inhibition with TTX for 48 hours was found to induce synaptic scaling only in juvenile (P15) but not in adults (P30) (Echegoyen et al., 2007). To test if the difference could be due to some particularities of our techniques for making slices, the experiments were repeated on mouse organotypic slices, in similar age and conditions to the Stellwagen paper (Stellwagen and Malenka, 2006). Once again, no synaptic scaling was observed, whether the slices were treated with TTX or CNQX/APV. The mEPSCs amplitude in control conditions was higher than that observed by Stellwagen et al, which could

suggest a problem in the detection of smaller events in my experiments. However, if synaptic scaling occurred, an increase in mEPSCs frequency would then be observed after chronic activity blockade, as more quantal events would reach detection size. This phenomenon was not observed in my experiments, and the trend would tend more towards a decrease in amplitude in TTX or CNQX/APV-treated slices (figure 5-8B).

The frequency of miniature excitatory events can also be affected by long-term changes in activity, reflecting either presynaptic changes such as modification of the release probability (Branco et al., 2008; Weyhersmuller et al., 2011) or the insertion of AMPA receptors in silent synapses (Kerchner and Nicoll, 2008). In both series of experiments, the frequency of miniature excitatory events in CA1 cells of hippocampal organotypic slices was left unchanged by the treatment. The mEPSC frequencies ranged below 1 Hz, in accordance to what has been observed in the Malinow and the Goda labs (De Simoni et al., 2003; Barria and Malinow, 2005; Cingolani and Goda, 2008), or even to what has been reported in acute slices of similar age (Hsia et al., 1998). However, the frequency reported in the Stellwagen study is much higher, more than 2 Hz (Stellwagen and Malenka, 2006). In that study, the osmolarity of the ACSF, which is increased by addition of 20 µM of sucrose to increase the release probability and thus enables them to obtain enough minis in a shorter period of time, is probably responsible for the difference. It is possible, however, that small differences in the preparation and maintenance of cultures affect the global connectivity and excitability of the network, thus modifying spontaneous and miniature activity in the cells by a homeostatic mechanism (Zhang et al., 2005), in a similar way that dissociated culture neurones are affected by changes in density (Ivenshitz and Segal, 2010). Similarly, the inclusion of the dorsal part of the hippocampus could result in differences in the plastic properties of the slices from those parts compared to slices obtained from ventral hippocampus only (Pandis et al., 2006). Indeed, gene expression and consequently receptor representations (NMDA-, AMPA-receptors) vary along the dorso-ventral axis of the hippocampus, conferring different plastic properties to neurones in those distant regions (see review Fanselow & Dong, 2010). These results suggest that synaptic scaling is very dependent on experimental preparation and suggests some age-dependent effects.

Chapter 6. Effect of partial deafferentation on CA1 dendritic spines is age-dependent

6.1 Introduction

During development, pyramidal cells in the CA1 area of the hippocampus undergo a major transformation of their dendritic tree, along with the pruning and later refining of their synaptic contacts. The dendritic spine population evolution reflects the changes in connectivity of the network.

During early post-natal days, the brain develops without many inputs from outside stimuli, relying on internal signals to make new branches and synapses.

The distribution of dendritic spines is in constant remodelling, the density increasing significantly from week to week, and the proportions of different spine types being altered in response to the evolving activity. Surprisingly, spines observed in acute slices, i.e. from neurones that develop in a living animal, present very similar evolution of their type distribution to spines growing in hippocampal organotypic cultures (De Simoni et al., 2003). Here I investigate the effect of a more dramatic alteration to the cell, using deafferentation of the Schaffer collateral, at two different developmental ages. Previous publication had already looked at similar effects on spine density in older preparations, but spine head diameter and spine length were not included in the analysis (McKinney et al., 1999)

The aim is to investigate how the dendritic spines shape and number are regulated after the loss of a major input, and whether homeostatic mechanisms aimed at maintaining the cells ability to function and communicate are age-dependent.

6.2 Development of dendritic spine density in organotypic slices

6.2.1 Increased spine density in hippocampal CA1 cells on organotypic slices between 7 and 21 DIV

The dendritic spines population during development in hippocampal slices was studied at different age during development with the new image analysis method.

Parasagittal slices from P5 male Sprague-Dawley rats were left to develop in the incubator for 7, 14 or 21 days, before being taken for imaging. Alexa 594 filled pyramidal CA1 cells were imaged with a confocal microscope, and the extracted tif files were deconvolved (figure 6-1A, C, E), before reconstruction of dendrites and spines with Imaris *Filament Tracer* (figure 6-1B, D, F).

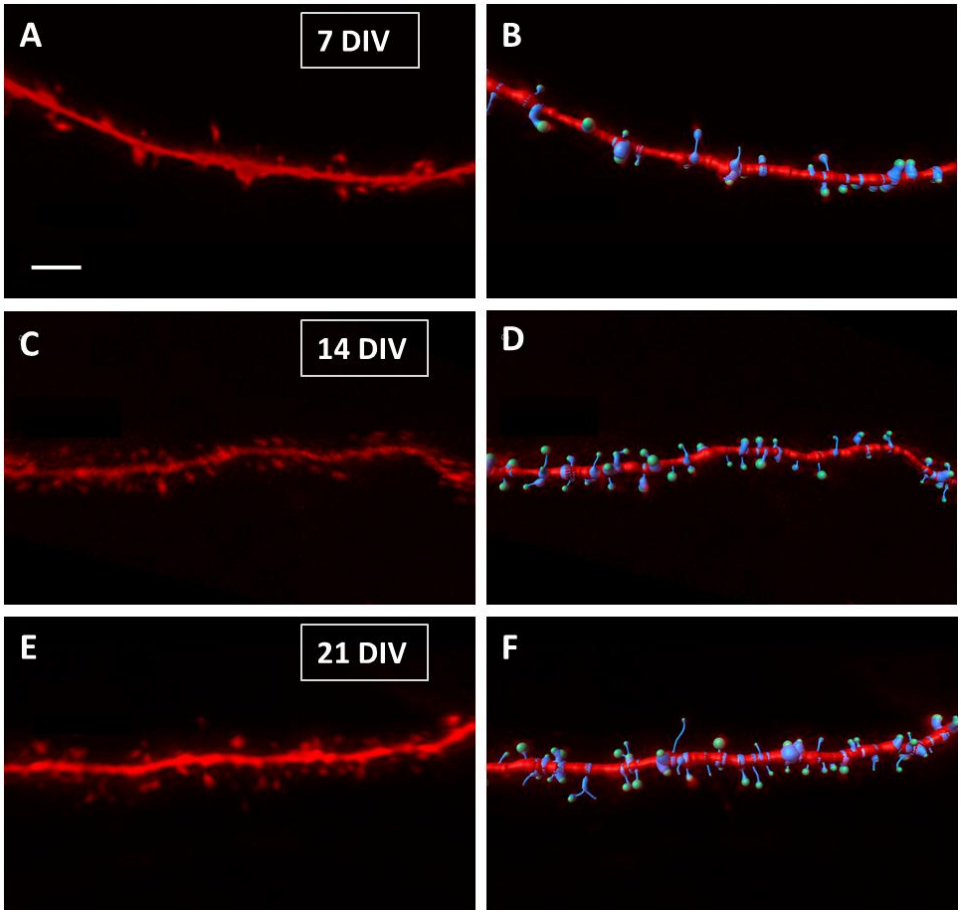

Figure 6-1: Image and Filament fit of CA1 dendritic spine at 7, 14 and 21 DIV.

Deconvolved image and 3D reconstruction with Imaris *Filament Tracer* of a segment of dendrite, on a hippocampal culture of 7 DIV (A&B), 14 DIV (C&D) and 21 DIV (E&F). Scale 3 µm.

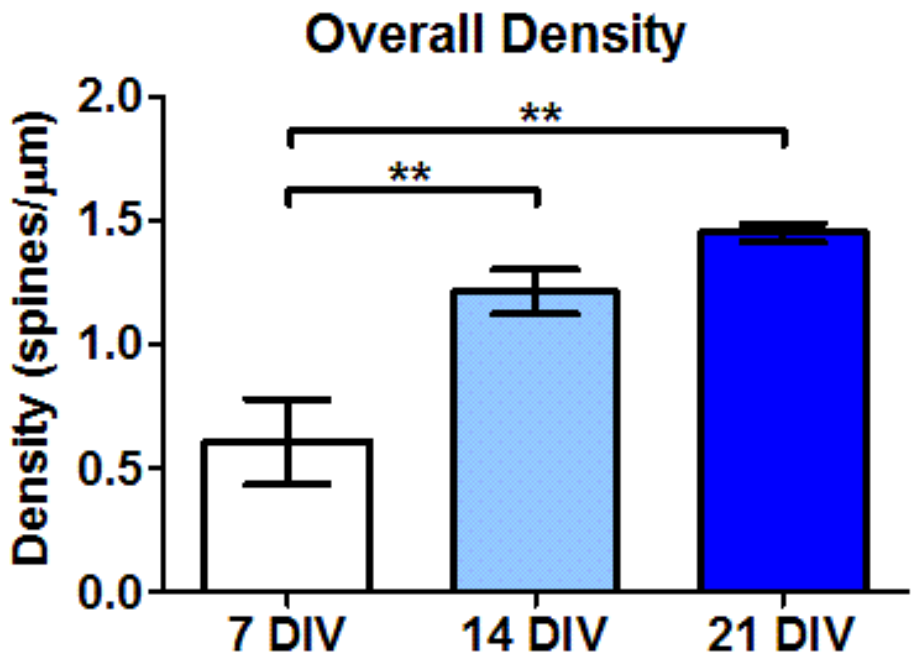

Figure 6-2: Spine density of pyramidal CA1 cells in hippocampal organotypic slices, analysed with Imaris 3D reconstruction.

Spine density was measures per cell, by adding the number of spines analysed on all the images from the same cell, using Imaris *Filament Tracer* on deconvolved data, and dividing it by the sum of the lengths of the segments analysed. The density increases between 7 and 21 days *in vitro* (mean ± SEM spines/µm; 7 DIV: 0.58±0.17, n=3; 14 DIV: 1.21±0.09, n=4; 21 DIV: 1.45±0.04, n=5). On the graph, ** for $p<0.01$, one-way ANOVA with Bonferroni's multiple comparison test, $p=0.0016$.

The density of dendritic spines increases from 7 to 21 DIV (figure 6-2), as confirmed by one-way ANOVA with Bonferroni's multiple comparison test ($p=0.0016$). The density was averaged per cell, by adding all the spines counted on the various sections of the dendritic tree, and divided by the sum of the length of these sections. The density increased from 0.58±0.17 spines/µm (n=3) at 7 DIV, to 1.21±0.09 spines/µm (n=4) at 14 DIV, to finally reach, at 21 DIV, 1.45±0.04 spines/µm (n=5).

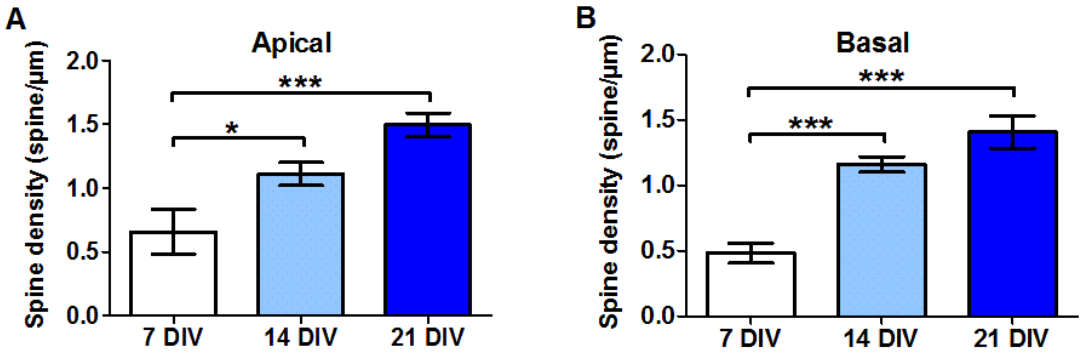

Figure 6-3: Density of spines from apical *vs* basal dendrites.

Spine density in apical (A) and basal (B) dendrites increased in a very similar manner with age (mean ± SEM, two-way ANOVA with Bonferroni's multiple comparison test; apical, 7 DIV: 0.65 ± 0.22 spines/µm, n=3, 14 DIV: 1.11 ± 0.10 spines/µm, n=4, 21 DIV: 1.49 ± 0.08 spines/µm, n=3, p=0.0133; basal, 7 DIV: 0.48 ± 0.09 spines/µm, n=3, 14 DIV: 1.16 ± 0.06 spines/µm, n=4, 21 DIV: 1.41 ± 0.15 spines/µm, n=3, age: p<0.0001, apical/basal: p>0.2, interaction p>0.8).

On a hippocampal slice, the tri-synaptic circuit is preserved (Förster and Frotscher, 1995; Gahwiler et al., 1997), and the dendrites preserve a structure similar to that of acute hippocampal slices, where cell bodies are maintained within a certain layer. Moreover, apical and basal dendrites preserve some specificity regarding their connections. However, the spreading of the slice during this time in culture means that the slice thickness decreases over time and the cells spread a little from their original position, enlarging the normally very tight cell body layer. It was therefore important to see if the distribution of spines was different between apical and basal dendrites, and if the evolution of density observed globally was also reflected in similar measures in both directions. The results from the analysis showed that the spine density increased throughout 3 weeks similarly in apical (figure 6-3A) and basal dendrites (figure 6-3B, two-way ANOVA with Bonferroni's post-test, age factor p<0.0001). The evolution of the apical and basal dendrite densities were paralleled, increasing steeply from 7 to 14 DIV, and plateauing around the same level by 21 DIV (two-way ANOVA, for apical/basal factor p>0.2, interaction p>0.8).

6.2.2 Stubby spines decrease is paralleled by an increase in more plastic spines

In Chapter 3, I have compared the distribution of visually identified spine categories from 7 and 14 DIV cultures. The results showed that user interpretation of spine type, combined with the flexibility of definitions, could lead to intra and inter-users variability and thus was not very reliable. Using the more objective method established later in Chapter 3, I reanalysed the dendritic spine population in control CA1 pyramidal cells at 7, 14 and 21 DIV (figure 6-4). The absence of neck distinguishes stubby spines from what is referred to in the literature as headed spines, i.e. spines which possess a head clearly separated from the parent dendrite by a neck. In this graph, I didn't separate filopodia from headed spines, as they are observed mainly up to 7 DIV (De Simoni et al., 2003), and represent only a very small fraction of spines after that (4-8%). The few very long filopodia were not included in the analysis

Figure 6-4 shows the evolution of these two populations, which play different roles during the earliest stages of development. Indeed, most synaptic contacts are formed on dendritic shafts or stubby spines in the first post natal days (Miller and Peters, 1981), after which spinogenesis is more abundant on filopodia or headed spines (Ziv and Smith, 1996; Fiala et al., 1998). Some of the data, acquired before the establishment of the new analytical method with Imaris, were insufficiently good to be included in the analysis, hence the number of cells included in this reanalysis is quite small. This reflects as well the various tedious former analyses, which was extremely time-consuming, and large sample analyses were hardly feasible.

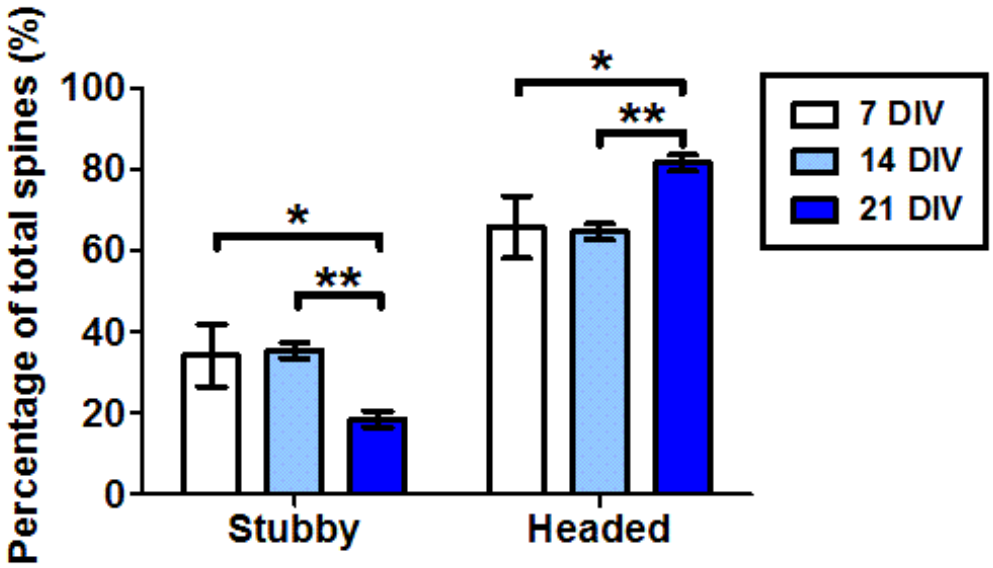

Figure 6-4: Representation of the different spine types automatically identified with Imaris at 7, 14 and 21 DIV.

The percentage of stubby spines decreases significantly between 7 and 21 DIV (mean ± SEM, one-way ANOVA with Bonferroni's post-test, p=0.0024, 7 DIV: n=2, 14 DIV: n=4, 21 DIV: n=4), leading to a parallel increase in headed spines representation.

The result reinforces previous data showing that the proportion of stubby spines decreases with development (mean ± SEM spines/µm, 7 DIV: 31.1 ± 4.3 (n=2); 14 DIV: 35.4 ± 2.2 (n=4); 21 DIV: 18.5 ± 2.3 (n=4); one-way ANOVA with Bonferroni's multiple comparison test, p=0.0024). As here spines are divided between stubby and headed spines, headed spines percentage is consequently increasing from 7 to 21 DIV, headed spines becoming ever more the dominant type of excitatory input recipient (mean ± SEM spines/µm, 7 DIV: 68.8 ± 4.3 (n=2); 14 DIV: 64.6 ± 2.2 (n=4); 21 DIV: 81.4 ± 2.3 (n=4); one-way ANOVA with Bonferroni's multiple comparison test).

In adults, the percentage of stubby spines is considerably smaller than during early development, although the overall spine density increases (Miller and Peters, 1981; Harris et al., 1992).

6.3 Effect of long-term deletion of Schaffer collateral input onto CA1 cells from 7 to 14 DIV on dendritic spines

6.3.1 Effect of partial deafferentation on CA1 cells spine density at 14 DIV

Based on data from previous publications in the lab, as well as the data shown above, the dendritic spine population of CA1 cells in organotypic slices develops very similarly to that of cells growing in living animals and studied in acute slices. It was interesting to study how the dendritic spine population in pyramidal cells would be affected by a dramatic alteration of their excitatory inputs. Note that this type of preparation is often used to study plasticity. Studying spine types after a long deafferentation was a good way of unveiling cell mechanisms for setting spine distribution in response to activity changes.

Is it autonomously regulated during early stages of development, as suggested in the theory of large initial pruning followed later by a refinement of connectivity? Or is it dependent on network activity? Or both? (Katz and Shatz, 1996; Yuste, 2010).

Hippocampal organotypic slices were left to recover for 7 DIV before cutting the CA3-CA1 pathways with a pair of small needles, removing a long but narrow stretch of the slice to avoid later regrowth of the axons (see Material & Methods). The incision was repeated after 3 days if some cells seemed to have reconnected. Finally, to test the efficiency of the deafferentation, crystals of the lipophilic dye DiO were carefully dropped on the CA3 body layer 24 hours before taking the slice for imaging. Fluorescent imaging confirmed that no CA3 axons were visible in the CA1 region, thus confirming that the cut was efficient.

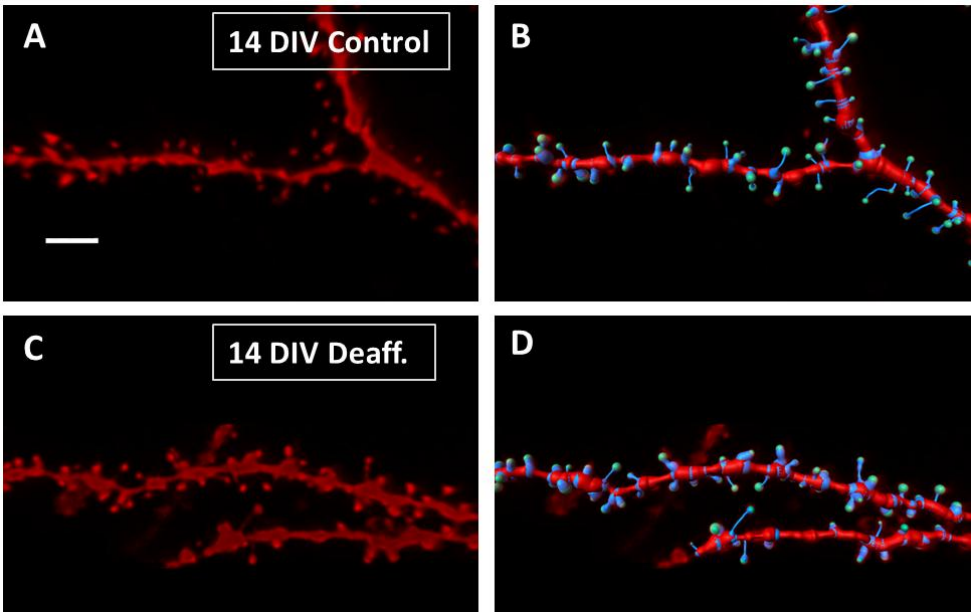

Figure 6-5: Deafferentation of CA1 cells in organotypic slices.

Image of 14 DIV dendritic branches from CA1 cells, in control (A) or deafferented slice (C), and their respective filaments constructed with Imaris (B and D). Scale 3 µm.

After 7 days without receiving the inputs from the Schaffer collateral, the slices tended to be thinner than the control ones, as observed by confocal microscopy from top to bottom of the slice, possibly resulting from an increased death rate of CA1 cells. However, when imaging the remaining healthy cells (figure 6-5), the spine population was surprisingly very similar in both cases (figure 6-6A). The total density in control slices (mean ± SEM: 1.21 ± 0.10 spines/µm, n=4) was not different from deafferented slices (1.14 ± 0.09 spines/µm, n=3; unpaired Student t-test, p=0.78).

In vivo and on acute slices, the Schaffer collateral pathway impinges largely onto proximal apical dendrites of CA1 neurones, but a small portion branches to innervate basal dendrites (Ishizuka et al., 1990; Li et al., 1994; De Simoni and Edwards, 2006). The effect of transection could therefore be significantly stronger in the apical than in the basal dendrites. Differentiating those two geographically distinct populations, the spine density seemed similarly unaffected in both regions by the deafferentation (apical, control: 1.20 ± 0.13, n=3, deafferented: 1.13 ± 0.12, n=3; basal, control: 1.13 ± 0.14, n=3, deafferented: 1.16 ± 0.08, n=3). As apical and basal spines are two non-overlapping and independent populations, two-way ANOVA was used to test the interaction between those factors, and results came up as non-significant (figure 6-6B, region effect: p=0.95; treatment effect: p=0.86).

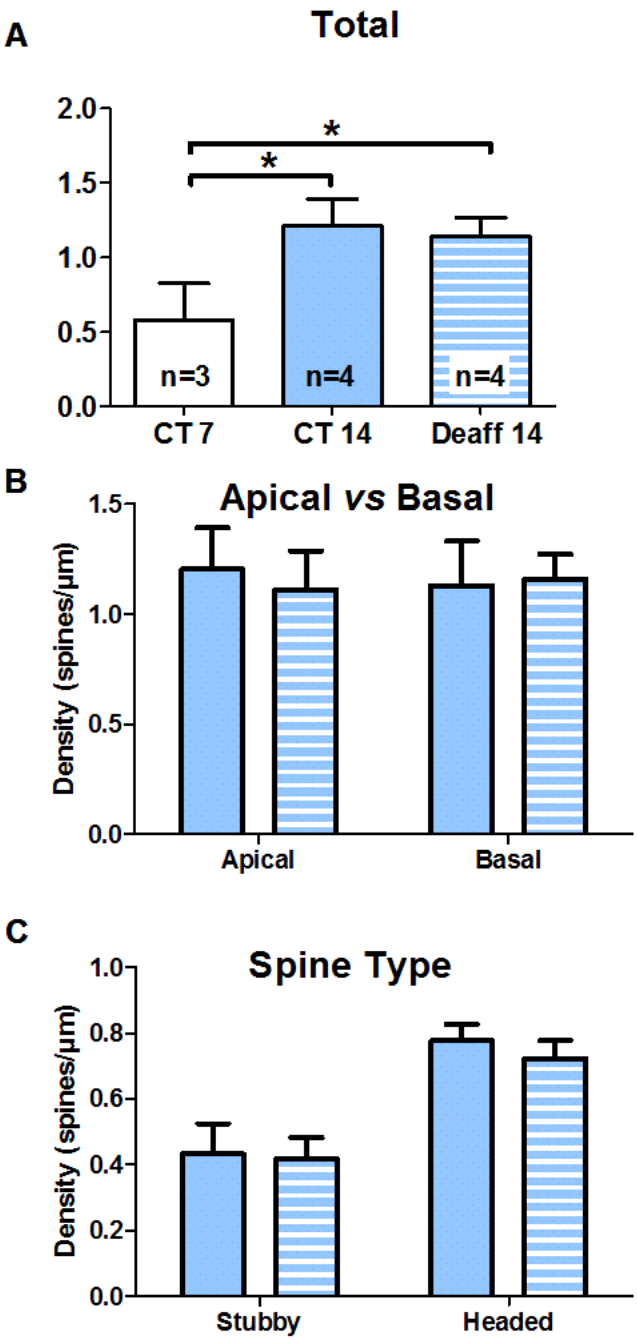

Figure 6-6: Effect of partial deafferentation to CA1 pyramidal cells spine density at 14 DIV.

(A) The overall density of spines is unaffected by 7 days of deafferentation (mean ± SEM spines/µm, control: 1.21 ± 0.10, n=4; deafferented: 1.14 ± 0.09, n=3) but both significantly increased from 7 DIV control (one-way ANOVA with Bonferroni's post-test). (B) No effect was visible in either apical or basal spine population (apical, control: 1.20 ± 0.13, n=3, deafferented: 1.13 ± 0.12, n=3; basal, control: 1.13 ± 0.14, n=3, deafferented: 1.16 ± 0.08, n=3; two-way ANOVA, $p>0.5$). (C) Density of stubby and headed spines was also unaffected (two-way ANOVA, $p>0.5$).

The density of stubby and headed spines was also compared in control and in deafferented CA1 neurones. A two-way ANOVA confirmed that the 7 days deafferentation had no effect on spine type density at the final age of 14 DIV (figure 6-6C, $p>0.5$).

6.3.2 Effect of deafferentation on headed spines dimension

In this section, I report the findings from deafferentation on the morphology of the most plastic spines, i.e. headed spines.

Using Imaris *Filament Tracer* to measure spines and remove stubby spines from the analysis of head and length dimensions, the comparison of spine heads from deafferented cultures to control ones revealed a significant increase ($p=0.01$) in spine head diameters on a whole cell level (figure 6-7A). The median diameter increased from 0.34 µm in control ($n=1000$) to 0.37 µm in deafferented cultures ($n=420$). That enlargement of spine head size was more pronounced in apical spines ($p<0.0001$), where the median head size jumped from 0.34 µm ($n=750$) to 0.43 µm ($n=194$) after a week of deafferentation (figure 6-7B). In the basal dendrites (figure 6-7C), which are more prone to CA1-CA1 connections in organotypic slices (De Simoni and Edwards, 2006), the spine head size was unchanged (control: 0.32 µm, $n=174$; deafferented: 0.33 µm, $n=192$; $p=0.26$).

Changes in dendritic spines morphology are the result of an alteration of the cellular environment, either as a direct consequence of the disturbance, or as a compensatory mechanism to maintain excitability while preserving relative synaptic weight (Turrigiano et al., 1998; reviewed in Turrigiano and Nelson, 2004). If the spine head size is proportional to the postsynaptic density (Harris and Stevens, 1989; Arellano et al., 2007a), and thus to a large extent to the synaptic strength (Matsuzaki et al., 2001), the spine neck has also a fundamental impact on the spine biophysical properties (Noguchi et al., 2005; Ashby et al., 2006).

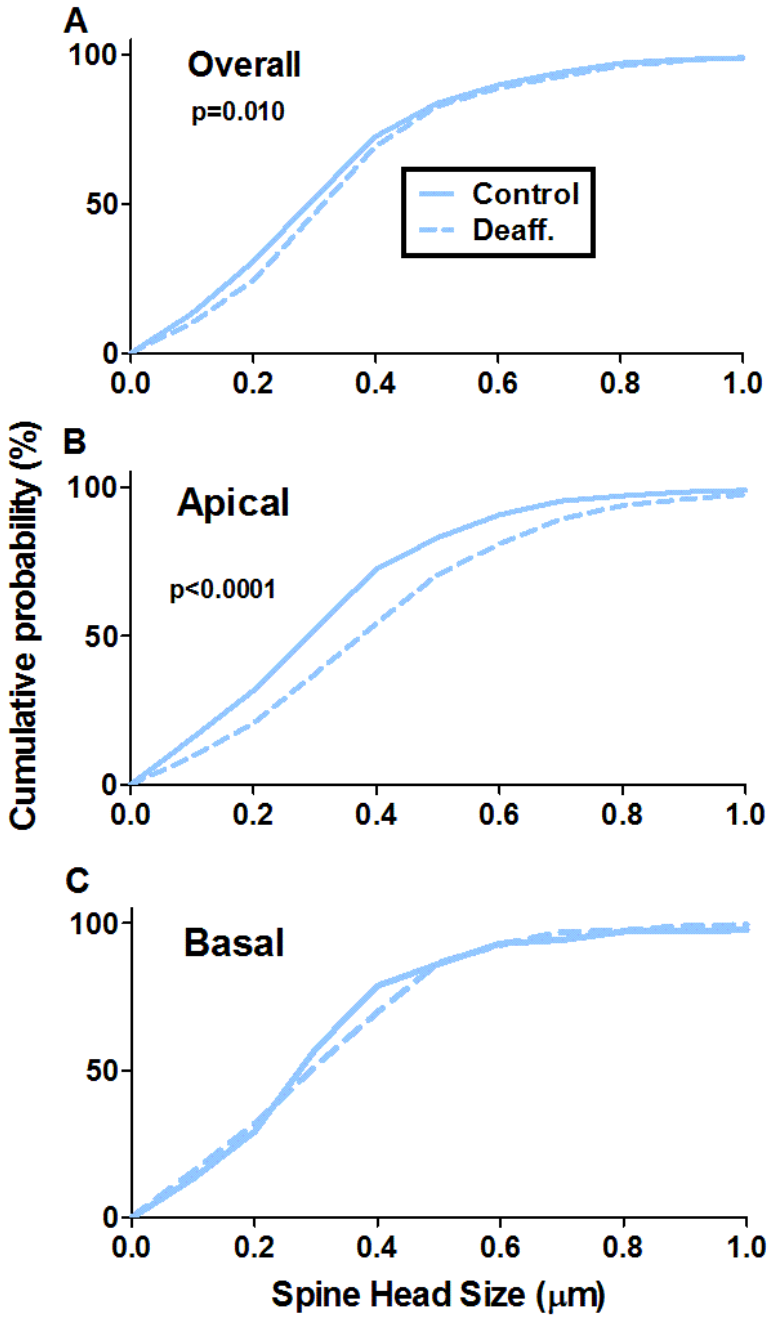

Figure 6-7: Effect of deafferentation on spine head size at 14 DIV.

The plots show the cumulative probability of spine head size, as measured by Imaris *Filament Tracer* with the *Approximate Circle* algorithm, after excluding stubby spines. (A) Deafferentation induced an increase in spine head diameter (control: 0.34 µm, n=1000; deafferented: 0.37 µm, n=420; p=0.0101). (B) The increased spine head size was predominant in apical dendrites (0.34 µm, n=750, *vs* 0.43 µm n=194; p<0.001). (C) In basal dendrites, the difference in spine head size was not significant (0.32 µm, n=174, *vs* 0.33 µm, n=192; p=0.26).

Spine length is a good indicator of spines properties modifications, as it affects the transmission of the signal from the head to the parent dendrite, and reciprocally. Here, when cultures of 7 DIV were deafferented and imaged 7 days later, the median spine length (figure 6-8A) was significantly shortened (p=0.0011), decreasing from 0.87 µm in control (n=1000) to 0.84 µm in deafferented slices (n=420). However, those changes were not detected in apical dendrites (figure 6-8B, control: 0.87 µm, n=750; deafferented: 0.89 µm, n=194; p=0.55). In basal dendrites (figure 6-8C), the trends towards shorter spines was not statistically significant (control: 0.90 µm, n=174; deafferented: 0.84 µm, n=192; p=0.12).

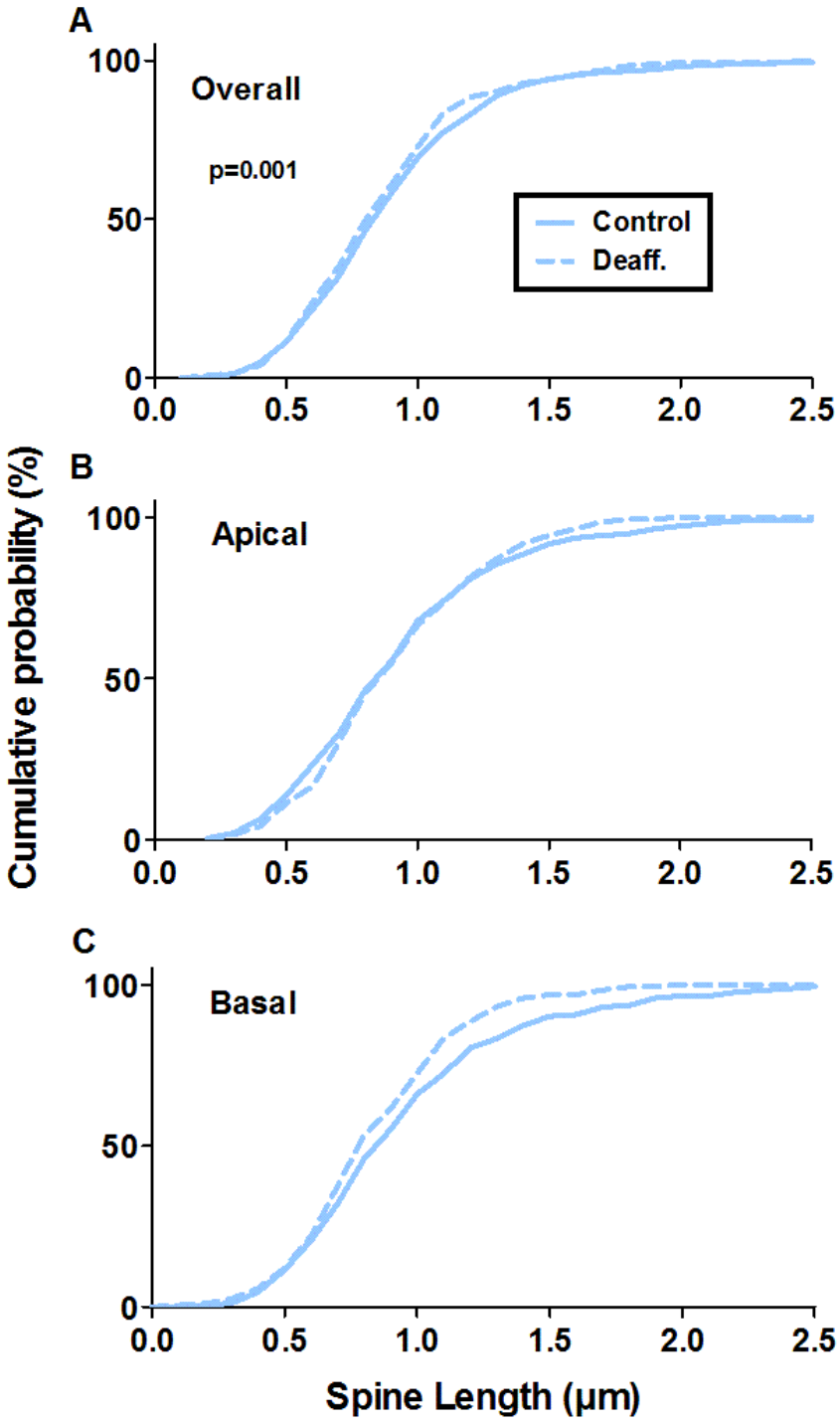

Figure 6-8: Effect of deafferentation on spine length at 14 DIV.

(A) Spine length was shortened by deafferentation on the whole cell level (control: 0.87 µm, n=1000; deafferented: 0.84 µm, n=420; p=0.0011). (B) The median spine length was not affected by the deafferentation in apical slices (control: 0.87 µm, n=750; deafferented: 0.89 µm, n=194; p=0.55). (C) In the basal dendrites, the spine length median was also not significantly changed (control: 0.90 µm, n=174; deafferented: 0.84 µm, n=192; p=0.12).

6.3.3 Why no change in spine density at an early age?

The effect of 7 days of deafferentation on CA1 pyramidal cells, when occurring during the rapid phase of development between the age of 7 and 14 DIV, resulted in less dramatic changes than I expected. First of all, the spine density, which was expected to be the first parameter affected by deafferentation of the major input to CA1 cells in organotypic slices, remained unchanged, in both apical and basal regions. This result was surprising as it was going against previously published data, which found a decrease in spine density in organotypic cultures with a similar transection performed here but on older cultures of 2 to 3 weeks (McKinney et al., 1999).

The trends observed in spine type distribution, also differs from the McKinney paper, which found a very significant increase in stubby spine representation (34 ± 4% to 61 ± 10%), while both mushroom and thin spines decreased. This result would tend towards a general reduction in spine length, a parameter which hasn't been looked at in that study, but which appears to be diminished in 14 DIV deafferented cultures.

I thus decided to see if our experimental and analytical methods allowed us to detect changes, by reproducing the deafferentation on slightly older culture, leaving 14 DIV to the hippocampal cultures to recover before transecting the Schaffer collaterals.

6.4 Effect of long-term deletion of the Schaffer collateral input onto CA1 cells from 14 to 21 DIV

6.4.1 Effect of deafferentation on spine density at 21 DIV

In this section, hippocampal slices cultures were left to develop undisturbed for 14 DIV before sectioning the Schaffer collateral pathway. As before, the slices were filled with Alexa 594, and imaged with confocal microscope and Fluoview software. Control and deafferented cultures were alternated randomly, in order to homogenise potential modifications of the culture and recording conditions. Figure 6-9 represent sample images of control (figure 6-9A) and deafferented (figure 6-9C) segment of dendrites, along their Imaris built-up filament.

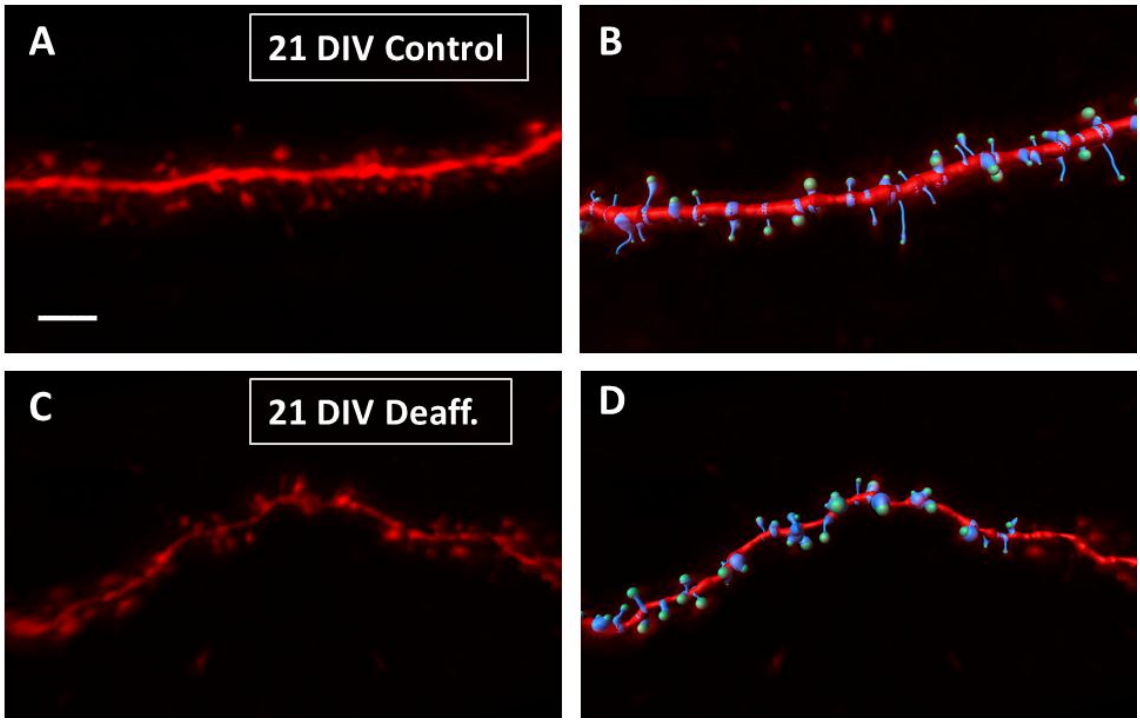

Figure 6-9: Effect of deafferentation for 7 days on CA1 pyramidal cells at 21 DIV.

Sample images of control (A) and deafferented (C) segment of dendrite, and their filament build up by Imaris *Filament Tracer*. Scale 3 µm.

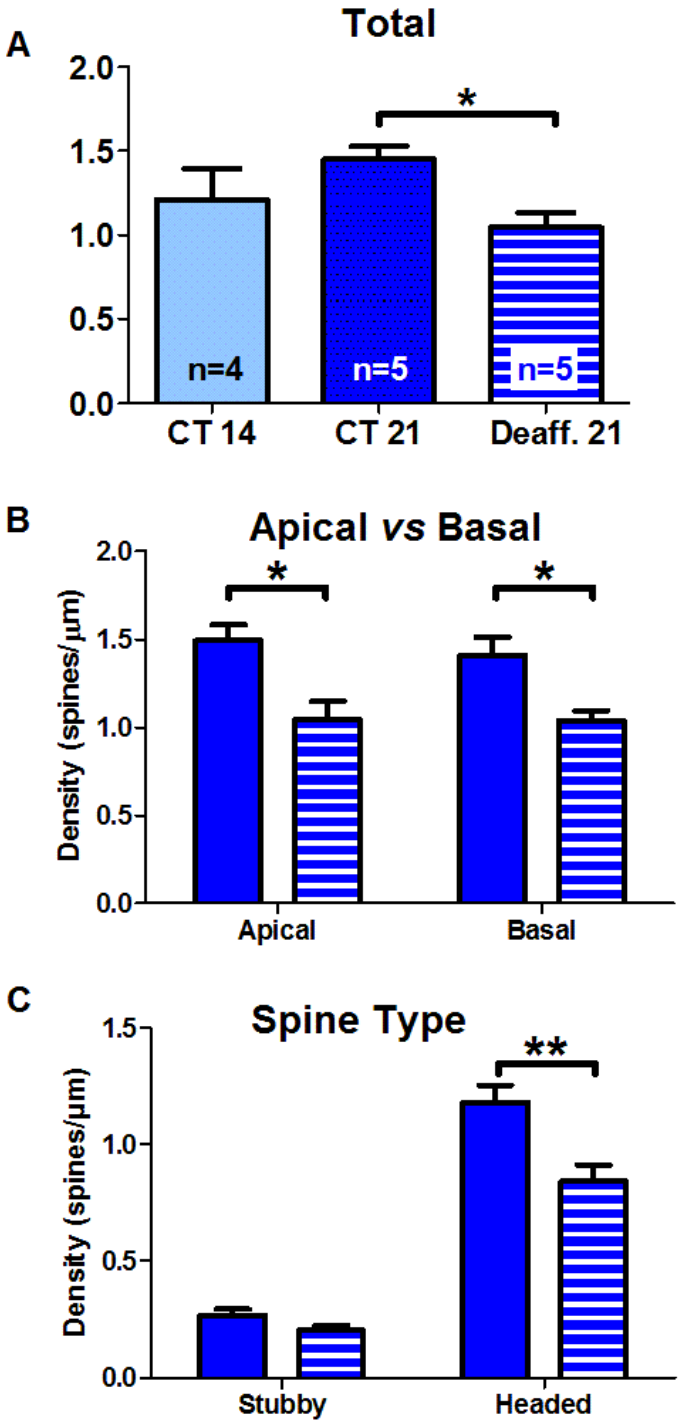

Figure 6-10: Density of spines at 21 DIV following a week of deafferentation.

Data showed as mean ± SEM of each condition, averaged per cell. (A) The overall density of spines was decreased by deafferentation (unpaired t-test, p=0.012). (B) Apical and basal spines were both scarcer following deafferentation (two-way ANOVA, treatment p=0.008, interaction p>0.6). (C) The decrease in spine density mainly affects headed spines (two-way ANOVA with Bonferroni's post-test, interaction p=0.02).

Dendritic spine density was largely reduced as a result of the deafferentation occurring from 14 to 21 DIV (figure 6-10A). The overall density dropped from 1.45 ± 0.08 spines/µm (n=4 cells) in control conditions to 1.04 ± 0.09 spines/µm (n=5) after 7 days of deafferentation, in agreement with the result from the McKinney study (McKinney et al., 1999), which found a very significant drop in density following one week of deafferentation in hippocampal slices of 2 or 3 weeks old. Their initial density was lower, 0.93 spines/µm, and decreased below 0.41 spines/µm ($p<0.0001$).

Apical and basal spine densities (figure 6-10B) were affected similarly by the deafferentation, both decreasing significantly (two-way ANOVA with Bonferroni's post-test, deafferentation $p=0.008$, apical/basal factor $p>0.6$, interaction $p>0.6$).

Density of headed spines decreased significantly following transection of the Schaffer collateral pathway (figure 6-10C, control: 1.18 ± 0.07 spines/µm, n=4; deafferented: 0.84 ± 0.07 spines/µm, n=5, two-way ANOVA with Bonferroni's post-test, spine type $p<0.0001$, treatment $p=0.0023$, interaction $p=0.023$), but the stubby spines only showed a trend in the same direction (stubby spines: control: 0.27 ± 0.03 spines/µm, n=4; deafferented: 0.20 ± 0.02 spines/µm, n=5).

6.4.2 Effect of deafferentation on spine types representation at 21 DIV

The representation of the different types of spines was not significantly affected by the deletion of the Schaffer collateral input for 7 days. The graph only shows stubby spine percentage, as headed spines are inversely linked to stubby spine proportion (figure 6-11). In former deafferentation studies, stubby spines were found to be dominant after deafferentation from CA3 inputs in pyramidal cells after 21 DIV, shifting from 34 ± 4 % in control to 61 ± 10 % in deafferented CA1 neurones (McKinney et al., 1999), mainly because stubby spine density has roughly maintained itself while thin and mushroom spines densities had dramatically decreased. In my hands, stubby and headed spines decreased in parallel, thus maintaining their relative percentage (unpaired t-test in overall, $p>0.5$). The proportions were unchanged in apical or basal dendrites (two-way ANOVA, $p>0.3$).

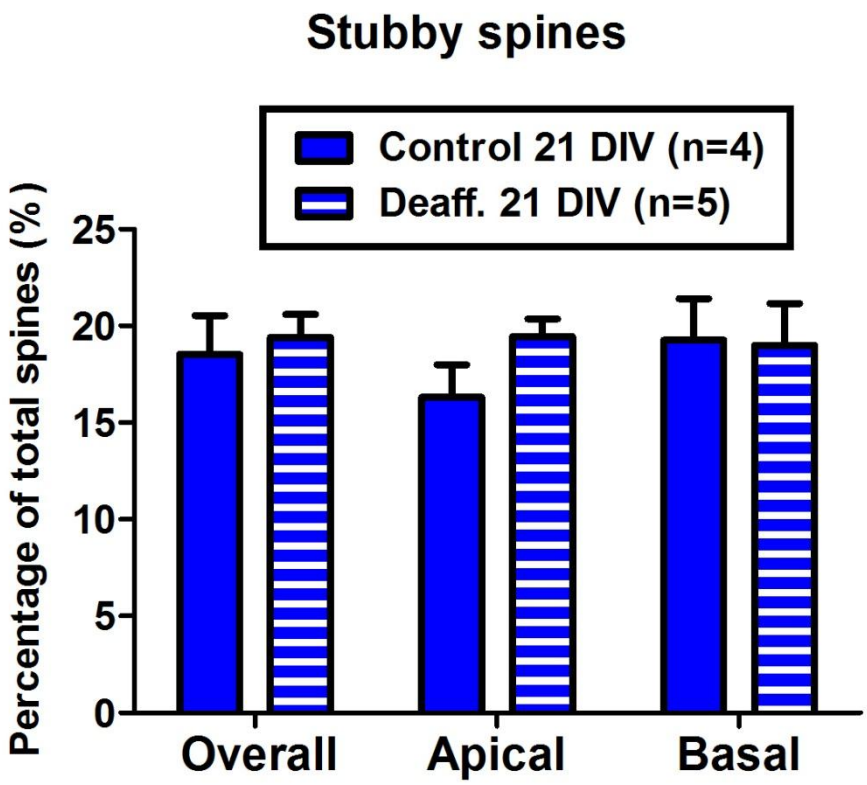

Figure 6-11: Effect of deafferentation at 21 DIV on stubby spine percentage, on the whole cell or selectively in the apical or basal dendrites.

Data is presented as mean ± SEM of total spine percentage. Stubby and headed spine densities decreased in parallel, thus leaving their proportions unchanged after deafferentation (two-way ANOVA on apical *vs* basal, p>0.3).

6.4.3 Effect of deafferentation on headed spines dimensions at 21 DIV

The lack of active input to CA1 neurones from CA3 axons for several days prior to imaging at 21 DIV was much stronger than what was observed on 14 DIV cultures.

The spine head size of the global population was strongly increased after deafferentation, as shown on the cumulative distribution (figure 6-12A). The median head diameter went from 0.28 µm (n=1600) to 0.35 µm (n=750), and the Mann-Whitney test for non-parametric distribution confirmed the difference in ranks among the 2 distributions were very significant (p<0.0001).

As shown on figure 6-12B, the shift towards larger heads was clearly predominant in apical spines (control: 0.28 µm, n=900; deafferented: 0.37 µm, n=450; p<0.0001), while

it was present to a lesser extent in basal dendrites (control: 0.27 µm, n=760; deafferented: 0.32 µm, n=365; p=0.020), as shown on figure 6-12C.

The spine length was also affected by the deafferentation, but compared to the deafferentation happening at an earlier age, which induced a decrease in the spine length median compared to control, the cumulative probability was now shifted towards larger values, i.e. longer spines (figure 6-13). On a whole cell level (figure 6-13A), the cumulative distribution of dendritic spine length were significantly different (Mann-Whitney test, $p<0.0001$), the median increasing from 0.85 µm (n=1600) to 0.93 µm (n=750). Similarly to what was observed in 14 DIV cultures, the change in spine length was not significant in either apical (figure 6-13B, p=0.47) or basal spine populations (figure 6-13C, p=0.105), but with a stronger trend in the basal dendrites (control: 0.86 µm, n=760; deafferented: 0.92 µm, n=0.92).

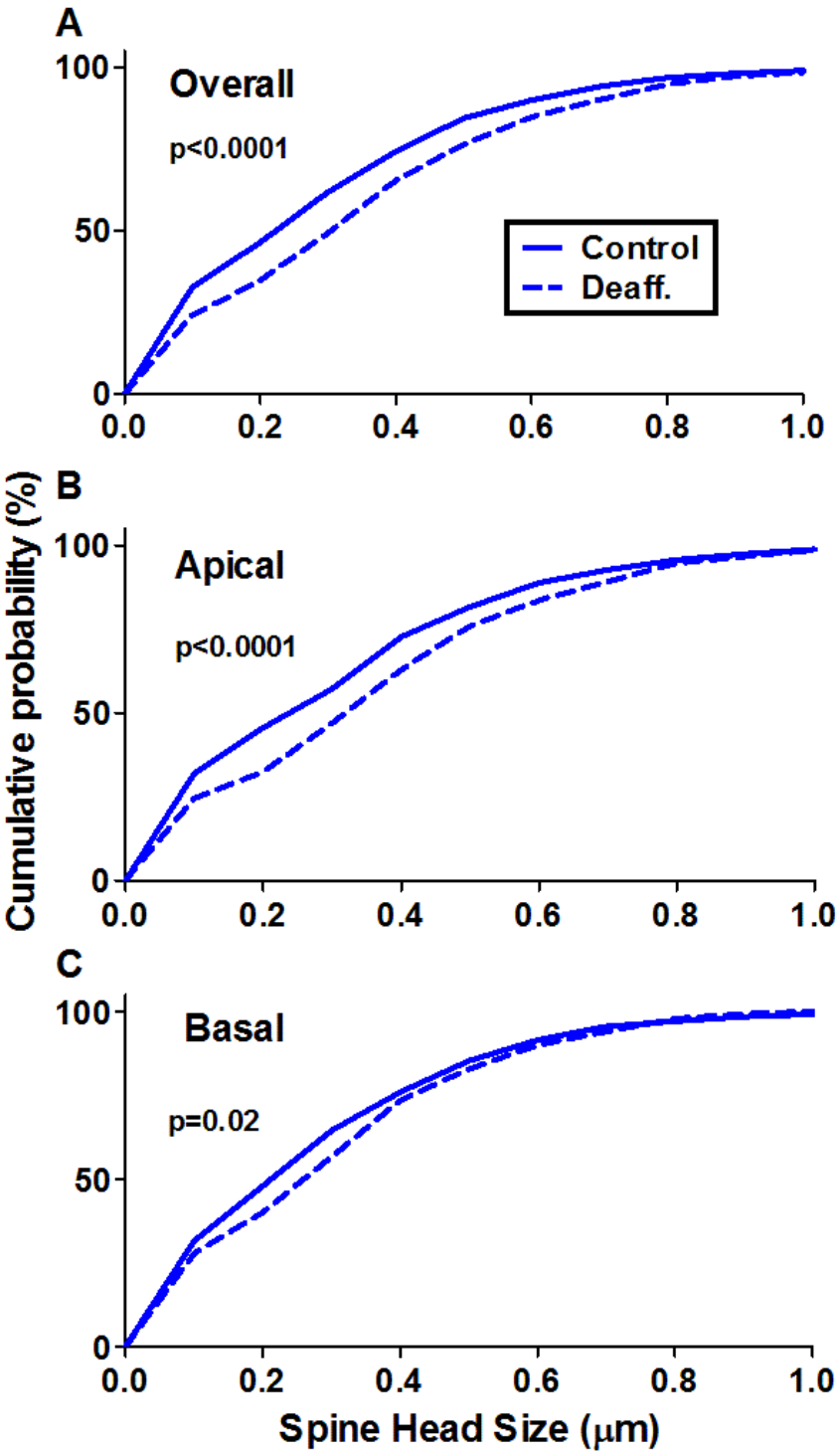

Figure 6-12: Effect of deafferentation on spine head size after deafferentation, on 21 DIV pyramidal cells.

(A) Spine head diameter was increased by deafferentation of the Schaffer collateral at 21 DIV (control: 0.28 µm, n=1600; deafferented: 0.35 µm, n=750; p<0.001). (B) Apical spines once again showed the greatest increase (control: 0.28 µm, n=900; deafferented: 0.37 µm, n=450; p<0.0001). (C) The effect was this time also visible in the basal dendrites (control: 0.27 µm, n=760; deafferented: 0.32 µm, n=365; p=0.0204).

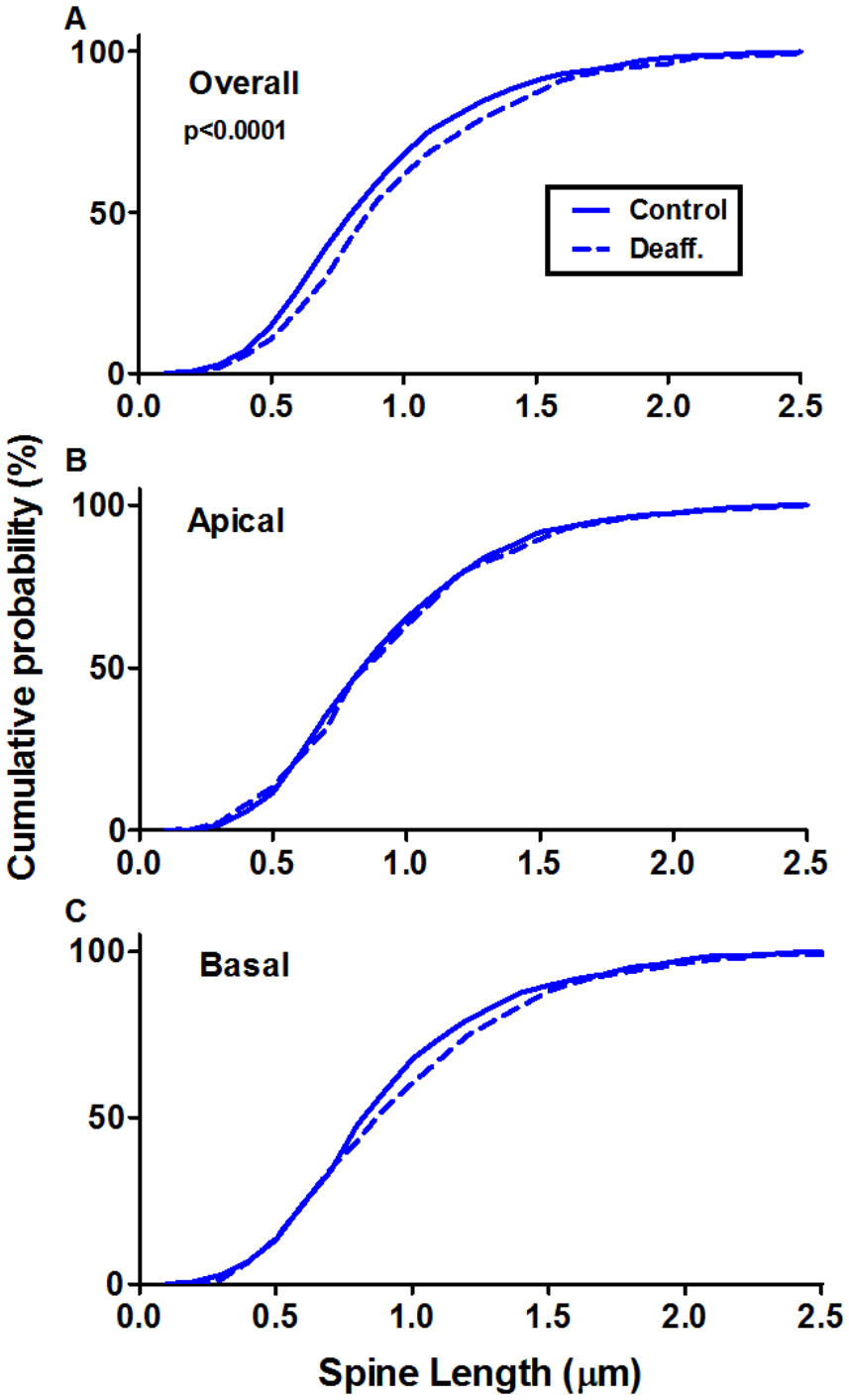

Figure 6-13: Effect of deafferentation on spine length at 21 DIV.

Similarly to what was observed at 14 DIV, the median spine length increased on the overall population of deafferented cells (A) (control: 0.85 µm, n=1600; deafferented: 0.93 µm, n=750; p<0.001), but significant difference were evident neither in the apical subpopulation (B) (control: 0.88 µm, n=900; deafferented: 0.90 µm, n=194; p=0.55) nor in the basal one (C) (control: 0.86 µm, n=760; deafferented: 0.92 µm, n=365; p=0.105).

6.5 Discussion

The aim of this chapter was to address the structural changes happening to a pyramidal neurone following the loss of input from a specific pathway via transection. This approach has previously been taken in older organotypic slices (McKinney et al., 1999), but had not been tested during earlier phase of development, when the density of dendritic spine is drastically increasing and their morphologies are still evolving (De Simoni et al., 2003). Moreover, the pathway specificity observed in the spine type representation has not plateaued between 7 and 14 DIV, but is much more stable between 14 and 21 DIV (De Simoni and Edwards, 2006).

As expected, the effect of deafferentation on CA1 neurones appears to be very dependent on the age of the preparation. Indeed, cutting the Schaffer collateral at 7 DIV and looking at spines at 14 DIV, the neurones showed no difference in spine density (figure 6-14), but an increase in spine head diameter, which is more pronounced in the apical dendrites. When the deafferentation was conducted at 14 and examined at 21 DIV, the density of spines was reduced compared with that of neurones in control slices, in accordance to previous observations made in organotypic slices of 3-4 weeks *in vitro* (McKinney et al., 1999). Also, studies from *in vivo* deafferentation of the entorhinal cortex to the dentate gyrus cells also found a 30% decrease in spine density after 5 days (Parnavelas et al., 1974). In the dentate gyrus, the removal of the entorhinal cortex induces the degeneration of the remaining presynaptic terminals which occurs mainly and almost completely during the first ten days following deafferentation (Matthews et al., 1976). This result strongly suggests that terminals of deafferented axons would have largely degenerated by the examination time. The labelling of CA3 axons with the lipophilic dye DiO did not show the presence of fluorescent axons in the CA1 area, making it likely that the presynaptic terminals of axons separated from the soma may have degenerated. Transection of axons induces an increase in axonal sprouting in CA3 neurones on organotypic slices (McKinney et al., 1997). Though unlikely, it cannot be totally excluded that CA3 neurones from deeper layers in the organotypic slice, not labelled by the crystals, may have established new connections to CA1 neurones.

Changes in spine density have been associated with several neurological diseases such as Down's syndrome, fragile X syndrome or epilepsy (reviewed in Hering and Sheng, 2001). It is highly likely that, following deafferentation, the normally very spiny excitatory neurones in the hippocampus need to maintain a certain global synaptic strength through connections in order to remain viable and avoid pathological functioning. Thus, the surviving neurones still have a reasonable density of dendritic spines, probably resulting from the remaining axons innervating CA1 cells which can increase the number of connections to individual neurones.

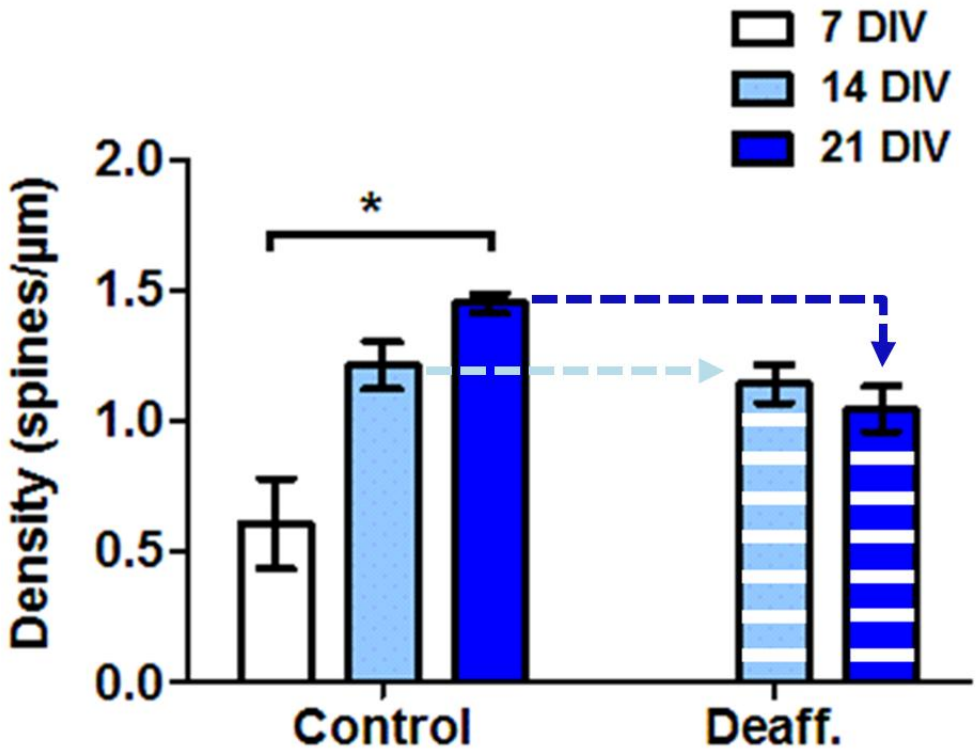

Figure 6-14: Summary of the effect of deafferentation on spine density.

Density increases similarly from 7 DIV to 14 DIV whether neurones received input or not from the Schaffer collateral. From 14 to 21 DIV, the lack of functional input from CA3 axons decreases density in deafferented neurones compared to control.

In older slices, transection of the Schaffer collateral increased median spine head size compared to control conditions at 21 DIV, more significantly in the apical than in the basal dendrites. This result also supports the hypothesis that smaller spines are lost more easily following deafferentation (reviewed in Takacs and Hamori, 1990), and the preferential loss of smaller spines would also contribute to increase the median head

size of spines, proportionally to the innervation of the region by CA3 axons. In older slices, basal dendrites are also slightly affected by a decrease in spine head size and spine density. These findings could reflect the sprouting of CA3 axons, occurring later in development in control organotypic slices, CA3 axons innervating preferentially CA1 *stratum radium* but are also found in a smaller proportion in the basal dendrites (De Simoni and Edwards, 2006).

It was interesting to bring together the results from control and deafferented at 14 and 21 DIV, to see the changes in spine head size on the same graph (figure 6-15). In transected slices of 21 DIV, the median spine head size was similar to the value of control 14 DIV cells, and all were significantly different from median head size in control at 21 DIV. The median spine head size in deafferented 21 DIV has not changed from control 14 DIV, thus diverging from the normal developmental decrease in spine head size. The fact that both spine head size and spine density are very similar in control at 14 DIV and deafferented at 21 DIV could suggest a developmental inhibition due to deafferentation occurring from 14 to 21 DIV, while the development from 7 to 14 DIV would be more cell-autonomous.

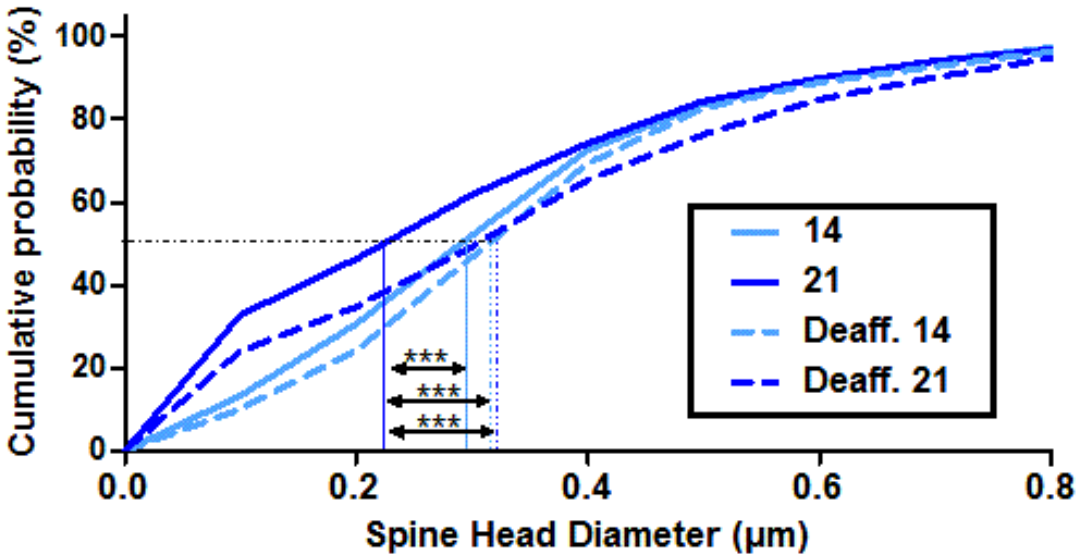

Figure 6-15: Summary of the effect of deafferentation on spine head size.

Transection of the Schaffer collateral from 14 DIV to 21 DIV prevented the change of spine head diameter observed normally during development between 14 and 21 DIV (Kruskal-Wallis with Dunn's post-test).

The deafferentation induced a decrease in spine length at 14 DIV and an increase at 21 DIV. Surprisingly, in both age groups, the dendritic spine length was affected on a whole cell level, but not significantly in either apical or basal dendrites. However, the global effect was reflected by a stronger trend in the same direction from the basal dendrites, suggesting that this region is implicated in the global effect observed. Elongation of dendritic spines has been observed in various contexts, such as in the cerebral cortex of fragile X syndrome mouse model (Irwin et al., 2000), following chronic activity deprivation in dissociated cultures (Papa and Segal, 1996), or by activation of signalling cascade involving Rap (Pak et al., 2001), actin-binding protein such as α-actinin or Drebrin (reviewed in Hotulainen and Hoogenraad, 2010) or mGluR type 1 (Vanderklish and Edelman, 2002). Elongation of dendritic spines seems to oppose the neck shortening and spine head enlargement observed following synaptic potentiation or regulation of spine morphology via the Ras/Rap signalling pathways (Fifkova and Anderson, 1981; Pak et al., 2001). That pathway has been recently involved in homeostatic plasticity (Lee et al., 2011), suggesting that changes in spine length following deafferentation could induce a modification of the Ras/Rap signalling. In the present study, the percentage of stubby spine was not increased, in contrast to previous findings (McKinney et al., 1999).

These results suggest that deafferentation has different effect on hippocampal slices neurones depending on the age at which the disruption happens. At 7 DIV, the slice is still in a developmental phase, where the spine density is rapidly increasing (De Simoni et al., 2003), and thus the deafferentation can be palliated by some rapid remodelling and axon sprouting.

Chapter 7. Effect of long-term blockade of CaMKII or PKA on dendritic spine population

7.1 Introduction

The dendritic tree and the population of spines it bears is the product of both autonomous and activity-driven changes. During development, the density of spines is increasing, while the proportion of the different spines is changing, thin spines taking over from filopodia or stubby spines, while mushroom spines remain stable around 15%. The different spine types reflect the previous activity experienced by the synapse, as well as by global changes in network activity which can induce homeostatic mechanisms in order to maintain the cell excitability.

To study homeostatic changes in hippocampal CA1 cells, evolution of synaptic currents have been mainly used as a measure of plasticity adaptation to long-term activity changes, usually consisting *in vitro* in 48 hours treatment with tetrodotoxin or a cocktail of AMPA/NMDA or $GABA_A$ receptors blockers. In this chapter, the approach taken was different, incubating organotypic hippocampal cultures for 7 days with inhibitors of specific kinases which, among other roles, are key factors for the induction and expression of LTP. The aim was to modify not directly the global activity of the network, but the ability of cells to express LTP. The two pathways targeted were the CaMKII-dependent LTP, which can be blocked by the CaMKII antagonist KN62 at 4 µm, and the PKA-dependent LTP, which can be blocked by the PKA type 1 antagonist Rp-cAMP at 200 µm. As discussed in the introduction, CaMKII and PKA have distinctive roles in LTP, CaMKII being essential for the establishment of LTP, while PKA is necessary for the maintenance and late-phase of LTP. The established correlation between dendritic spine size and the strength of the synapse enabled the use of imaging to study synaptic changes in CA1 pyramidal neurones after long-term treatments with the plasticity blockers KN62 and Rp-cAMP.

7.2 Effect on spine density

7.2.1 Preparation and imaging

The population of spines in apical and basal dendrites of CA1 pyramidal neurones was studied at 14 DIV, following 7 days treatment with control culture medium (control), or with the CaMKII antagonist KN62, or with the PKA antagonist Rp-cAMP. Figure 7-1 gathers a sample of images from each group, representing a segment of CA1 dendrite filled with Alexa 594, and after deconvolution, viewed with Imaris 3D reconstruction from the tif files.

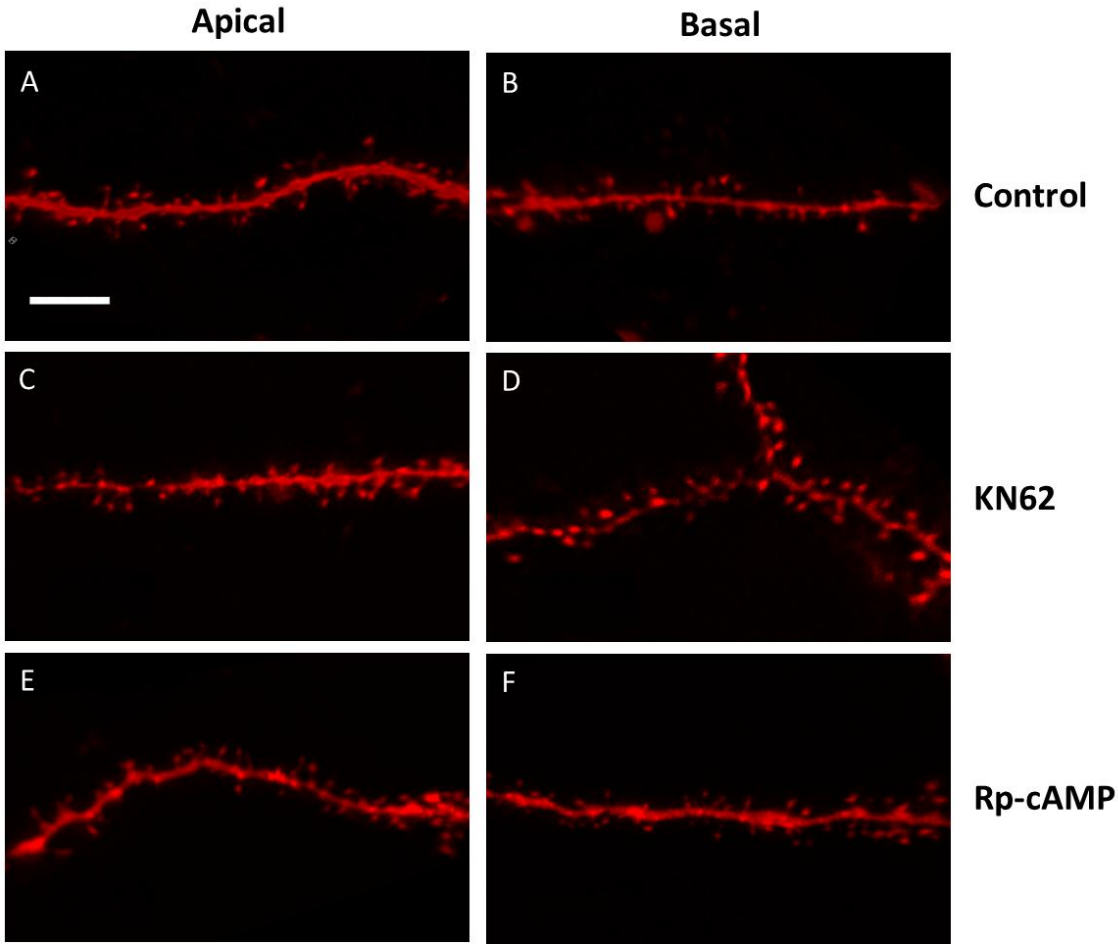

Figure 7-1: Deconvolved images of segments of CA1 dendrites in 14 DIV organotypic slices, filled with Alexa 594 and imaged with confocal microscopy.

The first column shows apical dendrites, while the second shows segments of basal dendrites, imaged at 14 DIV after a 7 days treatment with either control medium (A & B), or the CaMKII antagonist KN62 (C & D), or the PKA antagonist Rp-8-Br-cAMPs (called Rp-cAMP, E & F). Scale bar 5 µm.

7.2.2 Overall density of spines

The density per cell of dendritic spines was evaluated by adding the number of spines in each segment of the selected group, and dividing it by the total length of the selected segments.

The overall density of spines (figure 7-2A) was not affected by any of the three treatments (one-way ANOVA, p=0.61). In fact, the spine density remained very similar in the three groups, 1.09 ± 0.05 spines/µm in control (mean ± SEM, n=20 cells), 1.09 ± 0.05 spines/µm in KN62 treated slices (n=18) and finally 0.97 ± 0.12 spines/µm in PKA treated slices (n=5).

In order to compare later to what is happening specifically in apical and basal dendrites, graphs 7-2B and 7-2C show respectively the density of spines in apical and basal dendrites, under the three plasticity conditions. Similarly to what was observed on the overall population, the densities of apical (one-way ANOVA, p=0.56) and basal (p=0.89) were unaffected by long-term alteration of plasticity.

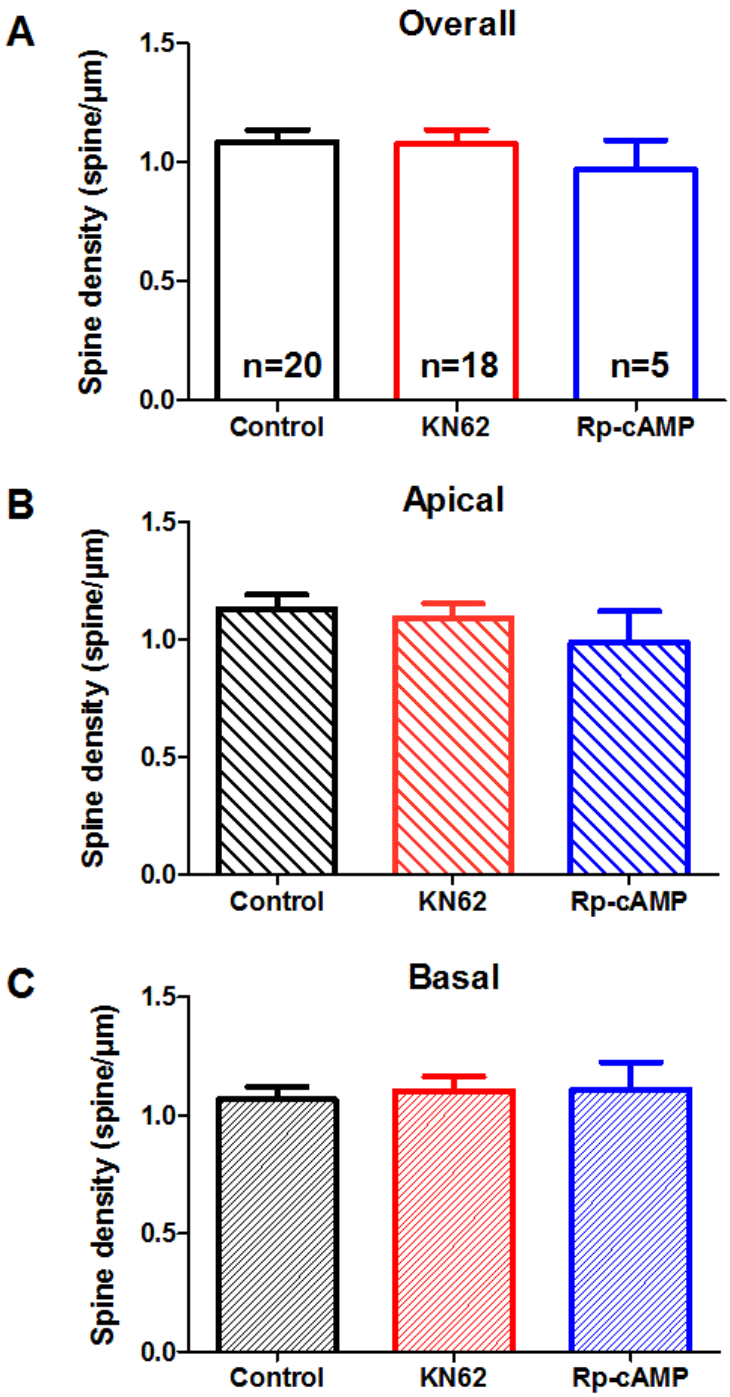

Figure 7-2: Density of dendritic spines following the 7 days treatment, in either apical, basal or overall.

The density of dendritic spines was unaffected by the long-term exposure to either CaMKII (red) or PKA (blue) antagonists, as confirmed by one-way ANOVA on the overall population (A, p=0.61), on the apical dendrites (B, p=0.56) or in the basal dendrites (C, p=0.89).

7.2.3 Effect of branching on apical spines

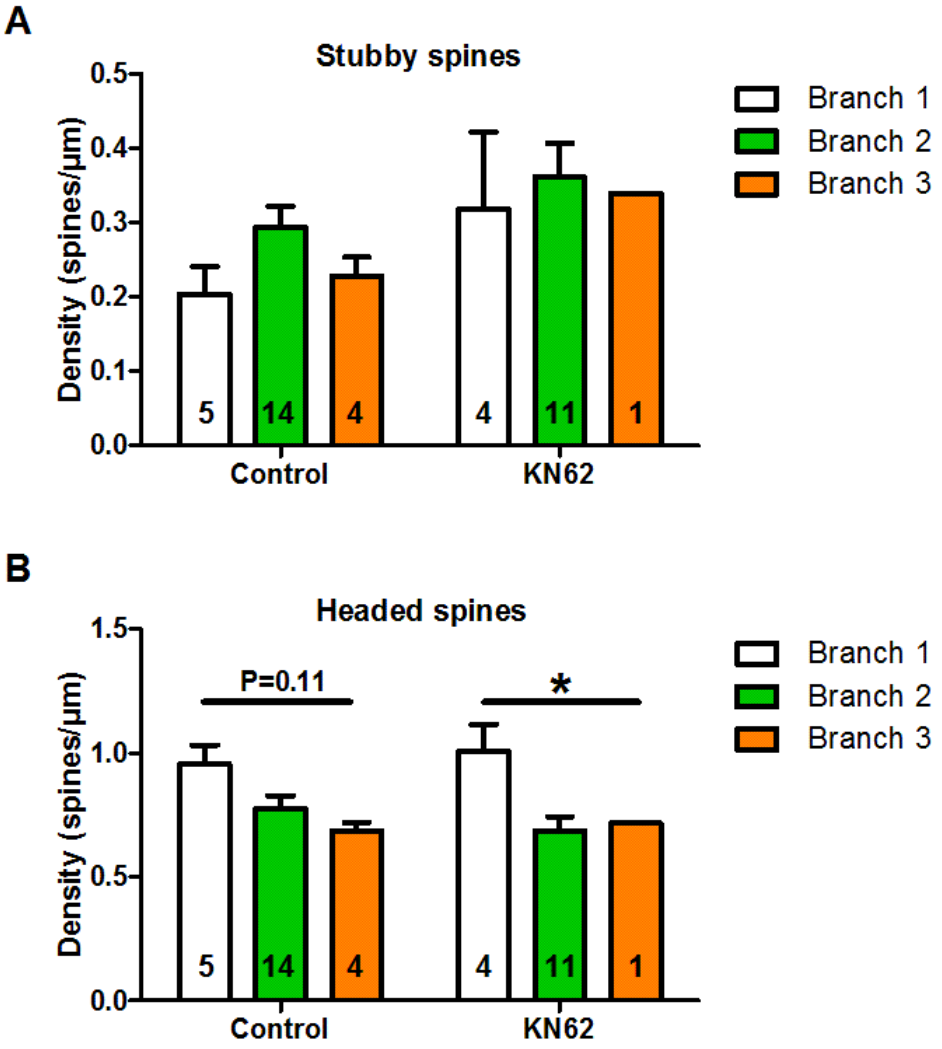

Figure 7-3: Density of spine in apical dendrites according to the degree of branching of the parent dendrite, in either control or KN62 treated CA1 cells.

(A) Cross-comparison of the density of stubby spines, between conditions and between branches (two-way ANOVA, interaction p=0.78). (B) The same cross-comparison in the headed spines brings a significant result among KN62 treated branches (p=0.026), while the same trend is observed in control, but to a much smaller degree (p=0.11).

The large sample of data available for control and KN62 treated cells allowed study of potential changes in dendritic spine population across the various degree of branching in the apical dendrites (figure 7-3). For this purpose, the density of spines in each branch was compared in control versus KN62 conditions using a two-way ANOVA. On

the overall density, no branch effect (p=0.20) or condition effect (p=0.42) were detected, nor was there an interaction (p=0.78). Densities of stubby and headed spines were compared separately, once again using a two-way ANOVA. In stubby spines (figure 7-3A), the comparison failed to find any significant difference between control and KN62 (p=0.11), or within each condition, between branches (p=0.66).

However, the results for headed spine density show some difference between branches in slices treated with KN62 (figure 7-3B). Indeed, the two-way ANOVA found a difference (p=0.026) in branches, which was confirmed with a Bonferroni's post-test between branches in KN62 conditions. While the trends towards a decrease in spine density with increasing branching failed to reach significance in control, it was significant in the presence of KN62 and furthermore, there was no significant difference between control and treated branches of the same order (two-way ANOVA, interaction: p>0.7).

7.3 Effect on spine type

7.3.1 Effect on density of each spine type

The total density of spines was found to be unchanged by the prolonged treatments with plasticity altering drugs, but this did not exclude the possibility that the density of each spine type was affected differently. Using two-way ANOVA to study the interaction between treatments and spine type, the overall population (not distinguishing between apical and basal) appeared to show no change (figure 7-4A, p=0.12). Similarly, the apical population taken separately did not show interaction between treatments in any spine type (figure 7-4B, p=0.17). However, the density of spines was affected by the treatments in basal dendrites (figure 7-4C), basal spines density increasing from 0.29 ± 0.02 spines/µm (mean ± SEM, n=18 cells) in control conditions to 0.41 ± 0.04 spines/µm (n=17) in KN62-treated slices (one-way ANOVA with Bonferroni's post-test, p<0.05), but was not affected by Rp-cAMP treatment.

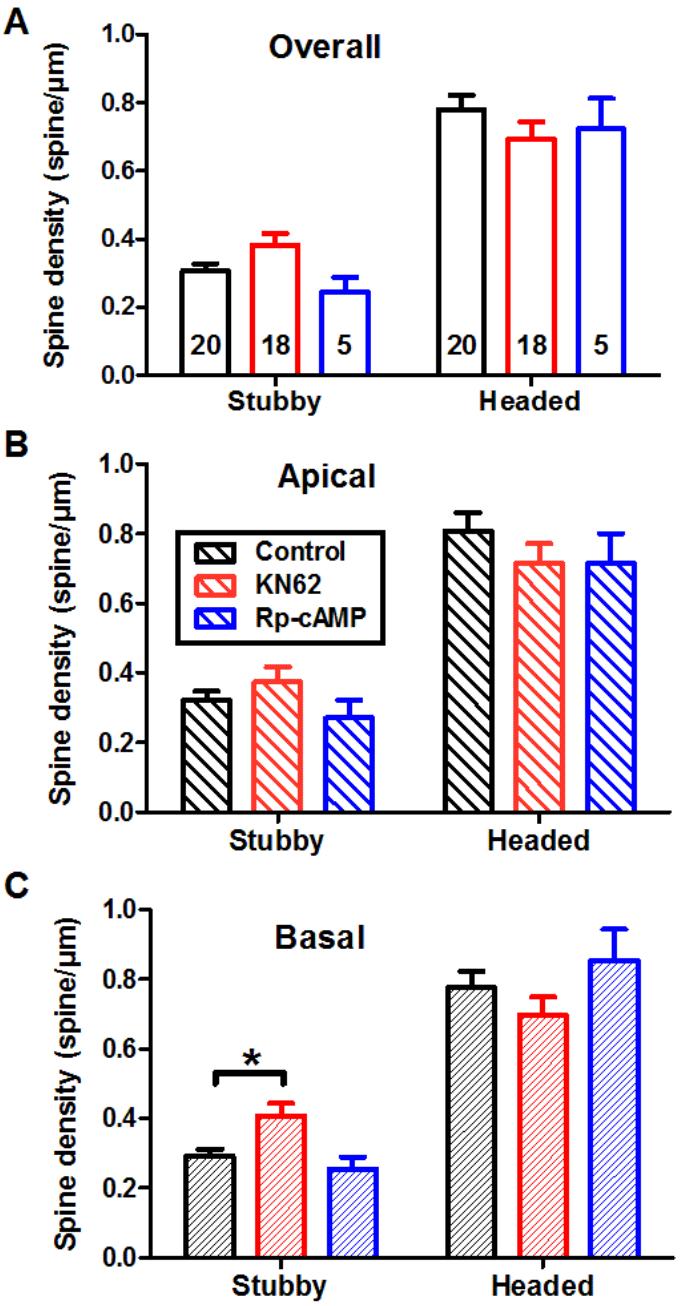

Figure 7-4: Effect of prolonged alteration of plasticity on the density of the different spine types.

Graphs shows mean and SEM of the total density of each spine type determined per cell and averaged across the cell sample. (A) The overall population is unchanged following any of the three treatments (two-way ANOVA, $p=0.13$). (B) In the apical dendrites, no interaction occurred between treatment and spine type (two-way ANOVA, $p=0.17$). (C) In the basal dendrites, stubby spines were affected by KN62-treatment (one-way ANOVA with Bonferroni's post-test, $p<0.05$).

7.3.2 Effect on spine types

The relative percentage of spine types can vary differently from individual spine type density. In organotypic as well as in acute slices, the percentage of mushroom spines, sometimes tagged “memory spines” (Bourne and Harris, 2007; Matsuzaki, 2007), surprisingly remains low, between 10-20% of the total population. In this section the percentage of spine type is calculated per cell, from the density of each type. The results from each cell are then pooled together to give the mean ± SEM, and result in each condition are compared for treatment effect with a one-way ANOVA and Bonferroni’s post-test. The numbers of cells used for each category are the same as for the calculation of density in the preceding section (number of cells, control: overall, n=20, apical n=19, basal n=18; KN62-treated: overall n=18, apical n=17, basal n=17; Rp-cAMP-treated: overall n=5, apical n=5, basal n=4).

Figure 7-5 presents in parallel the less plastic stubby spines and the more plastic headed spines. The overall proportion of stubby spine was significantly altered on the overall population (figure 7-5A, $p=0.019$) as well as in the basal dendrites (figure 7-5E, $p=0.012$). Apical dendrites were not affected by the treatment (figure 7-5C, $p=0.15$). In the basal dendrites, the percentage of stubby spines was increased and the percentage of headed was consequently decreased following the long-term blockage of CaMKII with KN62. However, on the overall population, a trend became evident between KN62 treatment and Rp-cAMP treatment (Bonferroni’s post-test, $p<0.05$). This result indicate a greater difference between KN62 and Rp-cAMP than with the control condition, possible sign that the effect of long-term incubation with KN62 and Rp-cAMP have opposite effects.

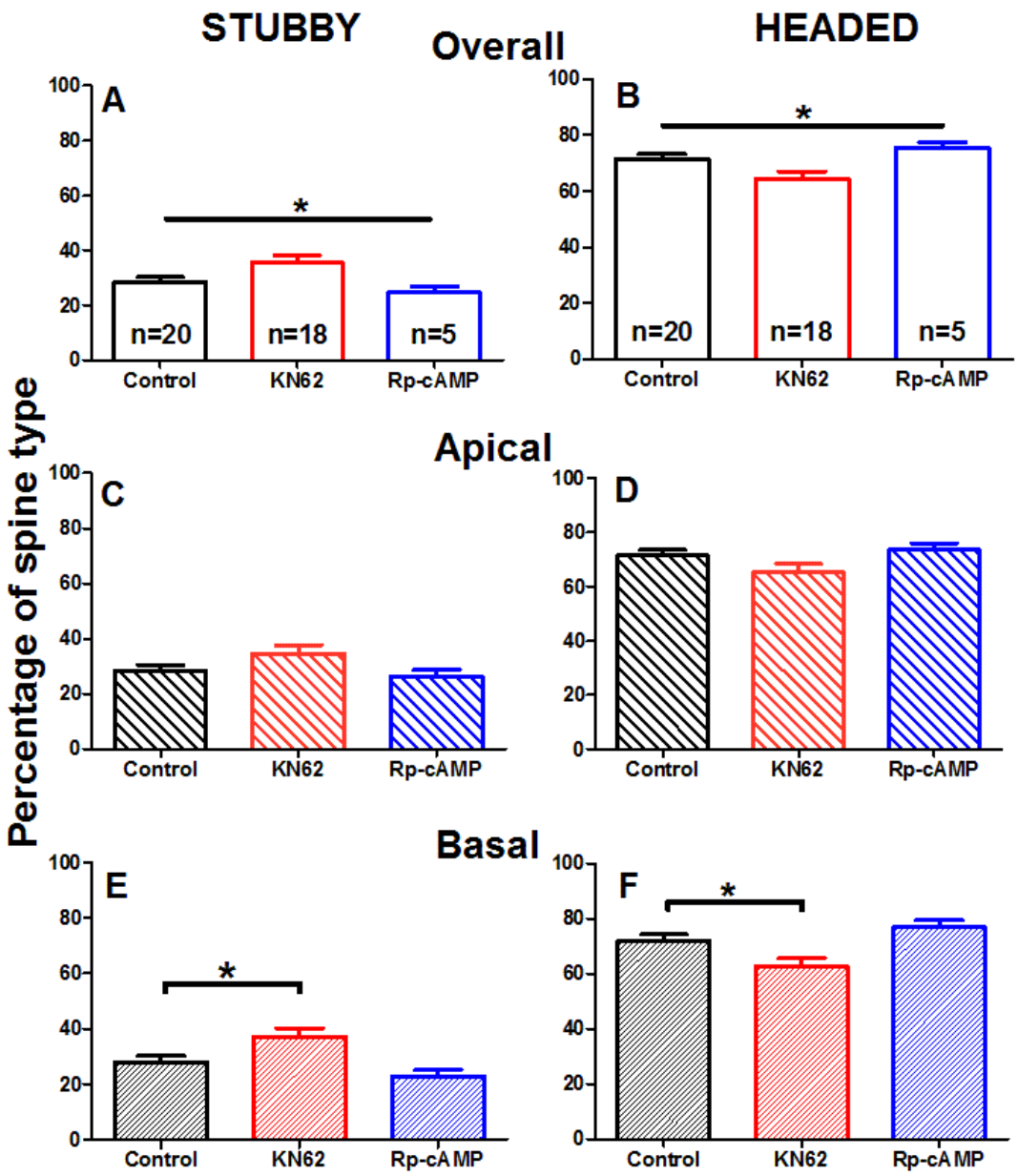

Figure 7-5: Effect of prolonged plasticity alteration on the representation of stubby and headed spines in the dendritic spine population.

Percentage of non-headed (=stubby) *vs* headed spines in overall (A & B), apical (C & D), and basal (E & F) dendrites, showing significance in one-way ANOVA (black line, no arrows, * for $p<0.05$) or Bonferroni's post-test (black line with downwards arrows).

7.4 Effect on spine shape

7.4.1 Spine head diameter

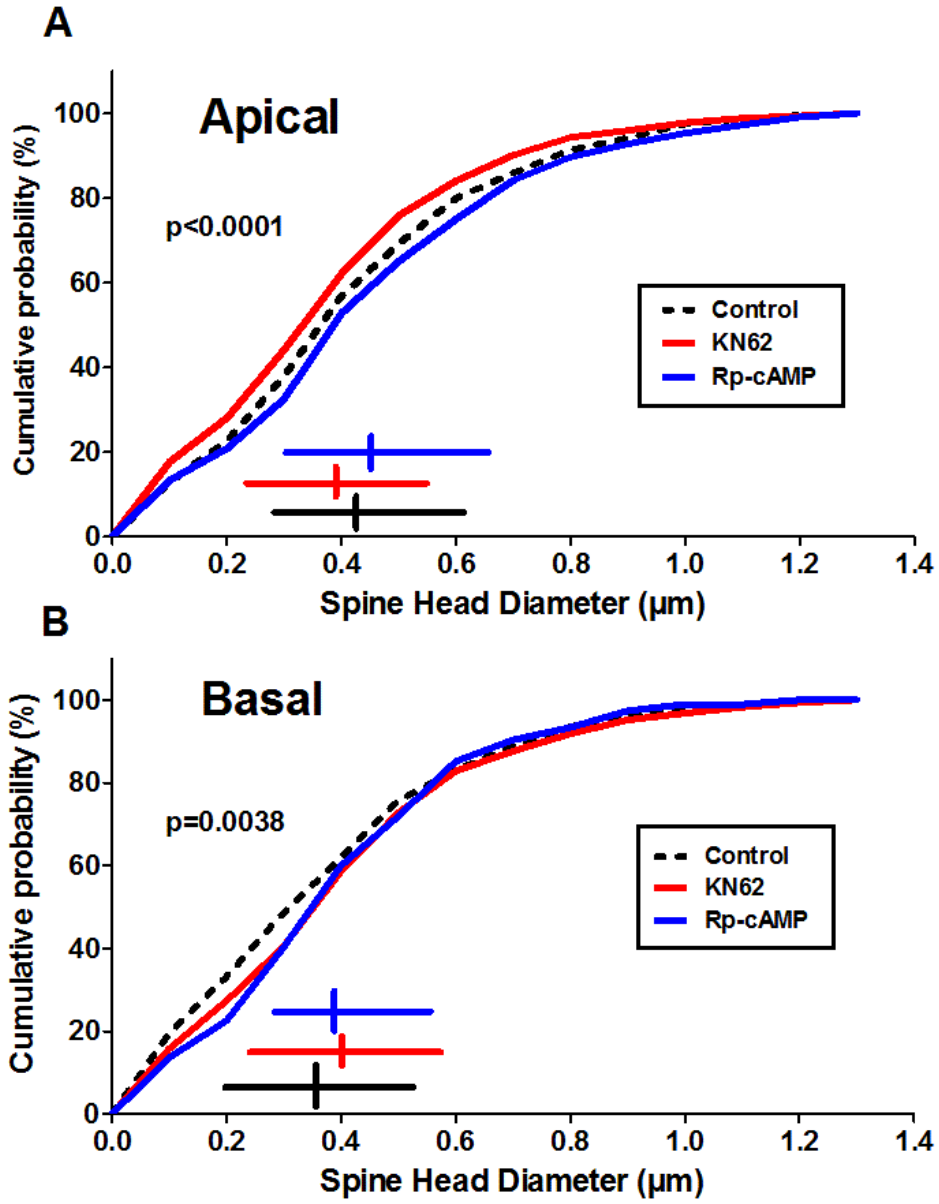

Figure 7-6: Distribution of spine head diameters in apical and basal dendrites of CA1 neurones in the three conditions tested.

The cumulative frequency distribution of spine head diameters shows that KN62 induced a decrease in spine head size in the apical (A) and an increase in the basal dendrites (B). Treatment with PKA inhibitor Rp-cAMP did not induce a significant change in spine head size in either apical or basal dendrites separately. The horizontal lines represent median, 1st and 3rd quartiles of each data set.

As mentioned previously, spine head diameter largely reflects synaptic strength, and as such global changes in their distribution can reveal whole cell changes in activity and plasticity. The population of spine head diameters was significantly affected by the long-term incubation with KN62 (red) or Rp-cAMP (blue), compared to control (black dotted line).

In the apical dendrites, similarly to what was observed with spine type density and percentage, KN62 and Rp-cAMP had opposite effects (figure 7-6A, Kruskal-Wallis $p<0.0001$). KN62 decreased the median spine head size (control, 0.41 µm, n=1350 *vs* KN62, 0.38 µm, n=810, Dunn's post-test $p<0.001$), equivalent to a 25% decrease in head volume. Rp-cAMP showed a trend towards increasing spine head size ($p<0.1$). The difference in head size became highly significant when Rp-cAMP was compared to KN62 (Rp-cAMP, 0.43 µm, n=360, Dunn's post-test $p<0.0001$).

In the basal dendrites (figure 7-6B), the spine head diameters were significantly larger in altered plasticity conditions (Kruskal-Wallis, $p=0.0038$), and Dunn's post-hoc test revealed the main difference to be between control (0.36 µm, n=1260 spines) and KN62 (0.40 µm, n=810, $p<0.001$), where the median spine head volume is increased by 40% under KN62 conditions.

Treatment with Rp-cAMP did not induce a significant increase in spine head size when looking separately at apical and basal dendrites ($p>0.05$). However, when pooled together, Rp-cAMP induced a small but highly statistically significant increase in spine head size on the overall population (control: 0.39 µm, n=1710; KN62: 0.38 µm, n=1260; Rp-cAMP: 0.42 µm, n=360; Kruskal-Wallis with Dunn's post-test, $p=0.012$, control *vs* KN62 $p>0.05$, control *vs* Rp-cAMP $p<0.001$).

7.4.2 Spine length

Analysis of the spine length revealed different effects of the treatments depending on the location of the parent dendrites. In the apical dendrites, the exposure to KN62 significantly reduced spine length (figure 7-7A, Kruskal-Wallis with Dunn's multiple comparison test, control *vs* KN62, $p<0.0001$). Interestingly, in the basal dendrites,

KN62 didn't show any effect on spine length, but Rp-cAMP did increase it significantly (figure 7-7B, control *vs* Rp-cAMP, p<0.0001). Spine length thus seemed to be affected very differently depending on the condition and location of the dendrite.

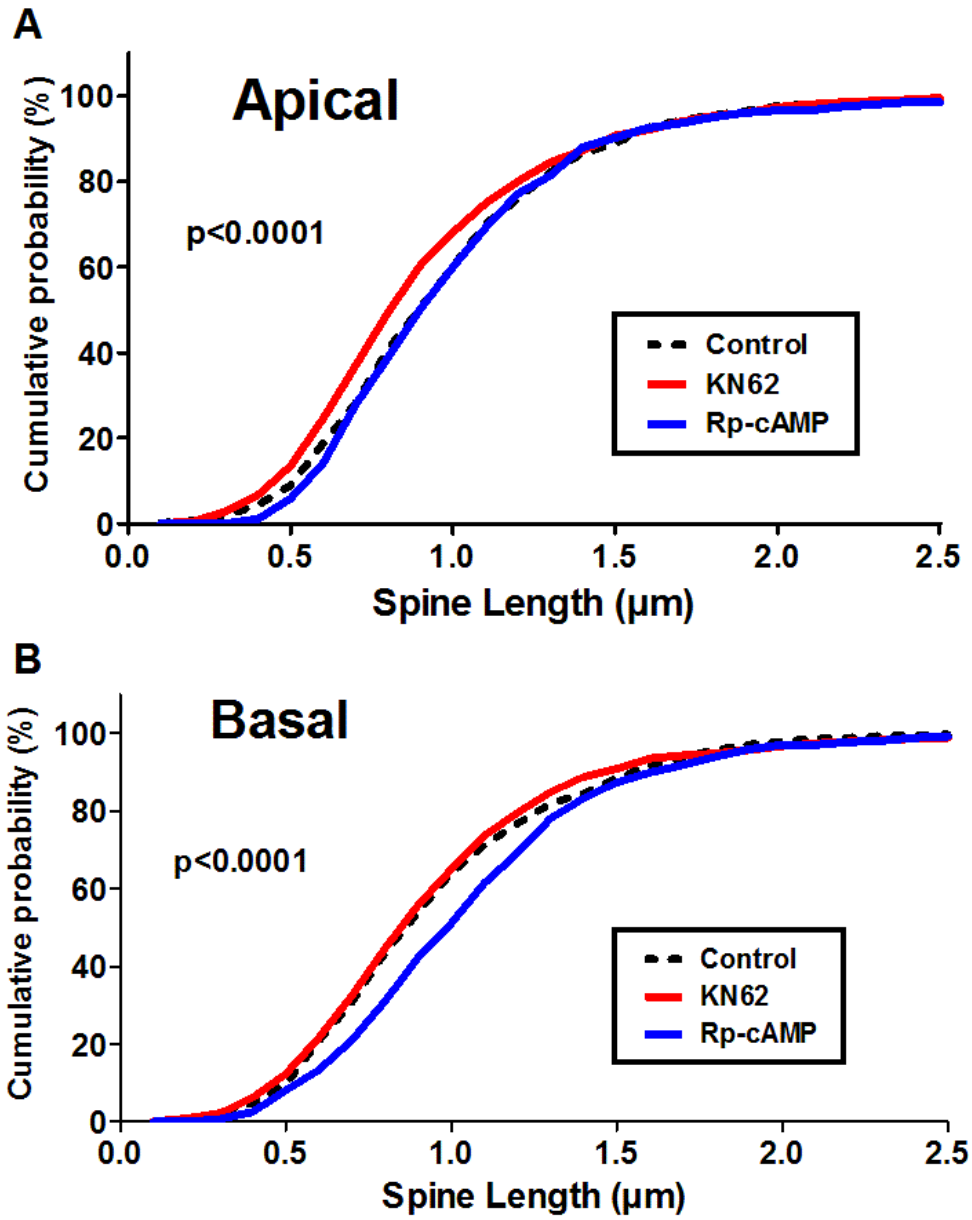

Figure 7-7: Distribution of spine length on apical and basal dendrites of CA1 neurones after 7 days treatments with plasticity blocker.

Cumulative frequency distribution of spine length in apical (A) or basal (B) dendrites of CA1 pyramidal neurones following 7 days treatment with KN62 or Rp-cAMP. KN62 significantly reduced spine length in the apical dendrites (A), while Rp-cAMP significantly increased spine length exclusively in the basal dendrites (B.) KN62 and Rp-cAMP have opposite effects in apical and basal branches (Kruskal-Wallis with Dunn's multiple comparison test).

7.5 Pathway specificity

Previous results from the Edwards lab have shown that the Schaffer collateral, which is the most active pathway in hippocampal organotypic slices, impinges more frequently on mushroom spines (~50%) than is observed on average across the cells (<15%) (De Simoni and Edwards, 2006). In my culture, and with the semi-automated analysis carried out in this work, the percentage of CA3 axons impinging on mushroom spines was not significantly different (12%) from the average percentage (15%). Since CaMKII and PKA are both responsible for the expression and maintenance of LTP in CA1 cells at 14 DIV, I tested the hypothesis that by blocking either molecule, the balance of the pathways would be altered.

However, I have showed in the introduction that mushroom spines were difficult to isolate automatically, and that the continuum of headed spines shape meant that it might be preferable not to try to distinguish them, otherwise taking the risk of identifying a very different sub-population to what was observed previously. Moreover, in Chapter 4, I have shown that the result obtained on control data with spines receiving only Schaffer collateral inputs suggest that I am looking at a different group of synapses than those reported as mushroom spines by De Simoni et al (2006).

However, though the isolated synapses might come from a more superficial or branching presynaptic axons, the experiment could still give interesting insight about whether and how changes in plasticity would induce changes in homeostatic mechanisms.

As mentioned previously, CA3 axons were labelled with DiO crystals dropped on the CA3 body layer 24 hours before imaging. The dye dissolves in the membranes of cells directly in contact with it, hence essentially cells on the top of the slice. Probably because of that, the axons labelled are predominantly visible in the apical dendrites of CA1 cells (figure 7-8A), and thus all connections here are from apical branches. An example of a putative synapse is visible on figure 7-8B, which is later verified by 3D reconstruction and visualisation with Imaris *Filament Tracer* (figure 7-8C).

Similarly to the analysis done in Chapter 4 when focusing on CA3-CA1 synapses, the data here is regrouped in contingency tables, and thus the graphs on figure 7-9 and 7-10 have no error bars, since they represent the percentage of each sub-group among the total population. A total of 10590 control spines, 7438 KN62-treated spines, and 3378 Rp-cAMP –treated spines were used for the analysis, including 27 confirmed CA3-CA1 synapses in control, 30 in KN62 and 21 in Rp-cAMP treatments.

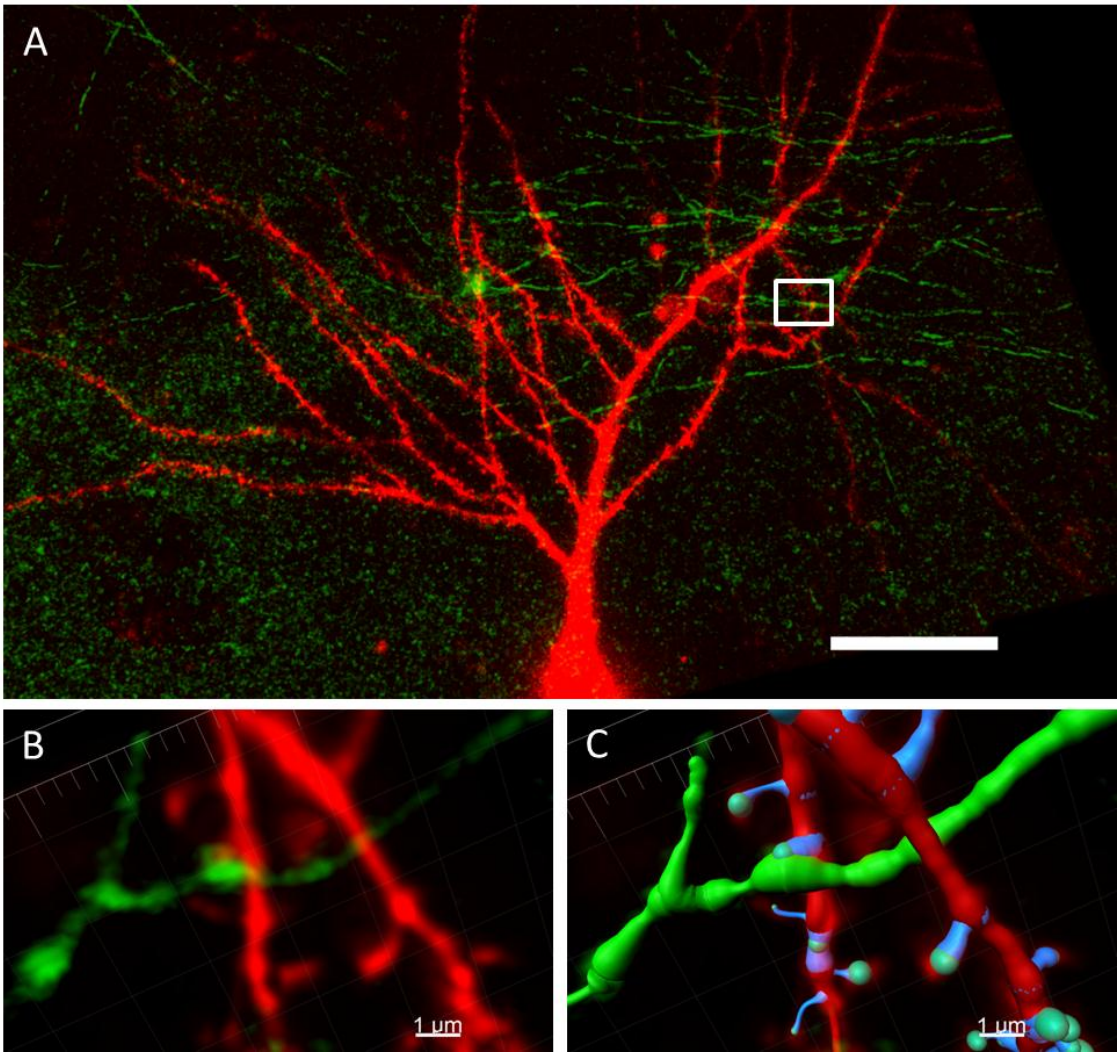

Figure 7-8: Confocal images (A & B) and Imaris *Filament Tracer* reconstruction (C) of CA1 apical dendrites (red) innervated by DiO labelled CA3 axons (green).

(A) Apical dendritic tree of a CA1 pyramidal neurone in an organotypic culture, showing intricate innervation by CA3 axons, labelled for 24 hours with DiO crystals (scale 10 µm). (B) Crop of a putative CA3-CA1 connection, which was confirmed by using 3D reconstruction and visualisation (C).

Figure 7-9 allows visualisation of the effect of treatment on the distribution of spine types in a pool of spine receiving either any input (figure 7-9A), or exclusively Schaffer collateral (figure 7-9B). A Pearson Chi-square test has been used to evaluate the interaction within each group between spine type and treatment.

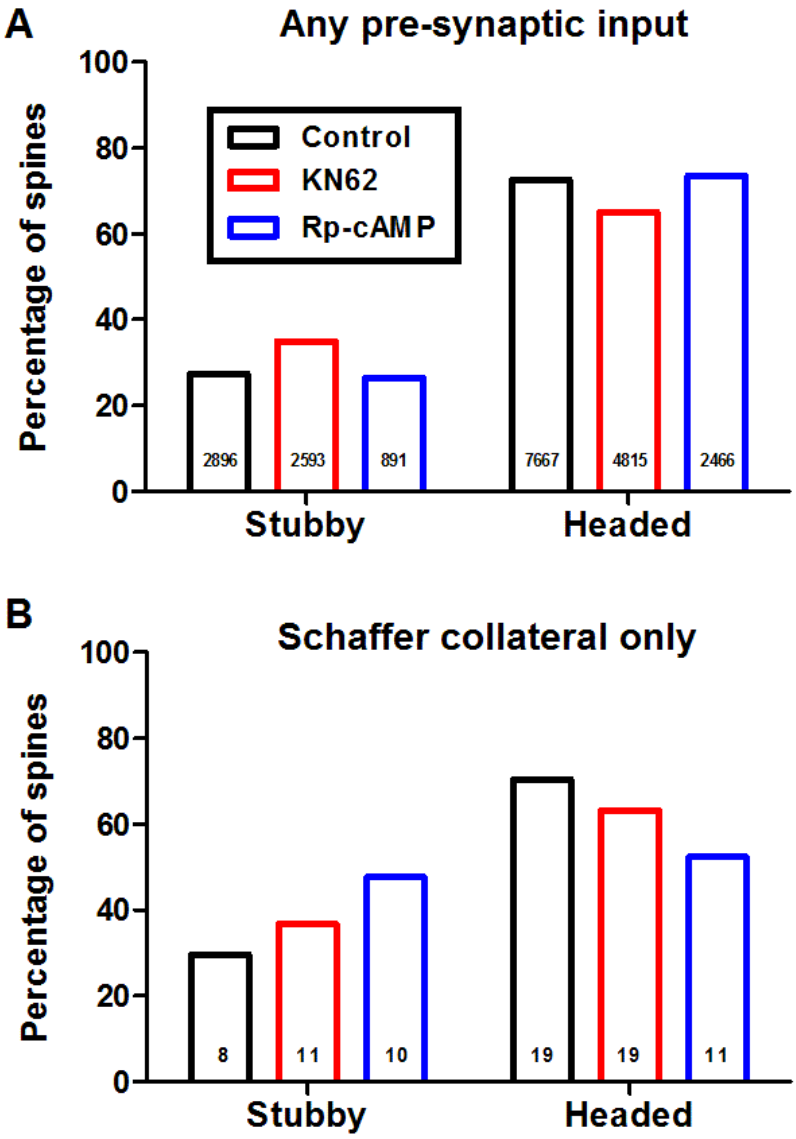

Figure 7-9: Percentage of spine types in the pooled population of spines, receiving input from either any presynaptic cell or specifically from CA3.

(A) All spines: Pearson Chi-square test evaluating the interaction between spine type and treatments found a clear difference between control and KN62 (Post-hoc Pearson Chi-square test, $p<0.0001$), but not between control and Rp-cAMP ($p=0.53$). (B) Schaffer collateral synapses: the trend came up as non-significant with the likelihood ratio ($p=0.80$), probably because of the smaller number of spines (stubby spine percentage: control, 29.6%, n=8; KN62, 36.7%, n=11; Rp-cAMP, 47.6%, n=10).

Figure 7-9A shows a similar effect to what was seen in section 7.3.2 of this chapter, when the focus was on the percentage of the different spine type. Previously, the data was compiled per cell; here the whole population of spines is used, without weighing for individual cells. The results from the Chi-square test gave the same result as those found previously: a very significant effect of KN62 compared to control ($p<0.0001$), but no effect of Rp-cAMP (control *vs* Rp-cAMP, $p=0.53$). The number of spines in the contingency table looking only at CA3-CA1 synapses is much smaller, and thus changes are less likely to come up as significant. Indeed, using the likelihood ratio, treatments appear to have no significant effect on the proportion of spine types ($p=0.80$).

To investigate further the effect of treatment on the Schaffer collateral activity and the spine types on which it impinges compared to the overall population of spine (all inputs), a new contingency table was created, and plotted per treatment (figure 7-10). Although there is no appropriate statistical test to compare overlapping distributions, the graph illustrates that only Rp-cAMP showed a trend towards an increase in stubby spines at CA3-CA1 synapses compared to the overall population. Once again, the spines identified here under SC seem to react differently to treatments than the overall spine population.

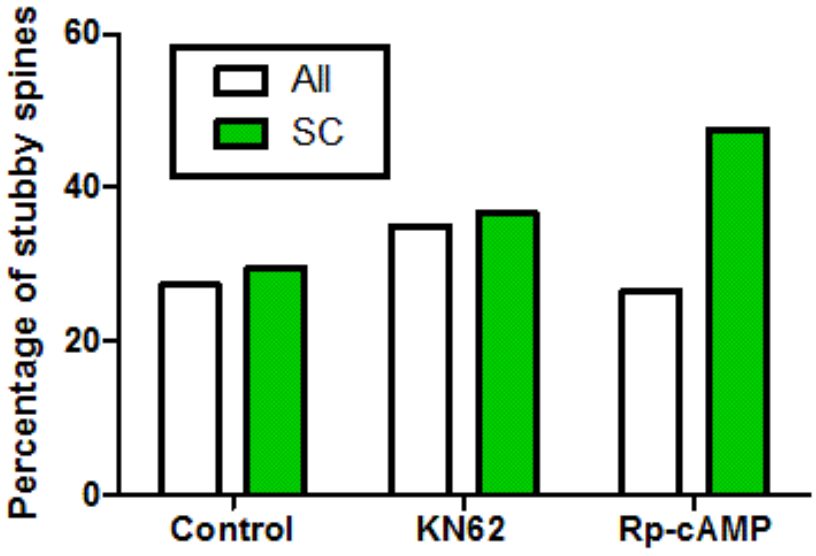

Figure 7-10: Percentage of the different spine type.

Contingency table of control, KN62 or Rp-cAMP treated CA1 neurones comparing the percentage of spines from each type according to the provenance of the presynaptic axon, either unknown (All) or Schaffer collateral only (SC).

7.6 Discussion

The work presented in this chapter investigated the effect of a less drastic alteration of the cells properties, in order to study homeostatic mechanisms of CA1 pyramidal neurones in 14 DIV organotypic cultures. I hypothesised that, since CA1 cells develop very similarly in organotypic slices and acute slices, synaptic changes occurring during development in organotypic slices were the result of LTP/LTD like phenomena, which shaped the synaptic network and set the characteristic distribution of the dendritic spine population. It was hypothesised that a seven day treatment with antagonists of key proteins for plasticity induction or maintenance such as CaMKII or PKA would induce changes in the ability of the cells to express LTP, and thus progressively compensate for this by homeostatic mechanisms. Also, since the Schaffer collateral pathway is the most active in organotypic slices, I hypothesised that the alteration of plasticity following the blockade of CaMKII or PKA would be more important on spines receiving input from this pathway.

Spine density. The experiments showed that plasticity alteration did not affect the overall density of spines. The maintenance of spine density is not surprising, especially in the light of the deafferentation results, which showed that spine density increase between 7 and 14 DIV is very robust and is probably the result of cell-autonomous development, independent of CaMKII or PKA.

Spine type. CaMKII inhibition did increase the proportion of stubby spines in both apical and basal dendrites to the detriment of headed spines, an alteration of dendritic spine morphology which implies changes in synaptic plasticity as stubby spines showing much faster decay of calcium transients (Majewska et al., 2000). CaMKII is fundamental in the induction phase of LTP after P10 (Lisman et al., 2002) and inhibition of CaMKII showed more significant differences on dendritic spine population than inhibition of PKA.

Spine head size. Spine dimensions were altered by the seven days incubation, KN62 and Rp-cAMP tending to show opposite effects: KN62 reduced dendritic spine head

size, while the antagonist of PKA showed a tendency to increase it, thus emphasising the different consequences of the two treatments. Rp-cAMP is an inhibitor of PKA type 1, which is essentially present in the cytoplasm while type 2 is mainly associated with the synaptic membrane (Michel and Scott, 2002). Inhibition of nuclear PKA results in deficient late but not early LTP in CA1 pyramidal neurones, expressing a parallel decrease in CREB phosphorylation (Matsushita et al., 2001), suggesting a dominant role for cytoplasmic PKA in the protein synthesis-dependent phase of LTP. Several hypotheses can be made to explain the different direction of the effect of Rp-cAMP in spine head size compared to CaMKII blockade.

1) PKA might not be directly involved in the setting of spine head size or in homeostatic plasticity.

2) It is also possible that the inhibition of PKA can be compensated over time by other signalling cascades involved in protein synthesis. Indeed, several papers report that the short term effects (12-48 hours) of chronic changes in activity -and potentially plasticity- can be reversed after 4 to 10 days. For instance, the overexpression of the inward rectifier Kir2.1 silences neurones for 48 hours, but longer incubation induces compensatory mechanisms restoring firing rates (Burrone et al., 2002). Similarly, the developmental increase in AMPA receptor numbers at synapses is prevented by blockade of NMDA receptors up to 4 days, but returns to control levels when the blockade persisted for 8 days (Zhu and Malinow, 2002). It can thus be hypothesised that the various cascades involved in the recruitment and synthesis of plasticity-related protein might be able to compensate for the blockade of PKA.

3) Another interesting hypothesis is that the soluble PKA type I is an intermediate of a global form of homeostatic plasticity. Thus, when CaMKII-dependent activity induces potentiation in the apical dendrites and thereby increases CA1 activity, the forward loop of CA1-CA1 synapses in the basal dendrites may activate soluble PKA which then transits to the nucleus to initiate synthesis of one or more enzymes that act as global regulator of plasticity. This hypothesis would reflect the general increase in spine head size observed with Rp-cAMP, and would also explain the increased difference observed between KN62-treated and Rp-cAMP-treated slices compared to control, since CaMKII-

dependent increase in apical head size would precede PKA's role in homeostatic plasticity.

Region-specific changes. The most interesting result from this section comes from the disappearance of the difference in spine head size between apical and basal dendrites following CaMKII inhibition for 7 days. In Chapter 4, the apical dendrites were shown to have larger spine heads on average than basal dendrites. The study of spines receiving input only from the Schaffer collateral did not produce the expected results, but on the contrary underlined a distinct population of spines, differing in spine length as well as in head size from the overall population and possibly receiving input from sprouting axons.

The overall difference between apical and basal spines is abolished in the presence of KN62 (figure 7-11). These results support the hypothesis that the differences between apical and basal dendrites in spine head diameters observed in control slices result from an activity-dependent competition between the different pathways, which induces homeostatic response in the weaker pathways to maintain the global synaptic output. Preventing the ability of neurones to express LTP abolished the pathway difference. The activity-dependent enlargement of spine head diameters was prevented in apical dendrites, while the opposite effect was observed in the basal dendrites. In control conditions, the CA1-CA1 synapses were mainly impinging on smaller spines (De Simoni and Edwards, 2006). Those results suggest that, following KN62 treatment, CA1-CA1 synapses, essentially present in the basal dendrites, are no more homeostatically down-regulated by the activity of the Schaffer collateral and contribute to the increase in spine head diameters observed in the basal dendrites compared to control conditions.

Another parameter affected very differently and locally in the two conditions is spine length: KN62 decreased length in the apical dendrites, while Rp-cAMP increased it in the basal dendrites, suggesting once more a regional effect of the inhibition of CaMKII and PKA, which may act differently at different types of synapses.

All results show a location-specific effect of the drugs, which could be the consequence of pathway specific responses. Mechanisms for the induction of plasticity and

homeostatic plasticity are synapse-specific (Kim and Tsien, 2008), and the different representation of afferent axons on apical and basal dendritic spines could be the cause of the treatment/pathway specific results. Those results point out the different mechanisms in which CaMKII and PKA are involved at distinct types of synapses and how these mechanisms are affecting different steps of the homeostatic process.

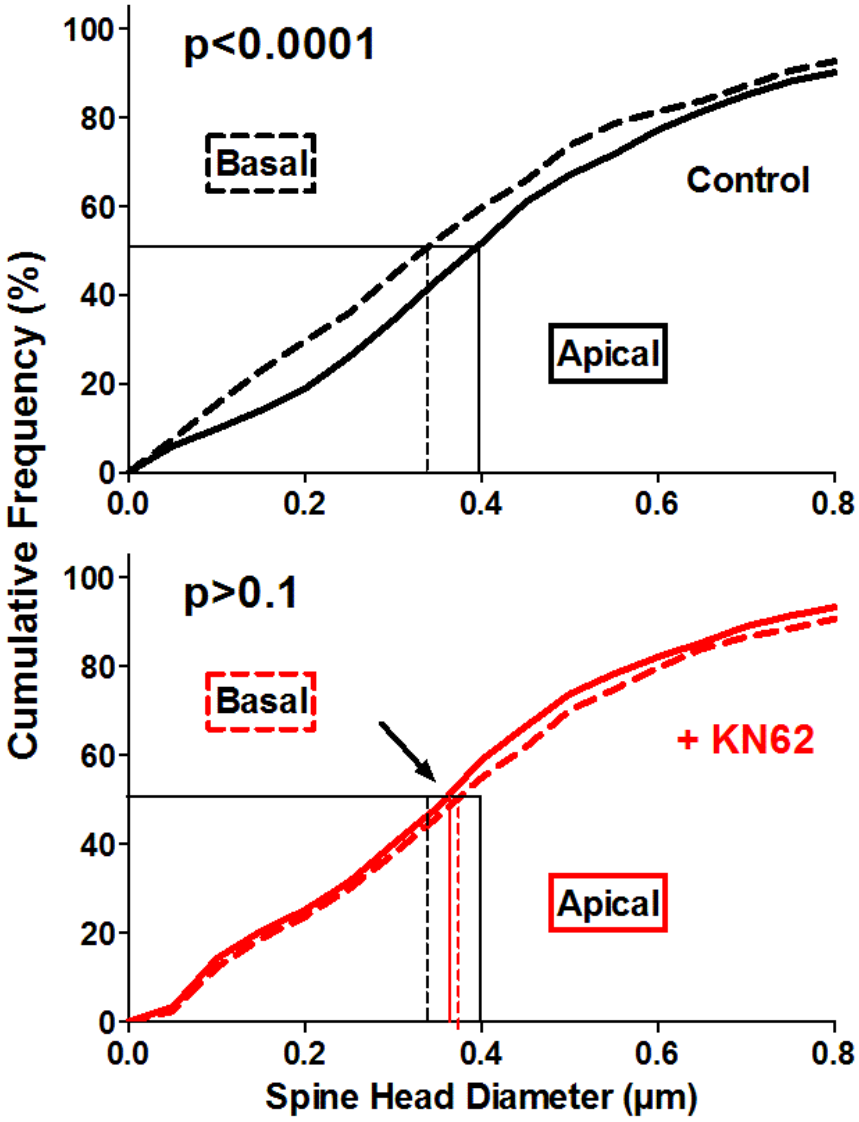

Figure 7-11: CaMKII inhibition prevents the difference of spine head size between apical and basal dendrites.

Apical dendrites, which are innervated by the active Schaffer collateral pathway, exhibit larger spines than the basal dendrites in control conditions. Following 7 days treatment with the CaMKII inhibitor KN62, the distributions of apical and basal dendritic spine head diameters are similar.

Chapter 8. General discussion

This work has focused on pathway dependent synaptic plasticity in developing neurones, mainly through the morphological changes of the postsynaptic dendritic spines. Synaptic changes have been studied by studying mEPSCs, spine density or individual spines, but few studies have focused on the distribution of dendritic spine morphological parameters such as head diameter and length following chronic modification of activity. Little is known about how activity-dependent and homeostatic plasticity are affected when the ability of neurones to express LTP or LTD is blocked during development. The large amount of knowledge gained lately, showing a tight relationship between spine morphology and functionality (Kasai et al., 2010), enables the study of both local and global changes in synaptic weight by studying the distribution and dimensions of dendritic spines in various conditions affecting plasticity.

After establishing a reliable method for analysing dendritic spines from confocal images, the dendritic spine population of CA1 pyramidal cells in developing organotypic slices was compared between control conditions and chronic modification of activity or plasticity. The results show that several factors tightly regulate the postsynaptic spines: neuronal network, age of the preparation and pathway-specific activity. Changes in dendritic spines seem to be localised to the regions most affected by the activity or plasticity inhibition and those adaptive modifications were increasing with the age and severity of the treatment. The cell global synaptic strength seems to be regulated by homeostatic mechanisms, possibly to ensure cellular and network stability.

8.1 Optimising dendritic spine analysis

Live-imaging of dendritic spines is a widely used technique, but image analyses vary largely across studies and need to be adapted for specific purposes. Optimisation of dendritic spine analysis has thus been the focus of a large part of my work, adapting the recent findings of the literature, suggesting a continuity of spine morphologies, to improve semi-automatic dendritic spine sorting with the commercial software *Filament Tracer* from Bitplane. Studying dendritic spines optically also implies working at resolution limits, and thus careful interpretation is required on the analysis of the statistical results.

8.1.1 Heterogeneity of dendritic spine types and analysis

A summary of dendritic spine type classification from several groups enables measurement of the discrepancy in the actual object categorised. Harris and colleagues' definition of dendritic spine types has been widely used, but this definition leaves many spines unclassified (Harris et al., 1992). Attempts by other labs to include all protrusions in the classification gave rise to less physiological distinctions between the different groups (Oray et al., 2006). The diversity of dendritic spine shapes (figure 1-3B) shows that several spines could fit in more than one type, suggesting a continuity of morphological shapes. In my experiments (Chap 3), I first attempted to make an automatic classification of dendritic spine types according to previous rules (De Simoni et al., 2003), by using dimensions extracted from 3D reconstructions. Trying several sets of parameters, it was very difficult to obtain a good match between the automatic and visual classifications, notably between thin and mushroom spines.

Some morphological parameters are more fundamental for synaptic plasticity, such as the presence of a neck constriction. The relative isolation of the head confers essential properties for synaptic plasticity such as increased Ca^{2+} gradients and retention of plasticity related protein (Bloodgood and Sabatini, 2005; Okamoto et al., 2007; Honkura et al., 2008). Stubby spines, characterised by the absence of constriction between their PSD and the parent dendrite, lack the ability to confine ions and proteins and, except at the first post natal days, rarely transform into a spine with a

head clearly separated from the dendrite by a neck constriction (Parnass et al., 2000; Petrak et al., 2005), called headed spines in this work. For plasticity studies based on morphological changes of dendritic spines, it is thus important to separate stubby and headed spines.

8.1.2 Limits of the analysis & significance of results

The limitations encountered with the image analysis software had also to be placed in the context of the analysis, which deals with object at the limit of optical resolution for light imaging. Indeed, the maximal resolution for confocal microscopy, in a supposedly perfect optical instrument, is limited by the wavelength and the numerical aperture. The resolution, i.e. the smallest distance between two objects to separate them, ranges around 0.2 µm at the excitation wavelength used with our confocal microscope. Very fine structures such as neck diameter cannot be resolved with confocal microscopy. When considering the head diameter of headed spines in control or treated slices, the difference between the means of the samples is usually less than 0.2 µm, and thus below resolution. It is important to remember, however, that the difference in the medians does not reflect an individual difference between two spines heads, but between the distributions of very large samples. Moreover, each measurement obtained with the *Approximate Circle* algorithm result from a 3D evaluation of the spine head and finally returns the diameter of a sphere of equivalent volume. The diameter is not a linear estimation of the head size, but takes into account the non-spherical geometry of spine heads.

It is therefore possible to study dendritic spine dimensions with confocal imaging and the appropriate analysis. It remains important to bear in mind that the values obtained for morphological parameters are not absolute measurements but represent a shift in the distribution between control and treated cells, extrapolated from 3D volumes rather than 2D projections.

8.2 Experimental variability & necessity of repeating basic findings in the model used

Homeostatic plasticity, which is by essence very sensitive to the neurones previous activity, is probably affected by the differences in basal activity of individual preparations. Small changes in procedures or protocols, across but also within one lab, could affect this basal activity of neurones and thereby plasticity. It is therefore essential to repeat previously published findings in one's model to set the starting point of further investigation.

8.2.1 Difference in culture preparation

The type of preparation used for studying synaptic plasticity mechanisms and the variability of living tissues can have a large impact on the experimental results. The issue was raised in my work following the absence of synaptic scaling observed in CA1 neurones from organotypic slices. In dissociated cultures, where synaptic scaling was established (Turrigiano et al., 1998), neuronal density in individual preparation impacts considerably on their development and physiological properties (Ivenshitz and Segal, 2010). In organotypic cultures, the estimation of equivalent ages across preparations can be difficult to establish. It is nevertheless an important factor for synaptic plasticity, since molecular pathways regulating plasticity are modified during development. For instance, LTP at CA3-CA1 synapses relies on PKA and GluR4 trafficking before P10 (Esteban et al., 2003; Yasuda et al., 2003), independently of CaMKII (Kirkwood et al., 1997), while LTP induction becomes CaMKII-dependent later (Silva et al., 1992; reviewed in Lisman et al., 2002). In the Edwards lab, the slices made from P5 male rat have been studied intensively and compared to acute slices of various ages in rat (De Simoni et al., 2003; De Simoni and Edwards, 2006). This enables a good comparison between findings in our cultures and the literature from acute slices. However the comparison becomes less relevant between slices made from various animals (mouse or rat) of different ages (P2-P8), since the synaptic plasticity of neurones develops differently during the first days *in vitro*, depending on the age of the pup when the slices were made (Muller et al., 1993).

The method used for slicing, whether it is with a vibratome (Edwards' lab, Malenka's lab) or a chopper (Malinow's lab), will affect the proportion of dorsal and ventral slices available, which express different levels of AMPA and NMDA receptors (Pandis et al., 2006) and thus could affect plasticity. Synaptic incorporation of AMPA receptors can be induced by phosphorylation of three different sites on the GluA1 subunit: at S831 by CaMKII (Mammen et al., 1997), at S845 by PKA (Esteban et al., 2003), or at S818 by PKC (Boehm et al., 2006). In basal conditions, the phosphorylation of these specific sites will affect the pathway required for synaptic plasticity (Lee et al., 2000). Similarly, the phosphorylation of CaMKII at T286/T305/T306 can also affect the direction of plasticity towards LTP or LTD (Pi et al., 2010), suggesting that basal network activity has fundamental implications for future plasticity.

When the focus is on LTP/LTD and homeostatic plasticity, it is important to establish the situation in the current model by repeating published experiments.

8.2.2 Variability of results and absence of published negative results

Small changes in experimental procedures can induce significant modification of results. When I compared my results to those gained previously in the lab, a few differences appear, such as the proportions of the different spine types, or the labelling of en passant axons. Although I was repeating carefully the protocols established in the lab, the absence of practical overlap with the previous users might have resulted in slight procedural differences which could explain the differences between my results and previously gained ones. This suggests that small experimental or analytical changes could involuntarily impact the results and that cross-experimenters comparison should always be considered carefully.

In similar developing cultures, the chronic inhibition of activity have led to contradictory results, such as increased mEPSCs amplitude (Stellwagen and Malenka, 2006), absence of activity-driven potentiation (Collin et al., 1997; Barria and Malinow, 2005), or absence of change from control conditions, as it was shown in Chapter 5. The

difficulty of publishing negative results biases biological findings available and could be misleading on the repeatability of experiments (Song et al., 2009). Although synaptic scaling has been observed in a large variety of preparations at different ages (for reviews, see Turrigiano, 2008; Pozo and Goda, 2010), it cannot be assumed to work in different types of cultures and ages, and the literature available may not reflect the real situation about synaptic scaling.

8.3 Age-dependence of the activity-dependent and homeostatic synaptic plasticity

Synaptic plasticity is very dependent on both the past and present activity of the network, which adapts to ensure physiological levels of excitability. During development, the relative importance of the activity-dependent plasticity pathways is modified and, consequently, so is the homeostatic responses. The balance between autonomous and network-driven changes seems to be very dependent on the age of the neurones.

8.3.1 Following reorganisation

After a drastic modification of the network induced by the transection of Schaffer collateral afferents on CA1 cells, pyramidal neurones showed some clear age-dependent adaptation. Younger cultures seem less affected following reorganisation of the network, the density of dendritic spine increasing normally from 7 to 14 DIV after deafferentation. As has been observed *in vivo* in the visual cortex (Wierenga et al., 2006), autonomous development plays an important role in young hippocampal neurones, suggesting an important role for spontaneous neural activity during development (Katz and Shatz, 1996). When the structural reorganisation arrives later (from 14 DIV), spine density decreases significantly, as has been observed in this work and previously (McKinney et al., 1999). However, the decrease in density observed was not as dramatic as what has been observed in other types of preparation, where up to

80% of connections were degenerating after a week (Raisman and Field, 1973). Following deafferentation, it is probable that persisting axons from other neurones, such as from the entorhinal cortex in the apical or neighbouring CA1 cells in the basal, increase their sprouting and make up for some of the lost connections from the Schaffer collateral (Steward et al., 1988).

8.3.2 Following activity deprivation

In hippocampal slices, TTX-induced activity deprivation has been found to induce synaptic scaling in mature slices (21-35 DIV) (Aptowicz et al., 2004; Kim and Tsien, 2008). However, results in younger slices are more controversial, possibly because changes in preparation, such as postnatal days of pups when cultures are made, or the composition of culture medium, have stronger effects on developing neurones than in mature ones. Synaptic scaling has been observed in organotypic cultures from 9-15 DIV (Cingolani and Goda, 2008), but sometimes the conditions such as the absence of serum were slightly different (Tyler and Pozzo-Miller, 2003). At CA3-CA1 synapses *in vivo*, injection of TTX induced an increase in mEPSCs amplitude only in juvenile (P15) but not older rats (P30) (Echegoyen et al., 2007). In the visual cortex, monocular deprivation scaled up transmission in layer IV when the deprivation was carried out at P14 but not at P21 (Desai et al., 2002). Conversely, the same treatment in layer 2/3 was effective only when started after P21, suggesting that the developmental changes occur with various time-scale in the different layers. In hippocampal organotypic slices, several papers report inhibition of developmental changes following chronic activity deprivation. For instance, blockade of NMDA receptors for 24 hours before P8 prevented the developmental increase of AMPA receptor numbers at synapses (Zhu and Malinow, 2002; Barria and Malinow, 2005); two or three weeks exposure to TTX or APV prevented the developmental increase of spine density in CA1 cells (Collin et al., 1997). Similarly, neurones individually silenced before formation of the network received less synaptic inputs than control (Burrone et al., 2002). However, in the same study, neurones silenced at a later age showed a marked increase in mEPSCs frequency but no change in amplitude, thus showing age-dependent regulation. Silencing of

individual neurones or of the whole network is thus dependent on the developmental stage of the preparation.

In the context of my experiments, the blockade of both AMPA and NMDA receptors to induce synaptic scaling (Stellwagen and Malenka, 2006) could lead to mixed results: blockade of AMPA receptors induces a decrease in spine density (McKinney et al., 1999a; Mateos et al., 2007), while NMDA receptor blockade maintained spine density (McKinney et al., 1999). The cocktail CNQX/APV was found to induce synaptic scaling in mouse organotypic slices but failed to do so in dissociated hippocampal cultures (Ibata et al., 2008) or in my preparations. Having contrasting results when used separately, NMDA and AMPA receptor antagonists' combination could therefore lead to mixed results, the balance of their respective contribution being possibly driven by several factors such as age of the neurones and preparation.

Spine density was unchanged at younger age (P6-7 or P11-12) following chronic activity deprivation for 5 hours with TTX/APV/CNQX, while the same experiment conducted at a later age (P20-22) increased spine density (Kirov et al., 2004). The results confirmed what I observed in my experiments, i.e. that spine density is more robust early during development but more prone to activity-dependent or homeostatic changes after 2 weeks.

8.3.3 Developmental switch in PKA/CaMKII-dependent synaptic plasticity and GABA transmission

The age-dependent changes in plasticity observed previously can be related to important physiological and functional changes operating in developing neurones.

The literature reports a developmental switch for the induction of LTP in CA1 pyramidal neurones, which relies principally on PKA in P7-8 neonates (Zhu et al., 2000; Yasuda et al., 2003), before becoming CaMKII-dependent later (Silva et al., 1992; Matsuzaki et al., 2004). In the P10-20, CaMKII was found to be necessary and sufficient to induce LTP (Pettit et al., 1994), but other studies found additional mechanisms involving PKA and/or PKC in parallel with CaMKII (Wikström et al., 2003; Boehm et al., 2006). It is possible that blocking PKA or CaMKII after 7 DIV in our cultures could be

compensated at different levels by those parallel mechanisms, which would lead to the observed differences in effects on spine morphology. Blocking CaMKII had no global effect on spine head size but modified the distribution in opposite directions in apical and basal dendrites. Meanwhile, blocking PKA increased spine head size globally but showed only trends in the same direction in apical or basal. This could suggest that in one case, LTP cannot be induced and thus the activity-dependent settings between the pathway is prevented, while with PKA inhibition, LTP may be induced, leaving the balance between apical and basal unaltered, but the disrupted maintenance leads to compensating mechanisms occurring in both regions.

During the same period, another important switch occurs in pyramidal neurones: the neurotransmitter GABA progressively becomes inhibitory (Ben-Ari et al., 2007), but see (Rheims et al., 2009). At early ages, $GABA_A$ activation causes depolarisation because of the high intracellular concentration of Cl^- (Ben-Ari, 2002). After P10, changes in the type of Cl^- transporter expressed results in a decrease in the intracellular concentration of Cl^- and both GABA and glycine become inhibitors of synaptic transmission (Blaesse et al., 2009). In the organotypic cultures made from P5 rat used in my work, GABA may still play a depolarising role at 7 DIV, when most treatments are started, but depolarising $GABA_A$ currents disappear rapidly after P10 and should have negligible impact thereafter in my cultures.

In accordance with previous findings, the results gained from this work suggest that plasticity relies on different mechanisms depending on the developmental stage of the neurones and the network, and that several mechanisms work in parallel to ensure the development of a functional network. The complementarity of those pathways in development is far from being elucidated, and the development of *in vivo* imaging, already used successfully in the motor and visual cortex, is probably the next step in the investigation of the hippocampus. Those biological pathways regulating plasticity could also be synapse-specific, and thus have localised influence.

8.4 Balancing output globally to maintain synaptic weight

Synaptic scaling is one of the most studied types of homeostatic mechanism which enable maintenance of neuronal excitability. Homeostatic changes aiming at maintaining each neurone's ability to fire action potential can also have more local origins, and be regulated at a pathway level. In my experiments, I have confirmed that CA1 pyramidal neurones can compensate for activity-dependent activity by scaling down of synaptic weight in the less active pathways, but that blocking CaMKII prevented that pathway specificity, emphasising the complex balance between local and global plasticity to maintain the total synaptic weight.

8.4.1 Changes proportional to the activity disruption

In pathological conditions, the response of the system seems to parallel the severity of the disruption. The results from the deafferentation experiments showed that dendritic spine head diameters increased predominantly in the region previously receiving input from the Schaffer collaterals. Moreover, the increase in spine head size seemed to be proportional to the loss of spine density, thus partially balancing the total synaptic weight of the neurone. Those results could suggest that larger spines, which are considered more stable (Kasai et al., 2010), are maintained while the weakest synapses are eliminated. This phenomenon was observed *in vitro*, where selective loss of synapses with small PSDs followed AMPA receptor blockade (Mateos et al., 2007). Similarly, *in vivo*, dark rearing of mice was found to decrease spine density but to increase in parallel the proportion of larger spines, thus preserving the total synaptic area per unit length of dendrite (Wallace and Bear, 2004).

When the activity blockade is persistent, different homeostatic mechanisms can compensate, thus reducing the effect of activity deprivation on synaptic transmission (Burrone et al., 2002; Zhu and Malinow, 2002). Interestingly, synaptic scaling, a mechanism compensating for chronic activity blockade and originally considered to be global (Turrigiano et al., 1998), has recently been shown recently to occur similarly at

single synapses (Hou et al., 2008). Considering recent findings emphasising the role of dendritic branches as the fundamental unit of plasticity (Govindarajan et al., 2011), it can be hypothesised that the same is true of homeostatic plasticity, and that changes observed globally with mEPSCs or synapse-specifically with two photon imaging, are in fact two sides of the same phenomenon, regulated at the branch level (see 7.5.4).

8.4.2 Balance between activity-dependent and homeostatic changes

Activity-dependent plasticity is a major driver of network properties. The most active afferent pathway on CA1 neurones was found to impinge on larger spines, whether it is the entorhinal cortex *in vivo* (Megias et al., 2001; Nicholson et al., 2006) or the Schaffer collateral in organotypic slices (De Simoni and Edwards, 2006). Local increase in spine head size, specifically located in the apical dendrites, was also found to occur *in vivo* following learning in the Morris Water Maze (Beltran-Campos et al., 2011). In the present study, proximal apical dendrites of CA1 pyramidal neurones, which receive mainly input from the Schaffer collaterals, were found to have significantly larger spines than basal dendrites. Previous experiments in the lab found that the entorhinal cortex in organotypic slices impinged on smaller spines, thus suggesting a homeostatic mechanism regulating dendritic spine size in a pathway specific manner.

Blocking CaMKII for 7 days on organotypic slices abolished the pathway specificity observed, and apical and basal spine head size distributions became indistinguishable. CaMKII is necessary for the induction of LTP and the consequent synaptic enlargement (Pettit et al., 1994; Hayashi et al., 2000; Matsuzaki et al., 2004), but also for homeostatic changes, since changes in mEPSCs amplitude and frequency produced by blockade of AMPA receptors are prevented by CaMKII inhibition (Thiagarajan et al., 2002). However, CaMKII inhibition with a dominant negative form of CaMKII failed to affect TTX-induced synaptic scaling (Ibata et al., 2008). Blocking CaMKII resulted in a conjoint block of activity-dependent and homeostatic changes, which evened dendritic spine size across the dendritic tree. Similar balance between activity-dependent and homeostatic changes have been observed in the visual cortex, the bidirectional response to eyesight deprivation/open-eye input preserved the net sensory drive of

individual neurones, indicating overall response homeostasis (Mrsic-Flogel et al., 2007).

The interpretation of the results has to be placed in a larger context, remembering that several additional factors could contribute to the experimental findings. The most important factors are discussed below.

8.5 Broader picture of synaptic plasticity

Studying plasticity by imaging dendritic spines represents a different approach to mEPSCs recordings, which cannot give information about the localisation of the synaptic changes or the morphological transformations of spines. This approach, however, does not give a full picture of the mechanisms involved in plasticity, as it focuses on postsynaptic modifications, and it is worth mentioning a few of the other components which can also contribute to the result observed in the experiments presented in this work. However, from this postsynaptic approach, some interesting findings have been observed, showing the fundamental role played by local plasticity towards the maintenance of global functionality, setting an intermediary state between global and input-specific plasticity.

8.5.1 Presynaptic changes

Insertion and removal of AMPA receptors, though a fundamental hallmark of activity-dependent plasticity in the hippocampus (reviewed in Kerchner and Nicoll, 2008), is not the only characteristic of synaptic changes. Many publications have emphasised the role for a presynaptic site for LTP (Emptage et al., 2003; reviewed in Lisman, 2009). In dissociated cultures from the visual cortex, no presynaptic effects are observed before 3 weeks (Wierenga et al., 2005), but it may not necessarily be the case in the hippocampus, where several papers report presynaptic changes following chronic activity modification in dissociated cultures from 9-17 DIV (Branco et al., 2008; Zhao et al., 2011).

PKA and CaMKII are both present in the presynaptic terminals. PKA was found to modify presynaptic release probability at mossy fibre synapses (Weisskopf et al., 1994; Salin et al., 1996). CaMKII was also found to regulate a presynaptic form of LTP in dissociated hippocampal cultures (Ninan and Arancio, 2004).

Presynaptic changes, though detectable with mEPSCs recordings, would not be detected by the imaging studies, and could account for the differences in or the absence of synaptic modifications observed after deafferentation of blockade of plasticity with CaMKII or PKA inhibitors.

8.5.2 Interneurones and glial cells

Homeostatic plasticity also involves other types of cells participating in synaptic transmission such as interneurones and glial cells. For instance, the release of tumour necrosis factor alpha by glial cells was found to be necessary for synaptic scaling in hippocampal cultures (Stellwagen and Malenka, 2006). Interneurones, which are present in the hippocampus in different locations under various forms and densities (Freund and Buzsáki, 1996), play a fundamental role in the regulation of network excitability (Turrigiano and Nelson, 2004), and like excitatory synapses, can express plasticity (Kullmann and Lamsa, 2007). Interneurones can also show some forms of homeostatic plasticity (Rutherford et al., 1997), decreasing the number of $GABA_A$ receptors gathered at synapses in the neocortex (Kilman et al., 2002), or by the insertion of sodium channels and the removal of potassium channels in the chick spinal cord (reviewed in Blankenship and Feller, 2010).

Interneurones do not express αCaMKII (Sik et al., 1998), but some forms of CaMKII-dependent synaptic plasticity can be observed, probably relying on βCaMKII (Lamsa et al., 2007). If strong activation of the synapses induces translocation of αCaMKII to excitatory synapses (Zhang et al., 2008), weaker stimulus lead to their translocation specifically to the postsynaptic site of inhibitory synapses in pyramidal neurones (Marsden et al., 2010). Thus CaMKII inhibition will also impact on inhibitory synapses. Moreover, like CA1 pyramidal neurones, interneurones in the CA1 region show

synapse-specific plasticity (Croce et al., 2010), suggesting that changes in the network such as deafferentation will affect interneurones activity in a pathway-specific manner, and could account for some of the differences between early and late transection.

8.5.3 PKA and CaMKII have multiple functions

At the intermediate age between the PKA-dependent (Yasuda et al., 2003) and CaMKII-dependent induction of LTP (Hayashi et al., 2000), both PKA and CaMKII cascades may be complementary for LTP induction. In acute hippocampal slices (P14-16), CaMKII-dependent induction of LTP was found to be paralleled by two other cascades involving PKA or PKC (Wikström et al., 2003). In the barrel cortex of adult mouse, a PKA-dependent LTP coexists with a CaMKII-dependent LTP (Hardingham et al., 2008), showing that PKA and CaMKII cascades can work in parallel to induce LTP in both developing and adult neurones. Moreover, when considering the implication of PKA for protein-synthesis dependent LTP, several cascades have emerged as potential candidates for plasticity related proteins, which could compensate for PKA inhibition. To cite just a few: tyrosine kinase B (Minichiello, 2009), mitogen-activate protein kinase (MAPK) (Sajikumar et al., 2005), protein kinase Mξ and BDNF (Sajikumar and Korte, 2011). CREB, the main downstream substrate of PKA for translational LTP can also be phosphorylated by other kinases such as MAPK or CaMKIV (Wu et al., 2001).

Another point to consider when interpreting results from CaMKII experiments is the fact that KN62, though originally thought to specifically inhibit CaMKII (Tokumitsu et al., 1990), also inhibits CaMKIV (Enslen et al., 1994). Recently, CaMKIV has been demonstrated to be involved in homeostatic plasticity, driving depression in optogenetically silenced neurones (Goold and Nicoll, 2010), or following global TTX-induced synaptic scaling (Ibata et al., 2008). Thus, blockade of CaMKIV with KN62 could have affected homeostatic plasticity, and be partly responsible for the absence of difference in the spine head size distribution between apical and basal dendrites following incubation with KN62.

8.5.4 The dendritic branch as preferential unit for plasticity

The simplest interpretation of the work presented here is that synaptic plasticity occurred at specific location, regulated by the activity of incoming axons at some synapses and homeostatic regulations at others. This distribution of synaptic changes is consistent with the model developed in recent years, where the dendritic branch is the intermediate functional unit for plasticity, whether activity-dependent (Mehta, 2004; Govindarajan et al., 2006) or homeostatic (Rabinowitch and Segev, 2008; Yu and Goda, 2009).

The hypothesis developed from the observation of local interactions between neighbouring synapses on the same branch. For instance, the induction of LTP at a single synapse was found to induce potentiation in neighbouring synapses (Engert and Bonhoeffer, 1997), by decreasing the threshold for LTP-induction at neighbouring synapses on the same dendrite (Harvey and Svoboda, 2007). Molecules involved in plasticity also propagate along the dendritic branch of stimulated synapses, as has been observed with CaMKII (Rose et al., 2009). According to the model of clustered plasticity developed by Tonegawa and colleagues, the cooperativity and associativity of L-LTP and L-LTD favours the formation of long-term memory engrams (Govindarajan et al., 2006). In this model, confirmed in their latest experimental paper (Govindarajan et al., 2011), synaptic tagging and capture of plasticity-related proteins is enhanced on individual dendritic branches instead of being dispersed throughout the dendritic tree.

In control conditions in my cultures, the population of dendritic spines had larger heads in proximal apical than in basal dendrites. The competition for newly-synthesised proteins and the facilitated tagging of spines in more activated branches could explain the pathway specificity observed in control organotypic slices. Specific investigation of clustering has not been carried out in my work, but could be of special interest in the perspective of the branch hypothesis.

Homeostatic changes have also been found to be regulated within specific dendritic subcompartments. Experimental studies found that the local block of activity increases

AMPA currents, accompanied by local dendritic protein synthesis (Sutton et al., 2006). Release probability of excitatory neurotransmitter was also homeostatically regulated by a local increase in activity, maintaining similar release probability at synapses on the same dendritic branch (Branco et al., 2008).

The hypothesis that local dendritic activity orchestrates synaptic plasticity was also proposed as a solution unifying maintenance of activity-dependent changes during homeostatic plasticity. In this model, the potentiation of one synapse induces tagging and potentiation of neighbouring synapses on the same branch. Reciprocally, homeostatic synaptic plasticity, occurring locally to compensate for the synaptic strengthening, also affects neighbouring synapses, thus preserving the activity-induced pattern. This model thus preserves learning-induced changes while maintaining neuronal output by homeostatic feedback mechanisms.

The result from the experiments presented here suggests another hypothesis combining local and global plasticity phenomena, which would also preserve activity-induced modification while maintaining the global synaptic output. In the proposed model (figure 8-1), CaMKII is involved in the establishment of the pathway specific pattern observed in CA1 pyramidal cells, where proximal apical dendrites have on average larger head size than basal. This local activity-dependent plasticity induces a feed-forward loop through CA1-CA1 connections in the basal dendrites, where soluble PKA type I is activated. PKA can then translocate to the nucleus to activate the synthesis of plasticity-related proteins, possibly including some phosphatases, which would then be translocated to both apical and basal dendrites where they can compensate for the global increase in synaptic output.

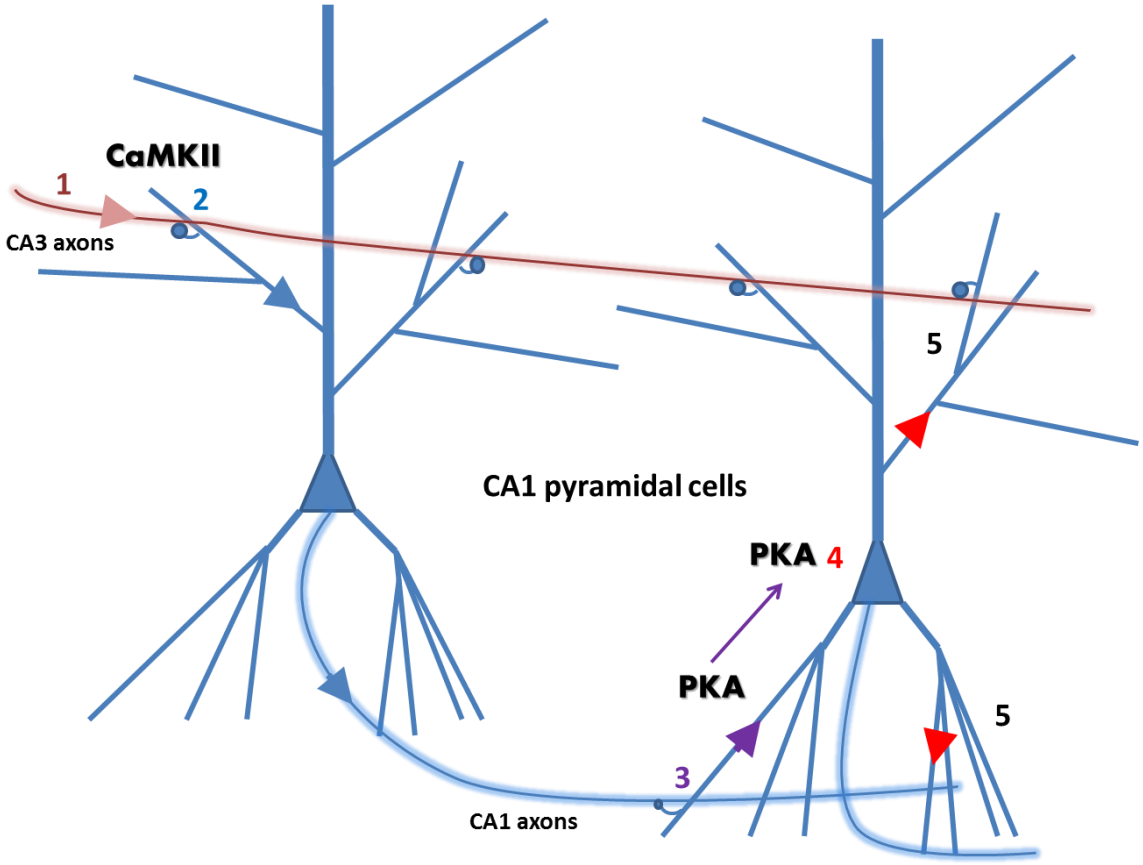

Figure 8-1: Schematic representation of the putative role of local and global plasticity, regulating synapses in both activity-dependent and homeostatic manners.

1) Activity of the Schaffer collateral in organotypic slices induces 2) a CaMKII-dependent enlargement of spine heads in the proximal apical dendrites. 3) Activity from CA3 neurones increases the output of CA1 cells, and thereby activates CA1-CA1 synapses in the basal dendrites. 4) Activated PKA type I, which is soluble, translocate to the nucleus, where it activates the transcription of protein involved in homeostatic regulations. 5) Those newly synthesised proteins diffuse to both apical and basal dendrites, globally reducing spine head size.

8.5.5 Implications for learning and disabilities

Homeostatic plasticity is a fundamental mechanism necessary for maintaining neuronal function within physiological limits. Throughout their lives, neurones have to efficiently transmit activity, modify synapses to retain specific information while controlling their overall excitability. The ability of the neuronal network to maintain a functional set point is particularly crucial during development, when the network is rapidly expanding and consequently the balance of excitation and inhibition has to be

adjusted constantly. The loss of homeostatic regulation may result in neurological diseases such as epilepsy, schizophrenia or mental retardation (Ramocki and Zoghbi, 2008; Chakravarthy et al., 2009). Abnormal regulation of a few genes and key proteins is sufficient to induce significant changes in the density and shape of dendritic spines, thereby altering synaptic transmission and possibly leading to neuropsychiatric phenotypes. A better understanding of dendritic spine plasticity and homeostatic regulation mechanisms could help to develop new therapeutic strategies to reduce the abnormal alterations of dendritic spines. For instance, it would be possible to prevent the known spine loss and following decline in cognitive functions associated with pathologies such as Down's syndrome or Alzheimer's disease, or following seizures (Ferrer and Gullotta, 1990; Knobloch and Mansuy, 2008).

8.6 Perspectives

In summary, my results show that activity-dependent and compensatory homeostatic changes operate in parallel in CA1 pyramidal neurones from developing organotypic slices, and can be abolished by inhibition of synaptic plasticity with an antagonist of CaMKII. The compensatory changes observed following CaMKII inhibition and deafferentation globally preserve the postsynaptic weight of individual neurones. Those changes can be presumed to maintain the stability of individual neurones and, by extension, of the network (Marder and Goaillard, 2006), furthermore preserving the ability to detect incoming information and to lay down new memories (Abraham, 2008). Another fundamental characteristic that emerges from these experiments is the age-dependence of plastic properties, emphasising the role of events happening during development on the setting of the basis of future learning potential.

The results also suggest that homeostasis may occur at many levels ranging from at least the level of individual pathways to scaling across the whole cell. The present study showed that intervention at the level of a single pathway by deafferentation or by influencing the capability of plasticity, thus affecting principally the most active

pathway, can cause more localised changes. The resulting homeostatic regulation of synaptic strength at a more local level is likely to be highly relevant for hippocampal function: it seems more physiological than global scaling in response to drastic up or down regulation of activity across the whole network, which probably rarely happens *in vivo* except in pathological cases such as epilepsy; it would also be more beneficial than input specific changes, which would lose the information previously encoded at single synapses. In that perspective, future investigations of local activity-dependent and homeostatic plasticity, such as clustering of larger spines, would bring insight into one of the fundamental mechanisms that maintains neuronal functionality throughout life.

List of References

Abel,T., and Nguyen,P.V. (2008). Regulation of hippocampus-dependent memory by cyclic AMP-dependent protein kinase. Prog. Brain Res. *169*, 97-115.

Abel,T., Nguyen,P.V., Barad,M., Deuel,T.A., Kandel,E.R., and Bourtchouladze,R. (1997). Genetic demonstration of a role for PKA in the late phase of LTP and in hippocampus-based long-term memory. Cell *88*, 615-626.

Abraham,W.C. (2008). Metaplasticity: tuning synapses and networks for plasticity. Nat. Rev. Neurosci. *9*, 387.

Abraham,W.C., and Williams,J.M. (2003). Properties and mechanisms of LTP maintenance. Neuroscientist. *9*, 463-474.

Abramowitz,M., and Davidson,M.W. Numerical Aperture and Resolution. Olympus Corporation. 2010. Online Source

Ahmed,T., and Frey,J.U. (2005). Plasticity-specific phosphorylation of CaMKII, MAP-kinases and CREB during late-LTP in rat hippocampal slices in vitro. Neuropharmacol. *49*, 477-492.

Ahmed,T., and Frey,J.U. (2005). Plasticity-specific phosphorylation of CaMKII, MAP-kinases and CREB during late-LTP in rat hippocampal slices in vitro. Neuropharmacol. 49, 477-492.

Andersen,P., Morris,R., Amaral,D., Bliss,T., and O'Keefe,J. (2007*). The hippocampus Book.* Oxford University Press, 1st Edition.

Andreasen,M., Lambert,J.D., and Jensen,M.S. (1989). Effects of new non-N-methyl-D-aspartate antagonists on synaptic transmission in the in vitro rat hippocampus. J. Physiol *414*, 317-336.

Andrásfalvy,B.K., and Magee,J.C. (2001). Distance-dependent increase in AMPA receptor number in the dendrites of adult hippocampal CA1 pyramidal neurons. J. Neurosci. *21*, 9151-9159.

Aniksztejn,L., Demarque,M., Morozov,Y., Ben Ari,Y., and Represa,A. (2001). Recurrent CA1 collateral axons in developing rat hippocampus. Brain Res. *913*, 195-200.

Aptowicz,C.O., Kunkler,P.E., and Kraig,R.P. (2004). Homeostatic plasticity in hippocampal slice cultures involves changes in voltage-gated Na^+ channel expression. Brain Res. *998*, 155-163.

Arellano,J.I., Benavides-Piccione,R., DeFelipe,J., and Yuste,R. (2007a). Ultrastructure of dendritic spines: correlation between synaptic and spine morphologies. Front Neurosci. *1*, 131-143.

Arellano,J.I., Espinosa,A., Fairen,A., Yuste,R., and DeFelipe,J. (2007b). Non-synaptic dendritic spines in neocortex. Neurosci. *145*, 464-469.

Ashby,M.C., Maier,S.R., Nishimune,A., and Henley,J.M. (2006). Lateral diffusion drives constitutive exchange of AMPA receptors at dendritic spines and is regulated by spine morphology. J. Neurosci. *26*, 7046-7055.

Bach,M.E., Barad,M., Son,H., Zhuo,M., Lu,Y.F., Shih,R., Mansuy,I., Hawkins,R.D., and Kandel,E.R. (1999). Age-related defects in spatial memory are correlated with defects in the late phase of hippocampal long-term potentiation in vitro and are attenuated by drugs that enhance the cAMP signaling pathway. Proc. Natl. Acad. Sci. U. S. A *96*, 5280-5285.

Bacskai,B.J., Hochner,B., Mahaut-Smith,M., Adams,S.R., Kaang,B.-K., Kandel,E.R., and Tsien,R.Y. (1993). Spatially resolved dynamics of cAMP and protein kinase A subunits in Aplysia sensory neurons. Science *260*, 222-226.

Bannister,N.J., and Larkman,A.U. (1995). Dendritic morphology of CA1 pyramidal neurones from the rat hippocampus: I. Branching patterns. J. Comp Neurol. *360*, 150-160.

Barria,A., and Malinow,R. (2002). Subunit-specific NMDA receptor trafficking to synapses. Neuron *35*, 345-353.

Barria,A., and Malinow,R. (2005). NMDA receptor subunit composition controls synaptic plasticity by regulating binding to CaMKII. Neuron *48*, 289-301.

Baude,A., Nusser,Z., Molnár,E., McIlhinney,R.A.J., and Somogyi,P. (1995). High resolution immunogold localization of AMPA type glutamate receptor subunits at synaptic and non-synaptic sites in rat hippocampus. Neurosci. *69*, 1031-1055.

Bear,M.F. (2003). Bidirectional synaptic plasticity: from theory to reality. Philos. Trans. R. Soc. Lond B Biol. Sci. *358*, 649-655.

Bear,M.F., and Abraham,W.C. (1996). Long-term depression in hippocampus. Annu. Rev. Neurosci. *19*, 437-462.

Beattie,E.C., Carroll,R.C., Yu,X., Morishita,W., Yasuda,H., Von Zastrow,M., and Malenka,R.C. (2000). Regulation of AMPA receptor endocytosis by a signaling mechanism shared with LTD. Nat. Neurosci. *3*, 1291-1300.

Becker,N., Wierenga,C.J., Fonseca,R., Bonhoeffer,T., and Nagerl,U.V. (2008). LTD induction causes morphological changes of presynaptic boutons and reduces their contacts with spines. Neuron *60*, 590-597.

Beique,J.C., Lin,D.T., Kang,M.G., Aizawa,H., Takamiya,K., and Huganir,R.L. (2006). Synapse-specific regulation of AMPA receptor function by PSD-95. Proc. Natl. Acad. Sci. U. S. A *103*, 19535-19540.

Bellone,C., and Nicoll,R.A. (2007). Rapid bidirectional switching of synaptic NMDA receptors. Neuron *55*, 779-785.

Beltran-Campos,V., Prado-Alcala,R.A., Leon-Jacinto,U., Aguilar-Vazquez,A., Quirarte,G.L., Ramirez-Amaya,V., and Diaz-Cintra,S. (2011). Increase of mushroom spine density in CA1 apical dendrites produced by water maze training is prevented by ovariectomy. Brain Res. *1369*, 119-130.

Ben-Ari,Y. (2002). Excitatory actions of gaba during development: the nature of the nurture. Nat. Rev. Neurosci. *3*, 728-739.

Ben-Ari,Y., Gaiarsa,J.L., Tyzio,R., and Khazipov,R. (2007). GABA: a pioneer transmitter that excites immature neurons and generates primitive oscillations. Physiol Rev. *87*, 1215-1284.

Benavides-Piccione,R., Ballesteros-Yanez,I., DeFelipe,J., and Yuste,R. (2002). Cortical area and species differences in dendritic spine morphology. J. Neurocytol. *31*, 337-346.

Bienenstock,E.L., Cooper,L.N., and Munro,P.W. (1982). Theory for the development of neuron selectivity: orientation specificity and binocular interaction in visual cortex. J. Neurosci. *2*, 32-48.

Biess,A., Korkotian,E., and Holcman,D. (2007). Diffusion in a dendritic spine: the role of geometry. Phys. Rev. E. Stat. Nonlin. Soft. Matter Phys. *76*, 021922.

Blackstad,T.W. (1958). On the termination of some afferents to the hippocampus and fascia dentata; an experimental study in the rat. Acta Anat. (Basel) *35*, 202-214.

Blaesse,P., Airaksinen,M.S., Rivera,C., and Kaila,K. (2009). Cation-chloride cotransporters and neuronal function. Neuron *61*, 820-838.

Blankenship,A.G., and Feller,M.B. (2010). Mechanisms underlying spontaneous patterned activity in developing neural circuits. Nat. Rev. Neurosci. *11*, 18-29.

Bliss,T.V., and Collingridge,G.L. (1993). A synaptic model of memory: long-term potentiation in the hippocampus. Nature *361*, 31-39.

Bloodgood,B.L., and Sabatini,B.L. (2005). Neuronal activity regulates diffusion across the neck of dendritic spines. Science *310*, 866-869.

Bloodgood,B.L., and Sabatini,B.L. (2007). Ca(2+) signaling in dendritic spines. Curr. Opin. Neurobiol. *17*, 345-351.

Boehm,J., Kang,M.G., Johnson,R.C., Esteban,J., Huganir,R.L., and Malinow,R. (2006). Synaptic incorporation of AMPA receptors during LTP is controlled by a PKC phosphorylation site on GluR1. Neuron *51*, 213-225.

Bourne,J., and Harris,K.M. (2007). Do thin spines learn to be mushroom spines that remember? Curr. Opin. Neurobiol. *17*, 381-386.

Bourne,J.N., and Harris,K.M. (2008). Balancing structure and function at hippocampal dendritic spines. Annu. Rev. Neurosci. *31*, 47-67.

Bourne,J.N., and Harris,K.M. (2010). Coordination of size and number of excitatory and inhibitory synapses results in a balanced structural plasticity along mature hippocampal CA1 dendrites during LTP. Hippocampus.

Bourne,J.N., Kirov,S.A., Sorra,K.E., and Harris,K.M. (2007). Warmer preparation of hippocampal slices prevents synapse proliferation that might obscure LTP-related structural plasticity. Neuropharmacol. *52*, 55-59.

Bradshaw,K.D., Emptage,N.J., and Bliss,T.V.P. (2003). A role for dendritic protein synthesis in hippocampal late LTP. Eur. J. Neurosci. *18*, 3150-3152.

Branco,T., Staras,K., Darcy,K.J., and Goda,Y. (2008). Local dendritic activity sets release probability at hippocampal synapses. Neuron *59*, 475-485.

Braun,A.P., and Schulman,H. (1995). The multifunctional calcium/calmodulin-dependent protein kinase: from form to function. Annu. Rev. Physiol *57*, 417-445.

Buchs,P.A., and Muller,D. (1996). Induction of long-term potentiation is associated with major ultrastructural changes of activated synapses. Proc. Natl. Acad. Sci. USA *93*, 8040-8045.

Burgin,K.E., Waxham,M.N., Rickling,S., Westgate,S.A., Mobley,W.C., and Kelly,P.T. (1990). In situ hybridization histochemistry of Ca2+/calmodulin-dependent protein kinase in developing rat brain. J. Neurosci. *10*, 1788-1798.

Burrone,J., O'Byrne,M., and Murthy,V.N. (2002). Multiple forms of synaptic plasticity triggered by selective suppression of activity in individual neurons. Nature *420*, 414-418.

Carroll,R.C., Lissin,D.V., Von Zastrow,M., Nicoll,R.A., and Malenka,R.C. (1999). Rapid redistribution of glutamate receptors contributes to long-term depression in hippocampal cultures. Nat. Neurosci. *2*, 454-460.

Chakravarthy,N., Tsakalis,K., Sabesan,S., and Iasemidis,L. (2009). Homeostasis of brain dynamics in epilepsy: a feedback control systems perspective of seizures. Ann. Biomed. Eng *37*, 565-585.

Chavis,P., and Westbrook,G. (2001). Integrins mediate functional pre- and postsynaptic maturation at a hippocampal synapse. Nature *411*, 317-321.

Cheng,D., Hoogenraad,C.C., Rush,J., Ramm,E., Schlager,M.A., Duong,D.M., Xu,P., Wijayawardana,S.R., Hanfelt,J., Nakagawa,T., Sheng,M., and Peng,J. (2006). Relative and absolute quantification of postsynaptic density proteome isolated from rat forebrain and cerebellum. Mol. Cell Proteomics. *5*, 1158-1170.

Cingolani,L.A., and Goda,Y. (2008). Differential involvement of beta3 integrin in pre- and postsynaptic forms of adaptation to chronic activity deprivation. Neuron Glia Biol. *4*, 179-187.

Claxton,N.S., Fellers,T.J., and Davidson,N. (2004). Laser Scanning Confocal Microscopy. Olympus Corporation and Department of Optical Microscopy and Digital Imaging, Florida State University. Olympus. Online Source

Clem,R.L., and Barth,A. (2006). Pathway-specific trafficking of native AMPARs by in vivo experience. Neuron *49*, 663-670.

Colbran,R.J. (2004). Targeting of calcium/calmodulin-dependent protein kinase II. Biochem. J. *378*, 1-16.

Collin,C., Miyaguchi,K., and Segal,M. (1997). Dendritic spine density and LTP induction in cultured hippocampal slices. J. Neurophysiol. *77*, 1614-1623.

Comery,T.A., Harris,J.B., Willems,P.J., Oostra,B.A., Irwin,S.A., Weiler,I.J., and Greenough,W.T. (1997). Abnormal dendritic spines in fragile X knockout mice: Maturation and pruning deficits. Proc. Natl. Acad. Sci. USA *94*, 5401-5404.

Cooke,S.F., and Bliss,T.V. (2006). Plasticity in the human central nervous system. Brain *129*, 1659-1673.

Cracco,J.B., Serrano,P., Moskowitz,S.I., Bergold,P.J., and Sacktor,T.C. (2005). Protein synthesis-dependent LTP in isolated dendrites of CA1 pyramidal cells. Hippocampus *15*, 551-556.

Croce,A., Pelletier,J.G., Tartas,M., and Lacaille,J.C. (2010). Afferent-specific properties of interneuron synapses underlie selective long-term regulation of feedback inhibitory circuits in CA1 hippocampus. J. Physiol *588*, 2091-2107.

Crump,F.T., Dillman,K.S., and Craig,A.M. (2001). cAMP-dependent protein kinase mediates activity-regulated synaptic targeting of NMDA receptors. J. Neurosci. *21*, 5079-5088.

Cruz-Martin,A., Crespo,M., and Portera-Cailliau,C. (2010). Delayed stabilization of dendritic spines in fragile X mice. J. Neurosci. *30*, 7793-7803.

Cull-Candy,S., Brickley,S., and Farrant,M. (2001). NMDA receptor subunits: diversity, development and disease. Curr. Opin. Neurobiol. 11, 327-335.

De Simoni,A., and Edwards,F.A. (2006). Pathway specificity of dendritic spine morphology in identified synapses onto rat hippocampal CA1 neurons in organotypic slices. Hippocampus *16*, 1111-1124.

De Simoni,A., Griesinger,C.B., and Edwards,F.A. (2003). Development of rat CA1 neurones in acute versus organotypic slices: role of experience in synaptic morphology and activity. J. Physiol *550*, 135-147.

Deisseroth,K., Bito,H., and Tsien,R.W. (1996). Signaling from synapse to nucleus: Postsynaptic CREB phosphorylation during multiple forms of hippocampal synaptic plasticity. Neuron *16*, 89-101.

Desai,N.S., Cudmore,R.H., Nelson,S.B., and Turrigiano,G.G. (2002). Critical periods for experience-dependent synaptic scaling in visual cortex. Nat. Neurosci. *5*, 783-789.

Deuchars,J., and Thomson,A.M. (1996). CA1 pyramid-pyramid connections in rat hippocampus in vitro: dual intracellular recordings with biocytin filling. Neurosci. *74*, 1009-1018.

Dhanrajan,T.M., Lynch,M.A., Kelly,A., Popov,V.I., Rusakov,D.A., and Stewart,M.G. (2004). Expression of long-term potentiation in aged rats involves perforated synapses but dendritic spine branching results from high-frequency stimulation alone. Hippocampus *14*, 255-264.

Dudek,S.M., and Bear,M.F. (1992). Homosynaptic long-term depression in area CA1 of hippocampus and effects of N-methyl-D-aspartate receptor blockade. Proc. Natl. Acad. Sci. USA *89*, 4363-4367.

Dudek,S.M., and Bear,M.F. (1993). Bidirectional long-term modification of synaptic effectiveness in the adult and immature hippocampus. J. Neurosci. *13*, 2910-2918.

Echegoyen,J., Neu,A., Graber,K.D., and Soltesz,I. (2007). Homeostatic plasticity studied using in vivo hippocampal activity-blockade: synaptic scaling, intrinsic plasticity and age-dependence. PLoS. ONE. *2*, e700.

Edwards,F.A. (1995). Anatomy and electrophysiology of fast central synapses lead to a structural model for long-term potentiation. Physiol. Rev. *75*, 759-787.

Edwards,F.A., Konnerth,A., Sakmann,B., and Takahashi,T. (1989). A thin slice preparation for patch clamp recordings from neurones of the mammalian central nervous system. Pflugers Arch. *414*, 600-612.

Elger,C.E., Helmstaedter,C., and Kurthen,M. (2004). Chronic epilepsy and cognition. Lancet Neurol. *3*, 663-672.

Emptage,N., Bliss,T.V.P., and Fine,A. (1999). Single synaptic events evoke NMDA receptor-mediated release of calcium from internal stores in hippocampal dendritic spines. Neuron *22*, 115-124.

Emptage,N.J., Reid,C.A., and Fine,A. (2001). Calcium stores in hippocampal synaptic boutons mediate short-term plasticity, store-operated Ca^{2+} entry, and spontaneous transmitter release. Neuron *29*, 197-208.

Emptage,N.J., Reid,C.A., Fine,A., and Bliss,T.V.P. (2003). Optical quantal analysis reveals a presynaptic component of LTP at hippocampal Schaffer-associational synapses. Neuron *38*, 797-804.

Engert,F., and Bonhoeffer,T. (1997). Synapse specificity of long-term potentiation breaks down at short distances. Nature *388*, 279-284.

Engert,F., and Bonhoeffer,T. (1999). Dendritic spine changes associated with hippocampal long-term synaptic plasticity. Nature *399*, 66-70.

Enoki,R., Hu,Y.L., Hamilton,D., and Fine,A. (2009). Expression of long-term plasticity at individual synapses in hippocampus is graded, bidirectional, and mainly presynaptic: optical quantal analysis. Neuron *62*, 242-253.

Enslen,H., Sun,P., Brickey,D., Soderling,S.H., Klamo,E., and Soderling,T.R. (1994). Characterization of Ca2+/calmodulin-dependent protein kinase IV. Role in transcriptional regulation. J. Biol. Chem. *269*, 15520-15527.

Esteban,J.A., Shi,S.H., Wilson,C., Nuriya,M., Huganir,R.L., and Malinow,R. (2003). PKA phosphorylation of AMPA receptor subunits controls synaptic trafficking underlying plasticity. Nat. Neurosci. *6*, 136-143.

Etkin,A., Alarcon,J.M., Weisberg,S.P., Touzani,K., Huang,Y.Y., Nordheim,A., and Kandel,E.R. (2006). A role in learning for SRF: deletion in the adult forebrain disrupts LTD and the formation of an immediate memory of a novel context. Neuron 50, 127-143.

Fanselow,M.S., and Dong,H.W. (2010). Are the dorsal and ventral hippocampus functionally distinct structures? Neuron 65, 7-19.

Ferrer,I., and Gullotta,F. (1990). Down's syndrome and Alzheimer's disease: dendritic spine counts in the hippocampus. Acta Neuropathol. *79*, 680-685.

Fiala,J.C., Feinberg,M., Popov,V., and Harris,K.M. (1998). Synaptogenesis via dendritic filopodia in developing hippocampal area CA1. J. Neurosci. *18*, 8900-8911.

Fifkova,E., and Anderson,C.L. (1981). Stimulation-induced changes in dimensions of stalks of dendritic spines in the dentate molecular layer. Exp. Neurol. *74*, 621-627.

Finnerty,G.T., Roberts,L.S., and Connors,B.W. (1999). Sensory experience modifies the short-term dynamics of neocortical synapses. Nature *400*, 367-371.

Fischer,M., Kaech,S., Wagner,U., Brinkhaus,H., and Matus,A. (2000). Glutamate receptors regulate actin-based plasticity in dendritic spines. Nat. Neurosci. *3*, 887-894.

Förster,E., and Frotscher,M. (1995). Developmental upregulation of the neural cell adhesion molecule VASE exon in slice cultures of rat hippocampus. Neurosci. Lett. *199*, 167-170.

Freund,T.F., and Buzsáki,G. (1996). Interneurons of the hippocampus. Hippocampus *6*, 347-470.

Frotscher,M., and Heimrich,B. (1995). Lamina-specific synaptic connections of hippocampal neurons in vitro. J. Neurobiol. *26*, 350-359.

Furukawa,H., Singh,S.K., Mancusso,R., and Gouaux,E. (2005). Subunit arrangement and function in NMDA receptors. Nature *438*, 185-192.

Gahwiler,B.H., Capogna,M., Debanne,D., McKinney,R.A., and Thompson,S.M. (1997). Organotypic slice cultures: a technique has come of age. Trends Neurosci. *20*, 471-477.

Gainey,M.A., Hurvitz-Wolff,J.R., Lambo,M.E., and Turrigiano,G.G. (2009). Synaptic scaling requires the GluR2 subunit of the AMPA receptor. J. Neurosci. *29*, 6479-6489.

Ge,Y., Dong,Z., Bagot,R.C., Howland,J.G., Phillips,A.G., Wong,T.P., and Wang,Y.T. (2010). Hippocampal long-term depression is required for the consolidation of spatial memory. Proc. Natl. Acad. Sci. U. S. A *107*, 16697-16702.

Giese,K.P., Fedorov,N.B., Filipkowski,R.K., and Silva,A.J. (1998). Autophosphorylation at Thr^{286} of the α calcium-calmodulin kinase II in LTP and learning. Science *279*, 870-873.

Goda,Y., and Stevens,C.F. (1998). Readily releasable pool size changes associated with long term depression. Proc. Natl. Acad. Sci. U. S. A *95*, 1283-1288.

Godement,P., Vanselow,J., Thanos,S., and Bonhoeffer,F. (1987). A study in developing visual systems with a new method of staining neurones and their processes in fixed tissue. Development *101*, 697-713.

Goel,A., and Lee,H.K. (2007). Persistence of experience-induced homeostatic synaptic plasticity through adulthood in superficial layers of mouse visual cortex. J. Neurosci. *27*, 6692-6700.

Goldin,M., Segal,M., and Avignone,E. (2001). Functional plasticity triggers formation and pruning of dendritic spines in cultured hippocampal networks. J. Neurosci. *21*, 186-193.

Goold,C.P., and Nicoll,R.A. (2010). Single-cell optogenetic excitation drives homeostatic synaptic depression. Neuron *68*, 512-528.

Gottmann,K. (2008). Transsynaptic modulation of the synaptic vesicle cycle by cell-adhesion molecules. J. Neurosci. Res. *86*, 223-232.

Govindarajan,A., Israely,I., Huang,S.Y., and Tonegawa,S. (2011). The dendritic branch is the preferred integrative unit for protein synthesis-dependent LTP. Neuron *69*, 132-146.

Govindarajan,A., Kelleher,R.J., and Tonegawa,S. (2006). A clustered plasticity model of long-term memory engrams. Nat. Rev. Neurosci. *7*, 575-583.

Gray,E.G. (1959). Electron microscopy of synaptic contacts on dendrite spines of the cerebral cortex. Nature *183*, 1592-1593.

Gray,N.W., Weimer,R.M., Bureau,I., and Svoboda,K. (2006). Rapid redistribution of synaptic PSD-95 in the neocortex in vivo. PLoS. Biol. *4*, e370.

Hagiwara,M., Alberts,A., Brindle,P., Meinkoth,J., Feramisco,J., Deng,T., Karin,M., Shenolikar,S., and Montminy,M. (1992). Transcriptional attenuation following cAMP induction requires PP-1-mediated dephosphorylation of CREB. Cell *70*, 105-113.

Han,E.B., and Stevens,C.F. (2009). Development regulates a switch between post- and presynaptic strengthening in response to activity deprivation. Proc. Natl. Acad. Sci. U. S. A *106*, 10817-10822.

Hanson,P.I., Kapiloff,M.S., Lou,L.L., Rosenfeld,M.G., and Schulman,H. (1989). Expression of a multifunctional Ca2+/calmodulin-dependent protein kinase and mutational analysis of its autoregulation. Neuron *3*, 59-70.

Hardingham,N., Glazewski,S., Pakhotin,P., Mizuno,K., Chapman,P.F., Giese,K.P., and Fox,K. (2003). Neocortical long-term potentiation and experience-dependent synaptic plasticity require α-calcium/calmodulin-dependent protein kinase II autophosphorylation. J. Neurosci. *23*, 4428-4436.

Hardingham,N., Wright,N., Dachtler,J., and Fox,K. (2008). Sensory deprivation unmasks a PKA-dependent synaptic plasticity mechanism that operates in parallel with CaMKII. Neuron *60*, 861-874.

Harms,K.J., Rioult-Pedotti,M.S., Carter,D.R., and Dunaevsky,A. (2008). Transient spine expansion and learning-induced plasticity in layer 1 primary motor cortex. J. Neurosci. *28*, 5686-5690.

Harris,K.M., Jensen,F.E., and Tsao,B. (1992). Three-dimensional structure of dendritic spines and synapses in rat hippocampus (CA1) at postnatal day 15 and adult ages: Implications for the maturation of synaptic physiology and long- term potentiation. J. Neurosci. *12*, 2685-2705.

Harris,K.M., and Stevens,J.K. (1989). Dendritic spines of CA1 pyramidal cells in the rat hippocampus: Serial electron microscopy with reference to their biophysical characteristics. J. Neurosci. *9*, 2982-2997.

Harvey,C.D., and Svoboda,K. (2007). Locally dynamic synaptic learning rules in pyramidal neuron dendrites
4. Nature *450*, 1195-1200.

Hausser,M. (2001). Synaptic function: dendritic democracy. Curr. Biol. *11*, R10-R12.

Hayashi,Y., Shi,S.H., Esteban,J.A., Piccini,A., Poncer,J.C., and Malinow,R. (2000). Driving AMPA receptors into synapses by LTP and CaMKII: Requirement for GluR1 and PDZ domain interaction. Science *287*, 2262-2267.

Hebb,D.O. (1949). The organization of behavior (New York: Wiley).

Hering,H., and Sheng,M. (2001). Dendritic spines: Structure, dynamics and regulation. Nat. Rev. Neurosci. *2*, 880-888.

Hollmann,M., Hartley,M., and Heinemann,S. (1991). Ca2+ permeability of KA-AMPA--gated glutamate receptor channels depends on subunit composition. Science *252*, 851-853.

Hollmann,M., and Heinemann,S. (1994). Cloned glutamate receptors. Annu. Rev. Neurosci. *17*, 31-108.

Holopainen,I.E., and Lauren,H.B. (2003). Neuronal activity regulates GABAA receptor subunit expression in organotypic hippocampal slice cultures. Neurosci. *118*, 967-974.

Honkura,N., Matsuzaki,M., Noguchi,J., Ellis-Davies,G.C., and Kasai,H. (2008). The subspine organization of actin fibers regulates the structure and plasticity of dendritic spines. Neuron *57*, 719-729.

Hooks,B.M., and Chen,C. (2007). Critical periods in the visual system: changing views for a model of experience-dependent plasticity. Neuron *56*, 312-326.

Hotulainen,P., and Hoogenraad,C.C. (2010). Actin in dendritic spines: connecting dynamics to function. J. Cell Biol. *189*, 619-629.

Hou,Q., Zhang,D., Jarzylo,L., Huganir,R.L., and Man,H.Y. (2008). Homeostatic regulation of AMPA receptor expression at single hippocampal synapses. Proc. Natl. Acad. Sci. U. S. A *105*, 775-780.

Hsia,A.Y., Malenka,R.C., and Nicoll,R.A. (1998). Development of excitatory circuitry in the hippocampus. J. Neurophysiol. *79*, 2013-2024.

Hugel,S., Abegg,M., De,P., V, Caroni,P., Gahwiler,B.H., and McKinney,R.A. (2009). Dendritic spine morphology determines membrane-associated protein exchange between dendritic shafts and spine heads. Cereb. Cortex *19*, 697-702.

Ibata,K., Sun,Q., and Turrigiano,G.G. (2008). Rapid synaptic scaling induced by changes in postsynaptic firing. Neuron *57*, 819-826.

Irwin,S.A., Galvez,R., and Greenough,W.T. (2000). Dendritic spine structural anomalies in fragile-X mental retardation syndrome. Cerebral Cortex *10*, 1038-1044.

Isaac,J.T.R., Nicoll,R.A., and Malenka,R.C. (1995). Evidence for silent synapses: Implications for the expression of LTP. Neuron *15*, 427-434.

Isaacson,J.S., and Nicoll,R.A. (1993). The uptake inhibitor L-trans-PDC enhances responses to glutamate but fails to alter the kinetics of excitatory synaptic currents in the hippocampus. J. Neurophysiol. 70, 2187-2191.

Ishizuka,N., Cowan,W.M., and Amaral,D.G. (1995). A quantitative analysis of the dendritic organization of pyramidal cells in the rat hippocampus. J. Comp Neurol. *362*, 17-45.

Ishizuka,N., Weber,J., and Amaral,D.G. (1990). Organization of intrahippocampal projections originating from CA3 pyramidal cells in the rat. J. Comp Neurol. *295*, 580-623.

Ivenshitz,M., and Segal,M. (2010). Neuronal density determines network connectivity and spontaneous activity in cultured hippocampus. J. Neurophysiol.

Jaffe,D.B., and Carnevale,N.T. (1999). Passive normalization of synaptic integration influenced by dendritic architecture. J. Neurophysiol. *82*, 3268-3285.

Jakubs,K., Nanobashvili,A., Bonde,S., Ekdahl,C.T., Kokaia,Z., Kokaia,M., and Lindvall,O. (2006). Environment matters: synaptic properties of neurons born in the epileptic adult brain develop to reduce excitability. Neuron *52*, 1047-1059.

Jouvenceau,A., Hedou,G., Potier,B., Kollen,M., Dutar,P., and Mansuy,I.M. (2006). Partial inhibition of PP1 alters bidirectional synaptic plasticity in the hippocampus. Eur. J. Neurosci. *24*, 564-572.

Kandel,E.R. (2001). Neuroscience - The molecular biology of memory storage: A dialogue between genes and synapses. Science *294*, 1030-1038.

Kasai,H., Fukuda,M., Watanabe,S., Hayashi-Takagi,A., and Noguchi,J. (2010). Structural dynamics of dendritic spines in memory and cognition. Trends Neurosci. *33*, 121-129.

Kasai,H., Matsuzaki,M., Noguchi,J., Yasumatsu,N., and Nakahara,H. (2003). Structure-stability-function relationships of dendritic spines. Trends Neurosci. *26*, 360-368.

Kato,S., Sakatani,S., and Hirose,A. (2004). Influence of dendritic spine morphology on spatiotemporal change of calcium/calmoduline-dependent protein kinase density. Lecture Notes in Computer Science *3316*, 31-36.

Katz,B., and Miledi,R. (1967). The timing of calcium action during neuromuscular transmission. J. Physiol. *189*, 535-544.

Katz,L.C., and Shatz,C.J. (1996). Synaptic activity and the construction of cortical circuits. Science *274*, 1133-1138.

Kelleher,R.J., III, Govindarajan,A., and Tonegawa,S. (2004). Translational regulatory mechanisms in persistent forms of synaptic plasticity. Neuron *44*, 59-73.

Kemp,A., and Manahan-Vaughan,D. (2004). Hippocampal long-term depression and long-term potentiation encode different aspects of novelty acquisition. Proc. Natl. Acad. Sci. U. S. A *101*, 8192-8197.

Kemp,A., and Manahan-Vaughan,D. (2007). Hippocampal long-term depression: master or minion in declarative memory processes? Trends Neurosci. *30*, 111-118.

Kerchner,G.A., and Nicoll,R.A. (2008). Silent synapses and the emergence of a postsynaptic mechanism for LTP. Nat. Rev. Neurosci. *9*, 813-825.

Kessels,H.W., and Malinow,R. (2009). Synaptic AMPA receptor plasticity and behavior. Neuron *61*, 340-350.

Kilman,V., Van Rossum,M.C.W., and Turrigiano,G.G. (2002). Activity deprivation reduces miniature IPSC amplitude by decreasing the number of postsynaptic $GABA_A$ receptors clustered at neocortical synapses. J. Neurosci. *22*, 1328-1337.

Kim,J., and Tsien,R.W. (2008). Synapse-specific adaptations to inactivity in hippocampal circuits achieve homeostatic gain control while dampening network reverberation. Neuron *58*, 925-937.

Kirkwood,A., Silva,A., and Bear,M.F. (1997). Age-dependent decrease of synaptic plasticity in the neocortex of alphaCaMKII mutant mice. Proc. Natl. Acad. Sci. U. S. A *94*, 3380-3383.

Kirov,S.A., Goddard,C.A., and Harris,K.M. (2004). Age-dependence in the homeostatic upregulation of hippocampal dendritic spine number during blocked synaptic transmission. Neuropharmacol. *47*, 640-648.

Knafo,S., Alonso-Nanclares,L., Gonzalez-Soriano,J., Merino-Serrais,P., Fernaud-Espinosa,I., Ferrer,I., and DeFelipe,J. (2009). Widespread changes in dendritic spines in a model of Alzheimer's disease. Cereb. Cortex *19*, 586-592.

Knobloch,M., and Mansuy,I.M. (2008). Dendritic spine loss and synaptic alterations in Alzheimer's disease. Mol. Neurobiol. *37*, 73-82.

Kopec,C.D., Li,B., Wei,W., Boehm,J., and Malinow,R. (2006). Glutamate receptor exocytosis and spine enlargement during chemically induced long-term potentiation. J. Neurosci. *26*, 2000-2009.

Kopec,C.D., Real,E., Kessels,H.W., and Malinow,R. (2007). GluR1 links structural and functional plasticity at excitatory synapses. J. Neurosci. *27*, 13706-13718.

Korkotian,E., and Segal,M. (2001). Regulation of dendritic spine motility in cultured hippocampal neurons. J. Neurosci. *21*, 6115-6124.

Korkotian,E., and Segal,M. (2007). Morphological constraints on calcium dependent glutamate receptor trafficking into individual dendritic spine. Cell Calcium *42*, 41-57.

Kullmann,D.M. (1994). Amplitude fluctuations of dual-component EPSCs in hippocampal pyramidal cells: implications for long-term potentiation. Neuron *12*, 1111-1120.

Kullmann,D.M., and Lamsa,K.P. (2007). Long-term synaptic plasticity in hippocampal interneurons. Nat Rev. Neurosci. *8*, 687-699.

Lamsa,K.P., Heeroma,J.H., Somogyi,P., Rusakov,D.A., and Kullmann,D.M. (2007). Anti-Hebbian long-term potentiation in the hippocampal feedback inhibitory circuit. Science *315*, 1262-1266.

Landis,D.M.D., and Reese,T.S. (1983). Cytoplasmic organization in cerebellar dendritic spines. J. Cell Biol. *97*, 1169-1178.

Lee,H.K., Barbarosie,M., Kameyama,K., Bear,M.F., and Huganir,R.L. (2000). Regulation of distinct AMPA receptor phosphorylation sites during bidirectional synaptic plasticity. Nature *405*, 955-959.

Lee,K.J., Lee,Y., Rozeboom,A., Lee,J.Y., Udagawa,N., Hoe,H.S., and Pak,D.T. (2011). Requirement for Plk2 in orchestrated ras and rap signaling, homeostatic structural plasticity, and memory. Neuron *69*, 957-973.

Lee,M.C., Yasuda,R., and Ehlers,M.D. (2010). Metaplasticity at single glutamatergic synapses. Neuron *66*, 859-870.

Lee,S.J., Escobedo-Lozoya,Y., Szatmari,E.M., and Yasuda,R. (2009). Activation of CaMKII in single dendritic spines during long-term potentiation. Nature *458*, 299-304.

Lengyel,I., Voss,K., Cammarota,M., Bradshaw,K., Brent,V., Murphy,K.P., Giese,K.P., Rostas,J.A., and Bliss,T.V. (2004). Autonomous activity of CaMKII is only transiently increased following the induction of long-term potentiation in the rat hippocampus. Eur. J. Neurosci. *20*, 3063-3072.

Li,X.G., Somogyi,P., Ylinen,A., and Buzsaki,G. (1994). The hippocampal CA3 network: an in vivo intracellular labeling study. J. Comp Neurol. *339*, 181-208.

Liao,D., Hessler,N.A., and Malinow,R. (1995). Activation of postsynaptically silent synapses during pairing-induced LTP in CA1 region of hippocampal slice. Nature *375*, 400-404.

Lin,Y.C., and Redmond,L. (2008). CaMKIIbeta binding to stable F-actin in vivo regulates F-actin filament stability. Proc. Natl. Acad. Sci. U. S. A *105*, 15791-15796.

Lisman,J., Schulman,H., and Cline,H. (2002). The molecular basis of CaMKII function in synaptic and behavioural memory. Nat. Rev. Neurosci. *3*, 175-190.

Lisman,J.E. (2009). The pre/post LTP debate. Neuron *63*, 281-284.

Lledo,P.M., Hjelmstad,G.O., Mukherji,S., Soderling,T.R., Malenka,R.C., and Nicoll,R.A. (1995). Calcium calmodulin-dependent kinase II and long-term potentiation enhance synaptic transmission by the same mechanism. Proc. Natl. Acad. Sci. USA *92*, 11175-11179.

Lois,C., Hong,E.J., Pease,S., Brown,E.J., and Baltimore,D. (2002). Germline transmission and tissue-specific expression of transgenes delivered by lentiviral vectors. Science *295*, 868-872.

Lu,C., and Mattson,M.P. (2001). Dimethyl sulfoxide suppresses NMDA- and AMPA-induced ion currents and calcium influx and protects against excitotoxic death in hippocampal neurons. Exp. Neurol. *170*, 180-185.

Lynch,G., Larson,J., Kelso,S., Barrionuevo,G., and Schottler,F. (1983). Intracellular injections of EGTA block induction of hippocampal long-term potentiation. Nature *305*, 719-721.

Lynch,G., Rex,C.S., and Gall,C.M. (2007). LTP consolidation: substrates, explanatory power, and functional significance. Neuropharmacol. *52*, 12-23.

Magee,J.C., and Cook,E.P. (2000). Somatic EPSP amplitude is independent of synapse location in hippocampal pyramidal neurons. Nat. Neurosci. *3*, 895-903.

Majewska,A., Brown,E., Ross,J., and Yuste,R. (2000). Mechanisms of calcium decay kinetics in hippocampal spines: Role of spine calcium pumps and calcium diffusion through the spine neck in biochemical compartmentalization. J. Neurosci. *20*, 1722-1734.

Majewska,A., and Sur,M. (2003). Motility of dendritic spines in visual cortex in vivo: Changes during the critical period and effects of visual deprivation. Proc. Natl. Acad. Sci. USA *100*, 16024-16029.

Makino,H., and Malinow,R. (2009). AMPA receptor incorporation into synapses during LTP: the role of lateral movement and exocytosis. Neuron *64*, 381-390.

Malenka,R.C., and Bear,M.F. (2004). LTP and LTD; An Embarrassment of Riches. Neuron *44*, 5-21.

Malenka,R.C., Kauer,J.A., Perkel,D.J., Mauk,M.D., Kelly,P.T., Nicoll,R.A., and Waxham,M.N. (1989). An essential role for postsynaptic calmodulin and protein kinase activity in long-term potentiation. Nature *340*, 554-557.

Malenka,R.C., Lancaster,B., and Zucker,R.S. (1992). Temporal limits on the rise in postsynaptic calcium required for the induction of long-term potentiation. Neuron *9*, 121-128.

Malenka,R.C., and Nicoll,R.A. (1999). Long-term potentiation--a decade of progress? Science *285*, 1870-1874.

Malinow,R., Schulman,H., and Tsien,R.W. (1989). Inhibition of postsynaptic PKC or CaMKII blocks induction but not expression of LTP. Science *245*, 862-866.

Malinow,R., and Tsien,R.W. (1990). Presynaptic enhancement shown by whole-cell recordings of long- term potentiation in hippocampal slices. Nature *346*, 177-180.

Malinow,R., and Malenka,R.C. (2002). AMPA receptor trafficking and synaptic plasticity. Annu. Rev. Neurosci. *25*, 103-126.

Mammen,A.L., Kameyama,K., Roche,K.W., and Huganir,R.L. (1997). Phosphorylation of the alpha-amino-3-hydroxy-5-methylisoxazole4-propionic acid receptor GluR1 subunit by calcium/calmodulin-dependent kinase II. J. Biol. Chem. *272*, 32528-32533.

Man,H.Y., Sekine-Aizawa,Y., and Huganir,R.L. (2007). Regulation of α-amino-3-hydroxy-5-methyl-4-isoxazolepropionic acid receptor trafficking through PKA phosphorylation of the Glu receptor 1 subunit. Proc. Natl. Acad. Sci. U. S. A *104*, 3579-3584.

Manahan-Vaughan,D., and Braunewell,K.H. (1999). Novelty acquisition is associated with induction of hippocampal long-term depression. Proc. Natl. Acad. Sci. U. S. A *96*, 8739-8744.

Maravall,M., Koh,I.Y.Y., Lindquist,W.B., and Svoboda,K. (2004). Experience-dependent changes in basal dendritic branching of layer 2/3 pyramidal neurons during a critical period for developmental plasticity in rat barrel cortex. Cerebral Cortex *14*, 655-664.

Marder,E., and Goaillard,J.-M. (2006). Variability, compensation and homeostasis in neuron and network function. Nat. Rev. Neurosci. *7*, 563-574.

Marrs,G.S., Green,S.H., and Dailey,M.E. (2001). Rapid formation and remodeling of postsynaptic densities in developing dendrites. Nat. Neurosci. *4*, 1006-1013.

Marsden,K.C., Shemesh,A., Bayer,K.U., and Carroll,R.C. (2010). Selective translocation of Ca2+/calmodulin protein kinase IIalpha (CaMKIIalpha) to inhibitory synapses. Proc. Natl. Acad. Sci. U. S. A *107*, 20559-20564.

Martin,S.J., Grimwood,P.D., and Morris,R.G.M. (2000). Synaptic plasticity and memory: An evaluation of the hypothesis. Annu. Rev. Neurosci. *23*, 649-711.

Mateos,J.M., Luthi,A., Savic,N., Stierli,B., Streit,P., Gahwiler,B.H., and McKinney,R.A. (2007). Synaptic modifications at the CA3-CA1 synapse after chronic AMPA receptor blockade in rat hippocampal slices. J. Physiol *581*, 129-138.

Matsuo,N., Reijmers,L., and Mayford,M. (2008). Spine-type-specific recruitment of newly synthesized AMPA receptors with learning. Science *319*, 1104-1107.

Matsushita,M., Tomizawa,K., Moriwaki,A., Li,S.T., Terada,H., and Matsui,H. (2001). A high-efficiency protein transduction system demonstrating the role of PKA in long-lasting long-term potentiation. J. Neurosci. *21*, 6000-6007.

Matsuzaki,M. (2007). Factors critical for the plasticity of dendritic spines and memory storage. Neurosci. Res. *57*, 1-9.

Matsuzaki,M., Ellis-Davies,G.C.R., Nemoto,T., Miyashita,Y., Iino,M., and Kasai,H. (2001). Dendritic spine geometry is critical for AMPA receptor expression in hippocampal CA1 pyramidal neurons. Nat. Neurosci. *4*, 1086-1092.

Matsuzaki,M., Honkura,N., Ellis-Davies,G.C.R., and Kasai,H. (2004). Structural basis of long-term potentiation in single dendritic spines. Nature 429, 761-766.

Matthews,D.A., Cotman,C., and Lynch,G. (1976). An electron microscopic study of lesion-induced synaptogenesis in the dentate gyrus of the adult rat. I. Magnitude and time course of degeneration. Brain Res. *115*, 1-21.

Mayadevi,M., Praseeda,M., Kumar,K.S., and Omkumar,R.V. (2002). Sequence determinants on the NR2A and NR2B subunits of NMDA receptor responsible for specificity of phosphorylation by CaMKII. Biochim. Biophys. Acta *1598*, 40-45.

Mayford,M., Wang,J., Kandel,E.R., and O'Dell,T.J. (1995). CaMKII regulates the frequency-response function of hippocampal synapses for the production of both LTD and LTP. Cell *81*, 891-904.

McKinney,R.A., Capogna,M., Durr,R., Gahwiler,B.H., and Thompson,S.M. (1999). Miniature synaptic events maintain dendritic spines via AMPA receptor activation. Nat. Neurosci. *2*, 44-49.

McKinney,R.A., Debanne,D., Gähwiler,B.H., and Thompson,S.M. (1997). Lesion-induced axonal sprouting and hyperexcitability in the hippocampus *in vitro*: Implications for the genesis of posttraumatic epilepsy. Nature Med. *3*, 990-996.

McNair,K., Spike,R., Guilding,C., Prendergast,G.C., Stone,T.W., Cobb,S.R., and Morris,B.J. (2010). A role for RhoB in synaptic plasticity and the regulation of neuronal morphology. J. Neurosci. *30*, 3508-3517.

Megias,M., Emri,Z., Freund,T.F., and Gulyas,A.I. (2001). Total number and distribution of inhibitory and excitatory synapses on hippocampal CA1 pyramidal cells. Neurosci. *102*, 527-540.

Mehta,M.R. (2004). Cooperative LTP can map memory sequences on dendritic branches. Trends Neurosci. *27*, 69-72.

Michel,J.J., and Scott,J.D. (2002). AKAP mediated signal transduction. Annu. Rev. Pharmacol. Toxicol. *42*, 235-257.

Miller,M., and Peters,A. (1981). Maturation of rat visual cortex. II. A combined Golgi-electron microscope study of pyramidal neurons. J. Comp Neurol. *203*, 555-573.

Minichiello,L. (2009). TrkB signalling pathways in LTP and learning. Nat. Rev. Neurosci. *10*, 850-860.

Montminy,M. (1997). Transcriptional regulation by cyclic AMP. Annu. Rev. Biochem. *66*, 807-822.

Morris,R.G., Davis,S., and Butcher,S.P. (1990). Hippocampal synaptic plasticity and NMDA receptors: a role in information storage? Philos. Trans. R. Soc. Lond B Biol. Sci. *329*, 187-204.

Moser,E.I., Krobert,K.A., Moser,M.B., and Morris,R.G. (1998). Impaired spatial learning after saturation of long-term potentiation. Science *281*, 2038-2042.

Mrsic-Flogel,T.D., Hofer,S.B., Ohki,K., Reid,R.C., Bonhoeffer,T., and Hubener,M. (2007). Homeostatic regulation of eye-specific responses in visual cortex during ocular dominance plasticity. Neuron *54*, 961-972.

Muller,D., Buchs,P.A., and Stoppini,L. (1993). Time course of synaptic development in hippocampal organotypic cultures. Developmental Brain Research *71*, 93-100.

Murphy,D.D., and Segal,M. (1997). Morphological plasticity of dendritic spines in central neurons is mediated by activation of cAMP response element binding protein. Proc. Natl. Acad. Sci. USA *94*, 1482-1487.

Nägerl,U.V., Eberhorn,N., Cambridge,S.B., and Bonhoeffer,T. (2004). Bidirectional Activity-Dependent Morphological Plasticity in Hippocampal Neurons. Neuron *44*, 759-767.

Nakamura,Y., Wood,C.L., Patton,A.P., Jaafari,N., Henley,J.M., Mellor,J.R., and Hanley,J.G. (2011). PICK1 inhibition of the Arp2/3 complex controls dendritic spine size and synaptic plasticity. EMBO J. *30*, 719-730.

Neves,G., Cooke,S.F., and Bliss,T.V. (2008). Synaptic plasticity, memory and the hippocampus: a neural network approach to causality. Nat. Rev. Neurosci. *9*, 65-75.

Nguyen,P.V., and Kandel,E.R. (1996). A macromolecular synthesis-dependent late phase of long-term potentiation requiring cAMP in the medial perforant pathway of rat hippocampal slices. J. Neurosci. *16*, 3189-3198.

Nguyen,P.V., and Woo,N.H. (2003). Regulation of hippocampal synaptic plasticity by cyclic AMP-dependent protein kinases. Prog. Neurobiol. *71*, 401-437.

Nicholson,D.A., Trana,R., Katz,Y., Kath,W.L., Spruston,N., and Geinisman,Y. (2006). Distance-Dependent Differences in Synapse Number and AMPA Receptor Expression in Hippocampal CA1 Pyramidal Neurons. Neuron *50*, 431-442.

Ninan,I., and Arancio,O. (2004). Presynaptic CaMKII is necessary for synaptic plasticity in cultured hippocampal neurons. Neuron *42*, 129-141.

Noguchi,J., Matsuzaki,M., Ellis-Davies,G.C., and Kasai,H. (2005). Spine-neck geometry determines NMDA receptor-dependent Ca2+ signaling in dendrites. Neuron *46*, 609-622.

Okamoto,K., Bosch,M., and Hayashi,Y. (2009). The roles of CaMKII and F-actin in the structural plasticity of dendritic spines: a potential molecular identity of a synaptic tag? Physiology. (Bethesda) *24*, 357-366.

Okamoto,K., Nagai,T., Miyawaki,A., and Hayashi,Y. (2004). Rapid and persistent modulation of actin dynamics regulates postsynaptic reorganization underlying bidirectional plasticity. Nature Neuroscience 7, 1104-1112.

Okamoto,K., Narayanan,R., Lee,S.H., Murata,K., and Hayashi,Y. (2007). The role of CaMKII as an F-actin-bundling protein crucial for maintenance of dendritic spine structure. Proc. Natl. Acad. Sci. U. S. A *104*, 6418-6423.

Oray,S., Majewska,A., and Sur,M. (2006). Effects of synaptic activity on dendritic spine motility of developing cortical layer v pyramidal neurons. Cereb. Cortex *16*, 730-741.

Ostroff,L.E., Fiala,J.C., Allwardt,B., and Harris,K.M. (2002). Polyribosomes redistribute from dendritic shafts into spines with enlarged synapses during LTP in developing rat hippocampal slices. Neuron *35*, 535-545.

Otmakhov,N., Griffith,L.C., and Lisman,J.E. (1997). Postsynaptic inhibitors of calcium/calmodulin-dependent protein kinase type II block induction but not maintenance of pairing-induced long-term potentiation. J. Neurosci. *17*, 5357-5365.

Pak,D.T.S., Yang,S.Y., Rudolph-Correia,S., Kim,E., and Sheng,M. (2001). Regulation of dendritic spine morphology by SPAR, a PSD-95-associated RapGAP. Neuron *31*, 289-303.

Pandis,C., Sotiriou,E., Kouvaras,E., Asprodini,E., Papatheodoropoulos,C., and Angelatou,F. (2006). Differential expression of NMDA and AMPA receptor subunits in rat dorsal and ventral hippocampus. Neurosci. *140*, 163-175.

Papa,M., and Segal,M. (1996). Morphological plasticity in dendritic spines of cultured hippocampal neurons. Neurosci. *71*, 1005-1011.

Parnass,Z., Tashiro,A., and Yuste,R. (2000). Analysis of spine morphological plasticity in developing hippocampal pyramidal neurons. Hippocampus *10*, 561-568.

Parnavelas,J.G., Lynch,G., Brecha,N., Cotman,C.W., and Globus,A. (1974). Spine loss and regrowth in hippocampus following deafferentation. Nature *248*, 71-73.

Parsley,S.L., Pilgram,S.M., Soto,F., Giese,K.P., and Edwards,F.A. (2007). Enriching the environment of alphaCaMKIIT286A mutant mice reveals that LTD occurs in memory processing but must be subsequently reversed by LTP. Learn. Mem. *14*, 75-83.

Pastalkova,E., Serrano,P., Pinkhasova,D., Wallace,E., Fenton,A.A., and Sacktor,T.C. (2006). Storage of spatial information by the maintenance mechanism of LTP. Science *313*, 1141-1144.

Perez-Otano,I., and Ehlers,M.D. (2005). Homeostatic plasticity and NMDA receptor trafficking. Trends Neurosci. *28*, 229-238.

Petrak,L.J., Harris,K.M., and Kirov,S.A. (2005). Synaptogenesis on mature hippocampal dendrites occurs via filopodia and immature spines during blocked synaptic transmission. J. Comp Neurol. *484*, 183-190.

Pettit,D.L., Perlman,S., and Malinow,R. (1994). Potentiated transmission and prevention of further LTP by increased CaMKII activity in postsynaptic hippocampal slice neurons. Science *266*, 1881-1885.

Pi,H.J., Otmakhov,N., Lemelin,D., De,K.P., and Lisman,J. (2010). Autonomous CaMKII can promote either long-term potentiation or long-term depression, depending on the state of T305/T306 phosphorylation. J. Neurosci. *30*, 8704-8709.

Pokorny,J., and Yamamoto,T. (1981). Postnatal ontogenesis of hippocampal CA1 area in rats. I. Development of dendritic arborisation in pyramidal neurons. Brain Res. Bull. *7*, 113-120.

Pozo,K., and Goda,Y. (2010). Unraveling mechanisms of homeostatic synaptic plasticity. Neuron *66*, 337-351.

Quinlan,E.M., Lebel,D., Brosh,I., and Barkai,E. (2004). A molecular mechanism for stabilization of learning-induced synaptic modifications. Neuron *41*, 185-192.

Rabinowitch,I., and Segev,I. (2008). Two opposing plasticity mechanisms pulling a single synapse. Trends Neurosci. *31*, 377-383.

Raisman,G., and Field,P.M. (1973). A quantitative investigation of the development of collateral reinnervation after partial deafferentation of the septal nuclei. Brain Res. *50*, 241-264.

Rakic,P., Bourgeois,J.P., Eckenhoff,M.F., Zecevic,N., and Goldman-Rakic,P.S. (1986). Concurrent overproduction of synapses in diverse regions of the primate cerebral cortex. Science *232*, 232-235.

Ramocki,M.B., and Zoghbi,H.Y. (2008). Failure of neuronal homeostasis results in common neuropsychiatric phenotypes. Nature *455*, 912-918.

Ramón y Cajal,S. (1899). La textura del sistema nerviosa del hombre y los vertebrados.

Rasband,W.S. ImageJ. U.S.National Institutes of Health, Bethesda, Maryland, USA. 1997-2011.

Raymond,C.R. (2007). LTP forms 1, 2 and 3: different mechanisms for the "long" in long-term potentiation. Trends Neurosci. *30*, 167-175.

Rempel-Clower,N.L., Zola,S.M., Squire,L.R., and Amaral,D.G. (1996). Three cases of enduring memory impairment after bilateral damage limited to the hippocampal formation. J. Neurosci. *16*, 5233-5255.

Renner,M., Choquet,D., and Triller,A. (2009). Control of the postsynaptic membrane viscosity. J. Neurosci. *29*, 2926-2937.

Rheims,S., Holmgren,C.D., Chazal,G., Mulder,J., Harkany,T., Zilberter,T., and Zilberter,Y. (2009). GABA action in immature neocortical neurons directly depends on the availability of ketone bodies. J. Neurochem. *110*, 1330-1338.

Ridler,T.W., and Calvard,S. (1978). Picture thresholding using an iterative selection method. IEEE Trans. System, Man and Cybernetics *SMC-8*, 630-632.

Roberts,T.F., Tschida,K.A., Klein,M.E., and Mooney,R. (2010). Rapid spine stabilization and synaptic enhancement at the onset of behavioural learning. Nature *463*, 948-952.

Rodriguez,A., Ehlenberger,D.B., Dickstein,D.L., Hof,P.R., and Wearne,S.L. (2008). Automated three-dimensional detection and shape classification of dendritic spines from fluorescence microscopy images. PLoS. ONE. *3*, e1997.

Rose,J., Jin,S.X., and Craig,A.M. (2009). Heterosynaptic molecular dynamics: locally induced propagating synaptic accumulation of CaM kinase II. Neuron *61*, 351-358.

Royer,S., and Pare,D. (2003). Conservation of total synaptic weight through balanced synaptic depression and potentiation. Nature *422*, 518-522.

Ruiz-Marcos,A., and Valverde,F. (1969). The temporal evolution of the distribution of dendritic spines in the visual cortex of normal and dark raised mice. Exp. Brain Res. *8*, 284-294.

Rutherford,L.C., DeWan,A., Lauer,H.M., and Turrigiano,G.G. (1997). Brain-Derived Neurotrophic Factor Mediates the Activity-Dependent Regulation of Inhibition in Neocortical Cultures. J. Neurosci. *17*, 4527-4535.

Sabatini,B.L., Oertner,T.G., and Svoboda,K. (2002). The life cycle of Ca^{2+} ions in dendritic spines. Neuron *33*, 439-452.

Sajikumar,S., and Korte,M. (2011). Metaplasticity governs compartmentalization of synaptic tagging and capture through brain-derived neurotrophic factor (BDNF) and protein kinase Mzeta (PKMzeta). Proc. Natl. Acad. Sci. U. S. A *108*, 2551-2556.

Sajikumar,S., Navakkode,S., and Frey,J.U. (2005). Protein synthesis-dependent long-term functional plasticity: methods and techniques. Curr. Opin. Neurobiol. *15*, 607-613.

Salin,P.A., Malenka,R.C., and Nicoll,R.A. (1996). Cyclic AMP mediates a presynaptic form of LTP at cerebellar parallel fiber synapses. Neuron *16*, 797-803.

Savic,N., Lüthi,A., Gähwiler,B.H., and McKinney,R.A. (2003). *N*-methyl-D-aspartate receptor blockade during development lowers long-term potentiation threshold without affecting dynamic range of CA3-CA1 synapses. Proc. Natl. Acad. Sci. USA *100*, 5503-5508.

Savtchenko,L.P., and Rusakov,D.A. (2007). The optimal height of the synaptic cleft. Proc. Natl. Acad. Sci. U. S. A *104*, 1823-1828.

Scoville,W.B., and Milner,B. (1957). Loss of recent memory after bilateral hippocampal lesions. J. Neurol. Neurosurg. Psychiatry *20*, 11-21.

Serrano,P., Yao,Y., and Sacktor,T.C. (2005). Persistent phosphorylation by protein kinase Mzeta maintains late-phase long-term potentiation. J. Neurosci. *25*, 1979-1984.

Shen,K., Teruel,M.N., Subramanian,K., and Meyer,T. (1998). CaMKIIβ functions as an F-actin targeting module that localizes CaMKIIα/β heterooligomers to dendritic spines. Neuron *21*, 593-606.

Shepherd,J.D., and Bear,M.F. (2011). New views of Arc, a master regulator of synaptic plasticity. Nat. Neurosci. *14*, 279-284.

Shepherd,J.D., Rumbaugh,G., Wu,J., Chowdhury,S., Plath,N., Kuhl,D., Huganir,R.L., and Worley,P.F. (2006). Arc/Arg3.1 mediates homeostatic synaptic scaling of AMPA receptors. Neuron *52*, 475-484.

Shi,S.H., Hayashi,Y., Esteban,J.A., and Malinow,R. (2001). Subunit-specific rules governing AMPA receptor trafficking to synapses in hippocampal pyramidal neurons. Cell *105*, 331-343.

Shinoda,Y., Tominaga-Yoshino,K., and Ogura,A. (2003). The dendritic layer-specific persistent enhancement of synaptic transmission induced by repetitive activation of protein kinase A. Neurosci. Res. *47*, 191-200.

Sik,A., Hajos,N., Gulacsi,A., Mody,I., and Freund,T.F. (1998). The absence of a major Ca2+ signaling pathway in GABAergic neurons of the hippocampus. Proc. Natl. Acad. Sci. U. S. A *95*, 3245-3250.

Silva,A.J., Stevens,C.F., Tonegawa,S., and Wang,Y. (1992). Deficient hippocampal long-term potentiation in alpha-calcium- calmodulin kinase II mutant mice. Science *257*, 201-206.

Silver,R.A. (2010). Neuronal arithmetic. Nat. Rev. Neurosci. *11*, 474-489.

Skeberdis,V.A., Chevaleyre,V., Lau,C.G., Goldberg,J.H., Pettit,D.L., Suadicani,S.O., Lin,Y., Bennett,M.V., Yuste,R., Castillo,P.E., and Zukin,R.S. (2006). Protein kinase A regulates calcium permeability of NMDA receptors. Nat. Neurosci. *9*, 501-510.

Smith,D.L., Pozueta,J., Gong,B., Arancio,O., and Shelanski,M. (2009). Reversal of long-term dendritic spine alterations in Alzheimer disease models
1. Proc. Natl. Acad. Sci. U. S. A *106*, 16877-16882.

Sobczyk,A., and Svoboda,K. (2007). Activity-dependent plasticity of the NMDA-receptor fractional Ca2+ current. Neuron *53*, 17-24.

Song,F., Parekh-Bhurke,S., Hooper,L., Loke,Y.K., Ryder,J.J., Sutton,A.J., Hing,C.B., and Harvey,I. (2009). Extent of publication bias in different categories of research cohorts: a meta-analysis of empirical studies. BMC. Med. Res. Methodol. *9*, 79.

Sorra,K.E., and Harris,K.M. (1993). Occurrence and three-dimensional structure of multiple synapses between individual radiatum axons and their target pyramidal cells in hippocampal area CA1. J. Neurosci. *13*, 3736-3748.

Sorra,K.E., and Harris,K.M. (2000). Overview on the structure, composition, function, development, and plasticity of hippocampal dendritic spines. Hippocampus *10*, 501-511.

Sotelo,C. (1978). Purkinje cell ontogeny: formation and maintenance of spines. Prog. Brain Res. *48*, 149-170.

Sourdet,V., and Debanne,D. (1999). The role of dendritic filtering in associative long-term synaptic plasticity. Learn. Mem. *6*, 422-447.

Squire,L.R., Stark,C.E., and Clark,R.E. (2004). The medial temporal lobe. Annu. Rev. Neurosci. *27*, 279-306.

Stellwagen,D., and Malenka,R.C. (2006). Synaptic scaling mediated by glial TNF-alpha. Nature *440*, 1054-1059.

Steward,O., Vinsant,S.L., and Davis,L. (1988). The process of reinnervation in the dentate gyrus of adult rats: an ultrastructural study of changes in presynaptic terminals as a result of sprouting. J. Comp Neurol. *267*, 203-210.

Stoppini,L., Buchs,P.-A., and Muller,D. (1991). A simple method for organotypic cultures of nervous tissue. J. Neurosci. Meth. *37*, 173-182.

Sutton,M.A., Ito,H.T., Cressy,P., Kempf,C., Woo,J.C., and Schuman,E.M. (2006). Miniature neurotransmission stabilizes synaptic function via tonic suppression of local dendritic protein synthesis. Cell *125*, 785-799.

Swann,J.W., Al Noori,S., Jiang,M., and Lee,C.L. (2000). Spine loss and other dendritic abnormalities in epilepsy [In Process Citation]. Hippocampus *10*, 617-625.

Takacs,J., and Hamori,J. (1990). Morphological plasticity of dendrites in adult brain. Acta Neurobiol. Exp. *50*, 109-114.

Takahashi,T., Svoboda,K., and Malinow,R. (2003). Experience strengthening transmission by driving AMPA receptors into synapses. Science *299*, 1585-1588.

Takumi,Y., Ramírez-León,V., Laake,P., Rinvik,E., and Ottersen,O.P. (1999). Different modes of expression of AMPA and NMDA receptors in hippocampal synapses. Nat. Neurosci. *2*, 618-624.

Tao,H.Z.W., and Poo,M.M. (2001). Retrograde signaling at central synapses. Proc. Natl. Acad. Sci. USA *98*, 11009-11015.

Thiagarajan,T.C., Lindskog,M., and Tsien,R.W. (2005). Adaptation to synaptic inactivity in hippocampal neurons. Neuron *47*, 725-737.

Thiagarajan,T.C., Piedras-Renteria,E.S., and Tsien,R.W. (2002). alpha- and betaCaMKII. Inverse regulation by neuronal activity and opposing effects on synaptic strength. Neuron *36*, 1103-1114.

Tobimatsu,T., and Fujisawa,H. (1989). Tissue-specific expression of four types of rat calmodulin-dependent protein kinase II mRNAs. J. Biol. Chem. *264*, 17907-17912.

Tokumitsu,H., Chijiwa,T., Hagiwara,M., Mizutani,A., Terasawa,M., and Hidaka,H. (1990). KN-62, 1-[N,O-bis(5-isoquinolinesulfonyl)-N-methyl-L-tyrosyl]-4-phenylpiperazine, a specific inhibitor of Ca2+/calmodulin-dependent protein kinase II. J. Biol. Chem. *265*, 4315-4320.

Tonegawa,S., Nakazawa,K., and Wilson,M.A. (2003). Genetic neuroscience of mammalian learning and memory. Philos. Trans. R. Soc. Lond B Biol. Sci. *358*, 787-795.

Turrigiano,G.G. (2008). The self-tuning neuron: synaptic scaling of excitatory synapses. Cell *135*, 422-435.

Turrigiano,G.G., Leslie,K.R., Desai,N.S., Rutherford,L.C., and Nelson,S.B. (1998). Activity-dependent scaling of quantal amplitude in neocortical neurons. Nature *391*, 892-896.

Turrigiano,G.G., and Nelson,S.B. (2004). Homeostatic plasticity in the developing nervous system. Nat. Rev. Neurosci. *5*, 97-107.

Tyler,W.J., and Pozzo-Miller,L. (2003). Miniature synaptic transmission and BDNF modulate dendritic spine growth and form in rat CA1 neurones. J. Physiol *553*, 497-509.

University of Victoria,A.i.l. Epi-fluorescence with the microscope. 2005. Online Source

Vanderklish,P.W., and Edelman,G.M. (2002). Dendritic spines elongate after stimulation of group 1 metabotropic glutamate receptors in cultured hippocampal neurons. Proc. Natl. Acad. Sci. USA *99*, 1639-1644.

Villarreal,D.M., Do,V., Haddad,E., and Derrick,B.E. (2002). NMDA receptor antagonists sustain LTP and spatial memory: active processes mediate LTP decay. Nat. Neurosci. *5*, 48-52.

Wallace,W., and Bear,M.F. (2004). A morphological correlate of synaptic scaling in visual cortex. J. Neurosci. *24*, 6928-6938.

Weisskopf,M.G., Castillo,P.E., Zalutsky,R.A., and Nicoll,R.A. (1994). Mediation of hippocampal mossy fiber long-term potentiation by cyclic AMP. Science *265*, 1878-1882.

Weyhersmuller,A., Hallermann,S., Wagner,N., and Eilers,J. (2011). Rapid active zone remodeling during synaptic plasticity. J. Neurosci. *31*, 6041-6052.

Wierenga,C.J., Ibata,K., and Turrigiano,G.G. (2005). Postsynaptic expression of homeostatic plasticity at neocortical synapses. J. Neurosci. *25*, 2895-2905.

Wierenga,C.J., Walsh,M.F., and Turrigiano,G.G. (2006). Temporal regulation of the expression locus of homeostatic plasticity. J. Neurophysiol. *96*, 2127-2133.

Wikström,M.A., Matthews,P., Roberts,D., Collingridge,G.L., and Bortolotto,Z.A. (2003). Parallel kinase cascades are involved in the induction of LTP at hippocampal CA1 synapses. Neuropharmacol. *45*, 828-836.

Williams,J. (2003). Learning and behavior in children with epilepsy. Epilepsy Behav. *4*, 107-111.

Wilson,R.I., and Nicoll,R.A. (2001). Endogenous cannabinoids mediate retrograde signalling at hippocampal synapses. Nature *410*, 588-592.

Wong,M. (2005). Modulation of dendritic spines in epilepsy: cellular mechanisms and functional implications. Epilepsy Behav. *7*, 569-577.

Wong,S.T., Athos,J., Figueroa,X.A., Pineda,V.V., Schaefer,M.L., Chavkin,C.C., Muglia,L.J., and Storm,D.R. (1999). Calcium-stimulated adenylyl cyclase activity is critical for hippocampus-dependent long-term memory and late phase LTP. Neuron *23*, 787-798.

Wu,G.Y., Deisseroth,K., and Tsien,R.W. (2001). Activity-dependent CREB phosphorylation: Convergence of a fast, sensitive calmodulin kinase pathway and a slow, less sensitive mitogen-activated protein kinase pathway. Proc. Natl. Acad. Sci. USA *98*, 2808-2813.

Xia,Z., and Storm,D.R. (2005). The role of calmodulin as a signal integrator for synaptic plasticity. Nat. Rev. Neurosci. *6*, 267-276.

Xu,T., Yu,X., Perlik,A.J., Tobin,W.F., Zweig,J.A., Tennant,K., Jones,T., and Zuo,Y. (2009). Rapid formation and selective stabilization of synapses for enduring motor memories. Nature *462*, 915-919.

Yamamoto,K.K., Gonzalez,G.A., Biggs,W.H., III, and Montminy,M.R. (1988). Phosphorylation-induced binding and transcriptional efficacy of nuclear factor CREB. Nature *334*, 494-498.

Yamamoto,M., Urakubo,T., Tominaga-Yoshino,K., and Ogura,A. (2005). Long-lasting synapse formation in cultured rat hippocampal neurons after repeated PKA activation. Brain Res. *1042*, 6-16.

Yang,G., Pan,F., and Gan,W.B. (2009). Stably maintained dendritic spines are associated with lifelong memories. Nature *462*, 920-924.

Yang,H.W., Hu,X.D., Zhang,H.M., Xin,W.J., Li,M.T., Zhang,T., Zhou,L.J., and Liu,X.G. (2004). Roles of CaMKII, PKA, and PKC in the induction and maintenance of LTP of c-fiber-evoked field potentials in rat spinal dorsal horn. J. Neurophysiol. *91*, 1122-1133.

Yang,Y., Wang,X.B., Frerking,M., and Zhou,Q. (2008). Spine expansion and stabilization associated with long-term potentiation. J. Neurosci. *28*, 5740-5751.

Yasuda,H., Barth,A.L., Stellwagen,D., and Malenka,R.C. (2003). A developmental switch in the signaling cascades for LTP induction. Nat. Neurosci. *6*, 15-16.

Yasumatsu,N., Matsuzaki,M., Miyazaki,T., Noguchi,J., and Kasai,H. (2008). Principles of long-term dynamics of dendritic spines. J. Neurosci. *28*, 13592-13608.

Young,J.Z., Isiegas,C., Abel,T., and Nguyen,P.V. (2006). Metaplasticity of the late-phase of long-term potentiation: a critical role for protein kinase A in synaptic tagging. Eur. J. Neurosci. *23*, 1784-1794.

Yu,L.M., and Goda,Y. (2009). Dendritic signalling and homeostatic adaptation. Curr. Opin. Neurobiol. *19*, 327-335.

Yuste,R. (2010). Dendritic Spines, MIT Press, 1st Edition.

Yuste,R., and Bonhoeffer,T. (2004). Genesis of dendritic spines: Insights from ultrastructural and imaging studies. Nat. Rev. Neurosci. *5*, 24-34.

Yuste,R., and Denk,W. (1995). Dendritic spines as basic functional units of neuronal integration. Nature *375*, 682-684.

Yuste,R., Majewska,A., Cash,S.S., and Denk,W. (1999). Mechanisms of calcium influx into hippocampal spines: Heterogeneity among spines, coincidence detection by NMDA receptors, and optical quantal analysis. J. Neurosci. *19*, 1976-1987.

Zhang,J., Yang,Y., Li,H., Cao,J., and Xu,L. (2005). Amplitude/frequency of spontaneous mEPSC correlates to the degree of long-term depression in the CA1 region of the hippocampal slice. Brain Res. *1050*, 110-117.

Zhang,Y.P., Holbro,N., and Oertner,T.G. (2008). Optical induction of plasticity at single synapses reveals input-specific accumulation of alphaCaMKII. Proc. Natl. Acad. Sci. U. S. A *105*, 12039-12044.

Zhao,C., Dreosti,E., and Lagnado,L. (2011). Homeostatic synaptic plasticity through changes in presynaptic calcium influx. J. Neurosci. *31*, 7492-7496.

Zhou,Q., Homma,K.J., and Poo,M.M. (2004). Shrinkage of dendritic spines associated with long-term depression of hippocampal synapses. Neuron *44*, 749-757.

Zhou,X., Lin,D.S., Zheng,F., Sutton,M.A., and Wang,H. (2010). Intracellular calcium and calmodulin link brain-derived neurotrophic factor to p70S6 kinase phosphorylation and dendritic protein synthesis. J. Neurosci. Res. *88*, 1420-1432.

Zhu,J.J., Esteban,J.A., Hayashi,Y., and Malinow,R. (2000). Postnatal synaptic potentiation: Delivery of GluR4-containing AMPA receptors by spontaneous activity. Nat. Neurosci. *3*, 1098-1106.

Zhu,J.J., and Malinow,R. (2002). Acute versus chronic NMDA receptor blockade and synaptic AMPA receptor delivery. Nat. Neurosci. *5*, 513-514.

Ziv,N.E., and Smith,S.J. (1996). Evidence for a role of dendritic filopodia in synaptogenesis and spine formation. Neuron *17*, 91-102.